HRVATSKO DRUŠTVO
ZA STROJARSKE TEHNOLOGIJE

CROATIAN SOCIETY
FOR MECHANICAL TECHNOLOGIES

In association with:

*University of Split
Faculty of Electrical Engineering,
Mechanical Engineering and
Naval Architecture*

*Slovak Academy of Science
Institute of Materials and
Machine Mechanics*

*Sveučilište u Splitu
Sveučilišni
odjel za stručne studije*

*Croatian Society for
Materials and Tribology*

*Dublin Institute
of Technology*

*Rogante Engineering
Office*

ISSN 1847-7917

4th International Conference

Mechanical Technology and Structural Materials 2014

General sponsors:

City of Split
Split - Dalmatia County
Ministry of Science, Education and Sports Republic of Croatia

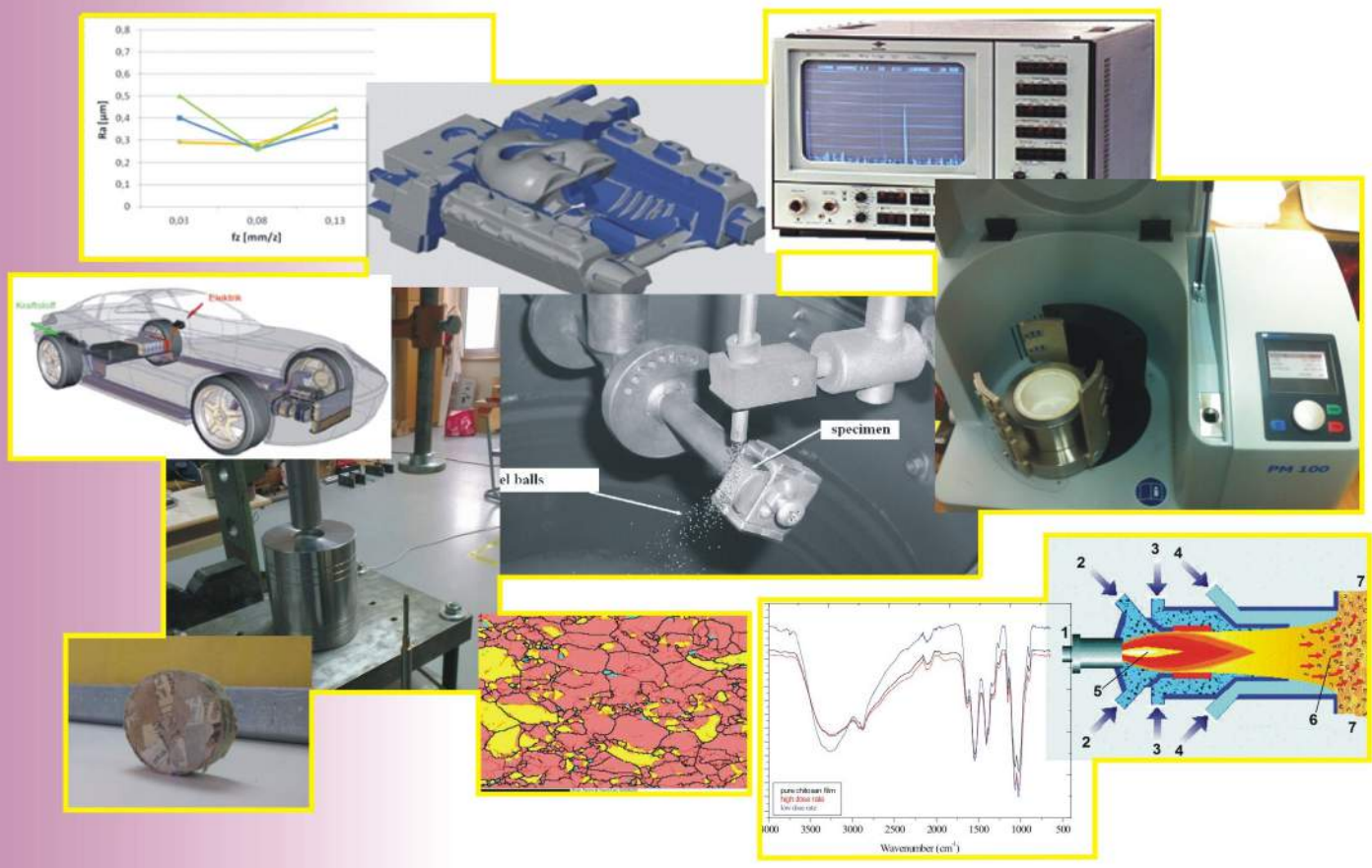

http://www.strojarska-tehnologija.hr

September, 25th - 26th, 2014.
from 9 a.m. to 2 p.m.
FESB, Ruđera Boškovića 32, Split

ZBORNIK RADOVA

CONFERENCE PROCEEDINGS

STROJARSKE TEHNOLOGIJE I KONSTRUKCIJSKI MATERIJALI

MECHANICAL TECHNOLOGIES AND STRUCTURAL MATERIALS

Split

Hrvatska / Croatia

25.-26. rujan / September 2014.

ORGANIZATOR / ORGANIZED BY:

HRVATSKO DRUŠTVO ZA STROJARSKE TEHNOLOGIJE, Hrvatska

CROATIAN SOCIETY FOR MECHANICAL TECHNOLOGIES, Croatia

SURGANIZATORI / CO-ORGANIZERS:

SVEUČILIŠTE U SPLITU
FAKULTET ELEKTROTEHNIKE, STROJARSTVA I BRODOGRADNJE

HRVATSKO DRUŠTVO ZA MATERIJALE I TRIBOLOGIJU

DUBLIN INSTITUTE OF TECHNOLOGY

SLOVAK ACADEMY OF SCIENCE INSTITUTE OF MATERIALS AND MACHINE MECHANICS

ROGANTE ENGINEERING OFFICE

SVEUČILIŠTE U SPLITU
SVEUČILIŠNI ODJEL ZA STRUČNE STUDIJE

SPONZORI / SPONSORS:

GRAD SPLIT

SPLITSKO-DALMATINSKA ŽUPANIJA

MINISTARSTVO ZNANOSTI, OBRAZOVANJA I ŠPORTA

EVN CROATIA PLIN d.o.o.

IZDAVAČ / PUBLISHER:

HRVATSKO DRUŠTVO ZA STROJARSKE TEHNOLOGIJE, Hrvatska

CROATIAN SOCIETY FOR MECHANICAL TECHNOLOGIES, Croatia

c/o FESB, Ruđera Boškovića 32, 21000 SPLIT

tel.: +385 21 305 910; fax.: +385 21 463 877

e-mail: info@strojarska-tehnologija.hr

http://www.strojarska-tehnologija.hr

UREDNIK / EDITOR:

dr.sc. Dražen Živković

ISSN 1847-7917

NAKLADA / ISSUE: 70

ORGANIZACIJSKI ODBOR
ORGANIZING COMMITEE:

- Igor GABRIĆ (Hrvatska) - Predsjednik
- Zvonko MRDULJAŠ (Hrvatska) - Dopredsjednik

- Ante ALUJEVIĆ (Hrvatska)
- Ante BAROVIĆ (Hrvatska)
- Nikša ČATIPOVIĆ (Hrvatska)
- Zvonimir DADIĆ (Hrvatska)
- Nikola GJELDUM (Hrvatska)
- Dario ILJKIĆ (Hrvatska)
- Sonja JOZIĆ (Hrvatska)
- Neven KUZMANIĆ (Hrvatska)
- Branimir LELA (Hrvatska)
- Petar LJUMOVIĆ (Hrvatska)
- Gojko MARIĆ (Hrvatska)
- Slaven ŠITIĆ (Hrvatska)

PROGRAMSKI I RECENZENTSKI ODBOR
PROGRAMME AND REVIEW COMMITEE:

- Dražen ŽIVKOVIĆ (Hrvatska) - Predsjednik
- Dražen BAJIĆ (Hrvatska) - Dopredsjednik

- Boris ANZULOVIĆ (Hrvatska)
- Frane BARBIR (Hrvatska)
- Franjo CAJNER (Hrvatska)
- Goran CUKOR (Hrvatska)
- Vinko IVUŠIĆ (Hrvatska)
- Zlatko JANKOSKI (Hrvatska)
- Jaroslav JERZ (Slovakia)
- David KENNEDY (Ireland)
- John LAWLOR (Ireland)
- Zoran PANDILOV (Macedonia)
- Mladen PERINIĆ (Hrvatska)
- Massimo ROGANTE (Italy)
- Zdravko SCHAUPERL (Hrvatska)
- Wilfried SIHN (Austria)
- František SIMANČIK (Bratislava)
- Božo SMOLJAN (Hrvatska)
- Goran ŠIMUNOVIĆ (Hrvatska)
- Katica ŠIMUNOVIĆ (Hrvatska)
- Matej VESENJAK (Slovenia)
- Ivica VEŽA (Hrvatska)

SADRŽAJ

1) Vladimir MESSERLE, Alexandr USTIMENKO, Oleg LAVRICHSHEV
"PLASMA-ENERGY TECHNOLOGIES OF FUEL PROCESSING" 1

2) Massimo ROGANTE, Katica ŠIMUNOVIĆ
„ENHANCED TOOL CONDITION MONITORING BY STATISTICAL ANALYSIS IN AUTOMATIC MACHINING OF AISI 1045 STEEL USING SINTERED CARBIDE INSERTS" 7

3) Katica ŠIMUNOVIĆ, Lidija VINKOVIĆ, Goran ŠIMUNOVIĆ, Tomislav ŠARIĆ, Sara HAVRLIŠAN
"MULTI-CRITERIA APPROACH TO THE INVENTORY CLASSIFICATION IN SMALL ENTERPRISE " 15

4) John KIJAK, David KENNEDY
"PUMP DESIGN AND DEVELOPMENT FOR HIGH SHEAR GROUT MIXING APPLICATIONS " 23

5) Cenk DENKTAŞ1, Derya YILMAZ BAYSOY, Erol KAM
„DOSE RATE DEPENDENT EFFECTS OF BETA AND GAMMA IRRADIATION ON CHITOSAN FILMS "..... 29

6) Ivica VEZA, Nikola GJELDUM, Marko MLADINEO
"LOGISTICS PERSONAL EXCELLENCE BY CONTINUOUS SELF-ASSESSMENT (LOPEC): PILOT-IMPLEMENTATION CASE STUDIES"..... 39

7) Jaroslav JERZ, Michal Bartko, Roman Florek, Ľubomír Orovčík
"ADVANCED SOLUTION FOR ENERGY STORAGE IN NET ZERO-ENERGY BUILDINGS" 47

8) Sonja JOZIĆ, Dražen BAJIĆ, Mario DRAGIČEVIĆ
„INVESTIGATION OF CUTTING PARAMETERS INFLUENCE DURING MILLING PROCESS APPLYING COLD COMPRESSED AIR" 55

9) Vedrana CVITANIĆ, Daniel IVANDIĆ, Branimir LELA
"COMPARISON OF ORTHOTROPIC CONSTITUTIVE MODELS IN PREDICTING SQUARE CUP DEEP DRAWING PROCESS OF AA2090-T3 SHEET " 61

10) Božo SMOLJAN, Dario ILJKIĆ, Zvonimir KOLUMBIĆ
"COMPUTER MODELLING OF AS QUENCHED HARDNESS AND MICROSTRUCTURE OF STEEL SHAFT " 71

11) Krešimir GRILEC, Lidija ĆURKOVIĆ, Marijana MAJIĆ RENJO, Suzana JAKOVLJEVIĆ, Vera REDE
„PARTICLE EROSION OF SOL-GEL TiO_2-ZrO_2 FILMS „..... 77

12) Branimir LELA, Marin BARIŠIĆ
"CARDBOARD BRIQUETTES FOR HEAT ENERGY PRODUCTION "..... 83

13) Filip VALE, Duško PAVLETIĆ, Graciela ŠTERPIN, Mladen PERINIĆ
"3D DIGITALISATOR MEASURING OF SAND CORE CASTING " 87

14) Marijana Majić RENJO, Lidija ĆURKOVIĆ, Krešimir GRILEC, Matija SAKOMAN, Suzana JAKOVLJEVIĆ
"SEM-EDS ANALYSIS OF SLIP CAST COMPOSITE Al_2O_3-ZrO_2 CERAMICS " 95

15) Graciela ŠTERPIN, Branimir TADIĆ, Goran CUKOR, Zoran JURKOVIĆ
„CREATING 3D MODELS WITH SCANNER DAVID SLS-1"..... 99

16) Marijana MAJIĆ RENJO, Lidija ĆURKOVIĆ, Krešimir GRILEC, Matija AKOMAN
"PREPARATION OF STABLE SUSPENSIONS FOR SLIP CASTING OF MONOLITHIC AND COMPOSITE CERAMICS" 107

17) Zvonimir DADIĆ, Dražen ŽIVKOVIĆ, Nikša ČATIPOVIĆ
"WEAR MECHANISMS OF MOLD FOR HIGH PRESSURE DIE CASTING IN LTH METAL CAST MANUFACTURING PLANT" 113

18) Nikša ČATIPOVIĆ, Dražen ŽIVKOVIĆ, Zvonimir DADIĆ
"COLD AND HOT FORGING DIE WEAR" 117

19) Elena PASHINSKA, Anna MAKSAKOVA, Anatoliy ZAVDOVEEV
"INFLUENCE OF DRAWING WITH SHEAR TECHNOLOGY ON THE STRUCTURE AND PROPERTIES OF LOW-CARBON WIRE" 125

20) Antonio MIJIĆ, Gojmir RADICA
"KONSTRUKCIJSKE KARAKTERISTIKE AKTIVNOG MODULARNOG MOTORA S UNUTRAŠNJIM IZGARANJEM" 131

ISSN 1847-7917

Plasma-Energy Technologies of Fuel Processing

Vladimir MESSERLE[1)]***, Alexandr USTIMENKO***[2)] ***and Oleg LAVRICHSHEV***[2)]

1) Combustion Problems Institute, Almaty, Kazakhstan, Institute of Thermophysics of SB RAS, Novosibirsk, Russia (Izgaranje Problemi Institute, Almaty, Kazahstan, Institut Thermophysics SB RAS, Novosibirsk, Rusija)

2) Research Institute of Experimental and Theoretical Physics, Almaty, Kazakhstan (Institut za istraživanje eksperimentalne i teorijske fizike, Almaty, Kazahstan)

ust@physics.kz

Keywords

fuel
plasma
ignition
complex processing
cracking
Plasmochemical reactor

Abstract: This paper presents the results of studies of plasma-assisted processing of gaseous and solid fuels. They are plasma ignition, gasification, hydrogenation, and complex processing of solid fuels and cracking of hydrocarbon gases. The application of these technologies to produce hydrogen, carbon, hydrocarbon gases, synthesis gas, valuable components from the mineral mass of coal meets modern ecological and economic requirements. Plasma ignition of coal results in the formation of highly reactive two-component fuel (fuel gas and coke residue) from low-rank coal. It is applicable at thermal power plants for oil-free boiler start-up and pulverized flame stabilization. At complex processing of coal simultaneously with gasification of organic matter in the same reactor coke carbon restores mineral mass of coal oxides and valuable components, such as industrial silicon, ferrosilicon, aluminum and carbosilicon and microelements of heavy metals (uranium, molybdenum, vanadium, and others) are formed. Plasmochemical hydrogenation of coal is a process of direct production of acetylene and alkenes in the gas phase. Plasmochemical cracking is to heat hydrocarbon gases in arc reactor to a temperature of pyrolysis with the formation of fine carbon and hydrogen in unified technological process.

Sažetak: U radu su prikazani rezultati istraživanja procesa obrade plinovitih i krutih goriva uz pomoć plazme. Procesi uključuju zapaljenje uz pomoć plazme, plinofikaciju, hidrogenaciju, složenu obrada krutih goriva i razlaganje ugljikovodičnih plinova. Primjena ovih tehnologija za proizvodnju vodika, ugljika, ugljikovodika, sintetskog plina i vrijednih komponenti iz mineralnog dijela ugljena zadovoljava moderne ekološke i ekonomske zahtjeve. Zapaljenje ugljena niske kvalitete uz pomoć plazme ima za rezultat stvaranje visoko reaktivnog dvo-komponentnog goriva (gorivog plina i preostalog koksa). Dobiveno gorivo primjenjivo je u termoelektranama i to za zagrijavanje peći i stabilizaciju plamena pri čemu nije potrebna upotreba sekundarnog goriva (mazuta). Tijekom obrade goriva dolazi do plinofikacije organskog dijela goriva, dok preostali čvrsti ugljik obnavlja mineralnu masu oksida ugljena i vrijednih komponenti, kao što su industrijski silicij, ferosilicij, aluminij, ugljikov silicij i mikro elementi teških metala (uran, molibden, vanadij i ostali). Plazma-kemijsko hidrogeniranje ugljena predstavlja postupak direktne proizvodnje acetilena i alkena iz plinovite faze. Plazma-kemijsko pucanje predstavlja proces grijanja plinovitih ugljikovodika u plazma reaktoru na temperaturu pirolize, pri čemu se jedinstvenim tehnološkim procesom formira fini ugljik i vodik.

1. Introduction

The world's heat-and-power engineering is currently and foreseeable future (till 2100 year) oriented to use fossil fuel, mainly coal. Fraction of coal in electric power production is 40 % and in heat – 24 %. Thus development of the technologies for efficient and ecology friendly utilization of coal is the prime task. Considered in this paper plasmochemical technologies meet these requirements. Actuality of fuel processing plasmochemical technologies is increasing in accordance with oil and gas reserves depletion, solid fuels quality and nuclear power plants growth rate decrease.

Application of plasmochemical technologies of pyrolysis, hydrogenation thermochemical preparation for combustion, gasification, hybrid (radiant-plasma) and complex processing of solid fuels and cracking of hydrocarbon gases [1-8] to produce desired products (hydrogen, carbon, hydrocarbon gases, synthesis gas, valuable components of the mineral mass of coal (MMC) including rare earth) meets modern ecological and economic requirements of the power industry, metallurgy and chemical industry. Technologies of solid fuel plasma conversion are characterized mainly by different concentration of gaseous oxidant (air, water steam, carbon dioxide, oxygen) and therefore by different excess oxidant ratio α_{ox} (Table 1). In the table $\alpha_{ox}=0$ corresponds to coal pyrolysis, and $\alpha_{ox}=1$ – complete gasification of coal when oxidant is air. Note, required quantity of air for combustion of 1 kg of the coal is 5.25 kg, i.e. 2.5 times more than for its complete gasification (α_{ox} = 1.0).

2. Plasma Technologies Discussion

Plasmochemical technology of cracking is to heat hydrocarbon gases in the combined electric arc reactor to a temperature of pyrolysis (1900-2300 K) with the formation of fine carbon and hydrogen in unified technological process. Plasmochemical hydrogenation of solid fuels, which is the pyrolysis of coal in a hydrogen atmosphere, provides acetylene and other unsaturated hydrocarbons (ethylene C_2H_4, propylene, C_3H_6, C_2H_6 ethane, etc.) from cheap low-rank coals by their treatment with hydrogen plasma. Plasmochemical hydrogenation of coal is a new process of direct production of acetylene and alkenes in the gas phase, in contrast to conventional hydrogenation (liquefaction) of coal [5]. As a result of experiments on low-rank coal hydrogenation in plasmochemical reactor (Fig. 1) at its power of 50 kW, coal consumption of 3 kg/h, and propane-butane mixture flow of 150 l/h gas of the following composition s obtained, mass %: C_2H_6=50, C_2H_2=30, C_2H_4=10.

Table 1. Air-coal mixture compound

No	α_{ox}	Weight, kg	
		coal	air
1	0	1000	0
2	0.17	1000	360
3	0.30	1000	640
4	0.50	1000	1067
5	0.75	1000	1600
6	1.00	1000	2133

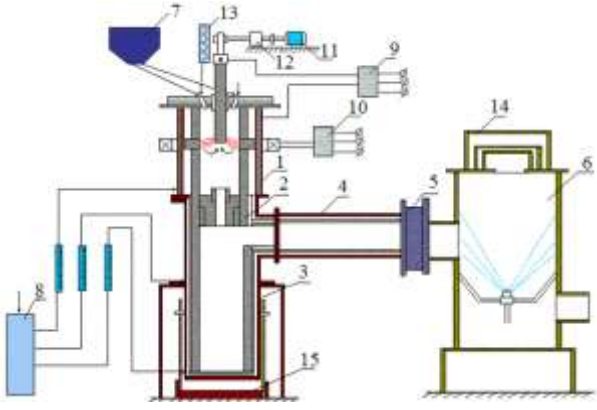

Figure 1. Layout of experimental installation for the plasmochemical processing of fuel: 1 – plasmochemical reactor; 2 – an orifice and a chamber for gas and slag separation; 3 – a slag catcher; 4 – chamber for oxidation; 5 – an orifice; 6 – scrubber; 7 – solid fuel feeding; 8 – water-cooling system; 9, 10 – power-supply system; 11, 12 – rode electrode mobility system; 13 – steam generator; 14 – safety valve; 15 –the slag catcher lift

Plasma ignition of coal is based on plasmochemical preparation of fuels for combustion, which results in the formation highly reactive two-component fuel (fuel gas and coke residue) from low-rank coal. Highly reactive two-component fuel (HTF) is formed already at T = 900-1200 K, which allows the process at relatively low specific power consumption (0.05-0.4 kWh/kg of coal) and leverage at TPP for oil-free boiler start-up and pulverized flame stabilization [3, 5 - 7]. In the framework of this concept some portion of pulverized solid fuel (PF) is separated from the main PF flow and undergone the activation by arc plasma in a special chamber with plasmatron – PFS (Figs. 2 and 3, stage (1). The air plasma flame is a source of heat and additional oxidation, it provides a high-temperature medium enriched with radicals, where the fuel mixture is heated, volatile components of coal are extracted, and carbon is partially gasified. This active blended fuel can ignite the main PF flow (Fig. 3, stage (2) supplied into the furnace. This technology provides boiler start-up and stabilization of PF flame and eliminates the necessity for additional highly reactive fuel. Figure 4 demonstrates the process of HTF self-ignition out-of-doors.

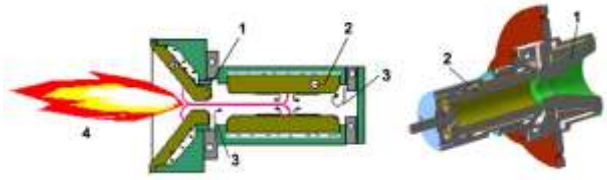

Figure 2. Sketch of the DC plasmatron: (1) anode, (2) cathode; (3) air and (4) plasma flame [7]

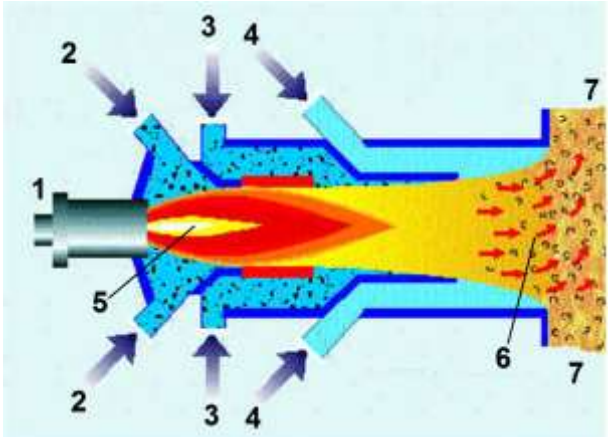

Figure 3. Sketch of the plasma-fuel system (PFS): (1) plasmatron, (2) primary air/coal mixture (stage 1), (3) primary air/coal mixture (stage 2), (4) secondary air, (5) plasma flame, (6) plasma activated pulverised coal flame and (7) furnace [7]

Plasma gasification, radiant-plasma and complex processing of coal to produce synthesis gas and valuable components from MMC were investigated using universal experimental setup (Fig. 1). Their essence is heating of coal dust by the arc plasma, which is oxidant, to complete gasification temperature at which the coal organic matter is transformed into an environmentally friendly fuel - synthesis gas free of ash particles, nitrogen oxides and sulfur oxides. At complex processing of coal simultaneously with gasification of organic matter in the same reaction volume coke carbon restores MMC oxides and valuable components, such as industrial silicon, ferrosilicon, aluminum and carbosilicon and microelements of rare metals: uranium, molybdenum, vanadium, and others, are formed. Material and heat balances-based integral parameters of the process were found. Table 2 shows typical results of plasma-steam gasification of low-rank brown coal of 28 % ash content and 13180 kJ/kg calorific value. Synthesis gas yield was 95.2 %, the degree of carbon gasification - 92.3 % and the degree of coal desulfurization - 95.2 %.

Figure 4. HTF flame (coal consumption is 1 t/h)

Essence of plasma technology for uranium, molybdenum and vanadium oxides from solid fuel is processing of the coal mixture with steam in the plasmochemical reactor 1 (Fig. 1) [6]. The process of uranium, molybdenum and vanadium extracting from coal (shale) using plasma heating is carried out as follows (Fig. 5). Coal dust from the hopper 1 and steam from the boiler 2 in a weight ratio coal - water steam equal to 8-12, enters the plasmochemical reactor 3. In the reactor 3 the steam plasma heats coal dust to the temperature of 2500-2900 K. As coal heating gasification of organic mass of coal is going on forming mainly synthesis gas and sublimation of vanadium, molybdenum and uranium in the form of oxides to the gas phase is taken place. Then the two-phase plasma flow (gas phase + molten slag) enters the chamber for gas and slag separation 4 (Fig. 5), slag goes to the slag catcher 5 and the gas directed to a series of heat exchangers 6, 8, 10 for step cooling and condensation of the separate target products. In the gas phase heat exchanger 6 is cooled to 2300-2400 K at which molybdenum oxides (Mo_nO_m) are condensed and trapped in the receiver 7. From the heat exchanger 6 gas enters the heat exchanger 8, where it is cooled to T = 2000-2200 K at which uranium oxides (U_nO_m) are condensed and trapped in the receiver 9. From the heat exchanger 8, the remaining exhaust gas enters the heat exchanger 10 where its temperature is reduced to T = 1800-1900 K, at which vanadium oxides (V_nO_m) are condensed and separated in the receiver 11. From the heat exchanger 10 the synthesis gas enters the utilization system 12. Table 4 shows the results of experiments on plasma processing of shale containing 0.02% of uranium.

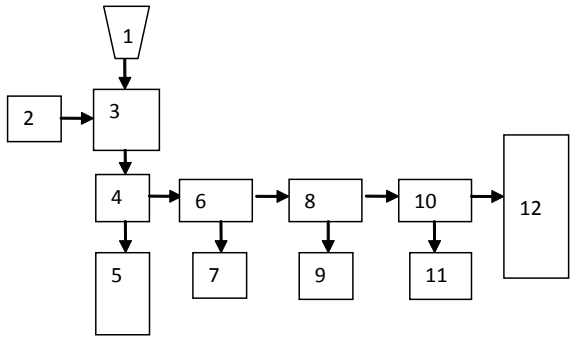

Figure 5. Block diagram of plasma process for uranium, molybdenum and vanadium extracting from coal: 1 – coal dust hopper, 2 – water steam generator, 3 – plasmochemical reactor, 4 – chamber for gas and slag separation, 5 – clag catcher, 6, 8, 10 – heat exchanger, 7, 9, 11 – receiver, 12 – system for exhaust gas utilization

Table 2. Integral parameters of plasma gasification of low-rank brown coal

T, K	Q_{sp}, kW·h/kg	CO	H_2	X_C, %	X_S, %
		Volume %			
3100	5.36	45.8	49.4	92.3	95.2

The degree of reduction of the solid residue samples from different sites of the installation for plasma chemical processing of fuel and from special bath melt around the graphite orifice 2 (Fig. 1) is presented in Table. 3. The table shows that the recovered material is located in the slag and presented in the form of ferrosilicon, silicon carbide and iron. The maximum degree of reduction of the MMC oxides reaches 47% in the slag from the walls of the reactor chamber in the arc zone of the maximum temperatures.

Table 3. Reduction degree (Θ) of MMC.

Site of sampling	T, K	Θ, %
Slag from the bath melt	2600-2800	8.5-44.0
Slag from the walls of the reactor chamber	2600-2900	16.5-47.3
Material from the slag catcher	2000-2200	6.7-8.3

At the radiant-plasma processing coal dust was exposed to pre-activation by an electron beam, and then processed into the plasmochemical reactor 1 (Fig. 1). The experiments were performed in the plasma gasifier of 100 kW nominal capacity. As a result of the measurements of the process material and heat balances

the following integral factors were found: the weight average temperature was 2200-2300 K, and the degree of carbon gasification was 82.4-83.2%. A significant positive effect of the preliminary radiant activation of pulverized coal to the yield of the synthesis gas during its processing was revealed. Synthesis gas yield at thermochemical preparation to burning of untreated coal dust was 24.5% and in the case of radiant activation of the coal synthesis gas yield reached 36.4%, which is 48% higher.

Table 4. Integral parameters of the process of plasma processing of uranium-bearing shale.

No	G_f, kg/h	G_{steam}, kg/h	$\gamma=G_{steam}/G_f$	T_{av}, K	Q_{sp}, kW h/kg	X_U, %	X_{Mo}, %	X_V, %	X_C, %
1	5.82	0	0	2900	2.84	48.0	54.5	58.6	56.2
2	8.40	0	0	2500	1.93	25.7	34.5	41.7	54.6
3	6.60	0.60	0.09	2700	2.20	78.6	79.0	81.3	66.4
4	4.33	0.40	0.09	3150	3.04	23.6	24.3	29.0	70.4

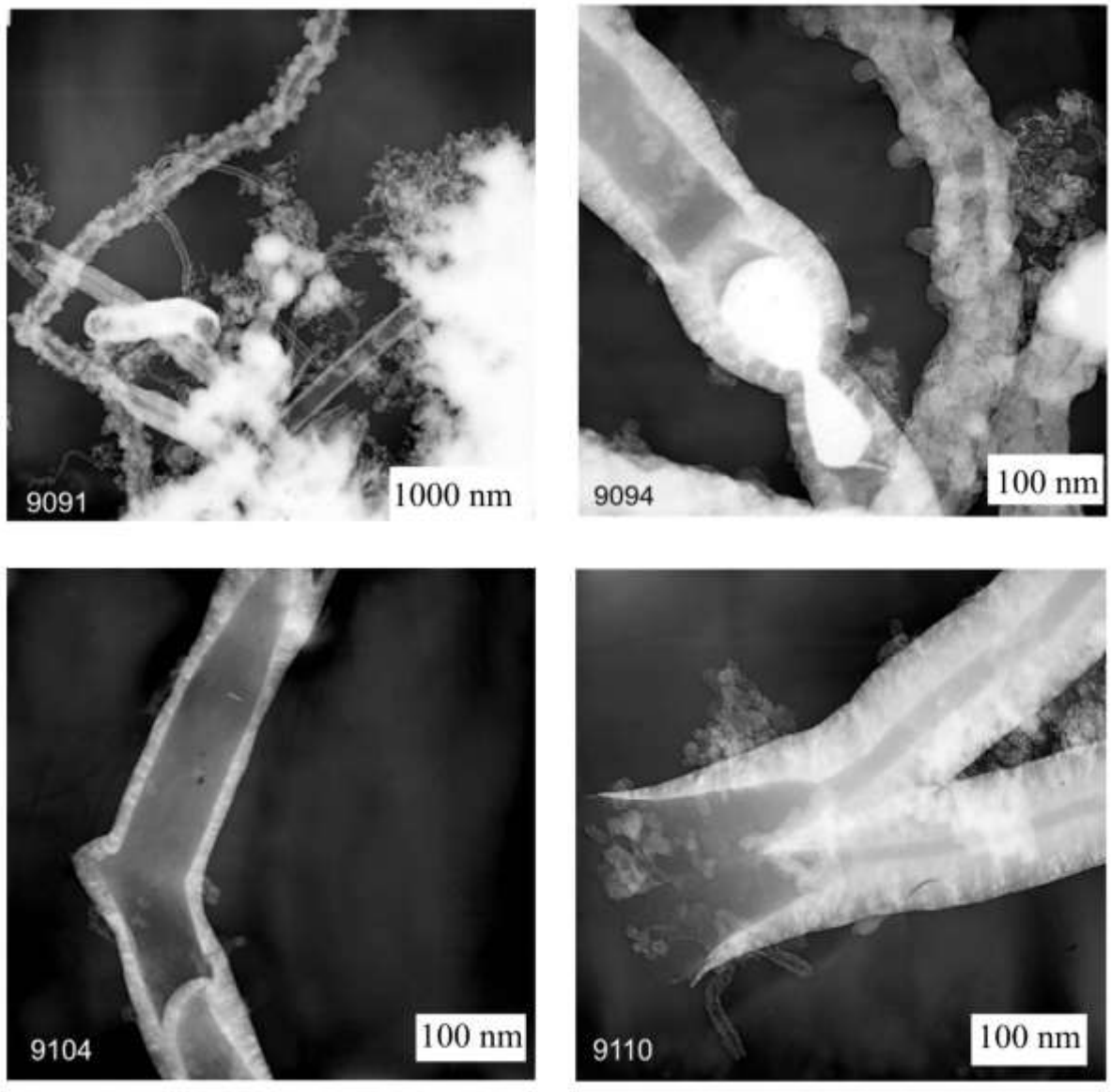

Figure 6. Photographs of carbon nanostructures through TEM [8]

Experiments on plasma pyrolysis (cracking) of propane-butane gas mixture were carried out in the plasmochemical reactor of 100 kW nominal power (Fig. 1). In the experiments propane-butane mixture flow was 300 l/min, and the electric power of the plasmochemical reactor was 60 kW [5]. During the experiments, hydrogen and carbon black were separated in the water-cooled chamber for gas and condensed phase separation 2. Hydrogen was withdrew into the oxidation chamber 4, and carbon landed on the reactor walls, water cooled copper spiral collectors beneath the lid and output orifice of the reactor, as well as slag catcher 3. After completion the experiments sampling from the aforementioned reactor units was carried out. Physico-chemical analysis of the samples of carbon black was performed using transmission electron microscopy (TEM). It showed that propane-butane mixture plasma pyrolysis products from the surface of the graphite electrode of the plasma reactor are different nanocarbon structures, mainly in the form of "colossal" nanotubes (Fig. 6) having high electrical conductivity and mechanical strength 30 times greater than the strength of Kevlar fabric [5]. On the negative 9091 sample is mainly composed of a "hairy" carbon nanotubes with a diameter of about 100 nm and a length greater than 5 microns. On the negative 9094 colossal carbon nanotubes with the inclusion of the teardrop shape metallic phase inside can be seen. Their diameter is 300 nm. Negative 9104 represents a "elbow" carbon nanotube with a diameter of 200 nm or more with an inner partition. Colossal nanotubes can be structures in the form of "octopus" (negative 9110). The diameter of the octopus in its ramifications is about 400 nm. Characteristically, the thickness of colossal nanotubes can range from 30 nm (negative 9104) to 100 nm (negatives 9094 and 9110).

The experimental results confirmed the possibility of producing hydrogen and condensed carbon-containing nanostructures in form of colossal carbon nanotubes. Based on these results, a technical solution for a pilot installation with power of 1 MW and a capacity on the natural gas source 330 Nm^3/h for the implementation of plasmochemical cracking of hydrocarbon gases was developed. The expected yield of the desired product was 74 % of carbon (171 kg/h) and 25 % of hydrogen (58 kg/h).

Table 5 summarizes the results of studies of plasmochemical processing of solid and gaseous fuels. Mass ratios solid fuel / oxidizer vary in the range of 1.3-2.75, ratio carbon / hydrogen reached 10 kg/kg, and the consumption of propane-butane mixture for processing in the plasmochemical reactor of 60 kW power is 18 m^3/h. Weight average temperature of the processes ranged from 800 to 3200 K. Since the plasmochemical preparation of coal for combustion is based on a partial gasification (conversion 15-30%), the temperature (800-1200 K) and the specific power consumption for the process (0.05-0.40 kW h/kg) are reasonable.

Table 5. The optimal ranges of recommended process parameters for plasmochemical processing of fuel.

Fuel / plasma forming gas	T, K	Specific power consumption, kW·h/kg of fuel	Fuel conversion rate, %	Concentration mg/Nm^3	
				NO_x	SO_x
1. Plasmochemical preparation of coal for combustion (air)					
1.5–2.5	800–1200	0.05–0.40	15–30	1–10	1–2
2. Complex processing of coal (water steam)					
1.3–2.75	2200–3100	2–4	90–100	1–2	1
3. Plasma gasification of coal (water steam)					
2.0–2.5	1600–2000	0.5–1.5	90–100	10–20	1–10
4. Radiant-plasma processing of coal (air)					
1.5–2.5	800–1200	0.1–0.45	22–45	1–10	1–2
5. Plasma processing of uranium-bearing solid fuels (water steam)					
8-12	2500-3150	2–4	55-70	1-3	1-2
6. Plasmochemical hydrogenation of coal (hydrogen)					
10	2800–3200	6.5–8	70–100	0	0
7. Plasmochemical cracking of a propane-butane mixture					
18 $м^3/ч$	1500–2500	2.2–3.8	98–100	0	0

At the complex processing of coal conversion of their mineral mass requires high temperatures (2200-3100 K), which leads to an increase in specific power consumption up to 2-4 kW h/kg. This will ensure a high degree of coal conversion (90-100%).

Plasma steam gasification provides mainly organic mass of coal transfer into the gaseous phase. That does not require so high temperature as at the complex processing, and allows the process at relatively low specific power consumption (0.5-1.5 kW h/kg), and achieving a high degree of conversion (90-100%).

Radiant-plasma processing of coal allows increasing the degree of conversion of the initial fuel by 48%.

At plasma processing of uranium-bearing shale, the following indicators have been achieved: at process temperatures 2700 - 2900 K degree of oil shale gasification was 56.2 - 66.4%, the efficiency of microelements transfer into the gas phase reached for uranium - 48.0 - 78.6%, molybdenum - 54.5 - 79.0%, and vanadium - 58.6 - 81.3%. These data are in qualitative agreement with the calculations by the program TERRA [6].

Plasmochemical hydrogenation of coal requires high temperatures (2800-3200 K), which leads to high specific power consumptions for the process (6.5-8 kW h/kg) in order to achieve a high conversion degree (70-100%) in direct (one-step) obtaining of acetylene and alkenes in gaseous phase.

To ensure high conversion degree of hydrocarbon gas (98-100%) in the combined plasmochemical reactor it is not required such a high temperature that enables the process at relatively low specific power consumption (2.2-3.8 kW h/kg).

Note that for all the studied processes of plasmochemical processing of fuels (Table 5) it is typical to have extremely low concentrations of emissions of nitrogen and sulfur oxides not exceeding 20 mg/Nm^3, which is much lower than when traditional fuels use.

REFERENCES

[1] Gorokhovski, M.; Karpenko, E.I.; Lockwood, F.C.; Messerle, V.E.; Trusov, B.G.; Ustimenko, A.B., Plasma technologies for solid fuels: experiment and theory. *Journal of the Energy Institute*. 78 (4), 2005, 157-171.

[2] Zhukov, M.F.; Kalinenko, R.A.; Levitski, A.A.; Polak, L.S., Plasmochemical processing of coal. (in Russian) Moscow: Science. 1990. 200 p.

[3] Messerle, V.E.; Ustimenko, A.B., Plasma ignition and combustion of solid fuel. (Scientific-and-technological basics). (in Russian). Saarbrucken, Germany: Palmarium Academic Publishing (ISBN: 978-3-8473-9845-5), 2012, 404 p. Available: http://ljubljuknigi.ru/

[4] Messerle, V.E.; Ustimenko, A.B., Radiant-plasma technology of coal processing. (in Russian). *KazNU Bulletin. Chemical series.* 4 (68), 2012, 107-113.

[5] Messerle, V.E.; Ustimenko, A.B., Plasmochemical technologies of fuel processing. (in Russian). *Izvestiya Vuzov (Proceedings of High Education). Chemistry and chemical technology*. 55 (4), 2012, 30-34.

[6] Karpenko, E.I.; Messerle, V.E., Plasma-power technologies of fuel utilization. (in Russian). Novosibirsk. V. 1. – Science, Siberian enterprise RAS. 1998, 385 p.

[7] Messerle, V.E.; Karpenko, E.I.; Ustimenko, A.B., Plasma Assisted Power Coal Combustion in the Furnace of Utility Boiler: Numerical Modelling and Full-Scale Test. *Fuel*. 126, 2014, 294-300

[8] Messerle, V.E.; Ustimenko, A.B., Plasma technologies for fuel Conversion. *High Temperature Material Processes*. 16 (2), 2012, 97–107.

ISSN 1847-7917

Enhanced tool condition monitoring by statistical analysis in automatic machining of AISI 1045 steel using sintered carbide inserts

Massimo ROGANTE[1)]***,***
Katica ŠIMUNOVIĆ[2)]
1) Rogante Engineering Office, Contrada San Michele 61, I-62012 Civitanova Marche, **Italy**
2) University of Osijek, Mechanical Engineering Faculty in Slavonski Brod, Trg I. Brlic-Mazuranic 2, HR-35000 Slavonski Brod, **Croatia**
main@roganteengineering.it
ksimun@sfsb.hr

Keywords
AISI 1045 steel
ANOVA
Dry machining
Regression models
Wear

Ključne riječi
AISI 1045 čelik
Analiza varijance
Obrada bez sredstva za hlađenje, ispiranje i podmazivanje
Regresijski modeli
Trošenje

Professional paper

Abstract: Semi-finishing and rough-shaping dry turning processes were performed on automatic lathe, applying three diverse measuring systems to the single point turning situation. Uncoated sintered carbide inserts were used in both processes, while TiC-TiN coated inserts were only used in the rough-shaping processes. The outputs measured were associated with the state and wear rate of the cutting tools.
The behaviour of the useful power output, the tool-holder shank vibrations and the surface roughness vs. pass number were investigated. Wear was assessed by the roughness checks on work pieces in the semi-finishing processes, and by the lathe motor's electrical input together with the vibration level in the rough-shaping processes.
In the present work, the single-factor analysis of variance for the responses - useful power, vibration acceleration and surface roughness - has been performed with the main aim to statistically make conclusions of the cutting speed significance and influence on the above mentioned responses. In addition, the regression models, i.e. the equations for the response variable (useful power and vibration acceleration) dependent on input variable (cutting speed) have been derived.
Finally, a comparison of the responses, respectively for uncoated and coated inserts for the same cutting speeds (125 and 140 m/min), has been carried out by using the hypothesis testing procedure.

Statistički pristup praćenju stanja alata pri obradi čelika AISI 1045 primjenom sinteriranih karbidnih reznih pločica

Stručni članak

Sažetak: U radu su prikazani rezultati istraživanja proces tokarenja (srednje fina i gruba obrada) bez sredstva za hlađenje, mjerenjem korisne snage, vibracija na držaču alata i površinske hrapavosti obratka. Za obje vrste obrade korištene su rezne pločice od tvrdog metala bez prevlake, dok su za grubu obradu korištene i pločice s TiC-TiN prevlakom. Obrada i mjerenje se provodilo u odnosu na istrošenje alata, promjenom brzine rezanja. S ciljem donošenja zaključka o statističkoj značajnosti i utjecaju brzine rezanja na tri odziva - korisnu snagu, vibracije i površinsku hrapavost, provedena je analiza varijance. Dobiveni su i regresijski modeli koji prikazuju ovisnost korisne snage i vibracija o brzini rezanja. Primjenom testiranja hipoteze uspoređeni su odzivi za alate s pločicama sa i bez prevlaka, za brzine rezanja 125 i 140 m/min.

1. Introduction

Assessment of the life of tool inserts is a key issue, though current production techniques are carefully planned. In metal turning, the best situation is typified by regular and uniform tool insert wear. The advancement and the extensive use of hard metal coated tool inserts in the latest years, has also given rise to a considerable growth in the chip volume removed per unit of machining time. A state-of-the-art design related to tool condition monitoring TCM systems is reported in [1]. In particular, automatic TCM systems were applied to computer numerical control (CNC) lathes and other machine tools, where the correlation of cutting power (or force) and wear mark width increase, provides information and warning signals to the operator [2], [3]. This information output, however, is not enough to monitor cutting tool conditions. An analysis of several steels was carried out, to develop a machinability control factor to assist in forecasting the steel machinability by using regular measurements [4].

Symbols/Oznake

R_a	- arithmetic mean surface roughness, µm - srednje aritmetičko odstupanje mjerenog profila, µm	F	- ratio between-treatment and within treatment mean square - omjer srednjeg kvadratnog odstupanja između razina i unutar razine
R_z	- ten points mean roughness, µm - prosječna hrapavost deset izbočina i udubina, µm	R^2	- coefficient of determination - koeficijent determinacije
R_p	- maximum peak height, µm - maksimalna visina vrha profila, µm	P_{us}	- useful power, W - korisna snaga, W
R_{max}	- maximum peak to valley height, µm - maksimalna visina profila, µm	t	- test statistics parameter - vrijednost t varijable
v	- cutting speed, m/min - brzina rezanja, m/min	T	- tool life, min - postojanost alata, min
n	- pass number - broj prolaza		**Subscripts/Indeksi**
VB	- flank medium wear, mm - trošenje stražnje površine alata, mm	t	- traces - tragovi
c	- craterization, mm - dubina kratera, mm	end	- tool life end - istrošenost alata
p	- tip wear, mm - trošenje vrha alata, mm		

Assessment of mechanical vibrations and shocks has confirmed its helpfulness in machining monitoring, as reported by some authors [1]. Measures for monitoring machine tool vibrations are set out in the ISO 13373-1 norm [5]. Single spectrum analysis was adopted to study the vibration signals created in turning processes, with the purpose of obtaining tool wear information. Nevertheless, also this single method is insufficient for applications in TCM. Surface roughness is a major indicator of surface quality on machined parts, and it is the result of a combination of process parameters involving tool geometry, cutting conditions and tool wear [1].

Various works were performed in the past by adopting one measuring system applied to the single point turning situation. Finally, a systematic and comparative investigation on the progressive wear of TNMG220408 and SNMM120408 uncoated and coated inserts in the dry machining of steels using CNC lathes, was carried out [1] in accordance with UNI-ISO 3685 standards [6], by adopting three measuring systems applied to the single point turning situation, i.e. through examining:

- the behaviour of usefully applied power of the lathe d. c. motor
- the tool-holder shank vibration levels
- the surface roughness of the work pieces vs. pass number.

This was done in connection with the progressive wear of these inserts, obtaining better information on tool life assessment and better understanding the tool wear processes. The life of the tool inserts was calculated, and its assessment criteria were defined with each test applied. The frequency ranges were matched to each turning process, and were related to the most relevant vibration amplitude values measured. The arithmetical mean roughness and flank medium wear average values were also calculated [1].

Gradual wear happens at three principal location on a cutting tool. Consequently, three main modes of tool wear exist, i.e. flank wear, crater wear and corner wear.

In the flank wear, the portion of the tool in contact with the finished part erodes, resulting in the gradual wearing away of the cutting edge (see Figure 1).

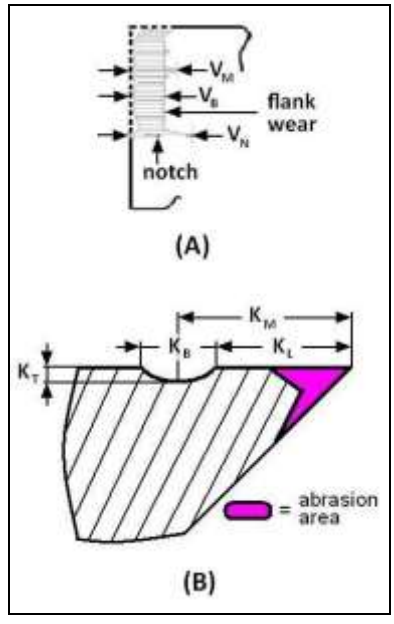

Figure 1. Flank wear (A) and crater wear (B)

Slika 1. Trošenje stražnje površine alata (A) i krater trošenje (B)

It is generally produced by abrasion, caused by hard constituents in the workpiece material, and it is the most preferred form of tool wear, since it offers predictable and stable tool life. V_B is the average value of the flank wear, V_M is the maximum width of the flank wear land in the central portion of the active cutting edge, V_N is the width of the flank wear land at the wear notch [6], [7], [8]. The width of the flank wear was measured by dividing the flank into three zones, i.e.: the curvilinear length connecting the tool tip with the cutting edge; the rectilinear length of the cutting edge (zone in which the measurement was carried out); the fourth part of the length of the cutting edge more far away from the tool tip. The crater wear is the tool wear in which contact with chips erodes the rake face, creating a concave depression in the face of the cutting tool above the cutting edge (see Figure 1). It is due to a chemical reaction between the workpiece material and the cutting tool and is amplified by cutting speed. K_M is the "distance to middle", K_B is the width, K_T is the depth and K_L is the "distance to start".

The Taylor's equation was finally determined for each insert studied. The parameters investigated showed that the results are directly influenced by the degree of the tool wear and also gave indications when the tool insert had reached the end of its life. Coated inserts permit nearly 50% longer machining time, a higher wear mark width and reduced applied power consumption, compared with uncoated inserts. The end of tool life in the semi-finishing processes, when compared to the rough-shaping processes referred to the higher power range used in the latter [1].

In the present work, to statistically make useful conclusions on the cutting speed significance and influence on the above mentioned responses, a single-factor analysis of variance for these responses has been performed. Moreover, the regression models, i.e. the equations for the response variable (useful power and vibration acceleration) dependent on input variable (cutting speed) have been derived. The respective responses for uncoated and coated inserts for the same cutting speeds (125 and 140 m/min) have been compared by adopting the procedure hypothesis testing.

2. The turning processes

The work piece material used was AISI 1045 normalised medium carbon steel. Hot rolled steel bars were used, having a maximum tensile stress of 65 kg/mm^2 and a tested hardness of ~191 HB; the latter value being within in the range of 180-200 HB as prescribed by the UNI-ISO 3685 standards [9]. The corresponding specific cutting force was 300 kg/mm^2. The bar lengths used were 310 mm for the semi-finishing, and 173 mm for the rough-shaping processes.

The initial diameter of the bars was 118 mm, while the minimum diameter of the bars reached during the tests, was fixed at 62 mm.

Tool inserts (Impero, Italy) with and without coating were used in the turning processes. These all had a nose radius of 0.8 mm in accordance with UNI 7736 standards [10]. Tungsten, titanium and tantalum sintered metal carbides were chosen as material components of the inserts used.

The semi-finishing tests were carried out using triangular inserts (ISO designation TNMG220408). The chemical composition of these inserts was (wt %): WC=71; TaC=12; Co=9; TiC=8. The tool holder used in these tests had an ISO designation of PTGNR2525-22. A first series of rough-shaping tests was carried out using square inserts (ISO designation SNMM120408) with the same material composition as the inserts employed in the semi-finishing tests. A second series of rough-shaping tests was carried out using square coated inserts ISO designation SNMM120408. The chemical composition of the body was (wt %): WC=69.5; TaC=12; Co=10.5; TiC=8; and the 3-5 μm thick coating of TiC-TiN was made with a chemical vapour deposition technique. The tool holder used in the rough-shaping tests has ISO designation of PSBNR2525-12. The geometry of the cutting inserts and other characteristics are reported in [1].

In all the tests the cutting depth and feed rate were chosen according to the UNI-ISO 3685 standards [6] and kept constant throughout each test period. The semi-finishing tests were carried out at the following cutting speeds (m/min): 125; 140; 160 and 180. A cutting depth of 2 mm and a feed rate of 0.22 mm/rev. were used. The first series of rough-shaping tests was carried out using the following cutting speeds (m/min): 90; 100; 112; 125 and 140. The second series of rough-shaping tests was carried out using the following cutting speeds (m/min): 125; 140; 160 and 180. For both series of rough-shaping processes, a cutting depth of 2 mm and a feed rate of 0.24 mm/rev were adopted. The following devices and instrumentations were used. A "Tekno3" lathe (Comev, Italy) provided with an "Elcon 5" CNC; a "SL150B" d.c. ammeter (Samar, Italy) and a "2480" d.c. voltmeter (Data Precision, USA) was connected respectively in series and parallel directly to the lathe motor terminals. This measured the required power and eliminated any contributions not directly due to the cutting processes. The following data was measured during the tests [1]:

during the pass:

- the effective power absorbed by the lathe motor
- the machining time by using a high precision chronometer
- the maximum accelerations of the tool-holder shank vibration vs. frequency
- the roughness parameters

at the end of certain passes:

- the flank medium wear and tool nose wear, using a "MK-3829" optical microscopy (PZO, Poland)
- the crater wear, using a dial gauge (Borletti, Italy).

The vibration levels were measured using a Brüel & Kjaer instrument (see the scheme in Figure 2).

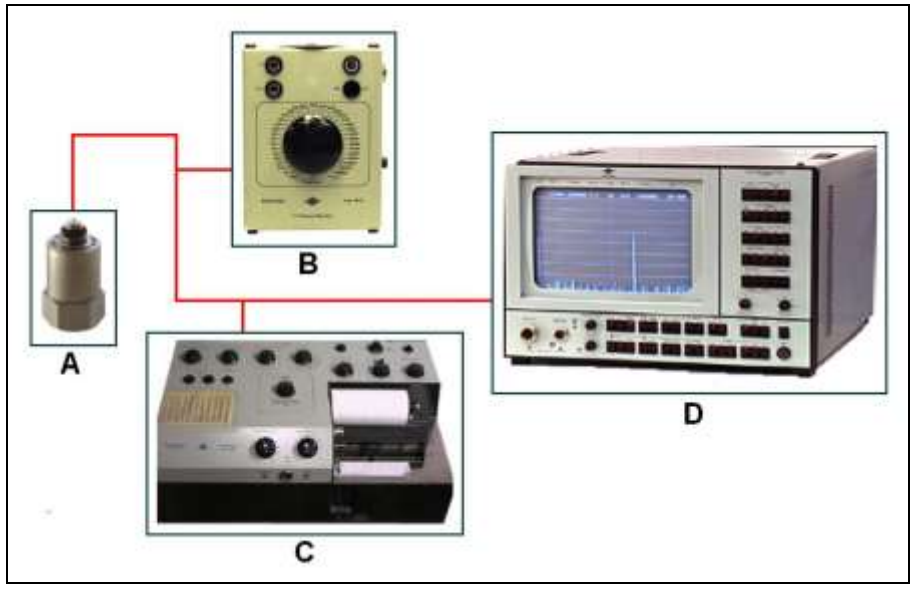

Figure 2. Scheme of the equipment (Brüel & Kjaer, Denmark) used for the vibration measurements: accelerometer (A); filter (B); graphic recorder (C); spectrum analyser (D).

Slika 2. Shema opreme (Brüel & Kjaer, Danska) za mjerenje vibracija: akcelerometar (A); filter (B); grafički snimač (C); analizator spektra (D).

With reference to Fig. 2, the "4384" piezoelectric, DeltaShear®, Unigain® accelerometer with top connector (A) is fixed on the tool-holder shank by a magnetic attachment. The vibration acceleration signal is amplified and documented by the "2307" graphic recorder (C), and examined by the "2031" spectrum analyser (D) using fast Fourier transform algorithms. A "1616" third octave filter set (B) valid for the frequency range 20 Hz – 40 kHz was set up before the signals were input in the analyser (D), to achieve a vibration spectrum in logarithmic scale (dB) for diverse frequency groups - 800; 1,250; 2,000; 3,150; 6,000 and 8,000 Hz - in place of acquiring a sole spectrum for the frequency full range 2,000-14,000 Hz.

Roughness profile R-parameters were computed by using a "Perthometer C5D" profilometer (Perthen, Germany) equipped with an "RT50e" pick-up and a "PPK" drive unit. The following roughness values were determined: arithmetic mean surface roughness R_a; ten points mean roughness R_z; maximum peak height R_p and maximum peak to valley height R_{max} [1].

In [1] the following results are reported and discussed:

- utilised power vs. pass number at different cutting speeds in the various tests.
- vibration accelerations of the tool-holder.
- the vibration accelerations vs. pass number at the different cutting speeds.
- the maximum amplitude of vibrations vs. pass number.
- R_a vs. pass number at the different cutting speeds.
- the average values of R_a.
- the average values of the flank medium wear.
- the monitoring parameters of the tool insert's condition during some passes of each turning process, together with data concerning the insert's end of life.
- the Taylor equations determined.

Table 1 [1] reports the monitoring parameters and life end data of the tool insert's used.

Table 1. Monitoring parameters and life end data of the tool inserts used [1]

Tablica 1. Parametri praćenja trošenja reznih pločica i podaci vezani za istrošenje [1]

Process-*v*	*n*	*VB*	*c*	*p*-	R_a	P_{us}	n_{end}	*T*
SF-125	6	0.15	c_t		3.3	2,470.91		
	9	0.20	c_t	0.1	3.2	2,519.68	9	25.37
SF-140	3	0.05			2.8	2,409.91		
	6	0.10			3.2	2,689.93		
	8				4.2	2,811.28	8	23.27
	10	0.25			5.5	2,989.08		

Extension of Table 1. Monitoring parameters and life end data of the tool insert's used [1]

Nastavak Tablica 1. Parametri praćenja trošenja reznih pločica i podaci vezani za istrošenje [1]

SF-160	5	0.10	c_t		2.5	3,078.64		
	8				3.3	3,301.51	8	21.47
	10	0.15			4.7	3,507.62		
SF-180	4	0.20	0.05		3.0	3,665.95		
	5				3.5	3,852.71	5	11.21
RS_{nc}-90	15	0.25				1,967.26		
	18	0.30	0.10	0.20		2,125.29	18	42.95
RS_{nc}-100	6	0.15			3.2	2,032.99		
	10	0.20		0.10	3.4	2,118.39		
	14	0.25		0.15	3.8	2,172.37		
	18	0.35		0.20	4.3	2,179.26		
	19	0.35	0.06			2,197.64	19	39.03
	21	0.40	0.07	0.30	4.3	2,475.60		
	23	0.40	0.10		4.1	2,804.02		
RS_{nc}-112	5	0.15	0.05	0.10	3.5	2,324.61		
	10	0.30		0.15	3.4	2,501.47		
	14	0.35		0.20	3.4	2,780.04		
	16	0.40	0.08		4.1	2,736.17	16	31.55
RS_{nc}-125	4	0.10	c_t		3.2	2,663.31		
	10	0.25	0.06	0.15	3.6	2,840.18		
	16	0.40		0.20	3.9	2,914.90		
	18	0.40	0.07	0.25	4.0	3,031.53	18	30.49
RS_{nc}-140	6	0.20	c_t	0.10	3.3	3,109.68		
	12	0.35	c_t	0.25	3.6	3,373.74		
	17	0.50	0.09	0.35	3.6	3,488.08	17	26.19
RS_c-125	7	0.05			3.1	2,163.00		
	13	0.20		0.10	4.4	2,478.80		
	20	0.30	c_t	0.20	5.7	2,474.63		
	26	0.40	c_t	0.25	6.3	2,617.36		
	29	0.50	0.03	0.30	6.3	2,896.44	29	48.34
RS_c-140	7	0.10		0.05	2.5	2,654.99		
	13	0.10		0.05	2.8	3,054.53		
	19	0.15		0.10	2.9	2,672.97		
	25	0.20		0.15	3.7	3,029.99		
	30	0.25	c_t		4.6	2,876.85	30	46.67
	31	0.25		0.20	4.6	3,010.13		
RS_c-160	8	0.15		0.05	2.0	3,422.70		
	14	0.25	c_t	0.10	3.3	3,426.66		
	20	0.30	c_t	0.15	5.7	4,006.07		
	23	0.40	c_t	0.30	6.4	4,174.25	23	32.92
RS_c-180	8	0.15		0.05	2.8	3,831.64		
	14	0.20		0.10	4.3	3,820.19		
	20	0.25	c_t	0.20	4.1	3,877.90		
	22	0.25	c_t		4.1	3,954.56	22	27.54

Notes. SF=semi-finishing test; RS_{nc}=rough-shaping test (uncoated inserts); RS_c=rough-shaping test (coated inserts). All values have been measured at the end of the referred machining pass.

3. Statistical analysis of the experimental data and discussion

After performing the experiments in the present work statistical methods have been used to analyse the obtained data. Statistical analysis of the measured responses has been performed by the use of the following licensed software: Design Expert [11], MS Excel [12] and MATLAB [13]. The single-factor analysis of variance is summarized in Table 2.

Table 2. Single-factor analysis of variance (factor: cutting speed)
Tablica 2. Analiza varijance s jednim promjenjivim faktorom (brzina rezanja)

Response	Type of machining	ANOVA parameters		Conclusion on factor	Regression model Coefficient of determination, R^2
		F (P-Value)	F_{crit}		
useful power	Semi-finishing *(Fig. 3 of [1])*	26.48 ($4.2*10^{-9}$)	2.87	significant	*Power*=18.5**cutting speed*+212.6 R^2 = 0.68 or *Power*=19.9**cutting speed*-13.99 R^2 = 0.77 (without the data for 11th machining pass of cutting speed 125 m/min)
	Rough-shaping Uncoated inserts *(Fig. 4 of [1])*	127.53 ($7.1*10^{-37}$)	2.47	significant	*Power*=27.7**cutting speed*-621.52 R^2 = 0.84
	Rough-shaping Coated inserts *(Fig. 5 of [1])*	178.3 ($2.01*10^{-40}$)	2.69	significant	*Power*=24.5**cutting speed*-577.03 R^2=0.81 or *Power*=-1324.5**cutting speed*+9.1 **cutting speed*^{2}-0.02**cutting speed*^{3}+65467.1 R^2=0.84
vibration acceleration	Rough-shaping Uncoated inserts *(Fig. 7 of [1])*	42.4 ($1.88*10^{-17}$)	2.51	significant	*Acceleration*=0.32**cutting speed* - 24.4 R^2=0.71
surface roughness	Semi-finishing *(Fig. 11 of [1])*	1.22 (0.33)	3.02	nonsignificant	-
	Rough-shaping Uncoated inserts *(Fig. 12 of [1])*	0.65 (0.59)	3.16	nonsignificant	-
	Rough-shaping Coated inserts *(Fig. 13 of [1])*	1.384 (0.277)	3.12	nonsignificant	-

The test statistic F (the ratio between-treatment mean square and within-treatment or error mean square) is larger than the critical F value (probability of the type I error, α = 0.05). Thus we reject null hypothesis and conclude that the treatment means differ; that is, the cutting speed setting significantly affects the mean useful power and mean vibration acceleration. Obviously, P-values are very small in those cases. The opposite is true for the surface roughness. Since the F ratio is smaller than critical F value, the null hypothesis has to be accepted, i.e. conclusion can be drawn that the cutting speed is no significant factor. This means that by changing the levels of cutting speed, the surface roughness means don't differ.

The results of the performed experiments are also presented in terms of the linear regression models (last column of Table 2), i.e. empirical models which are derived from the experimental data with the main aim to show the relationship between the responses (useful power and vibration acceleration, respectively) and input variable (cutting speed). These empirical models can be used to predict useful power and vibration acceleration at cutting speed settings within the region of experimentation. For all the models, coefficients of determination R^2 have been calculated. The quantity R^2 presents a portion of explained variability in total variability [14]. As can be seen from the last column of Table 2, a better semi-finishing model for useful power (with larger R^2 of 0.77 instead of 0.68) is obtained when the data for the 11th machining pass of cutting speed of 125 m/min was excluded (it seems to be outlier, see Figure 3).

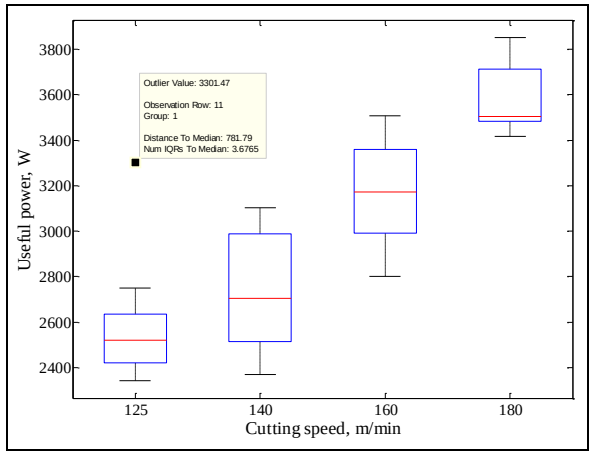

Figure 3. Comparative box plot (semi-finishing)
Slika 3. Box dijagram za četiri brzine (srednje fina obrada)

Regression models diagnostics have also been performed. For the sake of brevity, not all of the graphical presentations are shown. From the normal probability plot of internally studentized residuals (Figure 4) it can be seen that the residuals are approximately normally distributed because the plot resembles a straight line (useful power, rough-shaping, uncoated inserts).

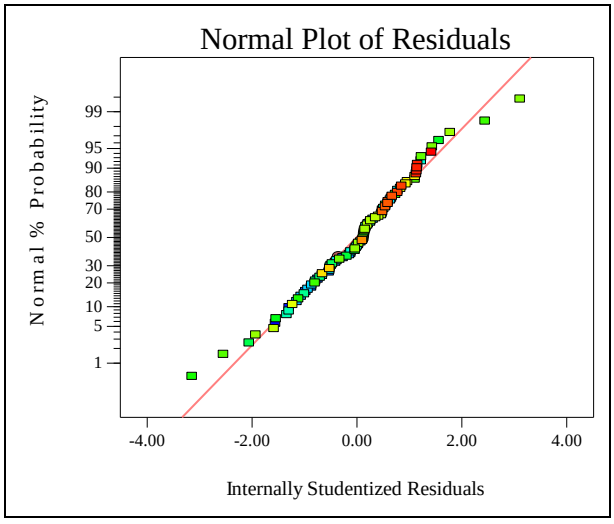

Figure 4. Normal probability plot of internally studentized residuals (useful power, rough-shaping, uncoated inserts)

Slika 4. Normalizirani papir vjerojatnosti ostataka (korisna snaga, gruba obrada, pločice bez prevlake)

The same is valid for other cases. The internally studentized residual is the transformed residual; that is, the residual divided by the estimated standard deviation of the residual. The same is true for the rough-shaping with coated inserts, where an improvement is obtained by adding a quadratic and even a cubic term to the model for useful power. Taking into account that we want to fit the lowest order polynomial that adequately describes the data [14], the linear model is also very satisfactory.

The empirical models relating the surface roughness to the cutting speed haven't been developed since there is no correlation between these two variables.

A cubic regression model, with a little bit higher coefficient of determination (0.84) than for the linear model (0.81) is shown in Figure 5 for the rough-shaping with coated inserts.

The plot of internally studentized residuals versus time order of data collection is presented in Figure 6 (vibration acceleration, rough-shaping, uncoated inserts). An approximately constant variance without change over time can be noticed; that is, the independence assumption on the errors has been proven.

Furthermore, a statistical inference procedure called hypothesis testing is used to compare the useful power as well as surface roughness of two different tools: with uncoated and coated inserts (for the same cutting speeds), see Table 3.

It should be noted that the procedure analysis of variance could also be applied (with a categorical single factor. The type of inserts varied over two levels – uncoated and coated).

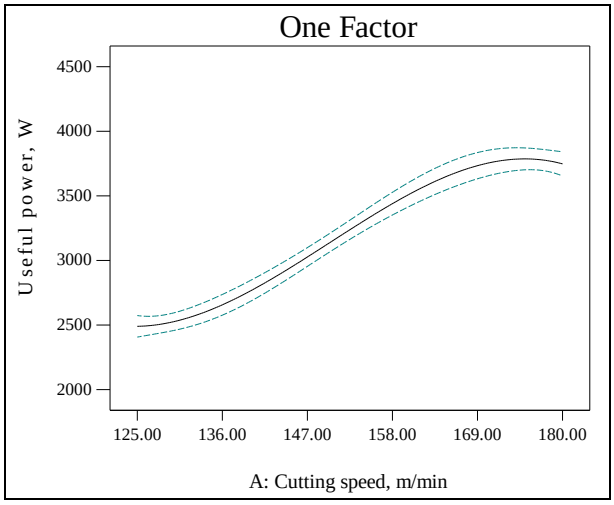

Figure 5. Cubic regression model graph (rough-shaping, coated inserts)

Slika 5. Kubični regresijski model (gruba obrada, pločice s prevlakom)

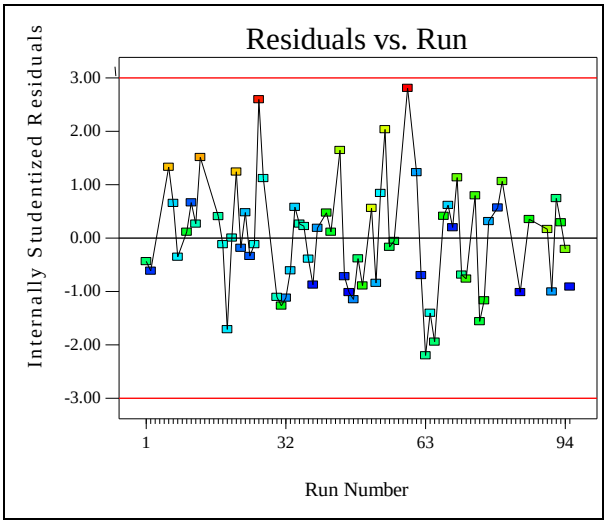

Figure 6. Plot of residuals versus run number (vibration acceleration; rough-shaping; uncoated inserts)

Slika 6. Dijagram ostaci – redoslijed izvođenja pokusa (vibracije; gruba obrada; pločice bez prevlake)

It is evident from Table 3 that there is a significant difference between the mean useful powers of the machining with uncoated and coated inserts for both cutting speeds. The test statistic *t* lies within the critical region. Therefore, the alternative hypothesis is accepted, i.e. the null hypothesis is rejected. The *F* test to compare variability in the data is used prior to the *t*-test. On the basis of the results of the *F* test, two-sample *t*-test

assuming equal variances is applied for a cutting speed of 125 m/min, and contrary two-sample *t*-test assuming unequal variances for a cutting speed of 140 m/min.
There is no significant difference between the mean surface roughness of the machining with uncoated and coated inserts for both cutting speeds. The test statistic *t* lies out of the critical region; therefore, the null hypothesis is accepted.

Table 3. Hypothesis testing – two-sample t-test
Tablica 3. Testiranje hipoteze – t-test za dva uzorka

Response	Inserts	Cutting speed m/min	*t*-test parameters	
			t (probability of *t*)	t_{crit}
useful power	uncoated	125	6.57 (3.62×10^{-8})	±2.01
	coated			
	uncoated	140	6.14 (1.44×10^{-6})	±2.05
	coated			
surface roughness	uncoated	125	0.39 (0.7)	±2.28
	coated			
	uncoated	140	-0.83 (0.45)	±2.77
	coated			

4. Conclusions

A systematic and comparative investigation on the progressive wear of TNMG220408 and SNMM120408 uncoated and coated inserts was carried out, examining the behaviour of usefully applied power, tool-holder shank vibrations and surface roughness vs. pass number, in connection with the progressive wear of these inserts. The inserts' life was calculated, and its assessment criteria were defined with each test applied. The frequency ranges, were matched to each turning process, and the arithmetical mean roughness and flank medium wear average values, were evaluated. The Taylor equation was also determined for each insert studied.
The procedure for the analysis of variance, hypothesis testing and regression analysis have been performed, thus completing the achieved information and demonstrating such to be very helpful in processing and analysing experimental data. By the use of statistical techniques, a decision making process is simpler and easier and thus more objective. Graphical presentations, very frequently adopted in processing and analysing experimental data can also be very useful.
The simultaneous adoption of the three different complementary measuring systems can finally be considered by the related industry to determine objective and definitive criteria for the life assessment of tool inserts.

REFERENCES

[1] Rogante M., (2009), *Wear characterisation and tool performance of sintered carbide inserts during automatic machining of AISI 1045 steel*, Journal of Materials Processing Technology 209 No. 10, p 4776-4783, Netherlands

[2] Sandwik Automation GmbH, (1992), *Plate sensor with integrated pre-amplifier for tool monitoring using strain gauge technology*, Press Release, Viernheim, Germany

[3] Sandwik Automation GmbH, (1992), *Modular sensor system for tool monitoring*, Press Release, Viernheim, Germany

[4] Paravicini Bagliani, E., (2005), *Development of an indicator for machinability rating of steel tubular products for mechanical applications*, La metallurgia italiana No. 11-12, p 47-52, Italy

[5] ISO norm 13373-1, (2002), *Condition monitoring and diagnostics of machines -Vibration condition monitoring*, Part 1: General procedures, p 51

[6] Boothroyd G., Knight W.A., (2006), *Fundamentals of Metal Machining and Machine Tools*, Third Edition, CRC Press Taylor & Francis, Boca Raton, FL, USA

[7] Luo X., Cheng K., Holt R., Liu X., (2005), *Modeling flank wear of carbide tool insert in metal cutting*, Wear 259, p 1235–1240, Netherlands

[8] Malakooti B., Deviprasad J., (1989), *An Interactive Multiple Criteria Approach for Parameter Selection in Metal Cutting*, Operations Research 37 No. 5, p 805-818, USA

[9] UNI-ISO norm 3685, (1981), *Tool-Life Testing with Single-Point Turning Tools*, UNI - Italian Organization for Standardization

[10] UNI norm 7736, (1977), *Inserti a più taglienti per utensili da taglio: codici di identificazione*, UNI - Italian Organization for Standardization

[11] Design Expert, version DX8, 8.0.7.1, Stat-Ease, Inc. Minneapolis, (2010)

[12] Microsoft Excel, version 2010, Microsoft, (2010)

[13] MATLAB, version 7.8.0.347 (R2009a), The MathWorks, (2009)

[14] Montgomery D. C., (2009), *Design and Analysis of Experiments*, Seventh Edition, John Wiley and Sons Inc, Hoboken, NJ, USA

ISSN 1847-7917

Višekriterijski pristup klasifikaciji zaliha u malom poduzeću

***Katica ŠIMUNOVIĆ*[1)], *Lidija VINKOVIĆ*[2)] , *Goran ŠIMUNOVIĆ*[1)] *Tomislav ŠARIĆ*[1)] *and Sara HAVRLIŠAN*[1)]**

1) University of Osijek, Mechanical Engineering Faculty in Slavonski Brod, Trg I. Brlic-Mazuranic 2, 35000 Slavonski Brod, **Croatia**
Sveučilište u Osijeku, Strojarski fakultet u Slavonskom Brodu, Trg I. Brlić-Mažuranić 2, 35000 Slavonski Brod, **Hrvatska**
2) Optics Wachtler, Petra Krešimira IV 39, 35000 Slavonski Brod, **Croatia**
Optika Wachtler, Petra Krešimira IV 39, 35000 Slavonski Brod, **Hrvatska**

katica.simunovic@sfsb.hr
lidijavinkov@gmail.com
goran.simunovic@sfsb.hr
tomislav.saric@sfsb.hr
sara.havrlisan@sfsb.hr

Keywords

ABC inventory classification
AHP methodology
Multi-criteria approach

Ključne riječi

ABC klasifikacija zaliha
AHP metodologija
Višekriterijski pristup

Original scientific paper

Sažetak: S ciljem učinkovitog upravljanja zalihama u malom poduzeću, predložena je višekriterijska klasifikacija zaliha te kriteriji. Predloženi kriteriji pored troška zaliha su bili potražnja, kvaliteta te kao četvrti kriterij - dobavljač. Na temelju predloženih kriterija, te višekriterijske klasifikacije zaliha primjenom metodologije analitički hijerarhijski proces (AHP) i aditivne metode, dokazano je da primjena samo jednoga kriterija - trošak zalihe (prema tradicionalnoj jednokriterijskoj ABC klasifikaciji), daje manje pouzdanu klasifikaciju, a da se višekriterijskim pristupom može donijeti pouzdanija odluka. Rezultati dobiveni jednokriterijskom i višekriterijskom klasifikacijom zaliha su uspoređeni te su doneseni zaključci o utjecaju težine pojedinoga kriterija.

Multi-criteria approach to the inventory classification in small enterprise

Izvorni znanstveni rad

Abstract: With the main aim of efficient inventory control in small enterprise, multi-criteria inventory classification and criteria have been proposed. Apart from the stock keeping units price, another proposed criteria were demand, quality and the fourth criterion - supplier. Based on the proposed criteria and multi-criteria inventory classification using the methodology of analytic hierarchy process (AHP) and additive method, it has been proven that the use of only one criterion, that is the stock keeping units price (according to the traditional one-criterion ABC classification) provide a less reliable classification. Just the opposite, by the multi-criteria approach, more reliable decisions can be made. Traditional and multi-criteria approaches have been compared and the conclusions were adopted on the impact of weight of each criterion.

1. Uvod

Zbog velike količine zaliha u većini poduzeća, velika se pažnja posvećuje klasifikaciji zaliha u različite klase ili skupine te se za različite skupine primjenjuju i različite vrste menadžerskih alata i načina upravljanja i praćenja.
ABC analiza je analitička metoda klasifikacije predmeta poslovanja (materijala, poluproizvoda i gotovih proizvoda) u skupine od kojih se svaka u odnosu prema cjelini odlikuje različitim, nejednakim značenjem za poslovanje, prema kojem se određuje i njihov tretman. ABC analiza se zasniva na poznatom "Paretovom pravilu" ili kako se još naziva pravilo 80:20. Pareto analiza dobila je naziv po talijanskom ekonomistu Vilfredu Paretu, koji je krajem 19. stoljeća postavio tvrdnju kako je samo relativno malo faktora od presudnog značenja za veliki postotak od ukupnih uzroka (reklamacija, defekata, problema itd.) kao i suprotno (tj. kritičnih nekoliko, a trivijalnih mnogo). Prema Pareto principu, svi događaji ili uzroci neke pojave nisu sa stajališta utjecaja jednakomjerno raspoređeni, već relativno malo uzroka tvori većinu utjecaja [1]. Ideja je da se klasificiraju slučajevi prema stupnju važnosti (udjelu), kako bi se potom usmjerilo na rješavanje najvažnijih, ne ulazeći pri tome u manje važne. ABC klasifikacija se provodi svrstavanjem predmeta poslovanja u tri skupine, A, B i C, primjenom kriterija koji karakteriziraju njihovo poslovno značenje. ABC klasifikacija zaliha, prema visini ulaganja sve zalihe klasificira u tri skupine:

- Skupina A – obuhvaća zalihe koje zahtijevaju najveća ulaganja i koje obično imaju visoku cijenu po jedinici i nizak koeficijent obrta. Količinski čine 10-20 % od ukupnih zaliha, a vrijednosno čine 80-90 % od ukupnih zaliha.
- Skupina B – obuhvaća zalihe koje imaju nižu cijenu po jedinici i viši koeficijent obrta od zaliha iz skupine A. Količinski čine oko 30 % od ukupnih zaliha, a vrijednosno oko 15 % od ukupnih zaliha.
- Skupina C – obuhvaća preostale zalihe koje zahtijevaju najmanja ulaganja. Ove zalihe količinski obično čine 50 % od ukupnih zaliha, a vrijednosno samo oko 5-10 % od ukupnih zaliha. Navedene granice nisu strogo određene.

Vrlo često, samo jedan kriterij nije dovoljan za učinkovitu odluku, odnosno klasifikaciju.

Symbols/Oznake

AHP	- Analitički hijerarhijski proces - Analytical hierarchy process	*K4*	- kriterij 4 - criterion 4
CI	- indeks konzistencije - consistency index	*n*	- broj kriterija - number of criteria
CR	- omjer konzistencije - consistency ratio	*RI*	- slučajni indeks - random index
K1	- kriterij 1 - criterion 1	SV_{ij}	- skalirana vrijednost za *j-ti* kriterij za *i-tu* alternativu - scaled value for the *j-th* criterion of the *i-th* alternative
K2	- kriterij 2 - criterion 2	V_{ri}	- ukupna vrijednost za *i-tu* alternativu - total value for the *i-th* alternative
K3	- kriterij 3 - criterion 3	w_j	- težina kriterija - criterion weight

Stoga, se metode višekriterijskog odlučivanja koriste u svim područjima ljudskih aktivnosti te tako i u području upravljanja zalihama [2-6]. Međutim, važno pitanje kojim se bave istraživači, je određivanje težina kriterija koje često podliježe subjektivnom pristupu (bez obzira što postoje metode kojima se subjektivnost želi maksimalno potisnuti). Rješavanjem problema subjektivnosti prilikom određivanja težina kriterija bavili su se autori [2] koji su predložili uključivanje referentnih jedinica u svaku klasu (u referentne jedinice uključene su preferencije donositelja odluke). Također, nije moguće definirati neke jedinstvene, odnosno univerzalne kriterije, jer oni ovise o pojedinom polju djelovanja ili čak i pojedinom poduzeću. U radu [6], pokazano je da se za poduzeće koje se bavi montažom gotovog proizvoda pojavljuju specifični kriteriji kod klasifikacije zaliha, a to su faktor kritičnosti (koliko o tome dijelu ovisi daljnji proces montaže) i vrijeme isporuke kada se radi o novom proizvodu-prototipu i uobičajeno vrijeme isporuke za već razvijen proizvod. Isto tako, i pri izboru dobavljača za ovakvo poduzeće, osim tradicionalnih kriterija (rok isporuke, cijena i paritet), autori [7] su predložili kriterij odgodu plaćanja, specifičan za područje Hrvatske, kao i kriterij pakiranje (jako važan zbog potrebe da se dijelovi namijenjeni montaži ne oštete).

Mnogi autori su pri višekriterijskom pristupu klasifikaciji zaliha primijenili metodologiju analitički hijerarhijski proces (AHP) [6-8]. AHP pristup utemeljio je 1980. godine Thomas Saaty [9, 10]. AHP metodologija omogućuje interaktivno strukturiranje (oblikovanje hijerarhije) problema kao pripremu scenarija odlučivanja, a zatim ocjenjivanje u parovima elemenata hijerarhije (ciljeva, kriterija i alternativa). Koraci metodologije su sljedeći:

- Razvije se hijerarhijski model problema odlučivanja s ciljem na vrhu, kriterijima i podkriterijima na nižim razinama, te alternativama na dnu modela.
- Iz procjena relativnih važnosti elemenata odgovarajuće razine hijerarhijske strukture problema, izračunaju se lokalne težine kriterija i podkriterija, a na posljednjoj razini prioriteti alternativa na osnovi lokalnih prioriteta. Izračunavanje težine kriterija računa se tako da se formira matrica omjera težina kriterija (Saatyeva skala od 1 do 9), u kojoj se u svakom stupcu i svakom redu nalaze vrijednosti procjena omjera između kriterija. Zatim se izračunaju sume stupaca, te se pomoću njih računa nova, normalizirana matrica, tako da se svaki element prethodne matrice podijeli sa sumom stupca kojem pripada. Težine se zatim izračunavaju kao prosječne vrijednosti pojedinih redova. Ukupni prioritet alternative se računa tako da se zbroje umnošci lokalnih prioriteta alternativa za pojedini kriterij i težina kriterija.
- Provodi se analiza osjetljivosti s ciljem da se vidi u kojoj mjeri se promjene ulaznih podataka odražavaju na ukupne prioritete alternativa.

AHP metodologija u postupka uspoređivanja u parovima, omogućuje praćenje konzistentnosti procjena [9-12]. Pomoću indeksa konzistencije *CI* i slučajnog indeksa *RI* (indeks konzistencije za matricu *n*-tog reda slučajno generiranih usporedbi u parovima), moguće je izračunati omjer konzistencije *CR*. Ako je za matricu usporedbi u parovima (relativnih važnosti), omjer konzistencije manji ili jednak 0,1, tada je procjena relativne važnosti kriterija (ili alternativa) prihvatljiva. Obrnuto, potrebno je otkriti razloge velike nekonzistentnosti procjena (ponovno napraviti usporedbu u parovima).

Na osnovi iskustva i pregleda dosadašnjih istraživanja, korištenjem integriranog pristupa - metodologije analitički hijerarhijski proces i aditivne metode, u radu su, osim uobičajenog kriterija, troška zaliha, predloženi i specifični kriteriji klasifikacije zaliha za malo optičarsko poduzeće te je problem riješen višekriterijski. Za usporedbu, prethodno su zalihe klasificirane prema jednom kriteriju.

2. Jednokriterijska ABC klasifikacija zaliha

U ovom poglavlju je obrađena jednokriterijska ABC analiza zaliha (naočalne leće i dioptrijski okviri) u malom optičarskom poduzeću. Kao kriterij za grupiranje dijelova na osnovi ABC klasifikacije uzeta je vrijednost repromaterijala na zalihi s 01.01.2013. odrađena po inventurnoj listi. Rezultati provedene ABC klasifikacije po jednom kriteriju su prikazani na slici 1.

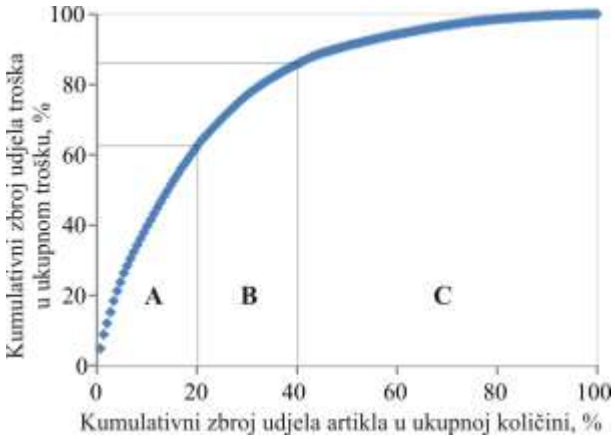

Slika 1. Dijagram ABC klasifikacije zaliha

Figure 1. ABC classification plot

Skupini A pripada 30 od 149 stavki odnosno 20,13 % artikala s najvećim izdvojenim novčanim sredstvima (62,62 % od ukupne vrijednosti). U novčanim sredstvima to je 1137913,87 kn od 1817173,22 kn. Skupina B nosi sljedećih 20,14 % artikala odnosno njezin udio u ukupnim troškovima zaliha iznosi 22,05 % ili 424492 kn. Skupini C pripada 89 od 149 artikala s vrijednošću od 14,02 % ukupnog troška ili 254767,68 kn. U skupini A se nalaze repromaterijali koje je potrebno imati na raspolaganju u kompletnom rasponu dioptrija kada se radi o naočalnim lećama, jer se najviše koriste, gotovo svakodnevno. U praksi nisu problem naočalne leće, jer one nemaju rok trajanja; najveći problem stvaraju dioptrijski okviri koji su podložni modi i trendovima. Dioptrijski okviri zahtijevaju stalnu kontrolu i praćenje. Problem nastaje kada se neki model prestane proizvoditi; tada za njega više nema mogućnosti narudžbe rezervnih dijelova. Iz tog razloga svaka tri mjeseca se prema dobavljačima šalju „lager" liste dioptrijskih okvira iz njihove ponude sa zahtjevom raspoloživosti rezervnih dijelova. U skupini C se nalazi i 40 artikala kojih na zalihi ima 1 ili 2 komada. Uglavnom su to okviri koji se vode kao zaliha, a zapravo su ostavljeni za rezervne dijelove jer su zadnji komadi iz kolekcija koje se više ne rade. Jedan od razloga ponekad prekomjernih zaliha su i ponude dobavljača koji vrlo često rabate i popuste vežu za količinu kupljene robe.

Povećane zalihe nastaju i kao posljedica skupe opreme za proizvodnju. Kada se ulože visoka novčana sredstva (nekoliko desetaka tisuća eura) u novi automat za brušenje naočalnih leća cilj je da se poveća i ubrza proizvodnja, a to je, pored ostalog, moguće većom zalihom repromaterijala.

3. Višekriterijska ABC klasifikacija zaliha – tri i četiri kriterija

Za višekriterijsku klasifikaciju zaliha po AHP modelu, osim kriterija troška zaliha, odabrana su još tri nova kriterija: potražnja, kvaliteta i dobavljač (slika 2). Što se tiče kriterija *potražnja*, on predstavlja potrebe tržišta za određenom vrstom naočalnih leća odnosno dioptrijskih okvira. Dioptrijski okviri su podložni modi i trendovima, ali prije svega se uzima u obzir cijena koštanja tako da se popune svi cjenovni rangovi. *Kvaliteta* je veoma važan kriterij. To znači da cijena koštanja mora biti sukladna kvaliteti proizvoda. U prodaji se nalaze okviri koji su na akciji i njihova cijena koštanja je jedna kuna, to ne znači da je njihova kvaliteta upitna nego su to okviri za koje se ne mogu dobiti originalni zamjenski dijelovi, jer se više ne proizvode. *Dobavljači* se prije svega biraju prema pozadinskoj podršci u smislu prezentacije proizvoda, mogućnosti narudžbe zamjenskih dijelova, reklamacija, a zatim sve druge stavke bitne za suradnju. Kriteriji potražnja, kvaliteta i dobavljač, vrednovani su ocjenama od 1 do 5 prema njihovoj važnosti s tim da je 1 najniža ocjena, a 5 najviša. *Cilj je da se u skupinu A, na koju se mora obratiti pozornost, izdvoje dijelovi s velikom vrijednosti zaliha, malom potražnjom, niskom kvalitetom i lošom komunikacijom s dobavljačem.*

U prvom slučaju promatrana su još dva nova kriterija, potražnja i kvaliteta (uz vrijednost zaliha), a u drugom slučaju, promatran je još jedan kriterij – dobavljač. Uključivanjem ovog zadnjeg kriterija – dobavljač, uz prije navedena tri kriterija, pokušat će se dokazati može li se dodavanjem još jednog kriterija što značajno promijeniti u klasifikaciji zaliha.

Slika 2. Predloženi kriteriji

Figure 2. Suggested criteria

Kako je objašnjeno u poglavlju 1, prema klasičnoj AHP metodologiji uspoređuju se osim kriterija i alternative

svaka sa svakom u odnosu na svaki kriterij. Kod klasifikacije zaliha, alternative se ne mogu uspoređivati zbog njihova velika broja (klasificirat će se 149 jedinica na zalihi). Broj usporedbi svake alternative sa svakom bi iznosio 11026 za svaki kriterij te bi ukupni broj usporedbi bio 44104; stoga se za višekriterijsku klasifikaciju zaliha koristila modificirana AHP metoda. Težine kriterija određene su po Saaty-evoj skali, a zatim je primijenjena aditivna metoda u kojoj su tako dobivene težine kriterija množene sa skaliranim (transformiranim vrijednostima) kriterija (*izraz 3.1, odnosno 3.2*). Kod linearne transformacije, za pozitivno usmjerene kriterije, podatak za *j-ti* kriterij *i-te* alternative se dijeli maksimalnim podatkom u *j-toj* koloni u matrici odluke, *izraz 3.1* [13]. Za pozitivno usmjerene kriterije, veća vrijednost kriterija znači veću važnost. S druge strane, za negativno usmjerene kriterije, manja vrijednost kriterija predstavlja veću važnost. Za negativno usmjerene kriterije, minimalni podatak u *j-toj* koloni u matrici odluke dijeli se s podatkom za *j-ti* kriterij *i-te* alternative, *izraz 3.2* [13]. Zatim se alternative (zalihe) poredaju po ukupnoj vrijednosti za pojedinu alternativu (*izraz 3.3*), od najveće prema najmanjoj vrijednosti.

$$SV_{ij} = \frac{x_{ij}}{\max\limits_{i} x_{ij}} \tag{3.1}$$

$$SV_{ij} = \frac{\min\limits_{i} x_{ij}}{x_{ij}} \tag{3.2}$$

$$V_{ri} = \sum_{j=1}^{n} w_j \cdot SV_{ij} \rightarrow \max. \tag{3.3}$$

gdje su:

V_{ri} - ukupna vrijednost za *i-tu* alternativu (i = 1, …, *m*)

w_j - težinski faktor (težina) za *j-ti* kriterij (j = 1, …, *n*)

SV_{ij} - skalirana vrijednost za *j-ti* kriterij za *i-tu* alternativu

n - broj kriterija.

Da bi se odredile težine kriterija, kriteriji su međusobno uspoređivani u parovima i na osnovi usporedbe prema Saaty-evoj skali, donesena je ocjena u kojoj je mjeri jedan kriterij važniji u odnosu na drugi (tablice 1 i 2). Potom su prema postupku opisanom u poglavlju 1, određene normalizirane tablice (tablice 3 i 4) iz kojih su dobivene težine kriterija. Klasifikacija u skupine A, B i C, je bila na osnovi pravila: prvih 20 % dijelova – skupina A, sljedećih 20 % dijelova - skupina B i ostalih 60 % - skupina C.

Tablica 1. Uspoređivanje tri kriterija u parovima

Table 1. Pair wise comparison of three criteria

	Potražnja K1	Kvaliteta K2	Vrijednost zalihe K3
Potražnja K1	1	2	3
Kvaliteta K2	1/2	1	2
Vrijednost zalihe K3	1/3	1/2	1

Tablica 2. Uspoređivanje četiri kriterija u parovima

Table 2. Pair wise comparison of four criteria

	Potražnja K1	Kvaliteta K2	Vrijednost zalihe K3	Dobavljač K4
Potražnja K1	1	2	3	3
Kvaliteta K2	1/2	1	2	3
Vrijednost zalihe K3	1/3	1/2	1	3
Dobavljač K4	1/3	1/3	1/3	1

Tablica 3. Normalizirana tablica i težine kriterija – tri kriterija

Table 3. Normalized table and criteria weights – three criteria

	Potražnja K1	Kvaliteta K2	Vrijednost zalihe K3	Težina
Potražnja K1	6/11	4/7	1/2	0,5390
Kvaliteta K2	3/11	2/7	1/3	0,2973
Vrijednost zalihe K3	2/11	1/7	1/6	0,1638

Tablica 4. Normalizirana tablica i težine kriterija – četiri kriterija

Table 4. Normalized table and criteria weights – four criteria

	Potražnja K1	Kvaliteta K2	Vrijednost zalihe K3	Dobavljač K4	Težina
Potražnja K1	6/13	12/23	9/19	3/10	0,4392
Kvaliteta K2	3/13	6/23	6/19	3/10	0,2769
Vrijednost zalihe K3	2/13	3/23	3/19	3/10	0,1855
Dobavljač K4	2/13	2/23	1/19	1/10	0,0984

4. Usporedba rezultata

U tablici 5 prikazana je usporedba tradicionalne ABC klasifikacije, te višekriterijske ABC klasifikacije s tri i četiri kriterija. Kriteriji su označeni od K1 do K4, prema tablicama 1, 2, 3 i 4. Uključivanjem četvrtog kriterija (dobavljač) u usporedbi s tri kriterija, samo 16 artikala je promijenilo svoje skupine (podebljana slova u posljednjoj koloni tablice 5).

Tablica 5. Usporedba tradicionalne ABC klasifikacije te višekriterijske s tri i četiri kriterija

Table 5. Comparison of traditional ABC classification and multi-criteria one with three and four criteria

R. br.	Šifra	K1	K2	K3	K4	1 kriterij	3 kriterija	4 kriterija
1	O475	4	4	88825	3	A	C	C
2	O275	4	4	72050	3	A	C	C
3	O982	3	4	58920	4	A	C	C
4	O572	4	4	57772	3	A	C	C
5	RL290	5	5	57710	4	A	C	C
6	RL999.99	1	5	50999,49	4	A	A	A
7	G1 2.00	5	2	46376	1	A	C	C
8	O879	2	4	44829	3	A	C	C
9	O999	1	4	37962	1	A	A	A
10	RL518	5	5	37814	4	A	C	C
11	RL299.99	1	5	35398,82	4	A	A	**B**
12	O1450	1	4	34800	1	A	A	A
13	O698	1	3	33504	1	A	A	A
14	OS300	1	3	32700	1	A	A	A
15	EL699.99	1	5	32199,54	4	A	A	**B**
16	O300	3	3	31500	2	A	C	C
17	O874	2	4	31464	3	A	C	C
18	EL199.99	1	3	30798,46	4	A	A	**B**
19	O676	3	3	29744	3	A	C	C
20	NL75	5	3	29325	2	A	C	C
21	O573	3	3	29223	3	A	C	C
22	O99	1	2	28809	1	A	A	A
23	O149	5	2	28012	1	A	C	C
24	EL399.99	3	4	27599,31	4	A	C	C
25	EL999.99	1	4	26999,73	4	A	A	**B**
26	O1389	2	4	25002	4	A	C	C
27	O926	3	4	25002	2	A	C	C
28	O565	3	4	24860	4	A	C	C
29	RL300	5	5	24000	4	A	C	C
30	O2643	1	5	23787	3	A	B	B
31	O465	4	4	23715	4	B	C	C
32	O249	5	2	19173	1	B	C	C
33	O365	2	4	18980	4	B	C	C
34	O600	2	4	18600	2	B	C	C
35	RL399.99	2	4	18399,54	4	B	C	C
36	O946	3	4	17974	3	B	C	C
37	O40	5	2	17960	1	B	C	C
38	O4490	1	5	17960	1	B	B	**A**
39	OSL290	1	3	16820	1	B	A	A
40	O462	3	4	16632	4	B	C	C
41	O1499	1	4	16489	1	B	B	**A**
42	O339	5	3	16272	3	B	C	C
43	O1246	1	4	16198	3	B	B	B
44	O577	3	3	15579	3	B	C	C
45	EL290	2	4	14790	4	B	C	C
46	O299	1	3	12558	1	B	A	A
47	EL499.99	2	4	12499,75	4	B	C	C
48	M2S	1	3	12446	1	B	A	A
49	O309	1	2	11742	1	B	A	A
50	MMS	1	2	11684	1	B	A	A
51	O674	3	3	10784	3	B	C	C
52	RL699.99	1	4	10499,85	4	B	B	B

Nastavak Tablice 5. Usporedba tradicionalne ABC klasifikacije te višekriterijske s tri i četiri kriterija

Exstension of Table 5. Comparison of traditional ABC classification and multi-criteria one with three and four criteria

R. br.	Šifra	K1	K2	K3	K4	1 kriterij	3 kriterija	4 kriterija
53	O1289	3	4	10312	4	B	C	C
54	G6 2/ 2	5	2	10138	1	B	C	C
55	O1446	2	4	10122	3	B	C	C
56	O3280	1	5	9840	1	B	B	B
57	O400	1	3	9200	2	B	A	**B**
58	O766	3	4	9192	4	B	C	C
59	G1 4.00	2	2	9108	1	B	C	C
60	O2943	1	5	8829	3	B	B	B
61	O1764	1	2	8820	1	C	A	A
62	O1068	2	4	8544	4	C	C	C
63	O199	5	2	7960	1	C	C	C
64	O474	3	3	7584	3	C	C	C
65	G6 2.00	5	2	7480	1	C	C	C
66	G6 4.00	5	2	6882	1	C	C	C
67	O772	3	4	6176	3	C	C	C
68	G6 6.00	3	2	5508	1	C	C	C
69	RL199.99	1	2	5199,74	4	C	A	**B**
70	O4940	1	1	4940	1	C	A	A
71	O352	2	3	4928	2	C	C	C
72	O375	3	4	4875	3	C	C	C
73	RL690	2	4	4830	4	C	C	C
74	G1 2/ 2	5	2	4680	1	C	C	C
75	O566	3	4	4528	4	C	C	C
76	O746	1	4	4476	3	C	B	B
77	O155	1	3	4340	1	C	A	A
78	O846	2	4	4230	3	C	C	C
79	EL300	2	4	4200	4	C	C	C
80	O456	3	3	4104	2	C	C	C
81	O678	3	4	4068	3	C	C	C
82	O451	3	4	4059	2	C	C	C
83	O569	1	4	3983	1	C	B	B
84	O795	2	4	3975	1	C	C	C
85	O990	1	4	3960	1	C	B	B
86	O200	4	2	3800	1	C	C	C
87	O472	3	3	3776	3	C	C	C
88	O910	2	4	3640	1	C	C	C
89	O1199	1	4	3597	1	C	B	B
90	O599	1	5	3594	1	C	B	B
91	O882	3	4	3528	4	C	C	C
92	O688	1	3	3440	2	C	A	**B**
93	EL1713	1	4	3426	4	C	B	B
94	O3340	1	5	3340	1	C	B	B
95	O549	1	3	3294	1	C	A	A
96	G1 6.00	3	2	3168	1	C	C	C
97	O3120	1	3	3120	1	C	A	A
98	O310	2	3	3100	1	C	C	C
99	O3100	1	3	3100	1	C	A	A
100	G6 4/2	5	2	2812	1	C	C	C
101	O2780	1	4	2780	1	C	B	B
102	O1386	3	4	2772	4	C	C	C
103	O682	3	4	2728	4	C	C	C
104	O1346	2	4	2692	3	C	C	C
105	O890	1	4	2670	1	C	B	B
106	O666	3	4	2664	4	C	C	C
107	O2640	1	5	2640	1	C	B	B
108	O2550	1	5	2550	1	C	B	B
109	O349	1	2	2443	3	C	A	**B**
110	RL1200	1	4	2400	4	C	B	B

Nastavak Tablice 5. Usporedba tradicionalne ABC klasifikacije te višekriterijske s tri i četiri kriterija

Exstension of Table 5. Comparison of traditional ABC classification and multi-criteria one with three and four criteria

R. br.	Šifra	K1	K2	K3	K4	1 kriterij	3 kriterija	4 kriterija
111	O790	1	3	2370	1	C	B	**A**
112	O774	3	4	2322	3	C	C	C
113	O558	3	3	2232	2	C	C	C
114	O880	1	4	1760	1	C	B	B
115	O866	3	4	1732	4	C	C	C
116	O1699	1	5	1699	1	C	B	B
117	O820	1	5	1640	1	C	B	B
118	O546	2	4	1638	3	C	C	C
119	O782	3	4	1564	4	C	C	C
120	O1489	3	4	1489	4	C	C	C
121	RL700	2	4	1400	4	C	C	C
122	O1399	1	5	1399	1	C	B	B
123	G1 4/ 4	4	2	1394	1	C	C	C
124	EL683	1	5	1366	4	C	C	C
125	O660	2	4	1320	1	C	C	C
126	O1286	3	4	1286	4	C	C	C
127	O255	4	2	1275	2	C	C	C
128	O1168	2	4	1168	4	C	C	C
129	G1 4/2	4	2	1125	1	C	C	C
130	G1 2/4	4	2	1106	4	C	C	C
131	O1082	3	4	1082	4	C	C	C
132	O1046	2	4	1046	3	C	C	C
133	O930	1	3	930	1	C	B	**A**
134	O449	1	3	898	1	C	B	**A**
135	O447	1	3	894	2	C	B	B
136	O209	1	2	836	2	C	A	A
137	O165	1	3	825	1	C	B	**A**
138	EL345	1	5	690	4	C	C	C
139	O665	2	4	665	1	C	C	C
140	O630	1	2	630	1	C	A	A
141	O198	1	3	594	1	C	B	**A**
142	O259	1	2	518	1	C	A	A
143	RL499.99	1	5	499,99	4	C	C	C
144	O490	1	3	490	1	C	B	**A**
145	O372	3	3	372	3	C	C	C
146	O369	3	3	369	1	C	C	C
147	O279	1	2	279	1	C	A	A
148	O239	1	2	239	1	C	A	A
149	G6 2/4	3	2	146	1	C	C	C

5. Zaključak

Primjenom tradicionalne jednokriterijske te višekriterijske ABC klasifikacije zaliha integriranom AHP i aditivnom metodom, može se zaključiti da klasifikacija zaliha, koja uzima u obzir samo jedan kriterij (trošak zalihe), daje različite rezultate u usporedbi s višekriterijskim pristupom. Kako je s četiri kriterija u usporedbi s tri kriterija, samo 16 dijelova promijenilo svoje skupine, može se zaključiti da uvođenje četvrtog kriterija nije značajno utjecalo na klasifikaciju. Stoga se daljnja analiza temelji na usporedbi jednokriterijske i trikriterijske klasifikacije zaliha. Uvođenjem dva nova kriterija (potražnja i kvaliteta), 83 artikla je promijenilo svoju skupinu, od kojih je 19 dijelova (tamno sivo obojano u tablici 5), prema jednokriterijskoj klasifikaciji zaliha bilo u prvoj skupini, a prema trikriterijskoj se ubrojilo čak u treću skupinu. To su bili repromaterijali s boljim ocjenama kvalitete i odličnom potražnjom (ova dva kriterija imaju veliku težinu), ali s višim troškom zaliha (manja težina toga kriterija). Kako je u ovom poduzeću dana manja težina na troškove, u skupini C koja nam nije zanimljiva, našli su se i relativno skupi repromaterijali.

Međutim potrebno je obratiti pozornost i na dijelove koji su prema jednom kriteriju bili u skupini C, a zatim su se prema klasifikaciji s tri kriterija, pojavili u skupini A (svijetlo sivo obojano u tablici 5). To su bili repromaterijali s malom potražnjom i niskom ocjenom kvalitete i srednjeg troška zaliha (njih 14) na koje bi trebalo obratiti posebnu pozornost, uz preostalih 16 u skupini A.

U svim problemima, potrebno je osim kvantitativnog pristupa, prokomentirati i situaciju u „pozadini". U današnje vrijeme, nije zanemariva činjenica da je recesija na našem području utjecala značajno i na potražnju. Primjer za to je dioptrijski okvir pod rednim brojem 26, prodajne cijene 1389,00 kn s vrijednošću zalihe 25002,00 kn. Okvir je vrlo dobre kvalitete, dobrog dobavljača no međutim potražnja na tržištu mu je dosta niska. Razlog tome je cijena. Kako je recesija zavladala svim segmentima života, tako nije zaobišla ni optiku. Na tržištu se javlja potreba za proizvodima odnosno dioptrijskim naočalama nižeg cjenovnog ranga. Isto tako, niža cijena ne mora značiti lošu kvalitetu. Primjer je dioptrijski okvir pod rednim brojem 63 čija je cijena 199,00 kn. To je okvir koji je na popustu i kod ocjenjivanja kvalitete dobio je ocjenu dva. To nije okvir trenutno loše kvalitete, ali je tako ocijenjen iz razloga što se na popustu nalaze okviri koji su izašli iz kolekcija te dobavljač pa tako i optika za njih nije u mogućnosti osigurati originalne rezervne dijelove. Dakle, i moda može utjecati na ocjene kriterija.

Daljnje istraživanje bi moglo uzeti u obzir sav materijal na zalihi (repromaterijal, pomoćni materijal, potrošni materijal i rezervni dijelovi). Time bi vjerojatno morali biti uključeni još neki kriteriji (na primjer kritičnost). U optici se svakodnevno koriste specijalne naljepnice, kao pomoćni materijal (naravno pored struje i vode), bez kojih se ne mogu izbrusiti leće. Bez obzira što je cijena jedne naljepnice samo 0,46 kn, radi se o važnoj vrsti materijala, jer ako bi zaliha bila nula kompletna proizvodnja bi stala.

Na kraju se može zaključiti da primjena i najsofisticiranije metode ne može uspjeti, ako se u početnoj fazi, ispravno ne odrede kriteriji i težine kriterija, a pri čemu je iskustvo čovjeka koji se bavi područjem u kojem se primjenjuje klasifikacija ili izbor neke alternative, zaista neprocjenjivo.

Zahvala

Autori rada zahvaljuju gospodinu Robertu Wachtleru na ustupljenim podacima o poslovanju poduzeća „Optika Wachtler".

LITERATURA

[1] Kondić, Ž. *Kvaliteta i metode poboljšavanja*. Varaždin; Zrinski, 2004, 545 str.

[2] Soylu, B., Akyol, B. *Multi-criteria inventory classification with reference items*. Computers & Industrial Engineering. 69 (2014), pp. 12-20

[3] Ramanathan, R. *ABC inventory classification with multiple-criteria using weighted linear optimization*. Computers and Operations Research. 33 (2006), pp. 695-700

[4] Ng, W.L. *A simple classifier for multiple criteria ABC analysis*. European Journal of Operational Research. 177 (2007), pp. 344-353

[5] Zhou, P., Fan, L. *A note on multi-criteria ABC inventory classification using weighted linear optimization*. European Journal of Operational Research. 182 (2007), pp. 1488-1491

[6] Šimunović, K., Draganjac, T., Šimunović, G. *Application of different quantitative techniques to inventory classification*. Tehnički vjesnik. 15 (2008), pp. 41-47

[7] Šimunović, K.; Draganjac, T.; Lujić, R. *Supplier selection using a multiple criteria decision making method*. Strojarstvo. 53 (2011), pp. 293-300

[8] Partovi, F.Y., Burton, J. *Using the analytic hierarchy process for ABC analysis*. International Journal of Production and Operations Management. 13 (1993), pp. 29-44

[9] Saaty, T.L. *The analytic hierarchy process*. McGraw Hill, New York, 1980.

[10] Saaty, T.L. *How to make a decision: the analytical hierarchy process*. European Journal of Operational Research. 48 (1990), 1; pp. 9-26

[11] Hunjak, T. *Višekriterijsko odlučivanje AHP metoda*.http://www.foi.hr/CMS_library/studiji/dodiplomski/IS/kolegiji/mzvo/ahp.pdf.

[12] Hunjak, T. *Matematički temelj AHP metode*. http://www.foi.hr/CMS_library/studiji/dodiplomski/IS/kolegiji/mzvo/MatematickiTemelj_AHPMetoda.pdf.

[13] Kalpić, D., Mornar, V. *Operacijska istraživanja*. Zagreb; Zeus, 1996, 261 str.

ISSN 1847-7917

Pump design and Development for High Shear Grout Mixing Applications

John KIJAK [1]***, David KENNEDY*** [2]
1) Department of Mechanical Engineering Dublin Institute of Technology DIT Bolton Street, Dublin 1, **Ireland**
2) Department of Mechanical Engineering Dublin Institute of Technology DIT Bolton Street, Dublin 1, **Ireland**

John.kijak@gmail.com
David.kennedy@dit.ie

Keywords

Grout pump
Impellor pump
Shearing
Vortex mixing

Professional paper

Abstract: The aim of this project was to design and develop a new pump for the mixing and pumping of grout cement. The initial design consisted of a cantilevered supported pump housing containing a centrifugal mill with a series of plate seals, gaskets, flanges and a single tapered bearing. To date, the initial pump has failed as evident from bearing and seal wear. Extensive research of the design features of grout mixing units from various competitors and suppliers was conducted [1]. Based on research undertaken a paddle pump design was developed incorporating dual end support, direct grout feed and improved sealing. Design calculations were used to size the hydraulic motor, the impeller shaft diameter, dynamic loading on bearings and their operational lifetime. The new pump unit, based on testing, delivers a suitable head of pressure for the mixing and shearing of the grout mix, leading to a consistent grout mix product. The performance of the pump was measured both physically and experimentally via the use of an industrial hydraulic power pack, capable of delivering the required power and pressure to enable the pump operate at industrial flow rates. Performance tests consisted of varying the flow rates of the grout material through the pump and measuring pressure head at the outlet. Results of the performance testing indicated that the pump operated to design specifications. The dual bearing system design proved satisfactory, with smooth operation even at higher ranges of industrial flow rates. The mechanical seals, selected for aggressive wear and corrosive environments remained leak proof as required. The new pump design features include a widened pumping impeller for increased shearing of the grout and gives higher volumetric flow rates. This offers advantages to the end user as it is more efficient, robust, maintainability and lest costly to manufacture. Figure 1. shows the assembled unit of the pump, hydraulic motor, holding tank, and the inlet and outlet ducts.

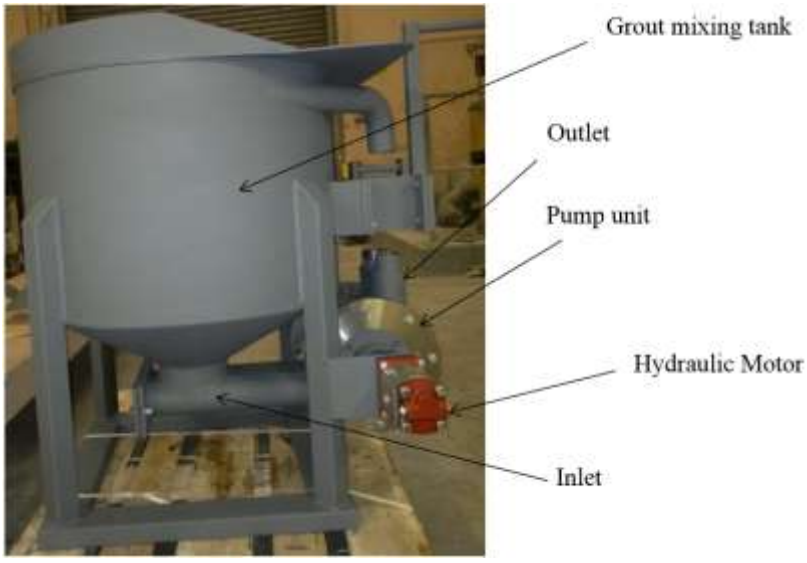

Figure 1. Pump unit with Hydraulic motor and mixing tank

1. Introduction

The main aim of this research was to design and develop a high shear colloidal mixing pump for grout material. Grout is used extensively in the construction industry for fixing foundations, re-setting sunken foundations, repairing culverts, preventing rising damp, and arresting subsoil movement/ landslides on a local basis. The formation of crack systems and voids in the subsoil reduces the load bearing capacity of a building's foundation, which may result in structural instability. Mixing grout involves shearing cement, water, sand and accelerating agents into a fine colloidal suspension. Wetting is necessary for batch quality and pumping involves transferring the slurry mix to the point of use. The technique involves circulating water in a vessel via a pump and adding the correct quantities of cement, sand and agents to produce a consistent paste. A vortex mixing effect is used to assist with the mixing as shown in Figure 2. This is generated by pumping the liquid tangentially into the mixing tank. The mix is then supplied to a second vessel where it is injected under high pressure through a hose and into the location underground or for culvert repairing.

The grout sets to provide structural rigidity and sealing against rising damp. Upon successful grouting, structural integrity is fully restored [2].

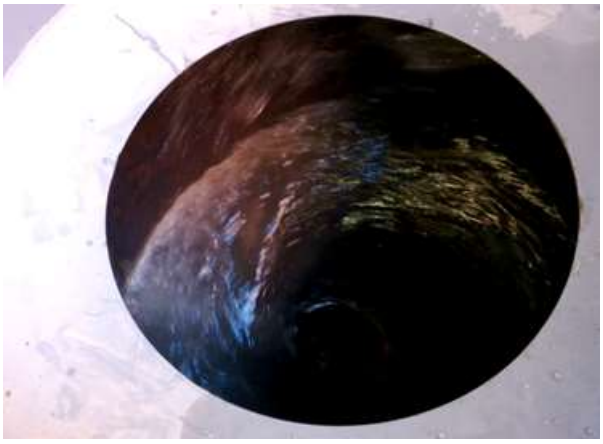

Figure 2. Vortex effect

2. Pump design

The pump was designed based on on-site mixing performance and industry knowledge coupled with faults identified with the existing pump unit and design calculations. The final design had to overcome initial design defects of the original pump and enhance technical capability with regard to performance, reliability, ease of maintenance and manufacturability. The initial pump had failed in terms of bearing performance, poor sealing, and high maintenance and manufacturing costs. The initial pump unit consisted of a modified centrifugal type pump, cantilevered impellor with one supporting bearing. The failed pump is shown in Figure 3. Figure 4. shows the component parts of this pump.

Figure 3. Pump bearing and component parts

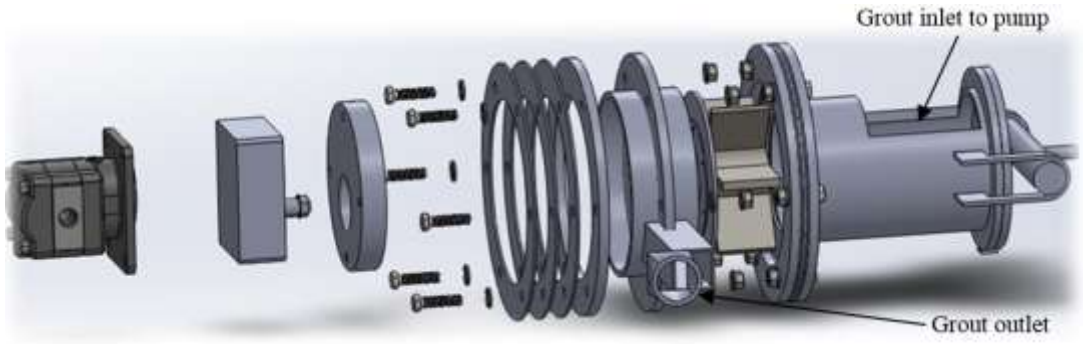

Figure 4. Exploded view of original pump unit

The Figures show the excess parts, seals, flanges and gaskets, supported by the bearing. The impellor is supported as a cantilever by the bearing and the overall pump unit is supported by the base of the mixing tank. The outlet from the pump is considerably smaller than the pump inlet which has the effect of causing back pressure in the pump. The new design overcame this by matching the cross sectional area of the outlet to the inlet. In order to improve the pump design and performance, a number of key design features were considered such as dual bearing support of the impellor shaft, direct impellor feed from the mixing tank, increased shearing areas, balancing inlet and outlet ducts, correct sizing of the motor for performance and efficiency and specifying components for operating conditions and loads. A key requirement of the design was to allow access to the pump for maintenance and inspections as this reduces downtime and increased availability. Figure 5 shows the pump impellor design, supported at each end and its accessibility on the grout pump equipment.

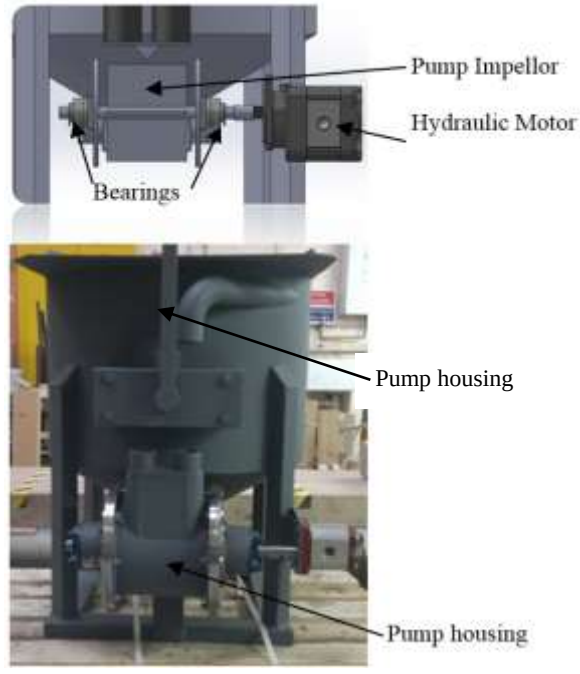

Figure 5. Redesigned pump

3. Operating conditions

The machine must be capable of mixing grout to meet the following specifications:

- Water/cement ratio = 0.4
- Mixing time of one minute (Multiple passes through pump)
- Impeller rpm > 1500
- The grout volume, based on the size of the mixing tank is 0.155m3
- Water and cement are added to the mixing drum to give a w/c ratio of 0.4
- Three bags of cement (150 kgs) added to 60l of water, giving a slurry mass of 210 kgs and overall 100 litre volume of grout mix.

The industry standard for recirculation flow rates in high shear colloidal mixing varies between 1000-1500 litres per minute and all calculations were based on the higher end of this range. The pump must deliver flow rates that produce turbulent, aggresive mixing.

Therefore the design flow rate: $= 1500 \frac{litres}{min} = \frac{90\ m^3}{hour}$ and the viscosity of the grout was 0.06 Pa.s [4].

- The System Flow rate = Q $= \frac{\mathbf{90}}{\mathbf{60 \times 60}} = \mathbf{0.025\ m^3/s}$

The entire mixing system consists of pipes/ducts and fittings of differing cross sectional areas as outlined in Figure 6. The flow rate of Q = 0.025 m^3/s remains constant through the entire system.

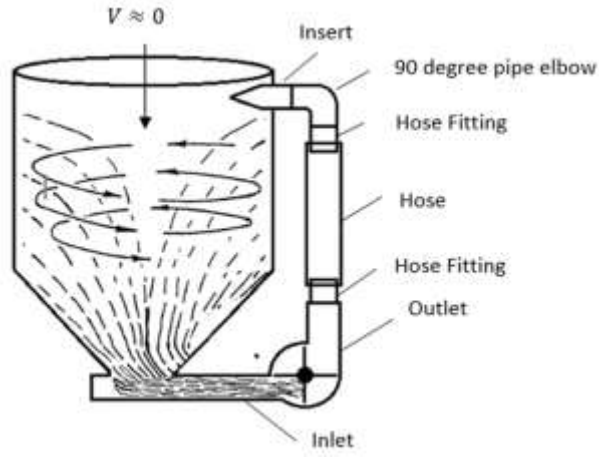

Figure 6. Schematic of mixing tank with variable cross sections

Major losses in the system are highlighted in Table 1. and the values derived in Column 8.

Table 1. values to determine head losses in the mixing system

Component	**Relative Roughness**	**Length** (m)	**Hydraulic Diameter** (m)	f_{moody} (Friction factor)	**Reynolds Number**	**Velocity** (m/s)	h_f (m) $\left(f\frac{L}{D}\frac{V^2}{2g}\right)$
Main tank	-	-	-	-	-	-	-
Inlet Duct	0.000526	0.365	0.095	0.032	11704	3.51	0.077
Outlet Duct	0.000526	0.07	0.095	0.032	11704	3.51	0.0148
Hose fitting	0.00607	0.046	0.0428	0.035	26017	17.36	0.577
Rubber Pinch hose	0.000147	0.282	0.068	0.0285	16374	6.88	0.285
Pipe elbow (90º)	0.00607	0.116	0.0428	0.035	26017	17.39	1.45
Insert pipe	0.00607	0.228	0.0428	0.035	26017	17.36	2.85

The overall design power required for the Grout pump for the mixing and pumping unit is was determined to be 12.56 kW.

4. Key Design improvements

The aim of this project was to improve the technical performance associated with a grout pump and mixing rig. To achieve this, a number of key objectives were addressed:

- To provide design documentation for the grout pump
- To design and develop a stationary mixing unit for testing machine performance
- To design and develop a high shear colloidal mixing pump
- To design for maintenance and accessibility
- To improve bearing performance problems and seal issues

The new design utilizes a twin bearing, positive displacement mixing unit with a widened impeller to provide increased shearing area and higher volume flow rates. The widened impeller is one of the key features of the mixing unit. It accounts for increased shearing area, and therefore more cement particles are wetted. In addition, the wider impeller displaces more volume per revolution, therefore increasing flow rates. Vortex formation is enhanced which improves mixing, wetting and turbulent flow in the mix. As a mixing unit, this new design has improved reliability, enhanced mixing capacity (due to high shearing area) and employs a better sealing system to cope with aggressive environments as shown in Figure 7. With the new design, the time taken for maintenance has been reduced from 1 day to 30 minutes. This is due to the simplified design of the new mixing unit. With only a flange to remove from the mill, access to the blades is immediate. The original machine suffered bearing failure as a result of a cantilevered impeller. Deflection of the impeller translated into additional dynamic loading on bearings, resulting in premature bearing fatigue and failure. This problem was solved with the use of a dual bearing system and eliminating the cantilever effect. The calculated value of dynamic loads on the bearings was found to be 5.41 kN which is well under the rated value of 14.6 kN [6]. The seal included a Tungsten Carbide shaft seal designed for abrasive environments.

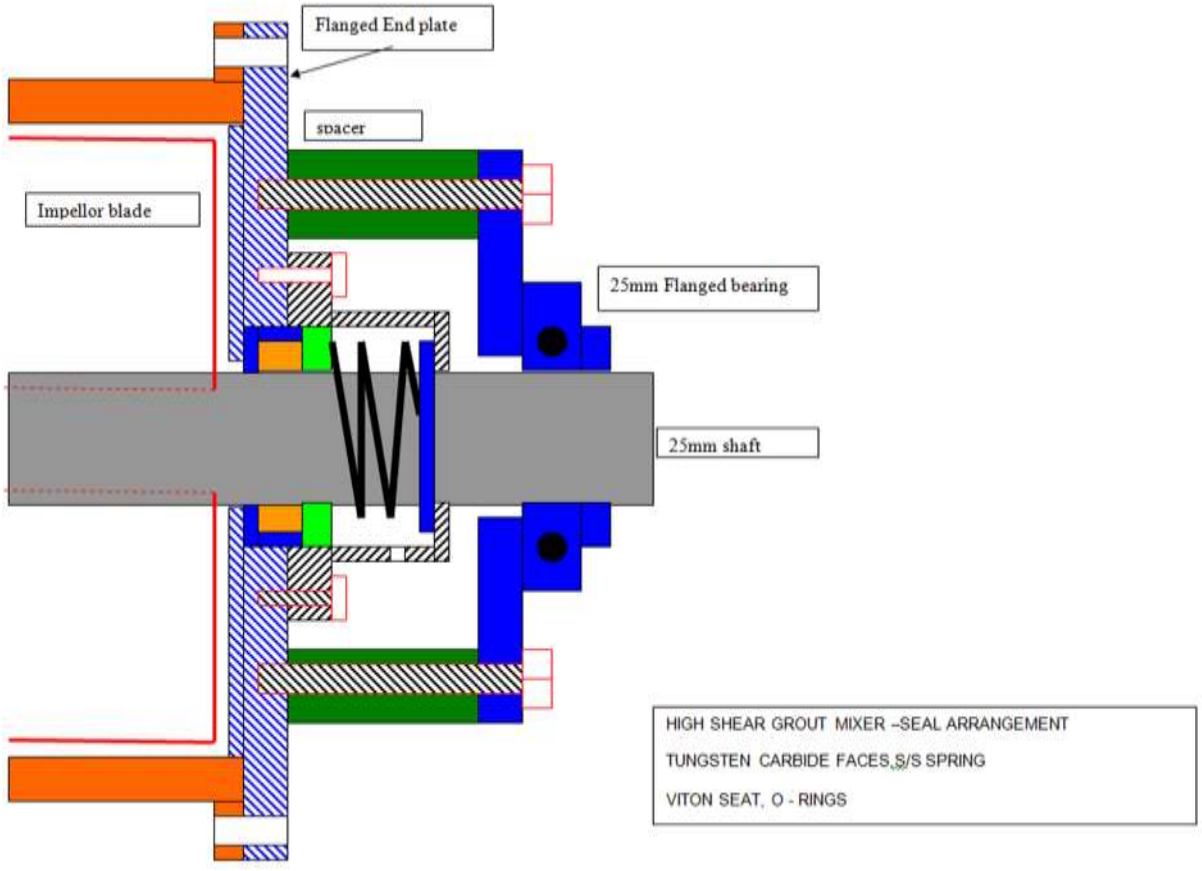

Figure 7. Bearing and seal system for grout pump

5. Testing and results

Preliminary operations with water proved satisfactory, generating a high speed and a vortex effect as required. This indicated that mixing should occur to requirements for the company involved. With the addition of cement and sand, the results of mixing was positive with a thourough homogenous mix obtained for a w/c ratio of 0.4 for grout. No leaks or part failure was observed. The power required to drive the impeller for mixing was calculated to be 12.56 kW. The overall torque on the impeller was calculated to be 66.63 Nm. The system was sized to cope with the highest industry standard flow rate of 1500 litres/min. Further testing is ongoing at the manufacturers plant and these involve standard cube tests of grout to determine strength and performance of the mixed product.

Acknowledgements

This work was sponsored by Engineers Ireland and TAL Construction Ltd., Cork, Ireland

REFERENCES

[1] *Bauma 2013 in Munich International Trade Fair for Construction Machinery*" bauma 2013 | N.p., n.d. Web. 2 June 2013. <http://www.bauma.de/en/>.

[2] Houlsby, A.C., 1990. *Construction and Design of Cement Grouting a Guide to Grouting in Rock Foundations*. John Wiley & Sons, New York, USA.

[3] http://www.haywardbaker.com *Cement grouting* http://www.haywardbaker.com/WhatWeDo/Techniques/Grouting/CementGrouting/default.aspx

[4] M.J. PITT (2000) *SPE Drilling and Completion* vol 15 no1 pages 3-6 "The Marsh Funnel and Drilling Fluid Viscosity: A New Equation for Field Use"

[5] Yunus A. Cengel, Fluid Mechanics, *Fundamentals and Applications*.

[6] Black, Rod. *Design and Manufacture And Integrated Approach*. Basingstoke: Palgrave Macmillan, 23. Print.

ISSN 1847-7917

Dose rate dependent effects of beta and gamma irradiation on chitosan films

Cenk DENKTAŞ[1]*, Derya YILMAZ BAYSOY[2], Erol KAM[1]
[1]Yildiz Technical University, Faculty of Art and Science, Dep. of Physics, Davutpasa Campus 34220 Esenler/Istanbul **Turkiye**
[2]Mimar Sinan Fine Arts University, Department of Physics, 34380, Sisli/Istanbul **Turkiye**
*denktas2010@gmail.com
cdenktas@yildiz.edu.tr

Abstract: Dose rate effects of beta and gamma irradiation on the physical properties and thermal properties of chitosan films have been investigated. After irradiation, the changes in the physical properties were obtained attenuated total reflection (ATR) method in IR spectrometer. The changes of thermal properties were evaluated by Thermo gravimetric (TG-DTA). IR spectroscopic analysis showed changes on microstructure of chitosan films after they had been exposed to doses of beta and gamma irradiation. Based upon the observation on the TGA analysis, the thermal stability of chitosan film is decreased and increased when exposed to doses for beta and gamma irradiation, respectively. FTIR spectroscopy showed that beta and gamma irradiation on chitosan films induced both collapse of the chitosan structure, improvement (or undetected crosslinking) and formation of new group in the chitosan films

Keywords
Chitosan,
Beta irradiation,
Gamma irradiation,
Dose rate
Thermal stability

1. Introduction

Chitosan, a polyelectrolyte prepared by N-deacetylation of chitin in a hot alkaline or acidic medium, has been intensively studied because of its interesting properties such as non-toxicity, biocompatibility, biodegradability, bioactivity, acceleration of wound healing, fat binding capacity etc. [1]. Chitosan has been used in a wide variety of applications, such as in medicine, pharmaceutical industry, biomedical applications, food, agricultural or environment protection [2]. The modification or degradation of chitosan is vital in order to enhance bio-compatibility, biodegradability in human body fluid (non-acidic) [3] and to minimize the potential chemical hazards [4].

Radiation processing (gamma rays, X-rays, beta rays, ion beams) [5]-[10], dry heat [11], pressure, steam or ethylene oxide can provide a useful tool for degradation or modification of different polymers [12], [13] and [14]. Among these methods, gamma rays emitted from a nuclear source (^{60}Co and ^{137}Ce) may be an attractive method [15] and [13]. It has been well known that polysaccharides such as chitosan can be degraded due to scission of glycosidic bonds by radiation [16] and [3]. In addition, some authors have reported that the gamma irradiation depending on the irradiation dose, could affect some properties of chitosan for applications [17]. The effect of beta irradiation on radiation processing of biopolymers and polymers has been studied, but not enough to be mentioned [18] and [19]. Furthermore, an electron beam or low energy beta irradiation may be used to induce effects such as chain scission and cross-linking (or enhancement) in polymers [5], [19]-[21]. Although the main interaction with matter is basically the same for gamma rays and beta particles, minor differences between the two modes remain [22], [23] and [24]. A significant difference exists between beta rays and gamma rays on polymers, which is related to dose rate (at low or high dose-rate) and often to oxidative degradation of material at or the reaction of the polymer surface with low dose-rates [5]. When gamma rays are compared with beta particles, the e-beam electrons have a much lower penetrating power than higher dose rates of gamma radiation; however, little information is available on the effects of beta irradiated chitosan films [25] and [26].

The aim of this work was to compare the effects of gamma and beta irradiation doses and dose rates on stability of chitosan films. Characterization of chitosan films were done by using different characterization techniques (ATR-FTIR and TG- DTA).

2. Experimental

2.1 Materials and Preparation

Chitosan (molecular weight 150.000) was provided by Fluka. Chitosan films were prepared based on the reported literatures. 1000 mg of chitosan was dissolved in 100 ml of distilled water 1 wt. % acetic acid solution at 80 ºC for 90 min to complete dissolution with magnetic stirrer. The solution was poured onto cleaned Petri dishes and dried in room temperature for 3 days to ensure removal of solvents. After drying, the films were skinned Petri dishes and kept in vacuum desiccators until use. The thickness of the obtained films was in the range of 50 nm.

Chitosan films were irradiated with ^{60}Co gamma source at two different dose rates of 0.51 kGy/h and 2.5 kGy/h, to absorbed doses up to 50 kGy and beta-rays irradiation of chitosan films were performed by ^{90}Sr/^{90}Y beta source with doses up to 5 kGy at two different dose rates of 0.05 kGy/h and 0.25 kGy/h.

2.2 Characterization of Chitosan Films

2.2.1 Fourier Transform IR (FTIR) Spectral Analysis

The microstructure changes were recorded using an attenuated total reflection (ATR) method in IR spectrometer by a Watson 1000 FTIR apparatus. Spectra were acquired for 100 scans between 400 and 4000 cm^{-1} at a resolution of 16 cm^{-1}. This spectrum were detected in more detail for chemical shifts, peak.

2.2.2 TG analysis (TGA)

The thermal properties of chitosan films were evaluated by TGA. Thermo gravimetric (TG) and Differential Thermal Analysis (DTA) measurements were carried out in nitrogen atmosphere at a heating rate 20 ºC/min over the temperature rate 20-500 ºC using Perkin Elmer TG/DTA 6300 EXSTAG. The DTA curves were recorded simultaneously.

3. Results and Discussion

3.1 FTIR spectral analysis

Fourier transform infrared spectroscopy (FTIR) reveals information about the molecular interactions of chemical components and is a useful technique to supplement micro-structural characterization of composite films [27]. The changes in the structure of chitosan films after they had been exposed to beta and gamma irradiation with different dose rates were examined by IR spectra and compared with the thermal properties. The chitosan spectrum was similar to previous reports and assignments of pure chitosan film are provided in Table 1. The infrared spectra of chitosan films before and after they had been exposed to beta and gamma irradiation with different dose rates are presented in Fig. 1. We observed changes in the absorbance or transmittance of specific chemical groups within an after radiation effects. From Fig.1 the O-H stretching band was affected and shifted (moved toward lower wavenumbers) from 3336 cm^{-1} to 3324 cm^{-1}, from 3336 cm^{-1} to 3334 cm^{-1}; from 3322 cm^{-1} to 3327 cm^{-1} and from 3322 cm^{-1} to 3314 cm^{-1} after beta and gamma irradiation, respectively. It is indicates that the intermolecular and intramolecular hydrogen bonds of chitosan can be weakened after radiation [28]. In addition, the decrease and increase in intensity of O-H stretching band of chitosan film is observed from Fig. 1a and Fig. 1b. The decrease of intensity is indicated to reduction in hydrogen-bond strength or the collapse of the chitosan structure and the increase of intensity can be pointed to improvement or undetected cross linking [29]-[32] and [1].

As shown in the Fig. 1a, the O-H stretching band of chitsan film is stable after high dose rate beta irradiation. The peaks at 2980 – 2820 cm^{-1} appeared in pure chitosan film, indicating of symmetric and asymmetric stretching of C-H [30]. Especially after low dose rate gamma irradiation, the increase of intensity of this band is observed. The amide band group at 1500 – 1700 cm^{-1} is observed in pure chitosan (from Fig. 1). From Fig. 1b, it can be seen that the intensity of the amide group peaks was increased and decreased after they had been exposed to low and high dose rates of gamma irradiation. First reason, this could be attributed to the additional number of amide I (C=O stretching) as the end group of chitosan polymeric chain that have been generated as a result of the depolymerisation reaction of chitosan film due to the gamma radiation exposure [3]. Second reason, this is ascribed to the partial involvement of amino groups in intra- and intermolecular hydrogen bonds [33]. The change in intensity of group bands within the β (1-4) glycoside range (1200 – 1000 cm^{-1}) is observed in Fig 1. The changes of these bands may have led to several effects on the amount, formation and distribution of hydroxyl group in the molecular chains of chitosan by glycosidic bonds [28] and [34].

Table1. Band Assignments for IR Spectrum of pure chitosan film

Wavenumber (cm^{-1})	Assignment
3000 – 3700	Broad band, O-H stretching superimposed to the N-H stretching band and inter hydrogen bonds of the polysaccharide [35]
2900	C-H stretching
1658	Amide I (C=O stretching) or δ(O-H) water bending [36]
1548	Amide II, N-H [36]
1439	CH_2 bending
1170 – 687	Specific band of the β (1-4) glycoside bridge [12]

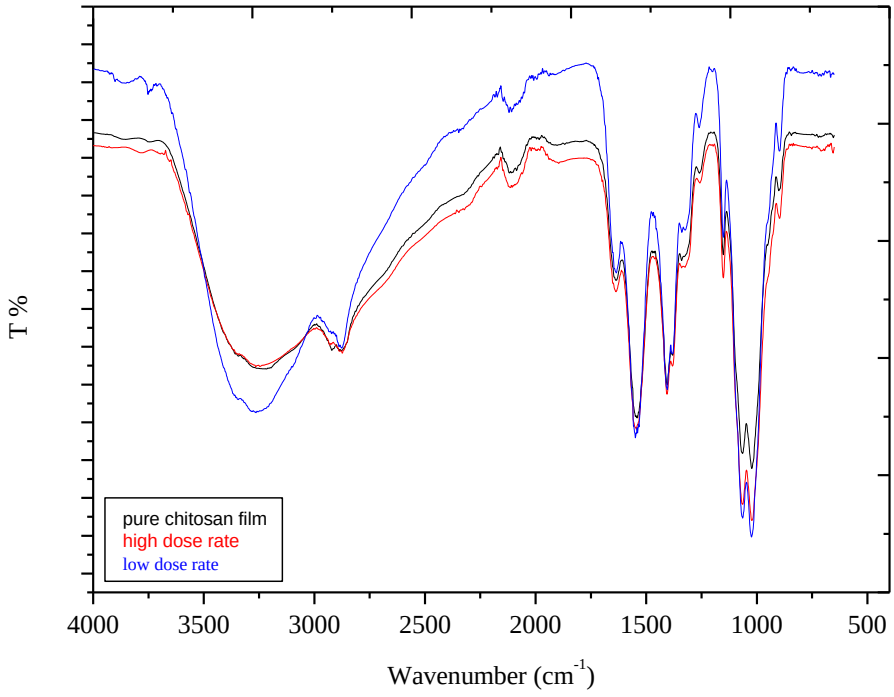

(a)

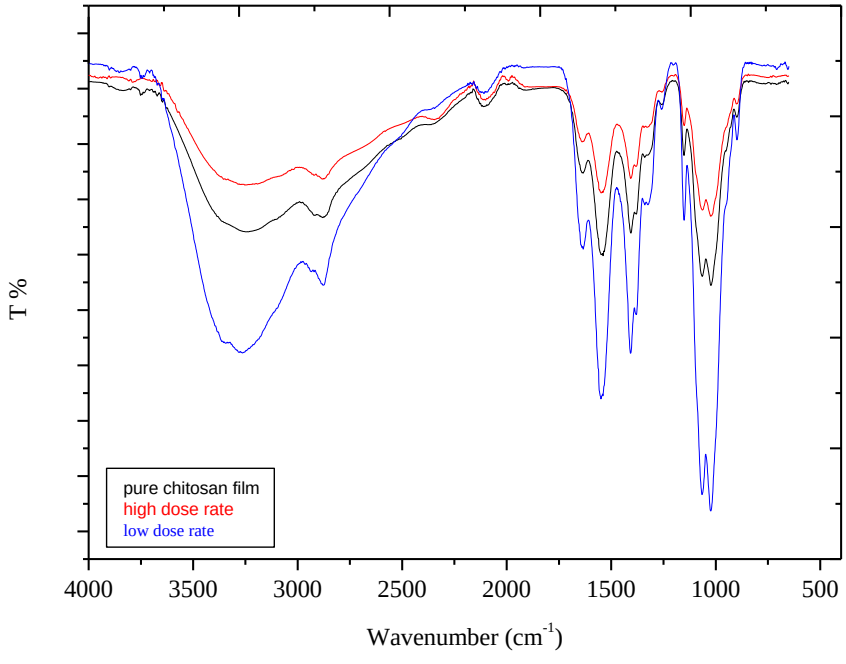

(**b**)

Figure 1. IR spectra of chitosan films before and after beta and gamma irradiation for different dose rate: (a) beta irradiation and (b) gamma irradiation

3.2 Thermogravimetric analysis (TGA)

TGA is considered as the most important method to illustrate the thermal stability over a wide range of temperature [37] and [38]. The changes of the weight loss in the chitosan films as a function of temperature are commonly determined by the technique of TGA. TGA curves of chitosan films, before and after exposure to by dose rates of beta and gamma irradiation, are shown in Fig. 2. In the examination, degradation mechanism occurred in two stages as clearly seen in Fig. 2 [39]. For pure chitosan film (from Fig. 2a), the first region for losses of weight was observed in the temperature range of ≈ 27 – 146 ºC due to evaporation of intermediate and bound water or volatile materials (e.g., solvent) on the chitosan solution [38], [39] and [40] and showed a total weight loss of about ≈13 wt %. The second region of thermal degradation was on occurred in the temperature range of ≈187 – 472 ºC and showed a total weight loss of about 45.0 wt %. Here, the second degradation stage could be attributed to complex process including the dehydration, deacetylation and chain scission of the chitosan polymer and the initial water content does not affect the onset of decomposition temperature [38]-[42]. Then, thermal degradation is affected by the final OH groups that "attack" the basic chain, which bends under the influence of thermal energy and such a reaction can start at temperatures higher than 237 ºC [42]. The first region for losses of weight of chitosan films after they had been exposed to dose rates of beta irradiation took place finishes at around 150 ºC and 144 ºC whereas chitosan films after they had been exposed to dose rates of gamma irradiation exhibited it at around 149 ºC and 145 ºC as shown Fig. 2b- 2e, respectively. Fig. 2 shows the second region for thermal degradation of chitosan films after they had been exposed to dose rates of beta and gamma irradiation, respectively. Also, Table 2 and Table 3 summarize the thermal degradation values of the chitosan films taken from Fig. 2.

The differential thermal analyses (DTA) curves for chitosan films were shown in Fig. 3. In all the curves, both endothermic peak and exothermic peak was observed. In all the curves, an endothermic peak was observed around 75 ºC and exothermic peak was observed between 250 - 320 ºC The first endothermic peak is due to evaporation of absorbed water/dehydration and the exothermic peaks observe for decomposition for chitosan [35], [43]-[45].

Table 2.Thermal degradation values of the chitosan films after and before exposure by beta irradiation

	The first region decomposition, (ºC) weight loss, (%)	The second region decomposition, (ºC) weight loss, (%)
Pure chitosan film	27 – 146 (≈ 13)	187 – 472 (≈45)
High dose rate	26 – 150 (≈19)	166 – 476 (≈53)
Low dose rate	25 – 144 (≈ 17)	171 – 472 (≈ 45)

Table 3. Thermal degradation values of the chitosan films after and before exposure by gamma irradiation

	The first region decomposition, (ºC) weight loss, (%)	The second region decomposition, (ºC) weight loss, (%)
Pure chitosan film	27 – 146 (≈13)	187 – 472 (≈45)
High dose rate	24 – 149 (≈11)	182 – 477 (≈43)
Low dose rate	28 – 145 (≈7)	175 – 476 (≈45)

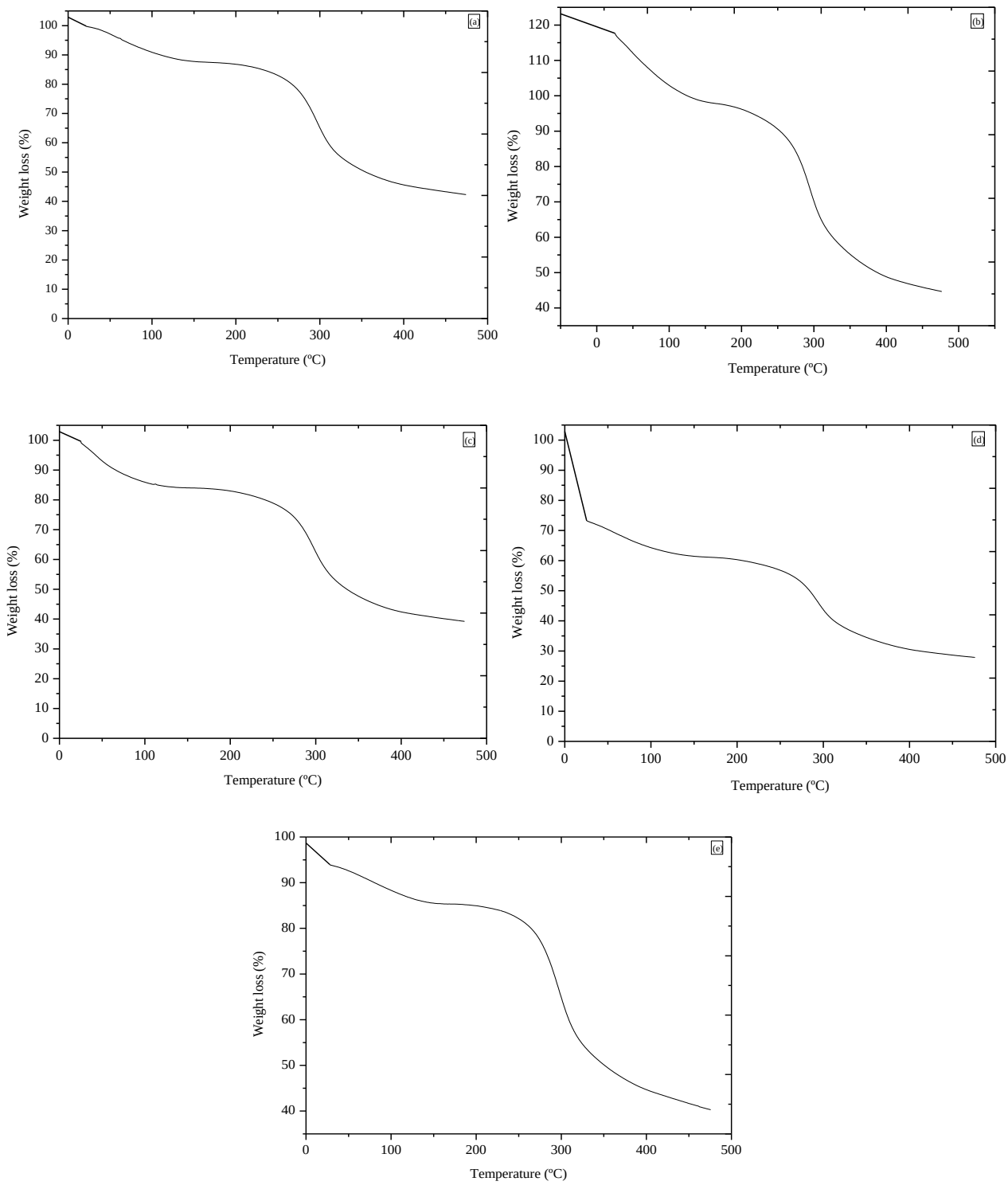

Figure 2. TG thermo grams of chitosan films before and after beta and gamma irradiation for different dose rate: (a) pure chitosan film, (b) high dose rate for beta irradiation, (c) low dose rate for beta irradiation, (d) high dose rate for gamma irradiation and (e) low dose rate for gamma irradiation.

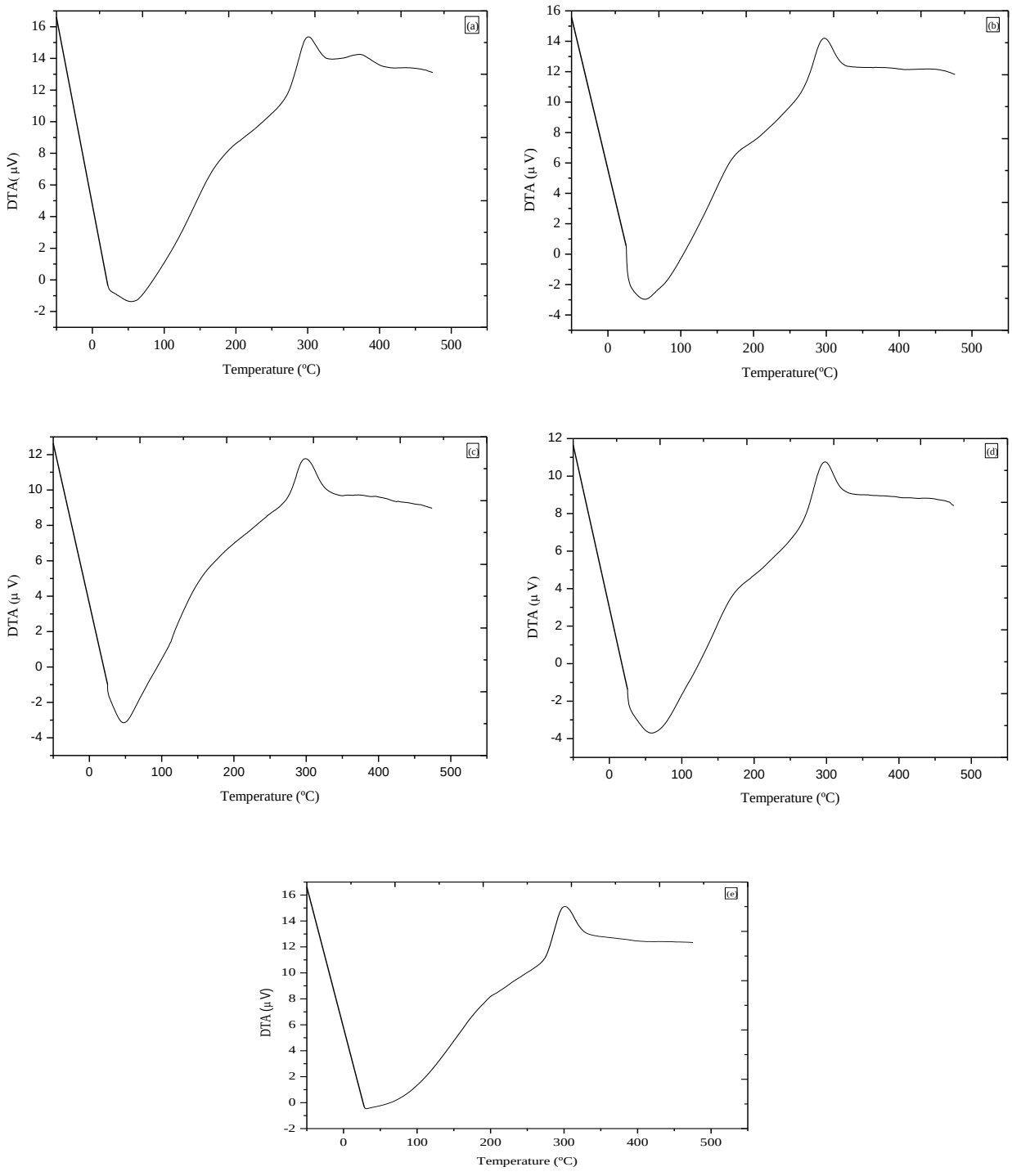

Figure 3. DTA curves of chitosan films before and after beta and gamma irradiation for different dose rate: (a) pure chitosan film, (b) high dose rate for beta irradiation, (c) low dose rate for beta irradiation, (d) high dose rate for gamma irradiation and (e) low dose rate for gamma irradiation.

4. Conclusion

Radiation degradation of chitosan films are one of the promising methods for by new product development for medical and environmental applications. The results presented in this study illustrate the effects of dose rate by beta and gamma irradiation on the microstructure and thermal properties of chitosan films. On the basis of the obtained results few points may be addressed:

(1) Further analysis using FT-IR revealed that there are no structural changes observed in chitosan films after exposure to beta and gamma radiation, where no new functional groups were detected for irradiated chitosan films.
(2) At lower dose rate improvement (or undetected crosslinking) was observed while at higher dose degradation by collapse of the structure (from Fig. 1a and Fig. 1g. in the region the O-H stretching band).
(3) The thermal stability of chitosan film is decreased and increased when the exposed to doses for beta and gamma irradiation, respectively.
(4) The results revealed that the beta irradiation have an important effect on the studied properties. Therefore, e-beam irradiation can be an efficient alternative method to produce modified chitosan in comparison to the gamma irradiation.
(5) The results of irradiation effects on chitosan films are shown depends on the high dose rate favors crosslinking reactions and low dose rates favor chain scission.

Acknowledgements

This study was supported by Yıldız Technical University Center Laboratory.

REFERENCES

[1] Wang, M., Xu, L., Zhai, M., Peng, J., Li, J., & Genshuan, W. (2008). γ-ray radiation-induced synthesis and Fe(III) ion adsorption of carboxymethylated chitosan hydrogels. Carbohydrate Polymers 74, 498–503.

[2] Duan, W., Chen, C., Jiang, L., & Li, G.H. (2008). Preparation and characterization of the graft copolymer of chitosan with poly[rosin-(2-acryloyloxy)ethyl ester]. Carbohydrate Polymers 73, 582–586.

[3] Zainol, I., Akil, H. Md., & Mastor, A. (2009) Effect of γ-irradiation on the physical and mechanical

[4] properties of chitosan powder. Materials Science and Engineering C 29, 292–297.

[5] Felinto, M.C.F.C., Para, D.F., da Silva, C.C., Angerami, J., Oliveira, M.J.A., & Lugão, A.B.(2007). The swelling behavior of chitosan hydrogels membranes obtained by UV- and γ-radiation. Nuclear Instruments and Methods in Physics Research B 265, 418–424.

[6] Chmielewski, A.G., Haji-Saeid, M., & Ahmed, S. (2005). Progress in radiation processing of polymers. Nuclear Instruments and Methods in Physics Research B 236, 44–54.

[7] Chmielewski, A.G. (2010). Chitosan and radiation chemistry. Radiation Physics and Chemistry 79, 272–275.

[8] Janik, I., Kasprzak, E., Al-Zier, A., Rosiak, J.M. (2003). Radiation crosslinking and scission parameters for poly(vinyl methyl ether) in aqueous solution. Nuclear Instruments and Methods in Physics Research B 208, 374–379.

[9] Makuuchi, K. (2010). Critical review of radiation processing of hydrogel and polysaccharide. Radiation Physics and Chemistry 79, 267–271.

[10] Choia, W.S., Ahnb, K.J., Leeb, D.W., Byunc, M.W. and Parkb, H.J. (2002). Preparation of chitosan oligomers by irradiation. Polymer Degradation and Stability 78, 533–538.

[11] Al-Assaf, S., Phillips, G.O., Williams, P.A. and du Plessis, T.A. (2007). Application of ionizing radiations to produce new polysaccharides and proteins with enhanced functionality. Nuclear Instruments and Methods in Physics Research B 265, 37–43.

[12] Ritthidej, G.C., Phaechamud, T., & Koizumi, T. (2002). Moist heat treatment on physicochemical change of chitosan salt films. International Journal of Pharmaceutics 232, 11–22.

[13] Feng, T., Du, Y., Li, J., Hu, Y., & Kennedy, J.F. (2008). Enhancement of antioxidant activity of chitosan by irradiation. Carbohydrate Polymers 73, 126–132.

[14] Lim, L.Y., Khor, E., & Koo, O. (1998). γ Irradiation of Chitosan. J Biomed Mater Res (Appl Biomater) 43, 282–290.

[15] Bartoníček, B., Plaček V., Hnát, V. (2007). Comparison of degradation effects induced by gamma radiation and electron beam radiation in two cable jacketing materials. Radiation Physics and Chemistry 76, 857–863.

[16] Huang, L., Zhai, M., Peng, J., Li, J., & Wei, G. (2007). Radiation-induced degradation of carboxymethylated chitosan in aqueous solution. Carbohydrate Polymers 67, 305–312.

[17] Nagasawa, N., Mitomo, H., Yoshii, F., Kume, T. (2000). Radiation-induced degradation of sodium alginate. Polymer Degradation and Stability 69, 279 – 285.

[18] Vilcáez, J., and Watanabe, T. (2009). Inhibitory Effect of Gamma-Irradiated Chitosan on the Growth of Denitrifiers. International Journal of Microbiology 2009, 5.

[19] Choi, J., Kim, J.K., Srinivasan, P., Kim, J.H., Park, H.J., Byun, M.W. and Lee, J.W (2009). Comparison of gamma ray and electron beam irradiation on extraction yield, morphological and antioxidant properties of polysaccharides from tamarind seed. Radiation Physics and Chemistry 78, 605–609.

[20] Raj, J.M. and Ranganathaiah, C. (2009). A free-volume study on the phase modifications brought out by e-beam and microwave irradiations in PP/NBR and PVC/SAN blends. Polymer Degradation and Stability 94, 397–403.

[21] Sangappa, S. Asha, T. Demappa, Ganesh Sanjeev, P. Parameswara, R. Somashekar (2009) Spectroscopic and thermal studies of 8 MeV electron beam irradiated HPMC films. Nuclear Instruments and Methods in Physics Research B 267, 2385–2389.

[22] Cairns, M.L., Sykes, A., Dickson, G.R., Orr, J.F., Farrar, D., Dumba, A., Buchanan, F.J. (2011). Through-thickness control of polymer bioresorption via electron beam irradiation. Acta Biomaterialia 7, 548–557.

[23] Woo, L., & Sandford, C.L. (2002). Comparison of electron beam irradiation with gamma processing for medical packaging materials. Radiation Physics and Chemistry 63, 845–850.

[24] Montanaria, L., Cilurzoa, F., Selmina, F., Contib, B., Gentab, I., Polettic, G., Orsini, F., & Valvo, L. (2003). P oly(lactide-co-glycolide) microspheres containing bupivacaine: comparison between gamma and beta irradiation effects. Journal of Controlled Release 90, 281–290.

[25] Silindir, M. And Özer, A.Y. (2009). Sterilization Methods and the Comparison of E-Beam Sterilization with Gamma Radiation sterilization. FABAD J. Pharm. Sci., 34, 43–53. Review Article.

[26] Silva, R.M., Elvira, C., Mano, J.F., Roman, J.S., & Reis, R.L. (2004). Influence of β-radiation sterilization in properties of new chitosan/soybean protein isolate membranes for guided bone regeneration. Journal of Materials Science: Materials in Medicine 15, 523-528.

[27] Gryczka, U., Dondi, D., Chmielewski, A.G., Migdal, W., Buttafava, A., & Faucitano, A. (2009). The mechanism of chitosan degradation by gamma and e-beam irradiation. Radiation Physics and Chemistry 78, 543–548.

[28] Riveroa, S., Garcíaa, M.A., & Pinotti, A. (2010). Crosslinking capacity of tannic acid in plasticized chitosan films. Carbohydrate Polymers 82, 270–276.

[29] El-Sawy, N.M., El-Rehim, H.A.A., Elbarbary, A.M., & Hegazy, E.S.A. (2010). Radiation induced degradation of chitosan for possible use as a growth promoter in agricultural purposes. Carbohydrate Polymers 79, 555–562.

[30] Choi, J., Kim, J.K., Kim, J.H., Kweon, D.K., & Lee, J.W. (2010). Degradation of hyaluronic acid powder by electron beam irradiation, gamma ray irradiation, microwave irradiation and thermal treatment: A comparative study. Carbohydrate Polymers 79, 1080–1085.

[31] Zawadzki, J., and Kaczmarek, H., (2010) Thermal treatment of chitosan in various conditions. Carbohydrate Polymers 80, 394 – 400.

[32] Kaczmarek, H., and Zawadzki, J. (2010) Chitosan pyrolysis and adsorption properties of chitosan and its carbonizate. Carbohydrate Polymers 345, 941–947.

[33] Yang Y. (2002). Performance Modification of Chitosan Membranes Induced by Gamma Irradiation. Journal Of Biomaterials Applications 16, 215 -226.

[34] Nawi, M.A., Jawad, A.H., Sabar, S., & Ngah, W.S.W. (2011). Photocatalytic-oxidation of solid state chitosan by immobilized bilayer assembly of TiO2–chitosan under a compact household fluorescent lamp irradiation. Carbohydrate Polymers 83, 1146-1152.

[35] Wasikiewicz, J.M., Yoshii, F., Nagasawa, N., Wach, R.A., Mitomo, H. (2005). Degradation of chitosan and sodium alginate by gamma radiation, sonochemical and ultraviolet methods. Radiation Physics and Chemistry 73, 287–295.

[36] Demetgül, C., & Serin, S. (2008). Synthesis and characterization of new vic-dioxime derivative of chitosan and its transition metal complexes. Carbohydrate Polymers 72, 506-512.

[37] Yue, W., He, R., Yao, P., & Wei, Y. (2009). Ultraviolet radiation-induced accelerated degradation of chitosan by ozone treatment. Carbohydrate Polymers 77, 639–642.

[38] Abdelrazek, E.M., Elashmawi, I.S., & Labeeb, S. (2010). Chitosan filler effects on the experimaental characterization, spectroscopic investigation and thermal studies of PVA/PVP blend films. Physica B 405, 2021-2027.

[39] Liu, H., Xie, F., Yu, L., Chen, L., & Li. (2009). Thermal processing of starch-based polymers. Progress in Polymer Science 34, 1348-1368.

[40] Julkaplia, N.M., & Akil, H.M. (2010). Thermal Properties of Kenaf-Filled Chitosan Biocomposites. Polymer-Plastics Technology and Engineering 49, 147–153.

[41] Xie, Y., Liu, X., & Chen, O. (2007). Synthesis and characterization of water-soluble chitosan derivate and its antibacterial activity. Carbohydrate Polymers 69, 142–147.

[42] Anithaa, A., Deepaa, N., Chennazhia, K.P., Naira, S.V., Tamurab, H., & Jayakumar,R. (2011). Development of mucoadhesive thiolated chitosan nanoparticles for biomedical applications. Carbohydrate Polymers 83, 66–73.

[43] Suljovrujic, E., Ignjatovic, N., Uskokovic,D., Mitric,M., Mitrovic, M., & Tomic, S. (2007). Radiation-induced degradation of hydroxyapatite/poly L-lactide composite biomaterial. Radiation Physics and Chemistry 76, 722–728.

[44] Khalid, M.N., agnely, F., Yagoubi, N., Grossiord, J.L. & Couarraze, G. (2002). Water state characterization, swelling behavior, thermal and mechanical properties of chitosan based networks. European Journal of Pharmaceutial Sciences 15, 425-432.

[45] Estrada, S.A.M., Pérez, C.A.M., Nava, J.G.C., Casillas, P.E.G., &-Armendariz, I.O. (2010). Synthesis and thermo-physical properties of chitosan/poly(dl-lactide-co-glycolide) composites prepared by thermally induced phase separation. Carbohydrate Polymers 81, 775–783.

[46] Shim, J.W., Nho, Y.C. (2003). Preparation of Poly(acrylic acid)–Chitosan Hydrogels by Gamma Irradiation and In Vitro Drug Release 90, 3660 – 3667.

ISSN 1847-7917

Logistics Personal Excellence by continuous Self-Assessment (LOPEC): Pilot-implementation case studies

Ivica VEZA[1)]***, Nikola GJELDUM***[1)] ***and Marko MLADINEO***[1)]

1) University of Split, Faculty of Electrical Engineering, Mechanical Engineering and Naval Architecture
Sveučilište u Splitu, Fakultet elektrotehnike, strojarstva i brodogradnje
R. Boskovica 32, 21000 Split, **Croatia**

iveza@fesb.hr
ngjeldum@fesb.hr
marko.mladineo@fesb.hr

Keywords

Personal Excellence
Self-Assessment
Lean Logistics
Learning Management System
Maturity Excellence Level

Ključne riječi

Osobna izvrsnost
Samoprocjena
Lean logistika
Sustav za upravljanje učenjem
Razina zrelosti izvrsnosti

Preliminary notes

Abstract: In a knowledge society where demands for skills, competencies and knowledge constantly increase and change, lifelong learning is a key strategy to adjust people's performance capabilities to new requirements and guarantee employability in the world of work. LOPEC aims in developing and offering special-tailored training for Lean Logistics and required basic skills for skilled workers on shop floor level. Needed know-how for today's challenges in logistics will be transferred. Thus, LOPEC is aiming at people enhancement as entry ticket to lifelong continuous learning by increasing the maturity level of personal logistic excellence. A common European view for "Logistics personal excellence" for skilled workers will ensure that the final product is an open product, using international, pan European validated standards. As results LOPEC will provide training modules for post-secondary education in the area of Lean Logistics, required basics skills and offers transparency of personal excellence, regarding the personal maturity level of hard and soft skills at any time. Furthermore, two case studies of LOPEC Pilot-implementation in Croatian companies are presented in this paper.

Prethodno priopćenje

Sažetak: U društvu znanja u kojem potreba za vještinama, kompetencijama i znanjem stalno raste i mijenja se, cjeloživotno učenje je ključna strategija za prilagodbu ljudskih mogućnosti novim zahtjevima, te je svojevrsna garancija za mogućnost zaposlenja. LOPEC cilja na razvoj i nuđenje specijalizirane obuke za Lean logistiku i traženih osnovnih vještina, za kvalificirane radnike na razini proizvodnog pogona. Transferirat će se znanja potrebna za svladavanje današnjih izazova u logistici. Stoga, LOPEC cilja na unaprjeđenje ljudskih sposobnosti kao na ključ za cjeloživotno kontinuirano učenje povećanjem razine zrelosti osobne logističke izvrsnosti. Zajedničko Europsko viđenje „Osobne logističke izvrsnosti" za kvalificirane radnike osigurat će da je finalni proizvod otvoren svima, korištenjem međunarodnih i Europskih standarda. Kao rezultat LOPEC će u bilo koje doba nuditi module za obuku za post-srednjoškolsko obrazovanje u području Lean logistike, traženih osnovnih vještina, te transparentnost po pitanju osobne izvrsnosti, s obzirom na osobnu razinu zrelosti po pitanju težih i lakših vještina. Nadalje, u ovom radu predstavljena su dva studija slučaja Pilot-implementacije LOPEC-a u hrvatska poduzeća.

1. Initial situation, challenges and motivation

The industrial sector is one of the most important assets of Europe's economic resources. With a contribution of almost 15% to the overall gross domestic product (GDP), it ensures 34.8 million jobs [1].

Facing global competition, companies are forced to continuously improve their manufacturing and logistics processes, machinery and equipment. For the implementation of modern and lean methods it is a crucial advantage to be able to use distinct capabilities of all possible employees [2]. Designing efficient processes challenges employees at all levels of the industrial hierarchy to be responsive and reactive to problems and to contribute to the continuous improvement of these processes, especially on the shop floor [2, 3]. The same applies to the changeability of companies, which can be substantially driven by the abilities and qualifications of employees [4]. Regularly, new services and processes close to production were developed or were taken into the portfolio of logistic enterprises, service providers and fields. For the execution and management of these logistics tasks, new

principles, approaches and methods were raised and applied within the last years. This includes implementation trends like the transfer of lean manufacturing methods to the field of logistics [5].
Skilled workers need the competence to change and adapt logistics processes through applying innovative methods, tools and techniques on operation level to meet customer requirements. Potentials for optimization should be recognized and realized by the workers themselves, without permanent instructions from management level. But the lack of skilled workers will increase in the next years [6]. In addition, a mind set by the skilled workers towards life-long learning must be established. Hence, lifelong learning is a key strategy to adjust people's performance capabilities for new requirements [7] because in a knowledge-driven society, demands for skills, competencies and knowledge constantly increase and change. But for skilled workers of the secondary educational level, the entrance into lifelong learning, starting with access to the tertiary educational level, is usually not possible or at least very difficult due to educational laws, certification requirements connected with the existing school education. Because of these aspects, the access to know-how in Lean Logistics usually remains undisclosed for skilled workers [8].
Nowadays, many organizations support their skilled workers by in-house trainings to close this gap. But they meet the challenge to design organizational personnel development and to support individual personal development in a coherent and balanced way [9, 10]. The dilemma of business, professional and private related objectives and its procedure of measurement is especially present in countries where labor plays a key role in manufacturing plants [11]. Currently, only assessment concepts to evaluate the position of a business in the market are available. The term "assessment" should not be confused with the other three 'A'-terms (Audits, Appraisal and Award). Often, they are mixed up and lead to a misunderstanding regarding the aims of self-assessment. The existing concepts and systems cannot be used to assess a "personal position of a skilled worker" regarding different maturity levels within his/her world of work and competences in Lean Logistics.

2. Scientific objectives and project goals

To implement the above mentioned challenges, the employed skilled workers have to be qualified and trained towards independent learning in order to design, plan and manage logistic systems at any time according to state-of-the- art of science and technology. Based on this demand, a common European vision is needed that claims major efforts to be oriented:

- on micro level, towards the support of a lifelong learning approach in European companies to ensure professional labor with continuous state-of-the-art knowledge and high performance skills,
- on meso level, towards securing, maintaining and building-up of production sites in Europe by own strength, especially by high employment and increasing empowerment of employees,
- on macro level, towards the speeding-up of the rate of industrial transformation in Europe.

The current situation and challenges can only be solved by a close cooperation between the vocational education and training (VET) organization and the world of work. Individual training modules can be compiled for skilled workers by understanding the demands of the professional life. The VET can contribute to the world of work to increase the employee skills and engagement, to raise the motivation of the skilled workers, to establish a more rapid training of new skilled workers as well as to strengthen the attraction for skilled logistics workers on the labor market. Understanding the different needs of skilled logistics workers across Europe will help to set up a customized self-assessment system as a contribution for continuous lifelong learning.

The focus of the research efforts at the Technical University of Vienna, Fraunhofer Austria Research, University of Reutlingen, is motivated through the following scientific objectives on a strategic perspective:

- Promotion of a common European view of "Logistics personal excellence" and its relevance not only for the management, but also for shop floor workers.
- Development of an educational environment for Lean Logistics in combination with the required basic skills to enable the knowledge transfer from management level to operation level.
- Definition of a learning pathway that allows skilled workers to participate in tertiary education. Thus, the gap between secondary and tertiary level as well as between continuing vocational training and higher education will be closed.
- Integration of the innovative training approach "learning factory" for life-long learning for skilled workers in the logistics sector.
- Development of a new approach of a self-assessment and a user training strategy towards "Personal Excellence in Lean Logistics". The methodology aims at providing a basis for a more systematic personal as well as professional development within the logistics sector.
- Usage of results as an international showcase for excellence in lifelong learning to persuade industry of transferability from personal to business improvements.
- Based on the scientific objectives, the following operative project goals are required to obtain the desired results:

- Determination of competencies and skills needed by a skilled worker in the context of Lean Logistics.
- Deflection of learning targets and definition of a systematic procedure to reach them.
- Setting up of a platform for life-long learning and as an instrument for advanced training in logistics techniques for employees at different levels of education.
- Establishing empowerment training (basic skills) and Lean Logistics learning modules for experienced skilled workers as a step to be enabled to graduate in a bachelor program.
- Implementation of the developed training modules into a blended learning approach, consisting of a web-based learning platform in combination with hands-on training in the learning factories of the project partners.
- Development and design of a self-assessment by adapting the business excellence approach towards a personal excellence approach. Therefore, the EFQM (European Foundation for Quality Management) model of excellence [12, 13] will be used as a basis. The model addresses the gap between organizational and personal self-assessment [14].
- Implementation of the personal self-assessment method into a software system as part of the software application "Group Opinion Analyzer" (GOA) that was developed by the previous European research project "SAETO" (Self-Assessment for Educational and Training Organizations) [15].
- Piloting the new solution in the four partner regions, with at least 12 test cases to collect feed-back from industrial end users.

3. Specifications of the LOPEC project

3.1. Consortium of LOPEC

All partners of the research project are themselves education or training organizations (ETO) from both the public and the private sector with a good link to VET. The Reutlingen University has a very close connection to the industry, resulting in the establishment of a corporation "Knowledge Foundation" for both continuous vocational training and academic education, with the curricula based on the needs of industry. Fraunhofer Austria has experience in developing business games, hands-on educational workshops and setting-up operation of a learning factory, which provide interactive training. Both universities, as well as the third academic partner, the Chair of industrial engineering (Department of engineering technology) at FESB, University of Split, are active in higher and advanced education and applied research in cooperation with industry in the fields of logistics, supply chain management, factory planning, process optimization and lean production. With the social research center of the University of Dortmund, Eurofortis SA, an adult education provider, IBK-Management Solution GmbH and the project coordinator, the consortium contains four of the original SAETO partners, thus facilitating knowledge transfer, expertise and experience within applying EFQM.

3.2. Definition of LOPEC target group as end-users

As described previously, LOPEC aims at skilled workers on the shop floor level. The project and its educational activities do not only focus on labor directly involved in production, the blue collar worker, but also on indirect or supporting labor, the white-collar worker. So both, a person who performs manual operation, typically in manufacturing or assembly, and a person who performs managerial or administrative work, typically in an office environment are addressed. Those types of classification result in the so-called "grey-collar worker" (Figure 1).

In the LOPEC project a grey-collar worker is an individual that acquired technical or economical skills through professional training or apprenticeship. Furthermore, the grey-collar worker requires leadership skills and social competences to promote improvements and changes within his or her work-group. This implies that the person is already a team leader or at least has the potential to become a team leader, who works well with others in a group setting and makes productive contributions through talent, knowledge and good work habits. At best, the grey-collar worker organizes people and resources toward the effective and efficient pursuit of predetermined objectives and has potential to stimulate the group to high performance. The methodological approach of LOPEC contains two important aspects that are integrated in one solution. On the one side, the self-assessment in terms of Lean Logistics, and on the other side, the self-assessment for the evaluation of the personal and professional development. Both approaches are presented in Section 4 and 5.

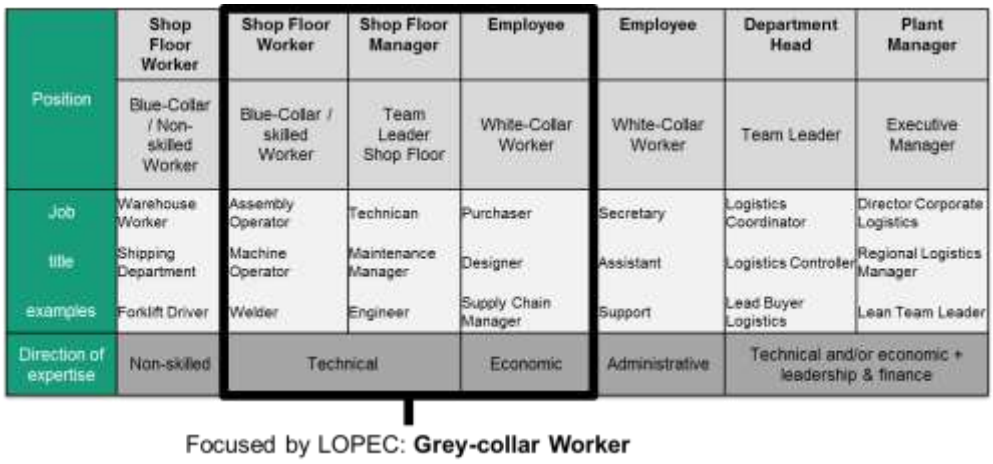

Figure 1. Definition of LOPEC target group as end-users
Slika 1. Definicija ciljane skupine krajnjih korisnika LOPEC-a

4. First LOPEC project results

The educational goal system of LOPEC is based on the fundamental mindset of Lean Management and Operational Excellence [16], with the essential objective on customer focus.

4.1. Definition of the LOPEC learning content

The grey-collar worker should be qualified to identify and to reduce waste sustainably to perfection. Parallel, he or she has to be experienced in additional disciplines and tools so that optimization tasks in regards of Lean Logistics can be developed, implemented and evaluated. If the individual grey- collar worker has no higher education diploma or a general qualification for university entrance, the gap of the required basic knowledge has to be identified and closed too. After reviewing the key literature, e.g. [17], the learning content of Lean Logistics got detailed into approx. 105 learning modules, with the categories as shown in Figure 2, each allocated to in-plant logistics or supply chains. As supporting subjects, 45 tools got detected as a need for grey- collar workers to be able to apply correlated Lean Logistics tools and methods. Analysing available and recommended pre-courses from different universities and countries resulted in three consolidated basic courses "Technics", "Mathematics" and "Informatics".

To support the learning progress of the learner and to build knowledge in a structured way, a learning path for Excellence in Lean Logistics was designed within LOPEC. This learning path divides the learning modules into 5 maturity levels which represent a performance improvement sequence (Figure 3).

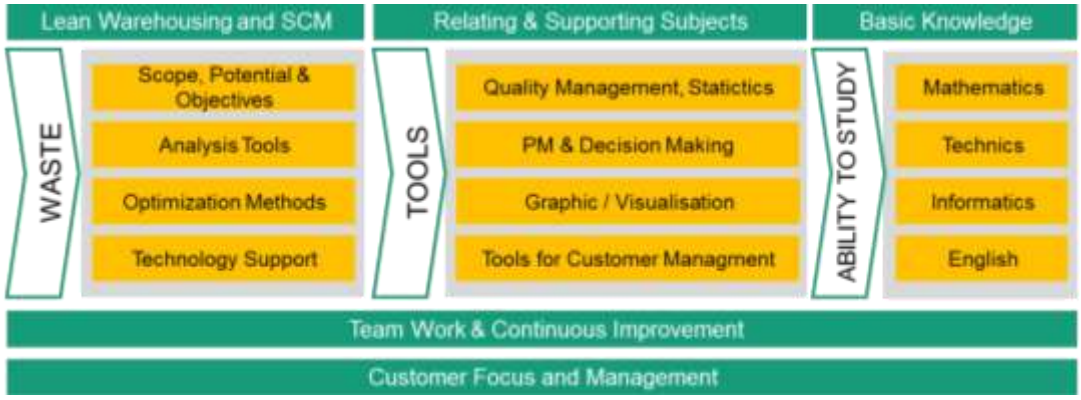

Figure 2. LOPEC content framework
Slika 2. LOPEC sadržajni okvir

In terms of Lean Logistics, Level 1 implies the philosophy of Lean Logistics and its principles, in particular the types of waste and material and information flow. Furthermore, analysis tools and optimization tools for the workplace of the grey-collar worker are focus of this Level. Level 2 expands Level 1

with workplace related material movement and handling issues up to production logistics, the wider working environment of the grey-collar worker. Level 3 concerns analysis tools and optimization methods regarding warehouse management, e.g. container strategies, C-part management or driverless transport systems. Additional, Level 3 covers the changeover from intra-logistics to supply chain management, which is the key aspect of Level 4, with has topics such as vendor managed inventory. Level 5 examines tools and methods that do not only affect the production and leadership-specific aspects in logistics sector and theirs correlation to external suppliers but also organizational, financial and terms of Lean Management.

To support the learning, understanding and especially the application of the Lean Logistics content, additional tools have to be known and practiced. Therefore, the chapters "tools for project management & decision making", "quality management tools", "statistical tools", "graphical tools & visual management", "creativity tools" and "tools for customer management" have been integrated into the content framework for each level.

Considering required logistics tools and methods focused on work place (Figure 3), the basic knowledge subjects "mathematics" and "technics", were analysed and as a result correlated to Maturity Level 1. In this context the learning units "materials" and "material handling" as well as "basic calculating" were most frequently applied.

Additionally analysis of assignment supported the conclusion that the application of computer technology is not stringently necessary for process optimization and avoiding waste regarding the LOPEC logistics methods on Level 1.

From Level 2 on, wider working environment, more complexity and interface related tasks require additional software and communication tools. In consequence of this assumption and the following analysis of Lean Logistics and additional tools, the basic course "Informatics", for example including the learning units "software", "e-Mail", "IT security", was assigned to Level 2.

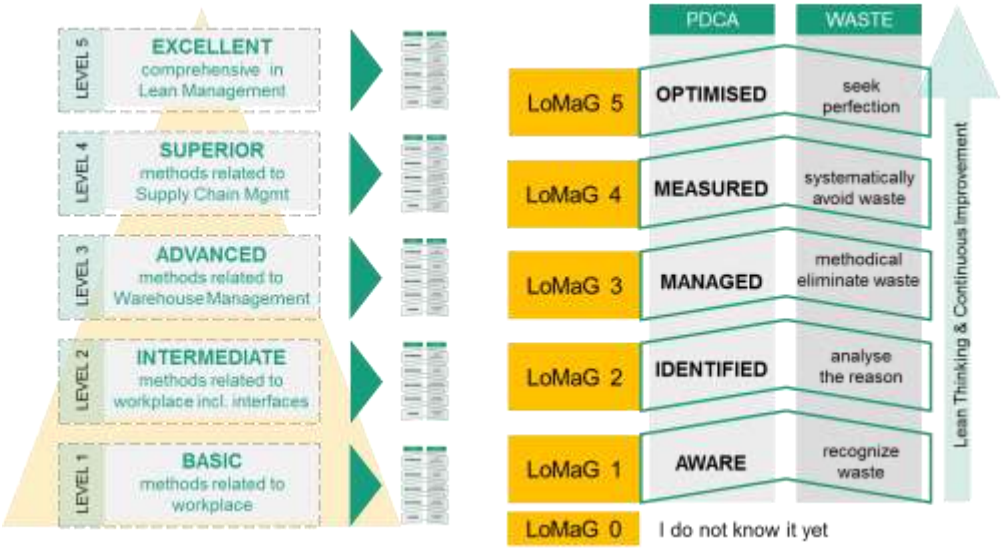

Figure 3. Maturity Excellence Levels in Lean Logistics and Logistics Maturity Grades (LoMaG)
Slika 3. Razine zrelosti izvrsnosti u Lean logistici i Ocjene logističke zrelosti (LoMaG)

Based on the focus "supply chain management" and in this context potentially persons of contact from abroad, an English skill of "B2" according to the "Common European Framework Language" (CEFR) is commended from Maturity Level 3. The present English skill should be proved by a certificate or comparable verification.

The current basic knowledge of the worker will be tested by single/multiple choice tests in Level 1 and 2.

4.2. Development of a Lean Logistics self-assessment (LOPEX) for continuous personal and professional development

Furthermore established logistics knowledge and skills have to be measured. The assessment procedure and the respective measurements covering all criteria must be developed to the appreciation level of a skilled worker to get short-term and long-term benefits towards life-long learning. A model was needed, that scales the achievement avoiding "waste" as essential point of Lean Logistics. Therefrom, the further way of proceeding is based on the PDCA-Circle by William Edwards Deming [18]. As result of the researched maturity models, a self-assessment ("LOPEX") with six Logistics Maturity Grades (LoMaG) was developed. Grade 0 means, that the worker doesn`t know the learning content/method yet. As a result of the adapted PDCA-Circle to Logistics Maturity Grades, the approach refers to "Aware" (Grade 1), "Identified" (Grade 2), "Managed" (Grade 3), "Measured" (Grade 4), "Optimized" (Grade 5).

Grade 1 and 2 indicate that the learner theoretically knows the learning content and that he or she can decide if the individual method or tool is relevant for his or her work place or production environment. The grades 3 to 5 measure the ability to apply and continuously optimize relevant methods by quantifying gained results in comparison to the previous ad hoc procedure.

To demonstrate the operative execution of the presented model, an example of a self-assessment question, using the Lean Logistics topic "clocked route traffic" [19], is following:

- LoMaG 0 – Unknown: "I am not familiar with this method."
- LoMaG 1– Aware: "Clocked route traffic is a method for production logistics."
- LoMaG 2 – Identified: "I can explain essential reasons for the usage of clocked route traffic."
- LoMaG 3 – Managed: "I can decide about static and dynamic routes and schedules as well as loading and unloading points."
- LoMaG 4 – Measured: "I can argue the advantages of clocked route traffic in comparison to single trips in our production."
- LoMaG 5 – Optimized: "I am involved in the optimization of cycle times, hauls and load trailers used."

The shop floor worker has to classify his or her knowledge and ability of application within the six grades. After choosing one grade, the assessment tool requires an argumentation or reference to validate the given answer.

Achieving Logistics Maturity Grade 4, which proves credits for further education, aiming at acquiring the needed recognition to enter a job-related bachelors program in logistics, requires the score of at least Logistics Maturity Grade 2 and overall sixty percent in each level.

4.3. Implementation of the LOPEC learning content into a Learning Management System

The developed learning units, modules and tests will be implemented in ILIAS, a web based Learning Management System (LMS). ILIAS meets all technical and didactical requirements for the application within LOPEC.

The developed LOPEC learning path can be easily transferred to ILIAS. Each course category will present one of the five Maturity Excellence Levels and contains the assigned Lean Logistics and basic knowledge learning units. The different roles and permissions for the LOPEC administrators, authors, trainers and learners are supported by a complex role and permission system. To monitor the learning progress numerous kinds of tests, especially single/multiple choice tests, can be implemented. Furthermore ILIAS is published under the General Public License and is free of charge.

ILIAS, as Learning Management System for the LOPEC solution, was also assessed in the validation by examination of the learning objectives, a survey of the skilled workers and trainers as well as a reflection process with the involved experts, the advisory board as well as industrial representatives.

5. Pilot-implementation case studies

To validate the systematic approach of the project, a pilot run was implemented in four regions (Austria, Croatia, Germany and Latvia) from March to June 2014. The piloting procedure contained the following milestones:

- Nomination of invited learners and selection of a trainer who supports the learner within the piloting organization,
- Setting up of a learning agreement, framework conditions and training targets between all stakeholders,
- Selection of relevant learning units within Lean Logistics Level 1 by the learner in agreement with the trainer,
- Review of selected units according to the defined priority,
- Start of optimization activities according to gained knowledge,
- Execution of self-assessments: LOPEX (and optionally PEX),
- Discussion of areas for personal and professional improvement between learner and trainer,
- Upgrade to next level, if one level is completed.

In Croatia, results of LOPEC have been implemented in two companies: Brodotrogir d.d. i Dalstroj d.d.

After restructuring process, Brodotrogir d.d. has been divided onto three parts based on three main business activities: shipbuilding, ship repair and marina & service. LOPEC was implemented for workers from shipbuilding and ship repair. Detail from training has been presented on Figure 4.

Dalstroj d.d. is a regional leader in the manufacturing of hydraulic, electrical and pneumatic deck equipment for the oil & gas industry, passenger and merchant navy, naval, scientific, research and other purpose vessels.

Training for both companies lasted for four weeks. Workers have been trained on 16 methods and tools from Lean logistic and basic logistic. In the first part of training workers have been introduced to basics of each method or tool, and after that they've tried to apply gained knowledge on problems from their daily work. Methods were implemented using team work, and that motivated workers and assured excellent results.

Few methods were accepted very well: Ishikawa diagram, Assembly game, Seven wastes, 5S, etc.

In the second part of training workers were tested using developed assessment methodology, i.e. LOPEX and LoMaG (Figure 3). It gave information how successful training was, and according to results it was very successful.

Figure 4. LOPEC training in company Brodotrogir d.d.
Slika 4. LOPEC obuka u poduzeću Brodotrogir d.d.

6. Conclusion

Logistics Personal Excellence by continuous Self-Assessment (LOPEC) educational goal system is based on the fundamental mind of Lean Thinking. It aims on training of grey-collar workers to have the ability to identify and to reduce waste until perfection. In addition, the LOPEC project team defined disciplines and tools that are essential for the development, implementation and evaluation of optimization tasks in regards of Lean Warehousing and Lean Supply Chain Management. Team also defined three more comprehensive goals (continuous improvement, customer focus and management, team work), that represent the basement of the LOPEC educational goal system, to achieve Operational Excellence.

Results of research on project LOPEC have been successfully implemented in Pilot-implementation projects in two Croatian companies. Considering implementation successful, further education is planned.

REFERENCES

[1] Eurostat: *National accounts by branches*. EU-27, 2009.

[2] Jovane, F.; Westkämper, E.; Williams, D. (2009): *The ManuFuture road: towards competitive and sustainable high-adding-value manufacturing*, Springer, Berlin Heidelberg.

[3] Werner, D. (2006): *Trends und Kosten der betrieblichen Weiterbildung*. Ergebnisse der IW-Weiterbildungserhebung, 2005 (IW-Trends Nr.1/2006).

[4] Abele, E.; Nyhuis, P.; Reinhart, G. (2008): *Wandlungsfähige Produktionssysteme: Heute die Industrie von morgen gestalten*, Verlag PZH Produktionstechnisches Zentrum, Garbsen.

[5] Meißner, S., Günthner, W. A. (20 09): *Lean Logistics: Ansatzpunkte der Gestaltung schlanker Logistiksysteme*, In ZWF: Zeitschrift für wissenschaftlichen Fabrikbetrieb 1 04.

[6] Borghans, L., Grip, A. (2000): *The Overeducated Worker? – The Economics of Skill Utilization*, Ed ward Elgar Publishing Limited, Glos.

[7] Editorial- Lifelong Learning & employability: *Lifelong learning in the Low Countries*. LLinE: Lifelong Learning in communication and citizen activity 2/2005. Europe Government

[8] Waters, D. (2003): *Global Logistics and Distribution Planning – Strategies for Management*, Kogan Page Limited, London.

[9] Throop, R., Castellucci, M. (2010): *Reaching your Potential – Personal and Professional Development*, Cengage Learning, Wadsworth.

[10] Wiese, B. (2004): *Individuelle Steuerung beruflicher Entwicklung – Kernkompetenzen Frankfurt/Main*. in der mordernen Arbeitswelt, Campus Verlag,

[11] Kalman, C., Liu, X. (2010): *Using and Developing Measurement Instruments in Science Education: A Rasch Modelling Approach*, Information Age Publishing, Charlotte.

[12] EFQM, 2012: *EFQM Excellence Model*, Brussels.

[13] Dalluege C.-A., 2012: *Exzellenz durch nachhaltige Unternehmensstrategien: EFQM im Mittelstand*, Haefner, Heidelberg.

[14] Lusthaus, C., Adrien, M., Anderson, G., Carden, F., Montalvan, G. (2002): *Organizational Assessmnet – A framework for Improving Performance*, International Development Research Centre, Washington.

[15] Dalluege, C.-A., Franz, H- W. (2011): *IQM – Integriertes Qualitätsmanagement in der Aus- und Weiterbildung: Selbstbewertung für EFQM, CAF, CIN EN ISO Bertelsmann*, Bielefeld. 9001/4 und andere QM-Systeme.

[16] Gleich, R.; Sauter, R. (2008): *Operational Excellence – Innovative Ansätze und Best Practices in der produzierenden Industrie*, Rudolf Haufe Verlag, München.

[17] Goldsby, T.; Martichenko, R. (2005): *Lean Six Sigma Logistics, Strategic Development to Operational Success*, J. Ross Publishing, Boca Raton, Florida.

[18] Geers, D.; Landgraf, K.; Jochem, R. (2010): Welchen *Beitrag leisten Reifegradmodelle bei der Qualitätsbewertung von Prozessen?* Jochem, R. (Hrsg.): Was kostet Qualität? Wirtschaftlichkeit von Qualitätermitteln, Hanser Verlag, München, S. 113-142.

[19] Günther, W., Durchholz, J., Klenk, E., Boppert, J. (2013): *Schlanke Logistikprozesse*, Springer Verlag, Berlin Heidelberg.

ISSN 1847-7917

Advanced solution for energy storage in net zero-energy buildings

Jaroslav JERZ [1)]**,**
František SIMANČÍK [1)]
Ľubomír OROVČÍK [1)2)]

1) Institute of Materials & Machine Mechanics, Slovak Academy of Sciences, Račianska 75, 83102 Bratislava 3, **Slovakia**
2) Faculty of Materials Science and Technology STU, Paulínska 16, 917 24 Trnava, **Slovakia**

ummsjerz@savba.sk

Keywords

energy efficiency,
zero-energy buildings,
advanced technologies,
aluminium foam,
heating/cooling panels,
phase changing material,
combined heat and power unit

Professional article

Abstract: Institute of Materials & Machine Mechanics (IMSAS) possesses the unique experience in the field of production heating/cooling wall and ceiling panels based on aluminium foams for future autonomous houses and buildings. These novel heating/cooling panels have been developed and successfully tested in pilot application in 260 m^2 open space office room. The low heat capacity of aluminium foam allows changing the temperature very quickly, whereas the temperature of the entire foam volume is always very uniform due to excellent thermal conductance of aluminium cell walls. The heat is transferred into or from the foam using foamed-in tubes, which are completely embedded in the foam, keeping excellent contact to cell wall aluminium. Good thermal conductance of the foam resulted in short length of embedded tubes, what is beneficial for low flow resistance and necessary pumping systems. The foamed panels can be partially impregnated at facing side by appropriate plaster, which improves the appearance and also serves as an absorber of potentially condensed air humidity. The developed panels provide an excellent alternative for large built-in ceiling radiators for efficient heating or cooling of rooms using low potential energy resources. The most appropriate ways of using these panels, which are able extremely to increases energy-efficiency in buildings has been outlined in this contribution. Moreover, patent pending technical solution based on simple Combined Heat and Power (CHP) unit for storage/dissipation of thermal energy equipped with mechanical system simultaneously produced the electricity covering partially the needs of the house using lifting force of compressed hot/cold air, are firstly introduced to scientific community in this article.

1. Introduction

The future energy systems providing its supply to houses and buildings will be surely based on entirely CO_2-free energy production. The development of energy storage and supply technologies should lead to economy based entirely on emission-free and inexhaustible energy sources, such as a solar, wind or geothermal.

The electricity and energy efficiency to produce it will play still quite a long time an important role in fulfilling constantly growing global energy demand. The challenges of sustainability, such as climate change, diminishing natural resources and further negative environmental effects necessitate a transition from power production based on the use of limited energy sources obtained from fossil fuel combustion to the more efficient energy systems with significantly lower emissions. The future economy will utilise the sun's energy either directly as solar power or heat or indirectly as hydro, wave and wind energy, bio energy and geothermal heat. The future eco-cities will be based on smart grids with eco-efficient construction utilizing exclusively ecological engineering materials, sustainable methods of energy production, transportation and storage as well as various advanced energy efficient heating/cooling solutions.

2. Net zero-energy buildings

Generelly, a net Zero-Energy Building (nZEB) is a building with greatly reduced energy needs through efficiency gains such that the balance of the energy needs can be supplied by renewable technologies [2]. The building connected to a district energy system which receives high temperature heat as well as electrical energy and provides heat in the same quality (exergy) at a lower temperature and at the same quantity of electrical energy to the district, is not balancing the exergy of heat it receives and provides. This building is still impacting the environment because

the negative exergy balance must be made up by the district at a cost of additional fuel spending and harmful emission even though energy amounts of the heat and power flow across the building district boundary are balanced. If the district generates power in the thermal power plant, and the building generates electric power in a micro-Combined Heat and Power (CHP) unit supported by using wind turbine, all have different environmental impacts and exergy. Therefore a Zero-Energy Building (ZEB) can be defined as a building, which has a total annual sum of zero exergy transfer across the building-district boundary in a district energy system, during all electric and any other transfer that is taking place in a certain period of time (A. J. Marszal and P. Heiselberg; 2011, [9]). In concept, energy needs for nZEB are greatly reduced through efficiency gains such that the balance of the energy needs can be supplied by renewable technologies. A nZEB optimally combines commercially available renewable energy technology with the state of the art energy efficiency construction techniques. There are no fossil fuels consumed in nZEBs and its annual energy consumption only slightly exceeds annual energy production.

EU has adopted these concepts to define energy saving and climate-change goals within the building sector. This topic is addressed in the continuation of the Energy performance in buildings directive of the EU [1]. ZEB has become by this way a general terms covering efforts significantly to improve the energy efficiency of buildings. According to Article 9 of the Directive 2010/31/EU of the European Parliament and of the Council of 19th May 2010 on the energy performance of buildings, even prescribes that in the end of 2020 should all member states of EU ensure that all new buildings are nearly ZEB, i.e. buildings that have a very high energy performance and nearly zero of very low amount of energy required should be covered to a very significant extent by energy from renewable sources, produced mainly on-site or nearby. The member states of EU shall furthermore, following the leading example of the public sector, develop policies and take measures such as the setting of targets in order to stimulate the transformation of buildings that are refurbished into nZEB, and inform the EC thereof in their national plans.

While fully energy-autonomous buildings – those not connected to an external energy infrastructure – the on-site energy systems (solar, wind and geothermal) as well as systems for energy storage must be dimensioned to guarantee the uninterrupted energy supply, the goal for nZEB is a neutral result for an energy or emission balance over the period of one year. This goal refers to calculated result for the balance between demand or consumption values and electricity fed into the grid. Interaction with an existing energy infrastructure is decisive to balance the energy supply and demand, both in terms of quantity and often also concerning the form of energy. The climatic condition in the Europe causes that seasonal compensation plays the dominant role from the energy point of view, whereas short-term equilibrating processes are most important regarding power. Seasonal storage within the building was unfortunately up to now deliberately omitted from the concept for nZEB. In particular, this could not be recently implemented rationally, as batteries are not suitable and building-integrated hydrogen systems are far from technical maturity [8], i.e. their excessively high price is today the main obstacle for their application and subsequent mass expansion in world markets. However, the feature that the nZEBs share with energy-autonomous buildings is the balanced energy budget, not just the low energy consumption as in the case of passive buildings.

Of course, that achievement of zero balance with solar energy alone causes in most cases unreasonably high costs for the purchase of required energy producing and storage systems. The significant use of wind power directly at the building is also limited to a few special cases. However, the co-generation (CHP) units integrated into the building energy systems are much more promising, specifically when they are based on renewable energy sources. They provide a number of new advanced technical solutions, one of which, based on the simultaneous utilization of geothermal heat obtained continuously from the earth's crust in the immediate vicinity of the building, is presented in the Section 5 of this contribution.

3. CO_2 reduction by CHP units

In countries with cold climate, space heating is a major energy consumer and thus a significant source of greenhouse gas emissions, i.e. emissions of any gases whose absorption of solar radiation is responsible for the greenhouse effect, including carbon dioxide, methane, ozone, and the fluorocarbons. CHP units as well as ground source heat pumps are generally seen to be among the best alternatives to reduce greenhouse gas emissions of space heating [10].

If CHP production is reduced due to heat pumps, the replacing electricity production would be mainly coal or gas (and with minor share peat or wood) condensing with the present fuel and CO_2 prices. The same situation remains both in the short and the mid-term, if climate policy is not dramatically stricter than at present. This statement for future can be justified by two aspects:

- ✓ For now, 50% of European electricity production is based on coal or gas condensing. These production methods have the most expensive marginal costs and thus are run up or down first when the consumption changes.
- ✓ In the future, it is very unlikely that peak loads caused by electrical heating or heat pumps are covered by nuclear or composite current source power due to their high investment costs. Wind and solar electricity production need regulating power.

Additionally, there is not enough hydropower for the whole Europe to level the diurnal, not even to talk about seasonal variation.

CHP is a very good alternative, when it replaces fossil-fuelled condensing power. The more of the time it does this, the better it is in terms of CO_2 emission reduction. The choice of heating system is not only dependent on economical rationality. There is normally only one district heating supplier in some specific area. To maintain the customer's trust, feeling of empowerment and freedom of choice, there should be e.g. different billing alternatives (although preferably cost-correlated as exactly as possible), active client hearing and openness in every sense. These could help to make the district heating system feel like the customer's own and flexible [10].

4. Energy storage technologies

The energy storage industry has continued recently to evolve and adapt to changing energy requirements and advances in technology. Energy storage systems suitable for future buildings and small houses provide a wide array of technological approaches to managing our power supply in order to create a more resilient energy infrastructure and bring cost savings to utilities and customers. Practically, 6 basic manners of energy storage are available at present:

- ✓ ***solid state batteries and supercaps*** – a range of electrochemical storage solutions, including advanced chemistry batteries and super capacitors,
- ✓ ***flow batteries*** – batteries where the energy is stored directly in the electrolyte solution for longer cycle life and quick response time (the rechargeability is provided by two chemical components dissolved in liquids contained within the system and most commonly separated by a membrane),
- ✓ ***flywheels*** – mechanical devices that harness rotational energy to deliver instantaneous electricity (flywheels employ kinetic energy stored in a rotating mass with very low frictional losses),
- ✓ ***compressed air energy storage*** – utilizing compressed air to create a potential energy reserve (energy generated during periods of low energy demand can be released to meet higher demand periods),
- ✓ ***thermal*** – capturing heat or cold to create energy on demand (thermal energy storage systems stock thermal energy by heating or cooling a storage medium so that the stored energy can be used at a later time for heating/cooling applications and power generation, they can help balance energy demand and supply on a daily, weekly and even seasonal basis, reduce peak demand, energy consumption, CO_2 emissions and costs, if their overall energy efficiency is increasing).
- ✓ ***pumped hydro power*** – creating large-scale water reservoirs of energy (a hydroelectric dam relies on water cascading down through the turbines to create electricity to be used on the grid). The case study of this technology is shown in Fig. 1.

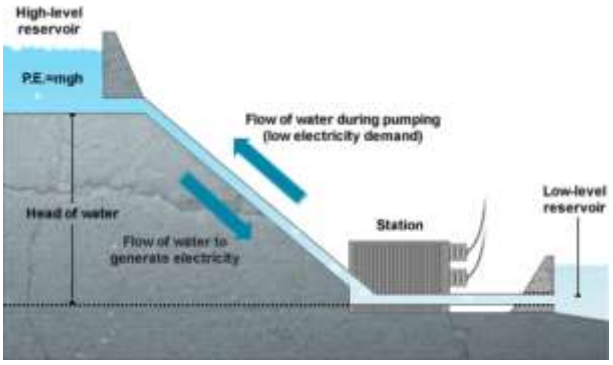

Figure 1. The case study by which an American wind power produced in North Dakota is stored by hydro "battery" in Manitoba's (Canada) hydro reservoir [12].

Energy from batteries is most expensive in terms of cost per kilowatt-hours (kWh). Improved runtimes, lower unit price and the convenience of recharging have shifted many portable applications previously reserved for primary batteries to rechargeable batteries. Table 1 compares the cost of power with rechargeable batteries. The cost is based on battery price and the number of possible discharge/charge cycles. The analysis does not include electricity for charging or the cost of purchasing and maintaining charging equipment. The table compares commercial battery packs used for communications, computing or medical devices. Older technologies have lower cost per kWh than newer systems.

Table 1. Energy and cost comparison using rechargeable batteries [14]

	Lead Acid	NiCd	NiMH	Li-ion
Capacity [mAh]	2,000	600	1,000	1,200
Battery voltage [V]	12	7.2	7.2	7.2
Energy per cycle [Wh]	24	4.5	7.5	8.6
Number of cycles	250	1,000	500	500
Battery cost [$US]	50	50	70	100
Cost per kWh [$US]	8.5	11.0	18.5	24.0

With dwindling fossil fuel supply associated with the need to reduce greenhouse gas emissions, governments as well as the private sector are beginning to focus on alternate energies. If we compare the cost to generate 1 kW of power by taking into account the initial investment, adding the consumption of fuel and including the eventual replacement of the system, power from the electrical utility grid is most cost-effective (consumers in industrial countries pay between $0.05 and $0.25US per kWh of energy and typical daily energy consumption per household is about 25 kWh) [14].

Flow batteries, such as vanadium redox flow batteries, are attractive due to their very long lifetimes even under consistently high discharge depths, their good scalability and their flexibility in managing power and storage capacity separately. They are generally not suitable for small-scale applications, however, and are therefore targeted more towards grid-scale energy storage. Drawbacks include fairly average round-trip efficiencies and significant costs for their operations and maintenance [15].

The company Aquiron Energy Inc. founded in 2008 by Prof. Jay Whitacre from Carnegie Mellon University in Pittsburgh, Pennsylvania (USA) developed patented [16] Aqueous Hybrid Ion (AHI™) battery technology which provides high performance, safe, sustainable and cost-effective energy storage for a diverse range of stationary applications. Using abundant, nontoxic materials (such as manganese oxide, sodium sulphate, carbon and cotton) and modern low cost manufacturing techniques, AHI™ batteries are ready to take on the global energy storage challenge.

Nevertheless, the excessively high price of batteries and building-integrated hydrogen storage systems is today the main obstacle for their application in small nZEB. The potential to reduce the energy consumption of small family house by storing energy obtained by renewable sources directly in house or in its immediate vicinity is therefore extremely hard achievable target if batteries, flywheels or hydrogen systems are used for this purpose. The energy storage systems based on compressed air energy storage, thermal storage as well as pumped hydro power storage seem to be unavoidable in order to have return-on-investment period below ten years in the case of small nZEB.

5. Heating and cooling of energy efficient buildings

The most convenient way how to decrease energy demands in the buildings is the utilization of renewable energy sources – the solar, wind or geothermal one. A main drawback of the solar source is its irregularity whereas it produces a lot of excess heat during the peak time and during the night. This excess heat is almost not possible to use. In case of cooling, it is an issue to eliminate overheating from the solar during the day what also requires additional energy inputs. That is why it is important to focus on development of new systems which will be able to cover these natural energy fall-outs by storing and subsequent later evolving the accumulated heat or cold according to the day-night cycle.

The thermal energy can be stored in standard buildings into massive inserts (i.e. clay bricks), but only sensible heat can be stored and the massive materials evolve this heat only in hand with continuously change of their temperature in this case. The sensible heat can also be stored also if the Phase Change Materials (PCMs) are used for thermal energy storage. However, their most important property is the phase change solid-liquid and vice versa at the temperature range between 23°C and 28°C. During this change a lot of latent heat is evolved or absorbed at almost constant temperature. The utilization of PCMs in larger volumes is strongly limited because of its low thermal conductivity. In this case solidification starts on the surface creating thus an isolating solid crust. That is why there is a need to combine PCMs and porous materials with higher thermal conductivity. Small empty pores can be filled with PCMs what ensures phase change in whole volume without creation of the isolating solid crust.

The aluminium foam panels made by foaming of foamable precursor with stainless tubes embedded in the structure of foam are therefore promising solution for energy efficient heating and cooling of walls/ceilings in interiors of buildings. The huge application potential mainly in the building and shipbuilding industry is expected thanks to their quick response to temperature changes due to excellent heat conduction of porous aluminium structure, lightweight design, self-supporting capability as well as shape and surface flexibility. The large active surface of foamed panels with extremely quick response to temperature changes enables to use heating/cooling fluids with the temperature nearly the same as is the achieved and maintained room temperature of interior air. This allows utilize various available alternative energy resources such as solar or geothermal energy very effectively for heating during winter, or even simply cold air during summer nights for cooling. The ceiling panels made of aluminium foam (fig. 2) supplemented with system containing the heat storage reservoir enables significantly to increase energy efficiency of interior heating and cooling. Moreover, this system enables to spend or release into the interior certain amount of heat at constant temperature in the case that aluminium foam is filled with PCMs melting or solidifying at desired temperature. This feature makes possible in combination with smart temperature control systems further energy cost savings for heating/air conditioning systems of future nZEB.

The patent application (PP 5040-2013, Inventors: J. Jerz and M. Bartko) "The method of operation of energy-autonomous buildings and power equipment" filled in December 2013 describes advanced technical solution for significant reduction of energy required for heating and air-conditioning of small nZEBs (fig. 3). According to this invention, the portion of the excess energy obtained from renewable sources is stored in the form of compressed hot/cold air in small heated/air conditioned room built in the close vicinity of the building above the well equipped with mechanical system connected to an electric power generator. The abovementioned mechanism submerged below the surface of the well is a small CHP unit able not only effectively store/dissipate the thermal energy into the

water in the well, but also to produce the electricity covering partially the needs of the building using lifting force of compressed hot/cold air released from the bottom of the well. The walls of the well are due to sufficient conduction of geothermal heat from earth crust jacketed by hollow aluminium profiles with cavities filled by PCMs according to this patent pending technical solution.

In order to test the various methods for production, transfer and consumption of energy obtained from renewable sources a Smart Grid laboratory (fig. 4) equipped with 29 kW photovoltaic power plant, concentrated thermo-solar panels, heat pumps for conversion of geothermal energy from four drilled 100 m deep drill holes, heat storage vessels and advanced control units has been built recently in the experimental hall of IMSAS in Bratislava. For IMSAS this creates an extraordinary possibility to build up the unique competency in this rapidly developing and very important research field. The orientation of future institute's research activities towards the research on advanced materials for the efficient use of renewable energy is thus foreseen.

6. Conclusions

The aluminium foam heating/cooling panels allows changing the temperature of interiors very quickly thanks to their low heat capacity, whereas the temperature of the entire foam volume is always very uniform due to excellent thermal conductance of aluminium cell walls. The panels provide an excellent alternative for large built-in ceiling radiators for efficient heating or cooling of rooms using low potential energy resources. Porous structure of aluminium foam allows evolve or absorb latent heat at almost constant temperature if pores are filled by PCMs with phase change at the temperature range between 23°C and 28°C. These features of aluminium foam panels in combination with smart temperature control systems allow significantly reduce energy consumption for heating/air conditioning systems of future nZEB. The energy storage systems based on compressed air energy storage, thermal storage as well as pumped hydro power storage seem to be unavoidable in order to have return-on-investment period below ten years in the case of energy efficient small family houses.

The invention "Method of operation of energy-autonomous buildings and power equipment" (PP 5040-2013) supports commercialization of advanced metallic materials utilized for significant reduction of energy needs and consumption in energy efficient buildings. This technical solution has a great potential to become the breakthrough by significant reduction of energy costs for building heating and air-conditioning and thus in the case of its successful commercialization may indicate the considerable shorten of the payback period for investment costs especially in the case of net zero energy small family houses.

7. Acknowledgements

The article was elaborated within the financial support of European Regional Development Fund under the project "ITMS 26240220028 – Efficient controlling of the production and consumption of energy from renewable sources (ENERGOZ)".

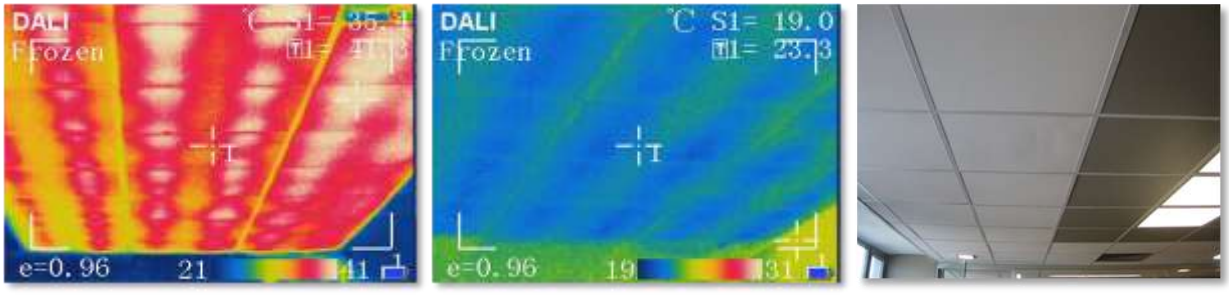

Figure 2. Distribution of temperature fields in the ceiling heating/cooling panels of aluminum foam captured using thermovision camera during heating (left) and cooling (center) in the open office space area 260 m^2 of company Sapa Profiles in Žiar nad Hronom, Slovakia.

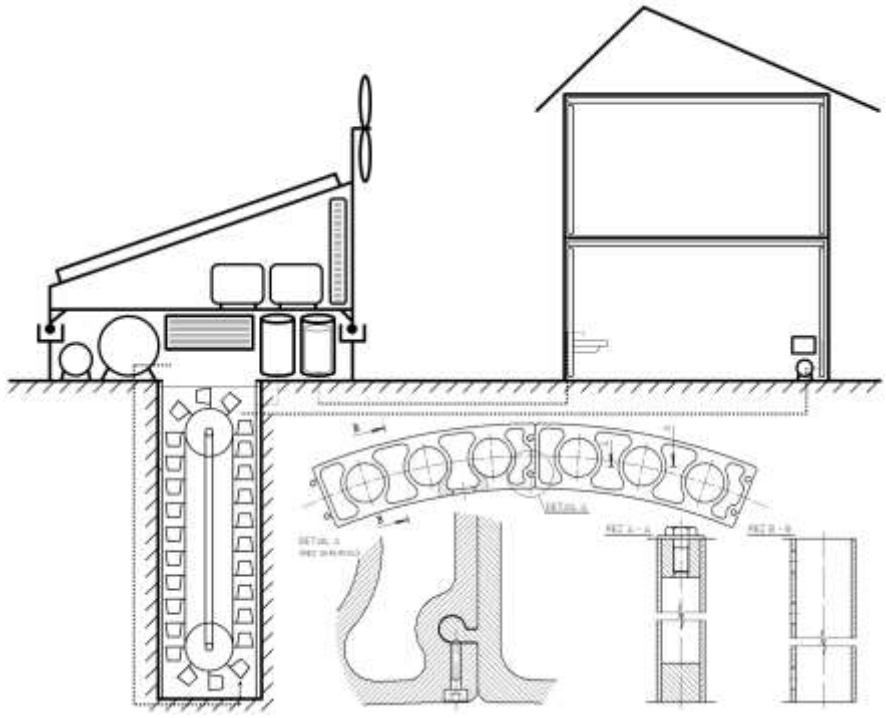

Figure 3. The illustration of basic principle of patent application (PP 5040-2013) of the invention "The method of operation of energy-autonomous buildings and power equipment" filled on 18th December 2013 in Slovakia.

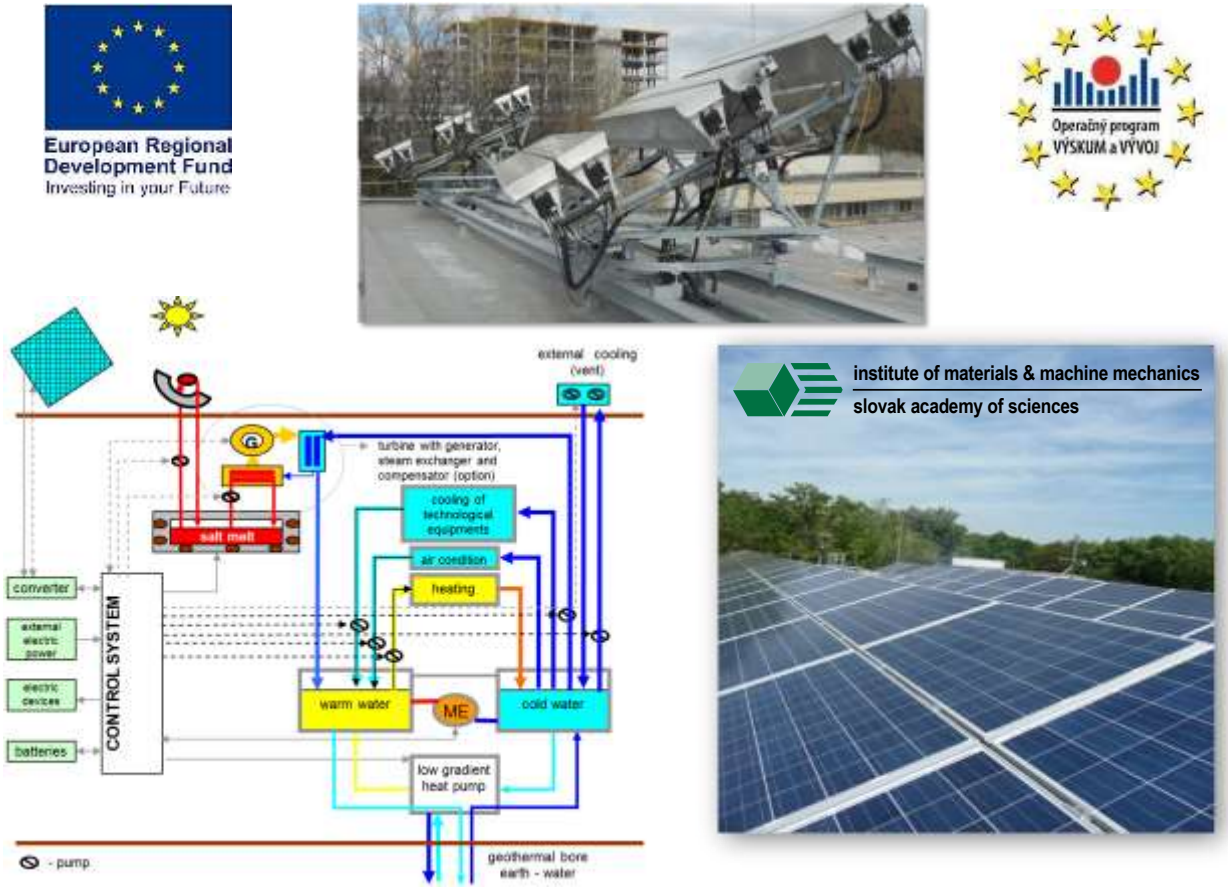

Figure 4. Smart Grid laboratory equipped with 29 kW photovoltaic power plant established in the experimental hall of IMSAS in Bratislava.

REFERENCES

[1] The Directive 2010/31/EU of the European Parliament and of the Council of 19th May 2010 on the energy performance of buildings, Official Journal of the European Union, 53 (2010)

[2] TORCELLINI. P. – PLES, S. – DERU. M. CRAWLEY, D. Zero Energy Buildings: A Critical Look at the Definition, ACEEE Summer Study, Pacific Grove, California, August 14−18, 2006 http://www.nrel.gov/sustainable_nrel/pdfs/ 39833.pdf

[3] JERZ, J. Research, Development and Technology Transfer (R & D & TT) in the Field of Engineering Materials and Related Technologies, Advances in Technology, Education and Development, Wim Kouwenhoven (Ed.), 2009. ISBN: 978-953-307-011-7, INTECH, available from: http://sciyo.com/articles/show/title/research-development-and-technology-transfer-r-amp-d-amp-tt-in-the-field-of-engineering-materials-an.

[4] JERZ, J. - WILFINGER, B. – HULA, R. C. - IŽDINSKÁ, Z. Knowledge management strengthens development of innovative products with extremely high added value. In ICERI Madrid 2011: *4th international conference of education, research and innovation*. ISBN 978-84-615-3324-4.

[5] JERZ, J. - OROVČÍK, Ľ. - WILFINGER, B. - HULA, R. C. Effective knowledge transfer of advanced technologies for production on innovative engineering materials into industry. In INTED 2012: *6th international technology, education and development conference*. - Valencia: IATED, 2012. pp. 0737-0745. ISBN 978-84-615-5563-5.

[6] JERZ, J. – WILFINGER, B. – HASENAUER, R. – FILO, P. – LAZAROVÁ, M. – TOROUD, T. Market entry of innovative products using

knowledge acquired by materials science and engineering. In INTED 2013: *7th international technology, education and development conference.* - Valencia: IATED, 2013, pp. 1378-1386. ISBN 978-84-616-2661-8

[7] LUNDSTRÖM P. – KANKAANPÄÄ, K. – REHELL, U.. CO_2-free energy production Fortum's long-term aspiration, http://www.fortum.com/en/mediaroom/pages/co2-free-energy-production-fortums-long-term-aspiration.aspx

[8] VOSS, K. – MUSALL, E. – LICHTMESS, M. From low-energy to net zero-energy buildings: Status and perspectives, In Journal of Green Building, 2011, Volume 6, No. 1, pp. 46 - 57 http://www.enob.info/fileadmin/media/Projektbilder/EnOB/Thema_Nullenergie/Journal_of_green_Building_FROM_LOW-ENERGY_TO_NET_ZERO-ENERGY_BUILDINGS.pdf

[9] MARSZAL A. J., HEISELBERG P., Zero Energy Building definition – a literature review, Aalborg University, Denmark, 2011, http://task40.iea-shc.org/data/sites/1/publications/T40A52-STA-Marzal-Report-2012-09.pdf

[10] RINNE S., SYRI S., Heat pumps versus combined heat and power production as CO_2 reduction measures in Finland, In Energy 57 (2013) pp. 308-318, http://dx.doi.org/10.1016/j.energy.2013.05.033

[11] http://energystorage.org/energy-storage/energy-storage-technologies

[12] http://nenmore.blogspot.sk/2014_02_01_archive.html

[13] http://www.irena.org/DocumentDownloads/Publications/IRENA-ETSAP%20Tech%20Brief%20E17%20Thermal%20Energy%20Storage.pdf

[14] http://batteryuniversity.com/learn/article/cost_of_power.

[15] http://theenergycollective.com/schalk-cloete/421716/seeking-consensus-internalized-costs-energy-storage-batteries

[16] WHITACRE J., HUMPHREYS D., YANG W., LYNCH-BELL E., MOHAMED A., WEBER E., BLACKWOOD D., US Patent 8298701, Aqueous electrolyte energy storage device, http://www.google.com/patents/US8298701

[17] http://en.wikipedia.org/wiki/Aquion_Energy

Investigation of cutting parameters influence during milling process applying cold compressed air

***Sonja JOZIĆ*[1)], *Dražen BAJIĆ*[1)] *Mario DRAGIČEVIĆ*[2)]**

1) University of Split
Faculty of Electrical Engineering
Mechanical Engineering and Naval Architect, R. Boškovića 32, Split,
Croatia

2) University of Mostar
Faculty of Mechanical Engineering and Comper Science
Matice hrvatske b.b.
88 000 Mostar
Bosnia and Hercegovina

sonja.jozic@fesb.hr;
drazen.bajic@fesb.hr;
mario.dragicevic@sve-mo.ba

Keywords

Alternaive types of cooling
Sustainable development
Vortex tube
Milling

Ključne riječi

Alternativne metode hlađenja
Održivi razvoj
Vrtložna cijev
Glodanje

Original scientific paper

Abstract: Cutting fluids are necessary for implementation of metal machining process. They have a huge impact on the tool life cycle, reducing the temperature in the cutting zone, elimination of separated chips and improvement of the product quality. Using of cutting fluids results in increase of the production cost and in detrimental impact on the environment and human health. Due to the reduction of negative impacts and implementation of environmental laws, the industry is forced to reduce the use of coolants. Alternative types of cooling in combination with new materials for making tools and special coatings represent an appropriate replacement of the cutting fluid. In this paper the influence of cutting parameters (cutting speed v_c, radial depth of cut a_e, feed per tooth f_t) on the surface roughness in the procedure of end milling along with dry machining, the use of emulsion cooling and compressed air cooling will be examined. Based on the change of input parameters, a decreasing and increasing trend of the surface roughness will be shown graphically.

Izvorni znanstveni rad

Sažetak: Sredstva za hlađenje, ispiranje i podmazivanje (SHIP) su neophodna za provedbu procesa strojne obrade metala. Ona imaju veliki utjecaj na životni vijek alata, smanjenje temperature u zoni rezanja, uklanjanje odvojene čestice i poboljšanje kvalitete proizvoda. Uporaba SHIP-a ima za posljedicu povećanje troškova proizvodnje, štetan utjecaj na okoliš i zdravlje čovjeka. Zbog smanjenja negativnih utjecaja i primjene zakona o zaštiti okoliša, industrija je primorana smanjiti upotrebu sredstava za hlađenje, ispiranje i podmazivanje. Alternativne vrste hlađenja, novi materijali za izradu alata i specijalne prevlake predstavljaju odgovarajuću zamjenu sredstvima za hlađenje, ispiranje i podmazivanje. U radu će se istražiti utjecaj parametara obrade (brzina rezanja v_c, radijalna dubina rezanja a_e, posmak po zubu f_t) na hrapavost obrađene površine pri postupku obodnog glodanja uz suhu strojnu obradu, upotrebu hlađenja emulzijom i hladnim komprimiranim zrakom. Na temelju promjene ulaznih parametara grafički će biti prikazan trend pada i rasta hrapavosti obrađene površine.

1. Introduction

One of the most frequently used procedure of metal processing in manufacturing industry is machining. Machining is performed on machine tools, which aim to, besides better productivity and efficiency, to get a high quality product as well. Machining represents tribological system in which tribological pair consists of cutting tool and workpiece. On a relatively small contact area tool-workpiece, very strong forces and cutting resistance appear, high specific pressures and temperatures are created, what causes tool wear. Having in mind that toll wear brings loss in machining, experts are forced to search for the possible solutions in order to cut down it. Just because of these reasons cutting fluids (CFs) are introduced in machining processes in order to improve previously mentioned characteristics which are appearing on contact areas tool-workpiece. Aside from cutting parameters, the CFs give a big contribution to the quality of the final product and lifetime of the tools. The use of CFs influences directly on the temperature dropping in the cutting zone, after which rapid occurrence of tool wear is decreased, and the quality of machined surface is increased. Besides from the fact that better conditions of machining process are improved by the right choice of CFs, there is also the possibility for the high speed machining and the hard machining, what can influence on abetment and using of new technologies and machining processes. Depending on the type of operation during machining process it is possible to distinguish different types of CFs, from simple oils to different water-based agents. Industrialization is limited by the legal framework, and it is forced to pay attention to ecological awareness development. Due to reduction of negative impacts on human health, water pollution and environment pollution, industry is forced to seek for the new technological solutions, so it is directing to dry machining. During dry machining, the tool is exposed to

Symbols/Oznake

CFs *SHIP*	- cutting fluids - Sredstva za hlađenje, ispiranje i podmazivanje	*fz*	- feed rate per tooth mm/z - posmak po zubu
v_c	- cutting speed, m/min - brzina rezanja	*Ra*	- Average surface roughnes, µm - Srednje aritmetičko odstupanje profila
a_e	- depth of cut, mm - radijalna dubina rezanja		

large mechanical, heating and chemical loads, which influence enhanced tool wear directly. Tools for dry machining should be designed specially in order to enable high heating resistance and minimum friction in the contact area tool-workpiece. Compensation of all functions vanished by eliminating CFs from the machining process is enabled by tools made of new materials, using tools with different coatings and trough alternative types of cooling.

2. Sustainable development

The idea of sustainable development grew from numerous environmental movements in earlier decades and was defined in 1987, by the World Commission on Environment and Development. The concept of sustainable economic development is that, form of economic development which aims to meet the needs of present consumption does not compromise or prejudice those of future generations. The Lowell Center for Sustainable Production (LCSP) defines sustainable production as the creation of goods and services using processes and systems that are non-polluting, conserving energy and natural resources, economically viable, safe and healthful for employees, communities and consumers. The environmental movement needs to address the global problems associated with climate change, global warming, depletion of natural resources, population growth, etc. The concept of sustainable production emerged at the United Nations Conference on Environment and Development in 1992 and is a key component of sustainable development, which balances three principal requirements: the social, economic and environmental objective, figure 1.

Achieving sustainable development will require changes in industrial processes, in the type and quantity of resources used, in the treatment of waste, in the control of emissions CO_2, and in the products produced [1]. During this critical time, an advanced manufacturing mode called green manufacturing (GM) as become popular as a sustainable development strategy in industrial processes and products [2]. GM is a modern manufacturing strategy integrating all the issues of manufacturing with its ultimate goal of reducing and minimizing resource consumption and environmental impacts like waste and pollution, during a product life cycle.

Figure 1. Sustainable Development Model

Slika 1. Model održivog razvoja

One of the most important manufacturing processes is the machining process. Machining process is constituted of major manufacturing activities which contribute the growth of the global economy. On the one hand, the research and development in the machining process have improved machining performance through greater productivity and quality by dint of advanced tool materials, while on the other hand through alternative types of cooling, environmentally and health friendly technologies are becoming increasingly important for achieving more environmentally acceptable, healthier, and safer machining [3, 4].

3. Alternative Types of Cooling

Alternative types of cooling are ecologically more acceptable than previously used cutting fluids. Appliance of alternative types of cooling is exclusively looked trough cutting parameters improvement with regard to conventional types and dry machining. In alternative types, water vapor could be used as cutting

fluid. Besides water vapor, some others types of cooling in combination with cold air with minimum quantity of MQL oil particles, cryogenic cooling as well as cold compressed air cooling are developed [5].

3.1. Minimum Quantity Lubrication and cooling in machining process

As its name implies, MQL endeavors to decrease quantity of liquid which is used in the cutting process. MQL method contains vegetable oils; therefore it is more ecologically acceptable. The control of MQL system is assured by control units (valves). It is necessary to assure proper regulation and needed air and oil quantity ratio in the system. The advantage over cutting fluids which are based on different emulsions in combination with oil has cryogenic cooling technique, which aims to accomplish better conditions (parameters) in machining process [6].

3.2. Cryogenic cooling in machining process

Cryogenic machining process implies the use of cryogenic fluids as cutting fluids. Liquid nitrogen is considered to be one of the most acceptable solutions of cryogenic machining. Nitrogen does not burn or support burning, it is lighter than air and it is hardly water-soluble. It is applied in liquid state at the temperature of -196°C and it is main cause of creating coldness in the zone in which it is applied because it absorbs heat [7]. Liquid nitrogen evaporates and forms protective coating, acting as lubricant. Advantage of liquid nitrogen cooling is seen trough decreased impacts on tool wear which prolongs the tool life cycle. Considering that liquid nitrogen decreases heat effect in the cutting zone significantly, quality of the machined surface. Friction is reduced in contact tool-processing item, what results with the reduce of cutting forces. Primary disadvantage is the high price of the system itself and its maintenance [8].

3.3. Cooling process with the use of cold compressed air

By the use of cold compressed air as a cutting fluid, it is possible to significantly decrease the total cost of manufacturing with relatively low cost of investment. Cold compressed air, as a cutting fluid, has a good characteristic of heat scattering in contact area tool-processing item, cooling of tool and processing item, as well as elimination of separated chips. From the effectiveness point of view, it reduces manufacturing costs, and it has no detrimental impact on the environment and human health. Cooling process with the use of cold compressed air is performed by vortex tube, also known as Ranque-Hilsch vortex tube, figure 2 [9,10].

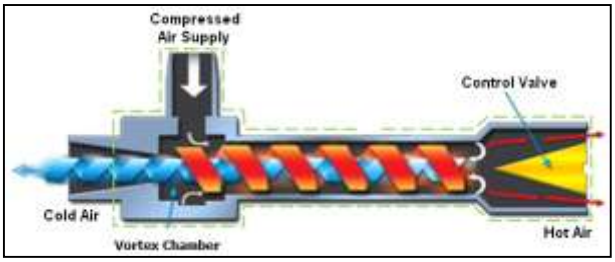

Figure 2. The Ranque-Hlisch Vortex Tube

Slika 2. Ranque-Hilsch vrtložna cijev [9]

The working principle of the Ranque-Hilsch vortex is based on the separation of incoming compressed air on two streams, the hot one and the cold one. Cold air stream leaves vortex through the central orifice diaphragm next to the inlet plane. In the same time, hot stream exits vortex through control valves at the far end of the tube. High appliance of vortex is based on its simplicity, compactness, as well as the fact that system itself has small mass and exceptionally quiet mode. The research results show that the advantage of using the vortex is extent of tool life cycle, decrease of temperature impacts and higher quality of machined area. Considering that the cooling media is cold compressed air, the procedure is considered to be the cleanest, and from the ecological point of view, the most acceptable method of cooling in machining process [11].

4. Experimental Research

The goal of the experiment is to try to determine dependence of the surface roughness on the particular influential factors based on a former literary research in the milling process. The experiment is performed on the vertical machining centre CNC SPINNER VC560 which uses software support of SINUMERIK 810D of the manufacturer SIEMENS. While performing the experiment, face and circumferential cutter COROMILL 390 cutting diameter 20 mm, product code R390-020A20-11M with three inserts code R390-11 T3 08M-PM. The symbol of insert quality is GC (Grade Coromant) 1025. Material of the workpiece is steel 42CrMo4. Dimensions of the workpiece are 250 × 110 × 110 mm, and chemical composition is shown in the table 1. Cooling process with the use of cold compressed air is enabled from the compressed air network with the device Cold Air Gun of the manufacturer Vortec. The surface roughness is measured by a device Mitutoyo SJ-301. The accuracy of this device is 0.01μm, all measurements are five times repeated, so the final result is measuring mean value.

Table 1. Chemical Composition of the processing item

Tablica 1. Kemijski sastav obradka

CHEMICAL COMPOSITION %								
C	Si	Mn	P	S	Cr	Ni	Mo	Cu
0.430	0.278	0.77	0.018	0.028	1.09	0.08	0.185	0.08

5. Experimental data processing and analysis

By the results processing of measured values, dependency graph of the average surface roughness parameter *Ra* to varied influential factors: cutting speed v_c, radial depth of cut a_e and feed per tooth f_t is obtained. In the graph, it is visible that in general, the surface roughness is decreased by machining with emulsion cooling or compressed air cooling in comparison with dry machining. An exception is machining by low feed per tooth, when during dry machining better quality of the machined surface is achieved. An advantage in view of quality of the machined surface for higher value of feed per tooth and radial depth of cut represents machining process by emulsion cooling, figure 3 and figure 5. Dry machining and emulsion machining showed notable increase, but also steady surface roughness while machining at lower cutting speed. Machining process at higher cutting speed represents sudden increase of the surface roughness in the case of dry machining, while with the other two methods surface roughness increase is minimum, figure 4.

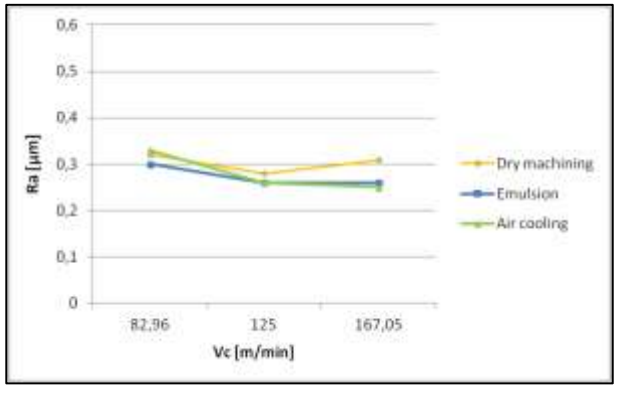

Figure 3. The surface roughness for different cutting speed v_c and constant parameters *fz*=0,8 mm/z and a_e=1,5 mm

Slika 3. Hrapavost obrađene površine za različite brzine rezanja v_c i konstantne parametre *fz*=0,8 mm/z i a_e=1,5 mm

The surface roughness trends of increase and decrease with regard to the radial depth of cut as variable parameter of machining is shown in the figure 4. An advantage compared to other two machining processes has cooling process with the use of cold compressed air. Machining process by emulsion cooling gets the same results as cooling process with the use of cold compressed air if radial depth of cut is a_e=1.5 mm. With the increase of depth of cut, the surface roughness is almost steady for all three types of processing.

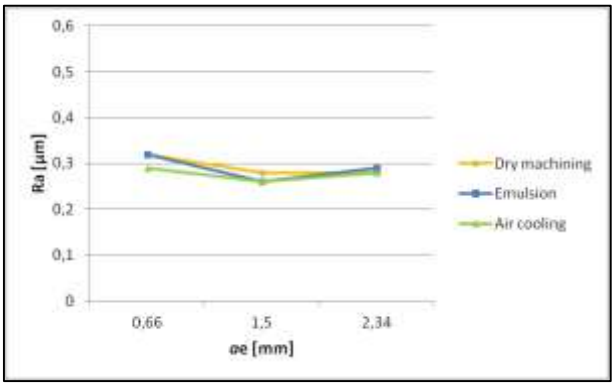

Figure 4. The surface roughness for different depth of cut a_e and constant parameters *fz*=0,8 mm/z and v_c=125 m/min

Slika 4. Hrapavost obrađene površine za različite dubine rezanja a_e i konstantne parametre *fz*=0,8 mm/z i v_c=125 m/min

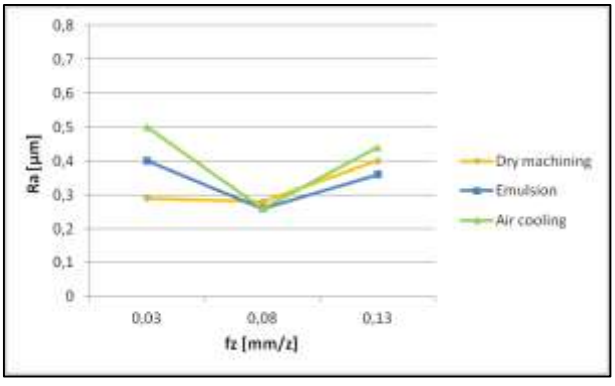

Figure 5. The surface roughness for different feed rate *fz* and constant parameters a_e=1,5 mm and v_c=125 m/min

Slika 5. Hrapavost obrađene površine za različite posmake rezanja *fz* i konstantne parametre a_e=1,5 mm i v_c=125 m/min

By the overview of experimental results, it can be concluded that cooling process with the use of cold

compressed air gives the best results of the surface roughness. Positive characteristic of all three types of processing in the view of quality depends on the change of input parameters.

6. Conclusion

By looking at the graph, it can be concluded that the surface roughness increases with the decrease of cutting speed v_c as well as by the increase of feed per tooth f_t and the radial depth of cut a_e. An impact of depth of cut on the surface roughness is dependent on two others parameters and it is manifested differently by all three types of cooling. Depending on a cutting fluid, the intensity of input parameters influence on the surface roughness is changed. For the actual values of input parameters, by which machining process is performed, the lowest surface roughness is achieved by cooling process with the use of cold compressed air, a little bit higher surface roughness is get by the emulsion cooling, and the highest surface roughness is appeared during dry machining. By defining cutting parameters with the use of various cutting tools and alternative types of cooling, it is possible to achieve high quality of the surface roughness. Different types of materials combined with cutting tools based on the change of input cutting parameters can give significantly different results from the ones obtained in this research. Therefore, optimal type of cooling by which the best surface roughness is achieved should be based on a large number of experiments.

Literatura

[1] Krajnc D., Glavic P., (2003), Indicators of sustainable production, production Faculty of Chemistry and Chemical Engineering, University of Maribor, Slovenia.

[2] Dixit U.S., Sarma D.K., Paulo Davim J., (2012) Environmentally Friendly Machining, Springer Briefs in Applied Sciences and Technology.

[3] Westkamper E., (2008), Manufuture and sustainable manufacturing, In Proceedings ofthe 41st CIRP conference on manufacturing systems. Japan, p. 11-14.

[4] Celent L., Bajić D., Jozić S., (2013), Effect of cooling with cold compresed air using Vortex tube on tool performance in milling process, 14th Internacional scientific conference on production engineering – CIM2013.

[5] Weinert K., Inasaki I., Sutherland J.W., Wakabayashi T., (2004), Dry Machining and Minimum Quantity Lubrication, CIRP- Anals, Manufacturing Technology Vol. 53

[6] Adler D. P., W-S Hii W., Michalek D. J., and Sutherland J. W., (2010), Examining the Role of Cutting Fluids in Machining and Efforts to Address Associated Environmental/Health Concerns, Department of Mechanical Engineering – Engineering Mechanics Sustainable Futures Institute Michigan Technological University.

[7] Paušavec F., Stoić A., Kopač J., (2009), The role of cryogenics in machining, Technical Gazette 16

[8] Slobodna enciklopedija Wikipedija:„Dušik", http://hr.wikipedia.org/wiki/Du%C5%A1ik (pristupljeno 6.2.2014.)

[9] Upendra S. G., Manoj K. J., Saurabh R., (2013), Thermodynamic Analysis Of Counter Flow Vortex Tube, International Journal of Engineering Research & Technology

[10] Byrne G., Dornfeld D., Denkena B., (2003), Advanced Cutting Technology, Laboratory for Manufacturing and Sustainability, University of California, Berkley

[11] De Vera G., (2010), The Ranque-Hilsch Vortex Tube,me.berkeley.ed

ISSN 1847-7917

Comparison of orthotropic constitutive models in predicting square cup deep drawing process of AA2090-T3 sheet

***Vedrana ČVITANIĆ*[1)], *Daniel IVANDIĆ*[2)] *and Branimir LELA*[1)]**

1) Faculty of Electrical Engineering, Mechanical Engineering and Naval Architecture, University of Split
Fakultet elektrotehnike, strojarstva i brodogradnje, Sveučilište u Splitu
Ruđera Boškovića 32, 21000 Split, **Croatia**
2) AD plastik
Matoševa 8, 21210 Solin, **Croatia**

vedrana.cvitanic@fesb.hr,
daniel.ivandic@gmail.com,
blela@fesb.hr

Keywords

Orthotropic material
Constitutive modeling
Flow rule
Orthotropic stress function
Finite element method
Square cup deep drawing

Ključne riječi

Ortotropan material
Konstitutivno modeliranje
Pravilo tečenja
Ortotropna funkcija naprezanja
Metoda konačnih elemenata
Kvadratično duboko vučenje

Original scientific paper

Abstract: In this article phenomenological elasto-plastic orthotropic material models are compared in predicting square cup deep drawing process of aluminum alloy AA2090-T3 sheet sample that shows pronounced plastic orthotropy. The analyzed material models are based on the isotropic hardening, associated or non-associated flow rule and symmetric orthotropic stress functions as yield function/plastic potential. The utilized orthotropic stress functions are quadratic Hill (1948) or non-quadratic Karafillis-Boyce (1993) stress function. The capabilities of the utilized stress functions under associated or non-associated flow rule in predicting orientation dependences of the uniaxial plastic material properties are demonstrated. Finite element simulations of the square cup drawing problem are performed with the finite element program ADINA 8.6. upgraded with the CBR shell element and the algorithmic formulations of the analyzed material models based on implicit return mapping. By comparing predictions obtained by the different material models influence of the flow rule and the functional form of the yield function/plastic potential is analyzed.

Izvorni znanstveni rad

Sažetak: U ovom radu uspoređene su fenomenološke ortotropne elasto-plastične konstitutivne formulacije u predviđanju postupka kvadratičnog dubokog vučenja lima aluminijske legure AA2090-T3. Analizirane formulacije temelje se na pridruženom ili nepridruženom pravilu tečenja, izotropnom očvršćivanju i koriste simetrične ortotropne funkcije naprezanja kao funkciju tečenja odnosno plastični potencijal. Korištene ortotropne funkcije naprezanja su kvadratična Hill (1948) i nekvadratična Karafillis-Boyce (1993) funkcija. U radu su prikazane mogućnosti analiziranih funkcija naprezanja u predviđanju orijentacijske ovisnosti naprezanja tečenja i Lankfordova parametra uz pretpostavku o pridruženom odnosno nepridruženom pravilu tečenja. Simulacije postupka kvadratičnog dubokog vučenja izvršene su korištenjem programa za analizu metodom konačnih elemenata ADINA 8.6 nadograđenim s CBR ljuskastim elementom i algoritamskim formulacijama analiziranih materijalnih modela temeljenim na postupku implicitnog povratnog projiciranja. Usporedbom predviđanja postupka dobivenih različitim materijalnim modelima, analiziran je utjecaj postavki modela na konačan rezultat predviđanja.

1. Introduction

Sheet metals exibit initial plastic anisotropy mainly due to the crystallographic texture caused by production rolling steps. The computer simulation codes, based on the finite element method, are widely used in the design and analysis of the sheet metal forming processes. Such approach requires numerically efficient material models that can accuratelly predict complex anisotropic plastic behaviour of the sheet materials. The phenomenological orthotropic plasticity theories are the most frequently applied for these purposes. The basis of the general phenomenological material model is a yield function representing a surface that separates the elastic and plastic regions in the stress space, a plastic potential function that governs the direction of the plastic strain rate in the stress space and a hardening rule by which evolution of the yield surface is described.

A common approach in metal plasticity is an assumption known as associated flow rule according to which yield fuction and plastic potential are identical. Application of associated flow rule in sheet metal plasticity caused development of complex yield functions that can simultaneously describe anisotropy of yielding and anisotropy of plastic flow, such as those proposed in [1], [2], [3], [4].

Symbols/Oznake

c	- weighting function parameter - parametar udjela funkcija
$C, \alpha_1, \alpha_2, \gamma_3$	- anisotropy parameters of Karafillis-Boyce (1993) stress function - anizotropni parametri Karafillis-Boyce (1993) funkcije naprezanja
$\mathbf{C^e}$	- tensor of elastic moduli - tenzor elastičnosti
$d\boldsymbol{\varepsilon}$	- strain tensor increment - inkrement tenzora deformacije
$d\boldsymbol{\varepsilon}^{\mathbf{e}}$	- elastic strain tensor increment - inkrement elastičnog tenzora deformacije
$d\boldsymbol{\varepsilon}^{\mathbf{p}}$	- plastic strain tensor increment - inkrement plastičnog tenzora deformacije
$d\bar{\varepsilon}^{\,p}$	- equivalent plastic strain increment - inkrement ekvivalentne plastične deformacije
$d\lambda$	- plastic multiplier, consistency parameter - plastični množitelj, parametar konzistentnosti
$d\boldsymbol{\sigma}$	- stress tensor increment - inkrement tenzora naprezanja
DX, DY, DD	- drawn-in lengths - duljine uvlačenja
$F,\ f_y$	- yield function, equivalent stress - funkcija tečenja, ekvivalentno naprezanje
f_p	- plastic potential function - funkcija plastičnog potencijala
m	- non-quadratic function exponent - eksponent nekvadratične funkcije tečenja
r	- Lankford parameter - Lankfordov parameter
$r_0,\ r_{45}, r_{90}$	- Lankford parameter for specimen orientations 0°, 45°, 90° - Lankfordovi parametri za uzorke orijentacija 0°, 45°, 90°
$\tilde{s}_1,\ \tilde{s}_2,\ \tilde{s}_3$	- principal values of the isotropic equivalent stress tensor - svojstvene vrijednosti ekvivalentnog izotropnog tenzora naprezanja
$\tilde{s}_{xx},\ \tilde{s}_{yy},\ \tilde{s}_{xy}, \tilde{s}_{zz}$	- isotropic equivalent stress tensor components - komponente ekvivalentnog izotropnog tenzora naprezanja

Greek letters/Grčka slova

$\bar{\varepsilon}^{\,p}$	- hardening parameter, equivalent plastic strain - parameter očvršćavanja, ekvivalentna plastična deformacija
κ	- hardening function - funkcija očvršćavanja
$\lambda_1, \lambda_2, \nu, \rho$	- anisotropy parameters of Hill (1948) stress function - anizotropni parametri Hill (1948) funkcije naprezanja
$\boldsymbol{\sigma}$	- stress tensor - tenzor naprezanja
σ_b	- equibiaxial yield stress - ujednačeno dvoosno naprezanje tečenja
σ_y	- yield stress for referent direction - naprezanje tečenja za referentni pravac
$\sigma_{xx}, \sigma_{yy}, \sigma_{xy}$	- stress tensor components - komponente tenzora naprezanja
$\sigma_0, \sigma_{45}, \sigma_{90}$	- yield stresses for specimens orientations 0°, 45°, 90° - naprezanja tečenja za uzorke orijentacija 0°, 45°, 90°

However, functional complexity of these functions is not due to their improved physical interpretation of the anisotropic yielding, instead they represent a good aproximation of experimental data or predictions of the polycrystal plasticity theories. By application of non-associated flow rule, two behaviours, plastic yielding and plastic flow are described by two separate functions. In orthotopic sheet material models, these functions might have identical form but their parameters can be adjusted to the different sets of experimental data, yield function can be defined in terms of measured yield stresses and plastic potential in terms of measured plastic strain ratios. Recent studies show that such approach can result in acceptable predictions of the material behaviour even if simple stress functions are utilized [5], [6], [7], [8], [9], [10].

In this paper, associated and non-associated constitutive formulations, based on simple orthotropic four parametric stress functions, quadratic Hill (1948) [11] and non-quadratic Karafillis-Boyce (1993) [12], are considered. Hill (1948) stress function is the simplest orthotropic yield function and thus the most convenient for the numerical application. It is a quadratic function derived as an extension of the isotropic von Mises yield function. Karafillis-Boyce (1993) stress function is a linear combination of two convex non-quadratic functions whose exponent can be closely related to the crystalline structure of the material, thus enabling more reliable description of the material behaviour. In this paper, the analyzed formulations are compared in predicting complex square cup deep drawing process assuming material data of aluminium alloy AA2090-T3 sheet sample. The considered AA2090-T3 sheet material is highly textured and thus shows pronounced directional dependence of the uniaxial plastic material properties. Cylindrical cup drawing problem for this sheet sample became a standard benchmark problem in developing orthotropic sheet material formulations [7], [10], [13], [14], [15]. In the previous study conducted by the authors [7], associated and non-associated formulations based on Hill (1948) and Karafillis-Boyce (1993) stress functions were analyzed in predicting cylindrical cup drawing for this material. Obtained results demonstrate that the earing predictions are strongly influenced by the strain ratio representation, i.e. by the choice of the plastic potential function. Furthermore, it was concluded that the functional form of the utilized stress functions significantly influences the predictions while the non-associated formulations result in certain improvements compared to the associated formulations.

The purpose of the present paper is to detect the portion of the possible discrepancy in predictions of the square cup drawing process obtained by the considered material formulations. By comparing results, influence of the representation of the yielding and plastic flow, i.e. choice of the flow rule and the functional form of the yield function/plastic potential, is analyzed. The paper is organized as follows. In Section 2, basic equations of the analyzed constitutive formulations are briefly presented. The utilized Hill (1948) and Karafillis-Boyce (1993) stress functions are described in Section 3. In Section 4 calculated anisotropy parameters and predictions of the uniaxial plastic material properties obtained by the analyzed constitutive models are presented. In Section 5 formulations are compared in predicting cup contours and thickness strains for the certain values of punch travel.

2. Basic equations of elasto-plastic constitutive formulations

Assuming isotropic linear elasticity and additive decomposition of the strain tensor increment $d\boldsymbol{\varepsilon}$ into elastic $d\boldsymbol{\varepsilon}^{\mathbf{e}}$ and plastic part $d\boldsymbol{\varepsilon}^{\mathbf{p}}$, the stress tensor increment $d\boldsymbol{\sigma}$ reads

$$d\boldsymbol{\sigma} = \mathbf{C}^{\mathbf{e}} : d\boldsymbol{\varepsilon}^{\mathbf{e}} = \mathbf{C}^{\mathbf{e}} : (d\boldsymbol{\varepsilon} - d\boldsymbol{\varepsilon}^{\mathbf{p}}) \tag{1}$$

where $\mathbf{C}^{\mathbf{e}}$ is the tensor of elastic moduli. If isotropic hardening is assumed, the yield criterion is defined as

$$F = f_y(\boldsymbol{\sigma}) - \kappa(\bar{\varepsilon}^p) = 0 \tag{2}$$

where $f_y(\boldsymbol{\sigma})$ is a continuously differentiable function called the yield function, scalar $\bar{\varepsilon}^p$ is a hardening parameter and $\kappa(\bar{\varepsilon}^p)$ is a scalar function called hardening function representing a stress-strain relation. According to the plastic potential theory, the plastic part of the strain tensor increment is proportional to the gradient of the stress function $f_p(\boldsymbol{\sigma})$ named plastic potential function

$$d\boldsymbol{\varepsilon}^{\mathbf{p}} = d\lambda \frac{\partial f_p(\boldsymbol{\sigma})}{\partial \boldsymbol{\sigma}} \tag{3}$$

where $d\lambda$ is a non-negative scalar called plastic multiplier or consistency parameter. If plastic potential and yield function are not identical above evolution equation for the plastic strain tensor increment becomes the so-called non-associated flow rule. If the plastic potential and yield function are identical the so-called associated flow rule is reproduced. In the present formulation, hardening parameter is considered as an equivalent plastic strain that obeys the principle of the plastic work equivalence

$$f_y(\boldsymbol{\sigma})\, d\bar{\varepsilon}^p = \boldsymbol{\sigma} : d\boldsymbol{\varepsilon}^{\mathbf{p}} \tag{4}$$

If the plastic potential is a first order homogeneous function that obeys Euler′s identity, by using Eqs. (3) and (4) evolution equation for the hardening parameter reads

$$d\bar{\varepsilon}^p = d\lambda \frac{\boldsymbol{\sigma} : \partial f_p(\boldsymbol{\sigma}) / \partial \boldsymbol{\sigma}}{f_y(\boldsymbol{\sigma})} = d\lambda \frac{f_p(\boldsymbol{\sigma})}{f_y(\boldsymbol{\sigma})} \tag{5}$$

Since, for the elastic processes the incremental changes of the internal variables (plastic strain tensor and

hardening parameter) vanish and $d\lambda = 0$ applies, for a hardening material plastic multiplier obeys complementary conditions

$$d\lambda \geq 0, \quad F \leq 0, \quad d\lambda F = 0 \tag{6}$$

and consistency condition

$$d\lambda dF = 0 \tag{7}$$

Finite element implementation of the analyzed constitutive models requires numerical integration of the constitutive equations over a time increment, i.e. computational procedure for the calculation of the state variables (stress tensor and equivalent plastic strain) at the certain time step based on the known state variables at the previous time step and the known displacement field. In the present study computational procedure developed in [7] based on the incremental deformation theory [16] and implicit return mapping [17] is adopted.

3. Analyzed orthotropic stress functions

In the considered models, the functional form of the yield function of Hill (1948) [11] or Karafillis-Boyce (1993) [12] associated model is used as yield function and plastic potential function.

In sheet metal forming it is common practice to assume that the sheet is approximately subjected to plane stress conditions and that material exhibits orthotropic symmetry in plastic properties. Therefore, utilized functions are considered as functions of the in-plane stress components, σ_{xx}, σ_{yy} and σ_{xy}, where x-axis denotes the original sheet rolling direction and y-axis denotes the direction in sheet plane transverse to the rolling direction. The z-axis denotes the sheet normal direction.

The orthotropic yield function of Hill (1948) associated model is a quadratic function derived as an extension of the isotropic von Mises yield function. For the plane stress conditions, Hill (1948) yield criterion can be written in the following form

$$f_y = \sqrt{\lambda_1\sigma_{xx}^2 + \lambda_2\sigma_{yy}^2 - 2\nu\sigma_{xx}\sigma_{yy} + 2\rho\sigma_{xy}^2} = \sigma_y \tag{8}$$

where λ_1, λ_2, ν and ρ are anisotropic material parameters that are adjusted to experimental data and σ_y is the yield stress for the referent direction.

Karafillis and Boyce (1993) proposed yield criterion based on a linear combination of two convex non-quadratic functions

$$f_y = \left(\frac{1-c}{2}((\tilde{s}_1 - \tilde{s}_2)^m + (\tilde{s}_2 - \tilde{s}_3)^m + (\tilde{s}_3 - \tilde{s}_1)^m) + \frac{c}{2}\frac{3^m}{(2^{m-1}+1)}((\tilde{s}_1)^m + (\tilde{s}_2)^m + (\tilde{s}_3)^m) \right)^{1/m} = \sigma_y \tag{9}$$

where $\tilde{s}_1$, $\tilde{s}_2$, $\tilde{s}_3$ are the principal values of the so-called isotropic plasticity equivalent stress tensor, c is a weighting parameter and exponent m is an even number.

For plane stress conditions the principal values of the isotropic plasticity equivalent stress tensor can be calculated as

$$\tilde{s}_{1,2} = \frac{\tilde{s}_{xx} + \tilde{s}_{yy}}{2} \pm \sqrt{\left(\frac{\tilde{s}_{xx} - \tilde{s}_{yy}}{2}\right)^2 + \tilde{s}_{xy}^2}, \tag{10}$$

$$\tilde{s}_3 = \tilde{s}_{zz}$$

where

$$\begin{Bmatrix} \tilde{s}_{xx} \\ \tilde{s}_{yy} \\ \tilde{s}_{zz} \\ \tilde{s}_{xy} \end{Bmatrix} = C \begin{bmatrix} 1 & \beta_1 & \beta_2 & 0 \\ \beta_1 & \alpha_1 & \beta_3 & 0 \\ \beta_2 & \beta_3 & \alpha_2 & 0 \\ 0 & 0 & 0 & \gamma_3 \end{bmatrix} \begin{Bmatrix} \sigma_{xx} \\ \sigma_{yy} \\ \sigma_{zz} = 0 \\ \sigma_{xy} \end{Bmatrix} \tag{11}$$

and

$$\begin{aligned} \beta_1 &= (\alpha_2 - \alpha_1 - 1)/2, \\ \beta_2 &= (\alpha_1 - \alpha_2 - 1)/2, \\ \beta_3 &= (1 - \alpha_1 - \alpha_2)/2 \end{aligned} \tag{12}$$

The constants C, α_1, α_2, γ_3 are anisotropic parameters. The stress components defined by Eq. (11) reduce to the components of the stress deviator tensor when $C = 2/3$, $\alpha_1 = \alpha_2 = 1$ and $\gamma_3 = 3/2$, i.e. when material is isotropic. In that case, if $c = 0$, Eq. (9) corresponds to Tresca yield criterion when $m \to \infty$, and von Mises yield criterion is reproduced for $m = 2$. For orthotropic material, if $c = 0$ and $m = 2$ Hill (1948) yield criterion is obtained. By varying the exponent m, Karafillis-Boyce (1993) yield criterion can be adjusted to the yield surfaces obtained by the polycrystalline theory of plasticity, i.e. exponent m can be closely related to the crystalline structure of material. Thus, when $c = 0$, recommended values for FCC materials are $m = 8$, and for BCC materials $m = 6$.

4. Calculated anisotropy parameters and predictions of planar anisotropy

Hill (1948) stress function (8) and Karafillis-Boyce (1993) stress function (9) contain four adjustable parameters, (λ_1, λ_2, ν, ρ) and (C, α_1, α_2, γ_3) respectively, that can be adjusted to various experimental data. For Karafillis-Boyce (1993) function exponent $m = 8$ and function weighting parameter $c = 0$ are utilized. Under the associated flow rule the analyzed stress functions act as yield function as well as plastic potential, therefore they can be adjusted to the yield stresses or the experimental data indicating plastic flow. In the present article, the parameters of functions denoted as Hill-σ and KB-σ are defined in terms of three directional yield stresses obtained in the uniaxial tension of the specimens oriented at 0°, 45° and 90° to the rolling direction and equibiaxial yield stress. The associated yield stresses are denoted as σ_0, σ_{45}, σ_{90} and σ_b. The

parameters of functions denoted as Hill-r and KB-r are defined in terms of Lankford parameter that reads

$$r = d\varepsilon_{22}^p / d\varepsilon_{33}^p \quad (13)$$

where $d\varepsilon_{22}^p$ and $d\varepsilon_{33}^p$ are width and thickness plastic strain rate, respectively. In calculating parameters of the functions denoted as Hill-r and KB-r, three Lankford parameters obtained in the uniaxial tensions along 0°, 45° and 90° to the rolling direction are used. The associated values are denoted as r_0, r_{45} and r_{90}.

For Hill (1948) stress function calibration procedure results in explicit expressions for the anisotropy parameters. Thus, parameters adjusted to yield stresses read

$$\lambda_1 = 1, \quad \lambda_2 = (\sigma_0 / \sigma_{90})^2$$
$$\nu = 0.5(1 + (\sigma_0 / \sigma_{90})^2 + (\sigma_0 / \sigma_b)^2)$$
$$\rho = 2(\sigma_0 / \sigma_{45})^2 - 0.5(\sigma_0 / \sigma_b)^2 \quad (14)$$

and if calibration procedure is based on Lankford parameters, following is obtained

$$\lambda_1 = 1, \quad \lambda_2 = \frac{1 + 1/r_{90}}{1 + 1/r_0}$$
$$\nu = \frac{1}{1 + 1/r_0}, \ \rho = \frac{(1 + 2r_{45})(1/r_0 + 1/r_{90})}{2(1 + 1/r_0)} \quad (15)$$

For Karafillis-Boyce (1993) stress function calibration procedure leads to the system of non-linear equations that can be solved using a numerical iterative procedure.

Material data for the analyzed AA2090-T3 sheet sample are given in Table 1. Table 2 shows calculated anisotropy parameters for the considered material.

The capabilities of the utilized stress functions under associated or non-associated flow rule in predicting orientation dependences of the uniaxial plastic material properties are demonstrated in Figs. 1 and 2.

It can be observed that both functions show poor capability in predicting material behaviour under associated flow rule. If analyzed functions are adjusted to yield stresses they results in good description of the yield stress anisotropy but poor predictions of plastic strain ratio anisotropy. And vice, if functions are adjusted to plastic strain ratio they result in acceptable predictions of plastic strain ratio anisotropy but poor predictions of yield stresses. Furthermore, neither of the analyzed functions can reproduce experimental *r* value trend that shows two maximums between transverse and rolling direction. According to the results presented in Figs. 1 and 2 the improved prediction of material behaviour can be obtained if formulation is based on non-associated flow rule, namely if stress function adjusted to the yield stresses is utilized as yield function and stress function adjusted to Lankford parameters as plastic potential. Fig. 3 shows contours of the analyzed stress functions. The pronounced discrepancy between gradients of the functions with same functional form but different calibration procedure can be observed.

Table 1. Material data for AA2090-T3 sheet sample [13]

Tablica 1. Materijalni podaci za uzorak lima AA2090-T3 [13]

yield stress (MPa)/ naprezanje tečenja (MPa)	σ_0 279.6	σ_{15} 268.7	σ_{30} 254.4	σ_{45} 226.8	σ_{60} 226.4	σ_{75} 246.6	σ_{90} 254.4	σ_b 289.4
Lankford parameter/ Lankfordov parametar	r_0 0.211	r_{15} 0.327	r_{30} 0.692	r_{45} 1.577	r_{60} 1.039	r_{75} 0.538	r_{90} 0.692	
thickness/debljina: 1.60 mm, Young modulus/Youngov modul: 69 000 MPa Poisson ratio/Poissonov koeficijent: 0.33 true stress-strain curve for rolling direction/zakon očvršćivanja za pravac valjanja: $\kappa(\bar{\varepsilon}^p) = 646(0.025 + \bar{\varepsilon}^p)^{0.227}$ MPa								

Table 2. Calculated anisotropy parameters of the analyzed stress functions for AA2090-T3 sheet sample

Tablica 2. Vrijednosti parametara anizotropije analiziranih funkcija naprezanja za uzorak lima AA2090-T3

function label / oznaka funkcije	material data used / korišteni materijalni podaci	anisotropy parameters / parametri anizotropije			
Hill-σ	$\sigma_0, \sigma_{45}, \sigma_{90}, \sigma_b$	$\lambda_1 = 1.0000$	$\lambda_2 = 1.2070$	$\nu = 0.6368$	$\rho = 2.5729$
Hill-r	$r_0, r_{45}, r_{90}, \sigma_0$	$\lambda_1 = 1.0000$	$\lambda_2 = 0.4251$	$\nu = 0.1736$	$\rho = 2.2422$
KB-σ	$\sigma_0, \sigma_{45}, \sigma_{90}, \sigma_b$	$C = 0.6619$	$\alpha_1 = 1.1062$	$\alpha_2 = 0.9686$	$\gamma_3 = 1.9592$
KB-r	$r_0, r_{45}, r_{90}, \sigma_0$	$C = 0.6535$	$\alpha_1 = 0.8013$	$\alpha_2 = 1.0354$	$\gamma_3 = 1.7157$

a)

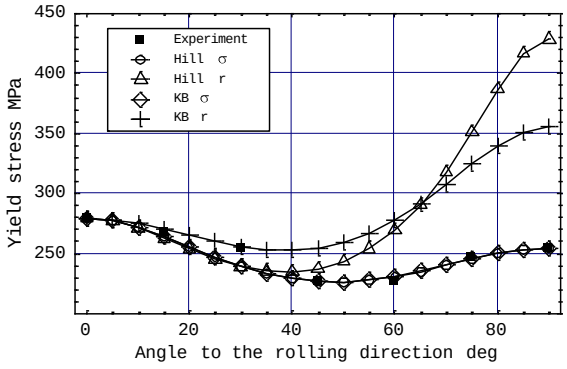

b)

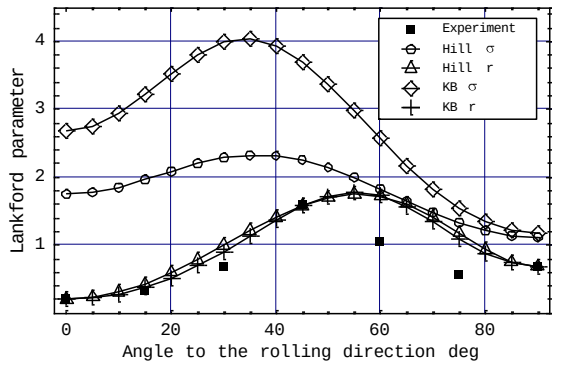

Figure 1. Experimental and predicted: a) yield stresses; b) Lankford parameters for AA2090-T3

Slika 1. Eksperimentalne vrijednosti i predviđanja: a) naprezanja tečenja; b) Lankfordovi parametri za AA2090-T3

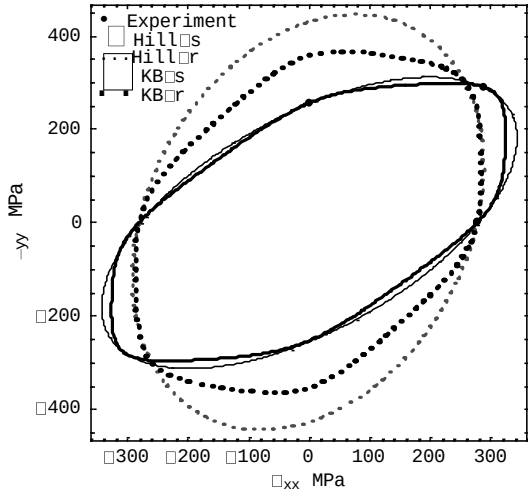

Figure 2. Contours of Hill and Karafillis-Boyce stress functions for AA2090-T3. Contours correspond to σ_{xy}=0.0

Slika 2. Konture Hill and Karafillis-Boyce funkcija naprezanja za AA2090-T3. Konture odgovaraju vrijednosti σ_{xy}=0.0

5. Simulations of square cup deep drawing for AA2090-T3 sheet sample

In this section, predictions of the associated and non-associated formulations based on quadratic Hill (1948) or non-quadratic Karafillis-Boyce (1993) stress functions are compared in predicting square cup deep drawing problem. For the considered forming process, process parameters, tool dimensions and initial blank length/width dimensions correspond to the benchmark mild steel square cup drawing test for NUMISHEET'93 [18], [19]. Instead of using material data for mild steel, in the present study, data for the AA2090-T3 sheet with 1.6 mm thickness listed in Table 1 are considered. As shown in Figs. 1 and 2, AA2090-T3 shows pronounced anisotropy in uniaxial plastic properties and the yield functions/plastic potentials utilized in the analyzed models are inherently different. Therefore, although experimental drawing process data are not available for the considered case, by analyzing results for this material, apparent insight into the influence of the functional form of the utilized stress functions and flow rule on the final predictions can be expected.

The simulations are performed with FE code ADINA 8.6 [20] upgraded with the updated Lagrangian formulation of the CBR shell element and the adopted stress integration procedure. A schematic view of the cup drawing problem in *x-z* plane and the geometry of tools in *x-y* plane are presented in Fig. 4. The initial square blank is 150×150 mm^2. The punch corner radius is 10 mm with shoulder radius of 8 mm and the die corner radius is 12 mm with shoulder radius of 5 mm. The blank holder force of 19.6 kN (4.9 kN for the one-quarter model) and a constant friction factor of 0.144 are utilized. Due to the shape geometry and material orthotropy, a one-quarter model of the cup is analyzed. One-quarter section of the blank is modelled by a regular 25×25 mesh of 4-node CBR shell elements and the blank holder, die and punch are modelled as rigid surfaces.

a) b)

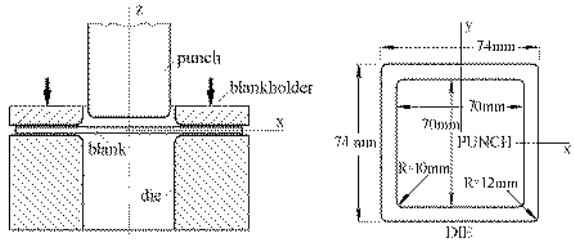

Figure 3. Square cup deep drawing problem: a) schematic view in *x-z* plane; b) geometry of tools in *x-y* plane

Slika 3. Postupak kvadratičnog dubokog vučenja: a) shematski prikaz u *x-z* ravnini; b) geometrija alata u *x-y* ravnini

For the frictional contact treatment, the constraint function algorithm available in ADINA 8.6 is employed. The classical Coulomb friction law and constant friction factor are used. The isotropic hardening is assumed and power hardening curve, specified in Tab. 1, describing the experimental stress-strain data for the rolling direction is utilized.

The contours of drawn cups and thickness strains for the blank rolling, transverse and diagonal direction at 20 and 30 mm punch travel predicted by the analyzed constitutive formulations are compared. The analysis is performed under the assumption that material with characteristics presented in Tab. 1 can withstand the whole deformation process without fracture. The analyzed constitutive formulations are label according to the utilized stress functions (Hill or Karafillis-Boyce) and flow rule (AFR for associated and NAFR non-associated flow rule). Full meaning of the labels is presented in Tab. 3. The analyzed associated formulations utilize stress function adjusted to strain ratios as plastic potential and as yield function. Non-associated formulations utilize stress function adjusted to strain ratios as plastic potential and function adjusted to yield stresses as yield function thus enabling more reliable representation of the material yielding.

Table 3. Formulation labels

Tablica 3. Oznake formulacija

formulation label / oznaka formulacije	yield function / funkcija tečenja	potential/ potencijal
AFR-Hill	Hill-r	Hill-r
NAFR-Hill	Hill-σ	Hill-r
AFR-KB	KB-r	KB-r
NAFR-KB	KB-σ	KB-r

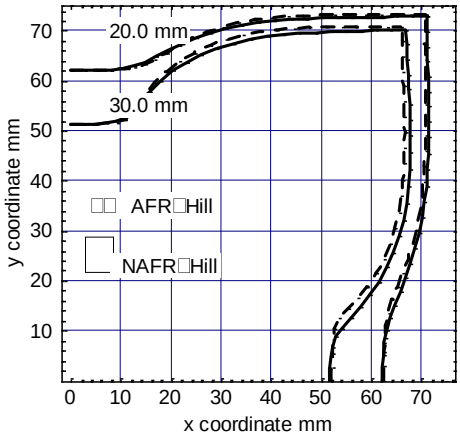

Figure 4. Contours of the square cup in the *x-y* plane at 20 and 30 mm punch travel predicted by formulations based on Hill (1948) function.

Slika 4. Predviđanja konture kvadratične posudice u *x-y* ravnini za pomak trna od 20 i 30 mm dobivene formulacijama temeljenim na Hill (1948) funkciji.

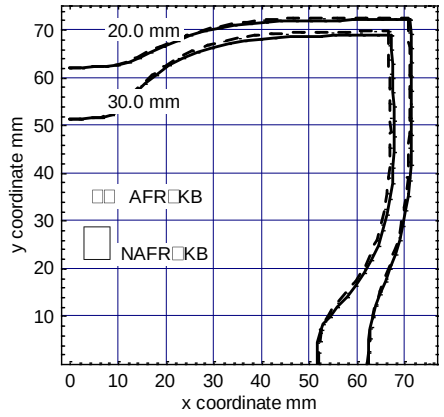

Figure 5. Contours of the square cup in the *x-y* plane at 20 and 30 mm punch travel predicted by formulations based on Karafillis-Boyce (1993) function

Slika 5. Predviđanja konture kvadratične posudice u *x-y* ravnini za pomak trna od 20 i 30 mm dobivene formulacijama temeljenim na Karafillis-Boyce (1993) funkciji

Figs. 4 and 5 show contours of the square cup in the *x-y* plane for the certain punch travel obtained by the analyzed formulations. Definitions of the draw-in lengths DX, DY and DD of the blank from the initial position are shown in Fig. 6, where DD presents the length reduction of the initially diagonal line. Predictions of the drawn-in lengths are compared in Tab. 4.

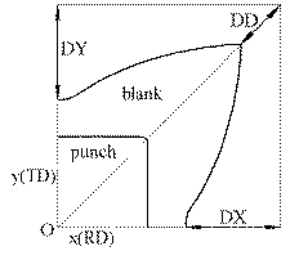

Figure 6. *x-y* projection of the deformed shape and definition of draw-in lengths

Slika 6. *x-y* projekcija deformirane posudice i definicije za duljine uvlačenja

Table 4. Comparison of draw-in lengths (units: mm)

Tablica 4. Usporedba duljina uvlačenja (units: mm)

	punch travel = 20 mm			punch travel = 30 mm		
formulation	DX	DY	DD	DX	DY	DD
AFR-Hill	12.43	12.97	4.23	22.86	23.76	9.16
NAFR-Hill	12.70	13.00	4.24	23.26	23.79	9.03
AFR-KB	12.44	12.90	4.63	22.97	23.74	9.65
NAFR-KB	12.73	12.96	4.69	23.37	23.74	9.71

Results presented in Figs. 4-5 and Tab. 4 demonstrate that analyzed models predict notable material orthotropic behaviour since they predict significant slope change of the initially diagonal line and certain discrepancy between DX and DY values. The differences between predicted contours are more pronounced for the greater punch travel. It can be observed that the application of non-associated flow rule, i.e. improvement of the yield stress representation, more affects the predictions for the formulations based on Hill (1948) stress function. Considering predictions presented in Tab. 4 it can be observed that the differences between predictions are the greatest for the DD values. Furthermore, formulations based on the non-quadratic Karafillis-Boyce (1993) stress function predict greater draw-in DD values compared to formulations based on quadratic Hill (1948) functions.

In Figs. 7 and 8 predictions of the thickness strain distributions along rolling, diagonal and transverse directions are presented. It can be observed that analyzed formulations predict quite similar trends of the distributions along all three directions. For the diagonal direction formulations predict significant stretching near the punch corner. For the rolling and transverse direction formulations predict less pronounced stretching followed by thickening. Predicted thickening is greater for the transverse than to the rolling direction that is in accordance with the predicted cup contours, namely the change of the diagonal line slope towards the transverse direction, as presented in Figs. 4 and 5.
The thickness strains predicted by the non-associated formulations are quite close except in the critical stretching area. The predicted thickness strains obtained by the associated formulation based on Hill (1948) stress function the mostly differ from the other predictions. As shown in Figs. 1 and 2, the analyzed non-associated formulations NAFR-Hill and NAFR-KB result in similar predictions of the directional yield stresses and their yield loci are quite close while there is a pronounced discrepancy between gradients of their plastic potentials. Compared to AFR-Hill, formulation AFR-KB results in yield stress representation and yield loci that are much closer to representations obtained by the non-associated formulations NAFR-Hill and NAFR-KB. These observations indicate that the yield stress representation, i.e. the choice of the yield function, has the major influence on the thickness strain predictions in this forming process.

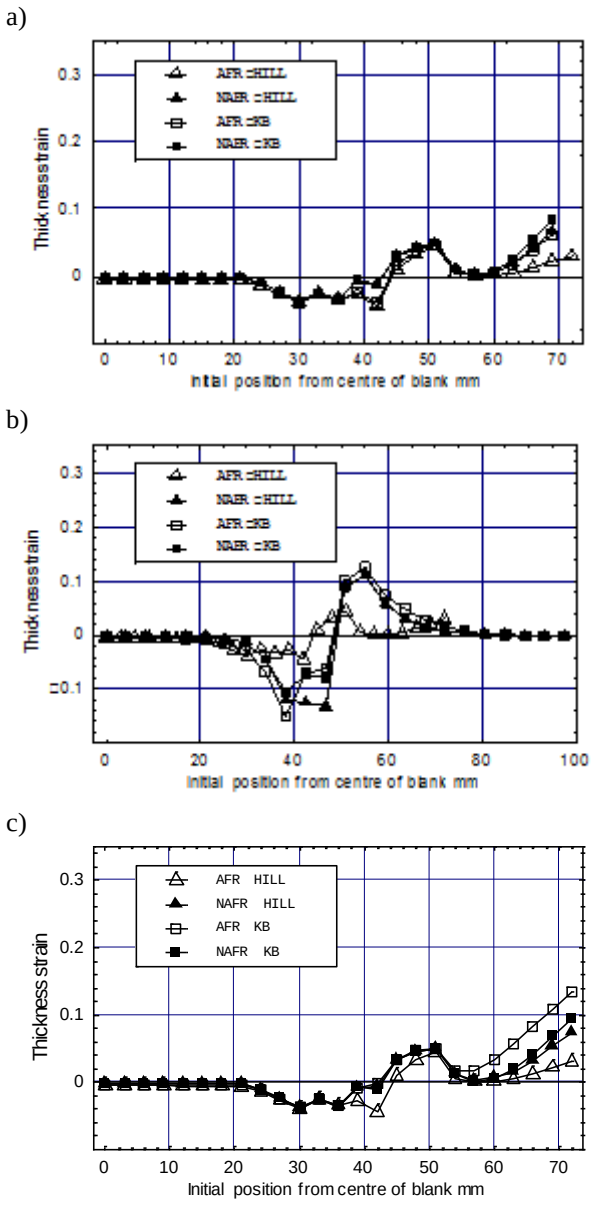

Figure 7. Predicted thickness strains at 20 mm punch travel along: a) rolling; b) diagonal c) transverse direction

Slika 7. Predviđanja deformacije debljine za pomak trna od 20 mm: a) pravac valjanja; b) dijagonalni pravac; c) poprečni pravac

a)

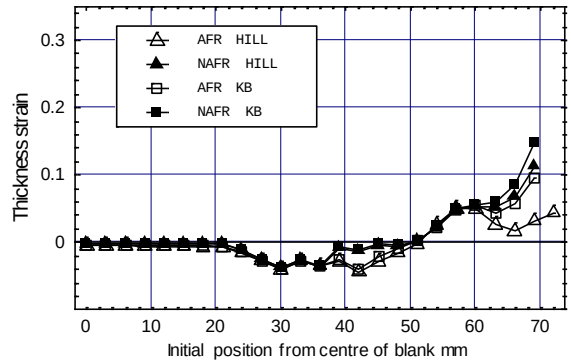

b)

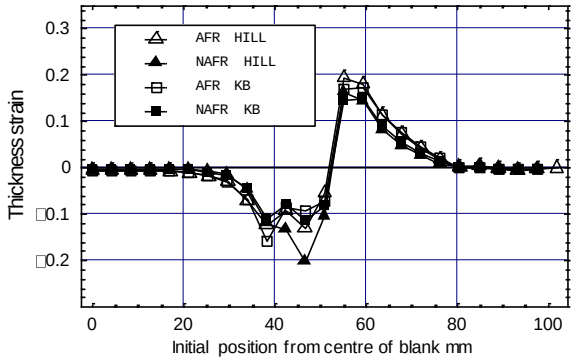

c)

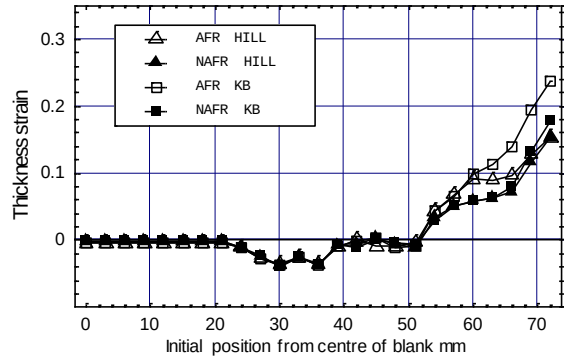

Figure 8. Predicted thickness strains at 30 mm punch travel along: a) rolling; b) diagonal; c) transverse direction.

Slika 8. Predviđanja deformacije debljine za pomak trna od 30 mm: a) pravac valjanja; b) dijagonalni pravac; c) poprečni pravac.

6. Conclusions

In the present paper, the orthotropic associated and non-associated formulations based on Hill (1948) or Karafillis-Boyce (1993) stress functions are compared in predicting square cup drawing process assuming material data for the aluminium alloy AA2090-T3 sheet sample. By considering predictions, influence of the yielding and plastic flow representation on the final predictions is analyzed. Considering overall cup drawing predictions it can be concluded that the results are more affected by the flow rule, i.e. the change of the yielding description, for the formulations based on the quadratic Hill (1948) stress functions than for the formulations based on non-quadratic Karafillis-Boyce (1993) stress functions. Furthermore, considering predictions of the thickness strain, it can be concluded that these predictions are the mostly influenced by the yield stress representation, i.e. by the choice of the yield function.

REFERENCES

[1] Barlat, F., Maeda, Y., Chung, K., Yanagawa, M., Brem, J.C., Hayashida, Y., Lege, D.J., Matsui, K., Murtha, S.J., Hattori, S., Becker, R.C., Makosey, S., (1997), *Yield function development for aluminium alloy sheets*, J. Mech. Phys. Solids 45, p 1727-1763.

[2] Barlat, F., Brem, J.C., Yoon, J.W., Chung, K., Dick, R.E., Lege, D.J., Pourboghrat, F., Choi, S.-H., Chu, E., (2003), *Plane stress yield function for aluminium alloy sheets – Part 1: Theory*, International Journal of Plasticity 19, p 1297-1319.

[3] Bron, F., Besson, J., (2004), *A yield function for anisotropic materials, application to aluminum alloys*, International Journal of Plasticity 20, p 937-963.

[4] Barlat, F., Aretz, H., Yoon, J.W., Karabin, M.E., Brem, J.C., Dick, R.E., (2005), *Linear transformation-based anisotropic yield functions*, International Journal of Plasticity 21, p 1009-1039.

[5] Lademo, O.-G., Hopperstad, O.S., Langseth, M., (1999), *An evaluation of yield criteria and flow rules for aluminium alloys*, International Journal of Plasticity 15, p 191-208.

[6] Stoughton, T.B., (2002), *A non-associated flow rule for sheet metal forming*, International Journal of Plasticity 18, p 687-714.

[7] Cvitanić, V., Vlak, F., Lozina, Ž., (2008), *A finite element formulation based on non-associated plasticity for sheet metal forming*, International Journal of Plasticity 24, p 646-687.

[8] Cvitanić, V., Vlak, F., Lozina, Ž., (2007), *An analysis of non-associated plasticity in deep drawing simulations*, Transactions of FAMENA 31, p 11-26.

[9] Cvitanić, V., Salečić, M., Vukasović, M., (2012), *Numerical simulations of S-rail forming for 6111-T4 sheet based on Hill stress function*, Book of abstracts, 7nd International congress of Croatian society of mechanics, Zadar, p 181-182.

[10] Cvitanić, V., Ivandić, D., Krstulović-Opara, L., (2013), *Influence of constitutive and process parameters on the cylindrical cup drawing*

predictions for AA2090-T3 sheet, Conference proceedings of the 3rd International conference MTSM 2013, Split, p 117-126.

[11] Hill, R., (1948), *Theory of yielding and plastic flow of anisotropic metals*, Proc. Roy.Soc. A 193, p 281-297.

[12] Karafillis, A.P., Boyce, M., (1993), *A general anisotropic yield criterion using bounds and a transformation weighting tensor*, J. Mech. Phys. Solids 41, p 1859-1886.

[13] Yoon, J.W., Barlat F., Chung, K, Pourboghrat, F., Yang, D.Y., (2000), *Earing prediction based on aysmmetric nonquadratic yield function*, International Journal of Plasticity 16, p 1075-1104.

[14] Yoon, J. W., Barlat, F., Dick, R. E., Karabin, M. E., (2006), *Prediction of six or eight ears in a drawn cup based on a new anisotropic yield function*, International Journal of Plasticity 22, p 174-193.

[15] Taherizadeh, A., Green, D.E., Ghaei, A., Yoon, J.W., (2010), *A non-associated constitutive model with mixed iso-kinematic hardening for finite element simulation of sheet metal forming*, International Journal of Plasticity 26, p 288-309.

[16] Yoon, J. W., Yang, D. Y., Chung, K., (1999), *Elasto-plastic finite element method based on incremental deformation theory and continuum based shell elements for planar anisotropic sheet materials*, Computer Methods in Applied Mechanics and Engineering 174, p 23-56.

[17] Simo, J. C., Hughes T.J.R., (1988), *Elastoplasticity and Viscoplasticity Computational Aspects*, Springer Verlag.

[18] Dankert, J., (1995), *Experimental investigation of a square cup deep drawing process*, Journal of Materials Processing Technology, 50, p 375-384.

[19] Ivandić, D., (2010) Diploma thesis (in Croatian), Faculty of Electrical Engineering, Mechanical Engineering and Naval Architecture, University of Split, Split, Croatia.

[20] ADINA 8.6, (2009), Theory and Modeling Guide, ADINA R&D Inc.

ISSN 1847-7917

Computer modelling of as quenched hardness and microstructure of steel shaft

***Božo SMOLJAN*[1)], *Dario ILJKIĆ*[1)] *and Zvonimir KOLUMBIĆ*[2)]**

1) Department of Materials Science and Engineering, University of Rijeka - Faculty of Engineering
Zavod za materijale, Sveučilište u Rijeci - Tehnički fakultet
Vukovarska 58, 51000 Rijeka, **Croatia**
2) Faculty of Humanities and Social Sciences, University of Rijeka
51000 Rijeka, **Croatia**

smoljan@riteh.hr
darioi@riteh.hr
zvonimir.kolumbic1@ri.t-com.hr

Keywords
Steel
Quenching
Computer modelling

Ključne riječi
Čelik
Kaljenje
Računalno modeliranje

Original scientific paper

Abstract: Thermo-metallurgical approach is applied to complete the numerical model of phenomena of steel quenching. Because of wide range of applicability and ease of use of finite volume method (FVM), this numerical method was suitable to create integrated computer program for simulation of transient temperature field, microstructure transformation and mechanical properties during quenching of steel components.
The computer model of steel quenching has been applied for simulation of quenching of steel component of complex form. By experimental verification of the computer simulation results it has been found out those phenomena of steel quenching could be successfully simulated by the proposed computer model.

Izvorni znanstveni rad

Sažetak: Numerički model fenomena kaljenja čelika dovršen je primjenom termo-metalurškog pristupa. Zbog široke primjene i jednostavne upotrebe metode konačnih volumena (FVM), ova je numerička metoda pogodna za izradu integriranog računalnog programa za simulaciju promjene temperaturnog polja, mikrostrukturnih transformacija i mehaničkih svojstava tijekom kaljenja čeličnih komponenti.
Računalni model kaljenja čelika primijenjen je u simulaciji čeličnog strojnog dijela složenog oblika. Eksperimentalnom verifikacijom rezultata računalne simulacije utvrđeno je da se proces kaljenja čelika može uspješno simulirati predloženim računalnim modelom.

1. Introduction

Quenching of steel is one of the most important factors in production and reliability of engineering components. Computer programs for simulation of the quenching can be developed by considering the issues as are achievement of desired mechanical property distribution, achievement of desired microstructure distribution, achievement of required workpiece shape. Computer simulation of quenching at the present has not developed enough [1]. Numerical model of heat transfer and mechanical properties based on finite volume method (FVM) recently are studied [2].
For the simulation of heat transfer which is thermodynamical problem, it is necessary to establish the appropriate algorithm which describes cooling process. Moreover, the accuracy of numerical simulation of thermal process directly depends on the applied input variables. Inverse heat transfer problems should be solute to determine heat transfer coefficients for quenching using experimentally evaluated cooling curve results [1]. To solve heat transfer problem using the experimentally predicted cooling curve, all of heat transfer parameters should be similar in simulation of thermal process as was in experimental evaluation of cooling curves [1]. Heat conductivity, heat capacity and other relevant material properties usually are estimated based on experimentally evaluated results of quenching of steel specimens [3].
Simulations of microstructural transformations are usually based on CCT diagrams using linear alignment with the actual chemical composition, or on thermo-kinetic expressions. The first approach is more consistent, but generally does not give accurate results. The second approach gives good results for the chemical composition of the steel, for which expressions have been established.
The structure transformations and hardness distribution can be estimated based on time relevant for structure transformation. It was accepted that cooling time from 800 to 500 °C, $t_{8/5}$, is relevant time for quenching. If the cooling time $t_{8/5}$ is equal for two different specimens, i.e. quenched workpiece and Jominy specimen, the hardness of these two specimens could be equal to each other [3, 4].

Symbols/Oznake

A_1	- equilibrium temperature of eutectoid transformation - ravnotežna temperatura eutektoidne transformacije
A_3	- equilibrium temperature at which transformation of austenite to ferrite begins - ravnotežna temperatura na kojoj počinje transformacija austenita u ferit
B_s	- temperature of start of bainitic transformation - temperatura početka bainitne transformacije
c	- specific heat capacity, $Jkg^{-1}K^{-1}$ - specifični toplinski kapacitet
H	- *Grossmann* severity of quenching - *Grossmann*ov intenzitet gašenja
HRC_{max}	- maximum hardness HRC in *Jominy* curve - maksimalna tvrdoća HRC na *Jominy*jevoj krivulji
HRC_{M50}	- hardness HRC of steel with 50 % of martensite in the microstructure - tvrdoća HRC čelika s 50 % martenzita u mikrostrukturi
HRC_{M95}	- hardness HRC of steel with 95 % of martensite in the microstructure - tvrdoća HRC čelika s 95 % martenzita u mikrostrukturi
HV_{P100}	- hardness HV of steel with 100 % of pearlite in the microstructure - tvrdoća HV čelika s 100 % perlita u mikrostrukturi
t_{M50}	- cooling time from 800 to 500 °C for characteristic points in *Jominy* specimen with 50 % of martensite in microstructure - vrijeme ohlađivanja od 800 do 500 °C za karakterističnu točku u *Jominy*jevom uzorku s 50 % martenzita u mikrostrukturi
HV_{P50}	- hardness HV of steel with 50 % of pearlite in the microstructure - tvrdoća HV čelika s 50 % perlita u mikrostrukturi
M_f	- temperature of finish of martensitic transformation - temperature završetka martenzitne pretvorbe
M_s	- temperature of start of martensitic transformation - temperature početka martenzitne pretvorbe
t	- time, s - vrijeme
$t_{8/5}$	- time of cooling from 800 to 500 °C, s - vrijeme ohlađivanja od 800 do 500 °C
t_{M95}	- cooling time from 800 to 500 °C for characteristic points in *Jominy* specimen with 95 % of martensite in microstructure - vrijeme ohlađivanja od 800 do 500 °C za karakterističnu točku u *Jominy*jevom uzorku s 95 % martenzita u mikrostrukturi
t_{P100}	- cooling time from 800 to 500 °C for characteristic points in *Jominy* specimen with 100 % of pearlite in microstructure - vrijeme ohlađivanja od 800 do 500 °C za karakterističnu točku u *Jominy*jevom uzorku s 100 % perlita u mikrostrukturi
t_{P50}	- cooling time from 800 to 500 °C for characteristic points in *Jominy* specimen with 50 % of pearlite in microstructure - vrijeme ohlađivanja od 800 do 500 °C za karakterističnu točku u *Jominy*jevom uzorku s 50 % perlita u mikrostrukturi
T	- temperature, K - temperatura

Greek letters/Grčka slova

α	- heat transfer coefficient, $Wm^{-2}K^{-1}$ - koeficijent prijelaza topline

Symbols/Oznake

λ	- coefficient of heat conductivity, $Wm^{-1}K^{-1}$ - koeficijent toplinske vodljivosti	**Subscripts/Indeksi**	
ρ	- density, kgm^{-3} - gustoća	f	- quenchant - medij za kaljenje
		s	- surface - površina

By involving the cooling time, $t_{8/5}$, the Jominy test results could be involved into the numerical model of steel hardening if the history of cooling of both, investigated specimen and Jominy specimen are similar [4].

2. Mathematical modelling of heat transfer

Modelling and computer simulation of heat transfer is in the root of all modelling and computer simulation of quenching.

The transient temperature field in an isotropic rigid body with coefficient of heat conductivity, $\lambda/Wm^{-1}K^{-1}$, density, ρ/kgm^{-3} and specific heat capacity, $c/Jkg^{-1}K^{-1}$, without heat sources can be described by Fourier's law of heat conduction:

$$\frac{\delta(c\rho T)}{\delta t} = div\lambda\ gradT \tag{1}$$

Characteristic boundary condition is:

$$-\lambda\frac{\delta T}{\delta n}\bigg|_s = \alpha(T_s - T_f) \tag{2}$$

where T_s/K is surface temperature, T_f/K is quenchant temperature, $\alpha/Wm^{-2}K^{-1}$ is heat transfer coefficient. Solution of Equation 1 can be found out using the finite volume method [3, 5].

Before setting of model of temperature field change in an isotropic rigid body input data, i.e., specific heat capacity of steel, c, heat conductivity coefficient of steel, λ, steel density, ρ, heat transfer coefficient of quenchant, α must be consistent with the achieved results of microstructure and mechanical properties. Optimization of input data should be done according to achieved results. Since variables ρ and c were accepted from literature, variables λ and α was estimated, i.e., calibrated, according to variables ρ and c. Input values of heat transfer and heat conductivity coefficients can be optimized using Crafts-Lamont diagrams for large spectra of a specimen bar diameter. Heat transfer coefficients of quenchants with different Grossmann severity of quenching were estimated simultaneously with estimation of heat conductivity coefficients of characteristic microstructure constituent [6, 7].

3. Mathematical modelling of hardness and microstructure composition

The hardness at workpiece points is estimated by the conversion of the calculated cooling time $t_{8/5}$ to the hardness by using both, the relation between cooling time, $t_{8/5}$ and Jominy distance and the Jominy hardenability curve [4]. Other mechanical properties of steel can be estimated based on as-quenched hardness of steel [2].

Contents of ferrite, pearlite, bainite, martensite and austenite at some temperature can be estimated using the diagram in the Figure 1.

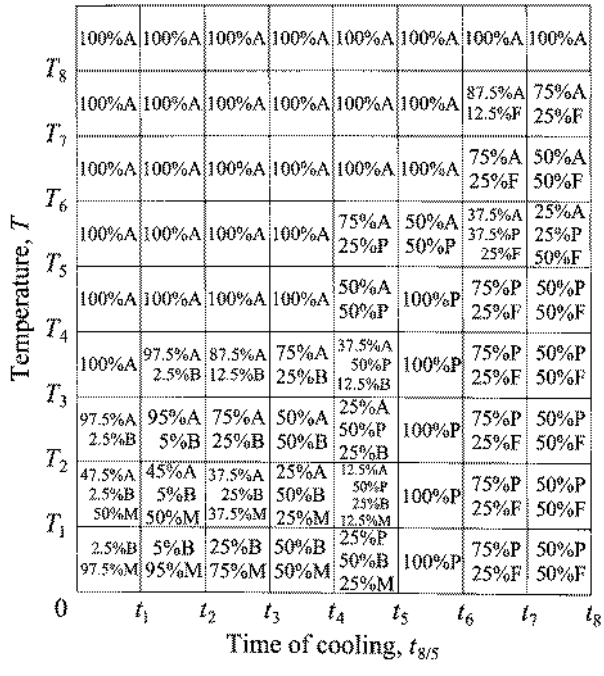

Figure 1. Contents of ferrite, pearlite, bainite, martensite and austenite at some temperature

Slika 1. Udjeli ferita, perlita, bainita, martenzita i austenita na određenoj temperaturi

Characteristic cooling times, t_i in diagram shown in Figure 1 are equal to:

$$t_1 = t_{M95} \quad (3a)$$

$$t_2 = \exp\left(\log t_{M95} + 0.25\left(\log t_{M50} - \log t_{M95}\right)\right) \quad (3b)$$

$$t_3 = \exp\left(\log t_{M95} + 0.75\left(\log t_{M50} - \log t_{M95}\right)\right) \quad (3c)$$

$$t_4 = \exp\left(\log t_{M50} + 0.25\left(\log t_{P100} - \log t_{M50}\right)\right) \quad (3d)$$

$$t_5 = \exp\left(\log t_{M50} + 0.75\left(\log t_{P100} - \log t_{M50}\right)\right) \quad (3e)$$

$$t_6 = \exp\left(\log t_{P100} + 0.25\left(\log t_{P50} - \log t_{P100}\right)\right) \quad (3f)$$

$$t_7 = \exp\left(\log t_{P100} + 0.75\left(\log t_{P50} - \log t_{P100}\right)\right) \quad (3g)$$

where t_{M95}, t_{M50}, t_{P100}, t_{P50} are cooling time from 800 to 500 °C for characteristic points in Jominy specimen with 95 % of martensite, 50 % of martensite, 100 % of pearlite and 50 % of pearlite in microstructure, respectively. The times t_{M95}, t_{M50}, t_{P100}, t_{P50} was estimated by the conversion of distance from a quenched end of Jominy specimen of characteristic microstructure composition to cooling time, $t_{8/5}$. [4]. If temperature in specimen point is higher than 500 °C, cooling time $t_{8/5}$ should be estimated by extrapolation.
Characteristic Jominy distance can be found out based on hardness of characteristic steel microstructure by set of Equations (4) shown in Table 1.

Table 1. Hardness of characteristic steel microstructure

Tablica 1. Tvrdoća karakterističnih mikrostruktura čelika

Microstructure	Hardness	
95 % martensite + 5 % bainite	$\mathrm{HRC}_{M95} = 0.93\mathrm{HRC}_{max}$	(4a)
50 % martensite + 50 % bainite	$\mathrm{HRC}_{M50} = 0.73\mathrm{HRC}_{max}$	(4b)
100 % pearlite	$\mathrm{HV}_{P100} = 0.2308\mathrm{HV}_{max} + 100$	(4c)
50 % pearlite + 50 % ferrite	$\mathrm{HV}_{P50} = 0.1504\mathrm{HV}_{max} + 100$	(4d)

Characteristic temperatures in diagram shown in Figure 1 are equal to:

$$T_1 = M_s - 0.75\left(M_s - M_f\right), \quad (5a)$$

$$T_2 = M_s - 0.25\left(M_s - M_f\right), \quad (5b)$$

$$T_3 = B_s - 0.75\left(B_s - M_s\right), \quad (5c)$$

$$T_4 = B_s - 0.25\left(B_s - M_s\right), \quad (5d)$$

$$T_5 = A_1 - 0.75\left(A_1 - B_s\right), \quad (5e)$$

$$T_6 = A_1 - 0.25\left(A_1 - B_s\right), \quad (5f)$$

$$T_7 = A_3 - 0.75\left(A_3 - A_1\right), \quad (5g)$$

$$T_8 = A_3 - 0.25\left(A_3 - A_1\right), \quad (5h)$$

Between critical temperatures A_3, B_s, M_s and M_f of austenite decomposition and hardenability properties, regression relations are established:

$$A_3 = 862 - 0.04\left(\mathrm{HRC}_{max.} - 20\right)^2 - \frac{2.5t_{8/5}}{\mathrm{HRC}_{max} - 20}, \quad (6a)$$

$$B_s = 586 - 0.02\left(\mathrm{HRC}_{max} - 20\right)^2 - \frac{12t_{8/5}}{\mathrm{HRC}_{max} - 20}, \quad (6b)$$

$$M_s = 502 - 0.09\left(\mathrm{HRC}_{max} - 20\right)^2 - \frac{3.5t_{8/5}}{\mathrm{HRC}_{max} - 20}, \quad (6c)$$

$$M_f = 502 - 0.2\left(\mathrm{HRC}_{max} - 20\right)^2 - \frac{3.5t_{8/5}}{\mathrm{HRC}_{max} - 20}, \quad (6d)$$

It was accepted that equilibrium temperature of eutectoid transformation A_1 is equal to 721 °C.

4. Application

The established relations were applied in computer simulation of mechanical properties and microstructure distribution of shaft made of low hardenability steel. Computer simulation of hardness and microstructure distribution of the as quenched workpiece was done using the computer software BS-QUENCHING [3]. Numerical simulation of the cooling time $t_{8/5}$ was based on finite volume method [3].
The shaft was quenched from 850 °C for 45 min/oil with *H*-value equal to 0.3. The chemical composition of investigated shaft is: 0.38 %C, 0.23 %Si, 0.64 %Mn, 0.019 %P, 0.013 %S, 0.99 %Cr, 0.16 %Mo. Jominy test results of the investigated steel are shown in Table 2. The geometry of the shaft is shown in Figure 2.

Table 2. Jominy test results of steel EN 42CrMo4

Tablica 2. Rezultati Jominyjevog pokusa čelika EN 42CrMo4

Jominy distance/mm	1.5	3	5	7	9	11	13
Hardness HRC	55	54	54	53	51	49	47
Jominy distance/mm	15	20	25	30	35	40	45
Hardness HRC	45	39	35	33	32	31	30
Jominy distance/mm	50	55	60	65	70	75	80
Hardness HRC	29	29	29	29	29	29	29

The distribution of hardness of the as quenched shaft is shown in Figure 3. The distribution of martensite, bainite and pearlite of as quenched shaft are shown in Figures 4-6.

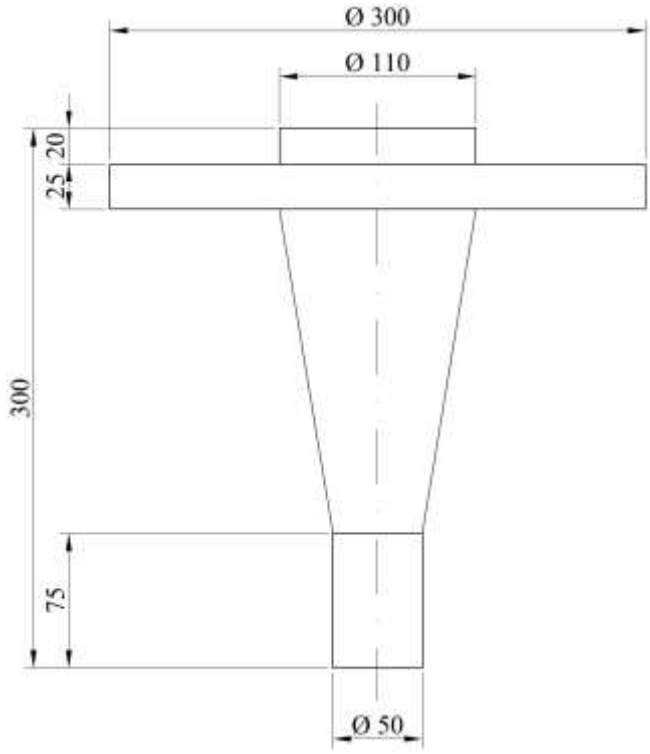

Figure 2. Geometry of the steel shaft

Slika 2. Geometrija čeličnog uzorka

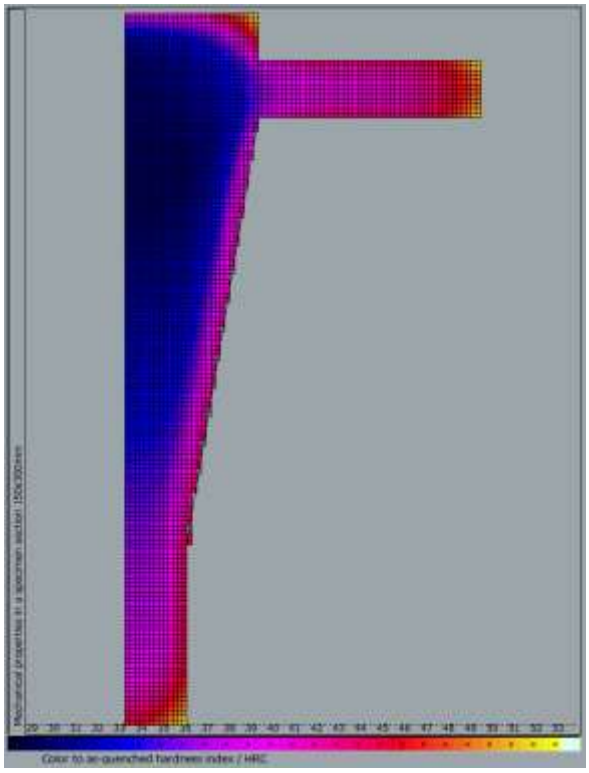

Figure 3. Distribution of hardness of as quenched shaft

Slika 3. Raspodjela tvrdoće kaljenog čeličnog uzorka

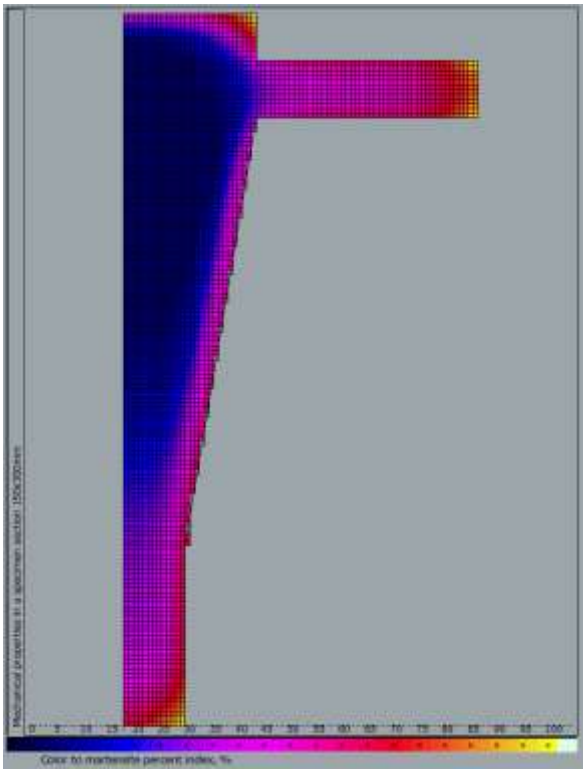

Figure 4. Distribution of martensite of as quenched shaft

Slika 4. Raspodjela martenzita kaljenog čeličnog uzorka

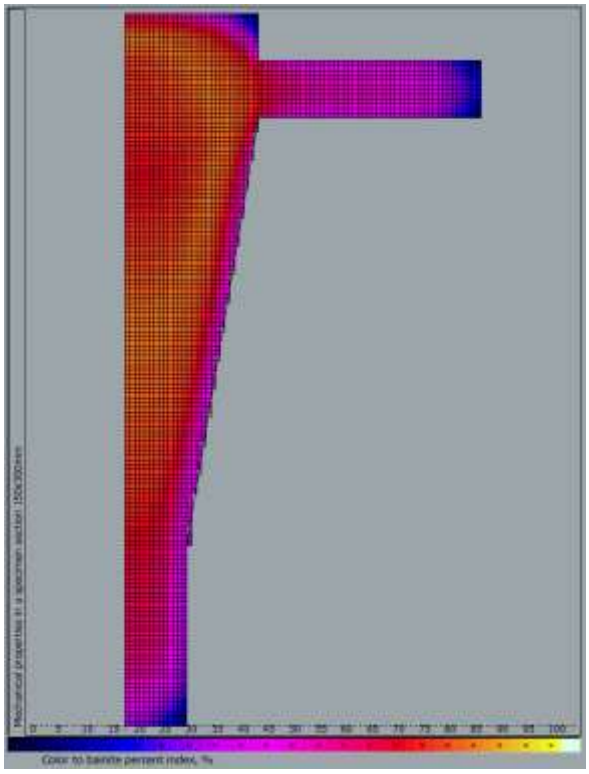

Figure 5. Distribution of bainite of as quenched shaft

Slika 5. Raspodjela bainita kaljenog čeličnog uzorka

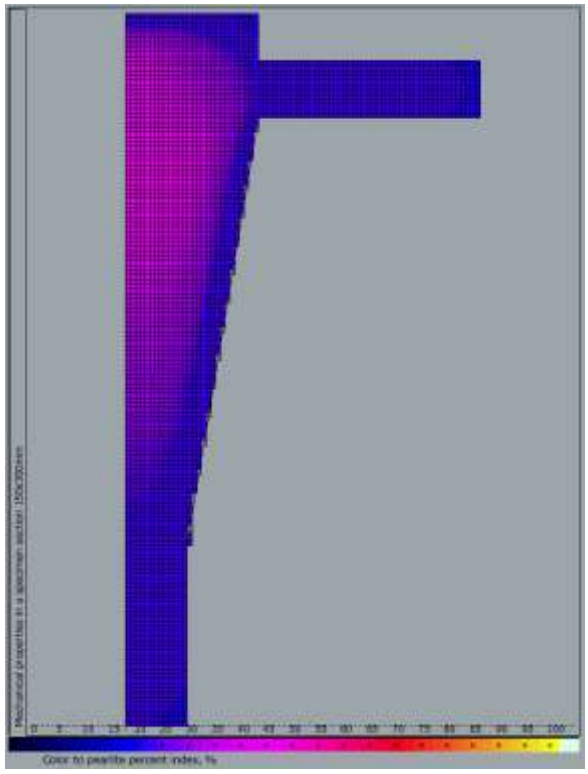

Figure 6. Distribution of pearlite of as quenched shaft

Slika 6. Raspodjela perlita kaljenog čeličnog uzorka

5. Conclusions

The mathematical model of steel quenching has been developed to predict the mechanical properties and microstructure distribution. The model is based on the finite volume method.

Input material data involved in mathematical model of quenching, i.e., density and specific heat capacity of steel have been accepted from literature. Heat transfer coefficient and heat conductivity coefficient have been successfully calibrated by based on results of quenching of steel specimen.

Hardness and microstructure composition in specimen points was calculated by the conversion of calculated time of cooling from 800 to 500 °C to hardness and microstructure composition.

A developed mathematical model has been applied in computer simulation of quenching of steel shaft, as well as, of die component of high hardenability steel. It can be concluded, that hardness and microstructure composition in quenched steel can be successfully calculated by proposed method.

ACKNOWLEDGEMENT

This work has been supported by University of Rijeka, Support No 13.09.1.1.02.

REFERENCES

[1] C. H. Gur, J. Pan, Handbook of Thermal Process Modeling Steels, CRC Press, 2008

[2] B. Smoljan, D. Iljkić, L. Pomenić, Mathematical modelling and computer simulation of mechanical properties of quenched and tempered steel, Int. J. Microstructure and Materials Properties, 2013, 8, 1/2, 97–112.

[3] B. Smoljan, Numerical simulation of as-quenched hardness in a steel specimen of complex form, Communications in Numerical Methods in Engineering, 1998, 14, 277-285.

[4] A. Rose, F. Wever, Atlas zur Wärmebehandlung der Stähle I, Verlag Stahleisen, Düsseldorf, 1954.

[5] S. Patankar, Numerical Heat Transfer and Fluid Flow, McGraw Hill Book Company, 1980.

[6] D. Iljkić, B. Smoljan, H. Novak, An analysis of thermal properties of steel during the quenching, Proceedings of the 3rd International conference "Mechanical Technologies and Structural Materials", MTSM2013, 26-27 September 2013, Split, Croatia.

[7] B. Smoljan, D. Iljkić, Computer Modeling of Mechanical Properties and Microsructure of Quenched Steel Specimen, Proceedings of the 5th International Conference on Thermal Process Modeling and Computer Simulation, 16-18 June 2014, Orlando, Florida USA.

ISSN 1847-7917

Particle erosion of sol-gel TiO_2-ZrO_2 films

Krešimir GRILEC, Lidija ĆURKOVIĆ, Marijana MAJIĆ RENJO, Suzana JAKOVLJEVIĆ and Vera REDE

1) University of Zagreb, Faculty of Mechanical Engineering and Naval Architecture,
Sveučilište u Zagrebu, Fakultet strojarstva i brodogradnje
Ivana Lučića 1, 10000 Zagreb, **Croatia**

kgrilec@fsb.hr

Keywords

Sol-gel
Thin films
Tribology
Particle erosion

Ključne riječi

Sol-gel
Tanke prevlake
Tribologija
Erozija česticama

Original scientific paper

Abstract: Wear resistance of metallic materials can be improved by modifying their surface with different coating deposition techniques, one of which is a sol-gel technology. In this paper, the erosive wear resistance of a ceramic nanostructured sol-gel TiO_2-ZrO_2 film deposited on the stainless steel substrate (X5CrNi18-10) by the dip coating technique has been described. Steel balls were used as an erodent, with the impact angle of 30° and 90°. The coating thickness, as well as chemical composition after erosion, was analyzed by the Glow Discharge Optical Emission Spectrometer (GD-OES). Obtained results showed that the erosive wear resistance of sol-gel TiO_2-ZrO_2 films does not depend significantly on the impact angle, if the applied erodents are steel balls. The coating is much harder than the substrate, so it is pressed into the substrate during the steel balls impacting.

Izvorni znanstveni rad

Sažetak: Otpornost trošenju metalnih materijala može se poboljšati modifikacijom njihove površine različitim metodama nanošenja prevlaka. U ovom radu ispitana je otpornost na erozijsko trošenje keramičke nanostrukturirane sol-gel TiO_2-ZrO_2 prevlake, nanesene na podlogu od nehrđajućeg čelika tehnikom uranjanja. Kao erodent korištene su čelične kuglice, pri čemu je kut upada iznosio 30° i 90°. Debljina prevlake i kemijski sastav površinskog sloja nakon erozije, određeni su optičkom emisijskom spektrometrijom s tinjajućim izbojem (GD-OES). Prema rezultatima ispitivanja, otpornost na erozijsko trošenje sol-gel TiO_2-ZrO_2 prevlaka ne ovisi značajno o kutu upada eroziva, ako su taj eroziv čelične kuglice. Uslijed udaraca čeličnih kuglica dolazi do djelomičnog utiskivanja prevlake u podlogu što je moguće zbog male tvrdoće podloge u odnosu na prevlaku.

1. Introduction

In order to improve properties of metallic materials, different ceramic coatings can be applied. Ceramic coatings can be deposited on metallic substrate by number of various techniques developed for this purpose. They include physical vapour deposition (PVD), chemical vapour deposition (CVD), electrochemical deposition, thermal spraying, plasma spraying and sol-gel processes, such as spin, dip and spray coating [1], [2].

The sol–gel method, also known as chemical solution deposition, is a wet-chemical technique, a process involving following steps: hydrolysis and polycondensation, gelation, aging, drying, densification and crystallization. The most important advantages of the sol-gel process are: low equipment costs, low processing temperature, good homogeneity, use of compounds that do not introduce impurities into the end product as initial substances, thus making it "green", waste-free technology. These advantages make the sol-gel process one of the most appropriate technologies for preparation of thin, nanostructured films [3]. Metal oxide nanostructures have been the focus of intensive research in the past years due to their potential application as catalysts for photodecomposition, semiconductors, in water treatment and so on [4]. Titanium and zirconium oxides are very promising candidates for future technology of thin layers because of their good mechanical, thermal and chemical properties [5].

Composite ZrO_2–TiO_2 films are also of significant scientific and technological importance, because several advantages can be derived from this binary composite system. The most attractive one is that the properties of the composite materials can be easily tailored by a simple control of the system. Moreover, the composite materials often exhibit better mechanical and thermal properties than the two participating components [6].

Symbols/Oznake

w(Me)	- mass portion of metal, % - maseni udio metala, %

2. Sample preparation

In this investigation, two samples (dimensions: 17×17×80 mm) of stainless steel X5CrNi18-10 (AISI 304) were used as substrates for sol-gel deposition. Prior to the coating deposition, samples were ground with SiC abrasive discs of different granulation (180–1000 grit) and then polished with diamond paste (3 μm and 0.25 μm). Thereafter, substrates were ultrasonically cleaned in acetone and subsequently dried in an oven at 100 °C for an hour.

For the preparation of sol (colloidal solution), the following components were used:

- 0.5 mol of titanium isopropoxide and 0.5 mol zirconium butoxide (ratio 1:1) as precursor,
- 0.8 mol acetylacetone as a chelating agent,
- 40 mol of *i*-propanol as a solvent,
- 0.05 mol of nitric acid as a catalyst,
- 5 mol of distilled water for hydrolysis.

The final precursor sol was yellow, transparent and homogeneous.

Coatings were deposited on 2 equal samples with rate of 1.7 mm/s. The substrates were held in solution for 3 minutes, in order to allow surface wetting. The samples were withdrawn from the sol with the same rate (figure 1). After each dipping, the samples were air dried for an hour and subsequently dried in the oven at 100 °C for an hour as well. The whole deposition procedure was repeated three times, in order to increase the coating thickness. Sample 1 was calcined after each dipping and drying procedure, while the sample 2 was calcined only after the third dipping and drying cycle. The calcination was conducted in the following way: samples were heated on 500 °C at the rate of 2 °C/min, hold on this temperature for an hour and then cooled down by the furnace cooling rate.

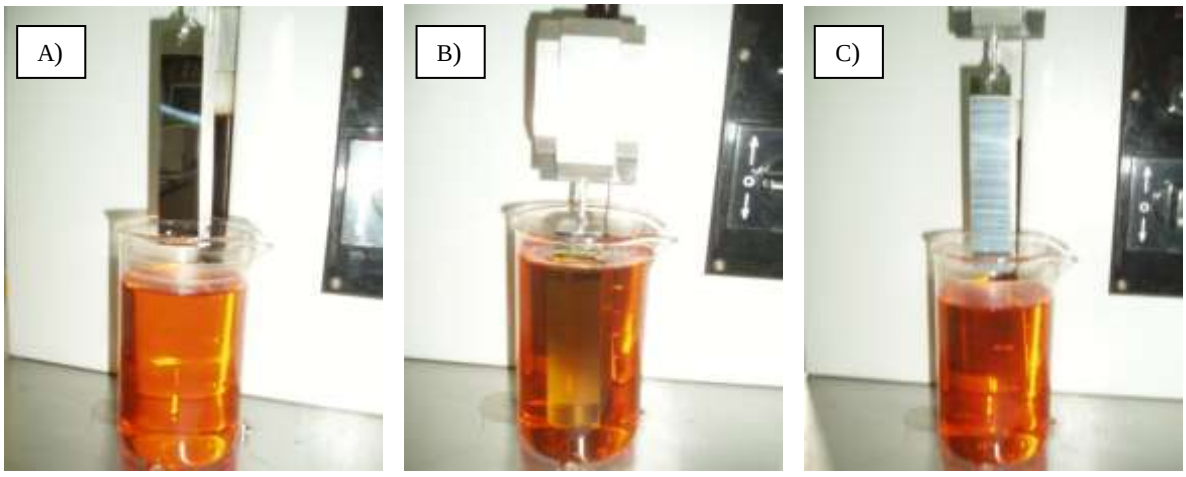

Figure 1. Deposition procedure: dipping (A); holding (B); withdrawing (C).
Slika 1. Postupak prevlačenja: uranjanje (A); držanje (B); izvlačenje (C).

3. Surface analysis of prepared samples

Figure 2 shows the surface of coated samples as seen with the optical microscope. The coating of the sample 2, which was calcined only once, after three dipping and drying procedures, is clearly cracked. It is assumed that the cracking occurred due to the calcination of three layers at the same time, that is, because the coating was thicker.

For chemical surface analysis of deposited coatings, glow discharge optical emission spectrometer (GDS 850A, Leco) was used. This device can be used for elemental bulk analysis, but it can also be used for determination of coating thickness and quantitative depth profiling (QDP). In other words, it can show the chemical composition of a coating, as well as the distribution of chemical elements from the surface to the substrate.

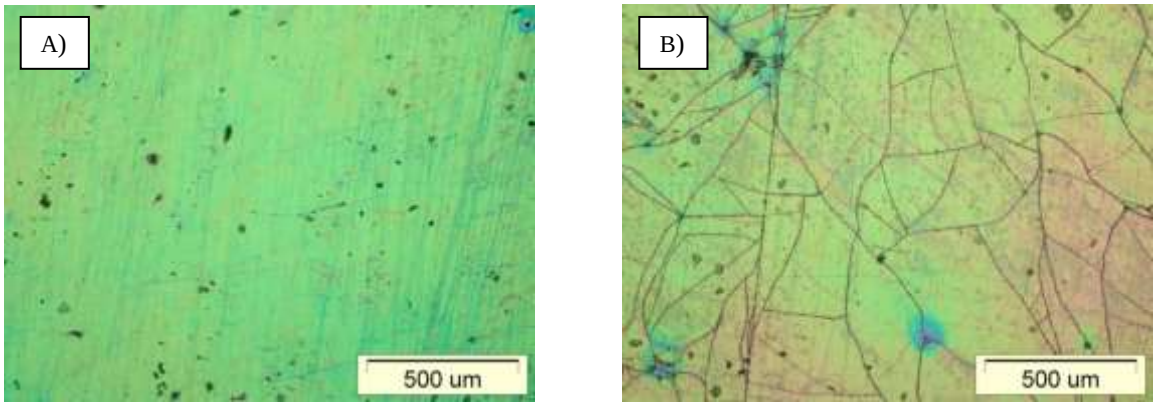

Figure 2. Optical microscope images of the obtained coatings: sample 1 (A); sample 2 (B)
Slika 2. Površina prevlaka snimljena svjetlosnim mikroskopom: uzorak 1 (A); uzorak 2 (B)

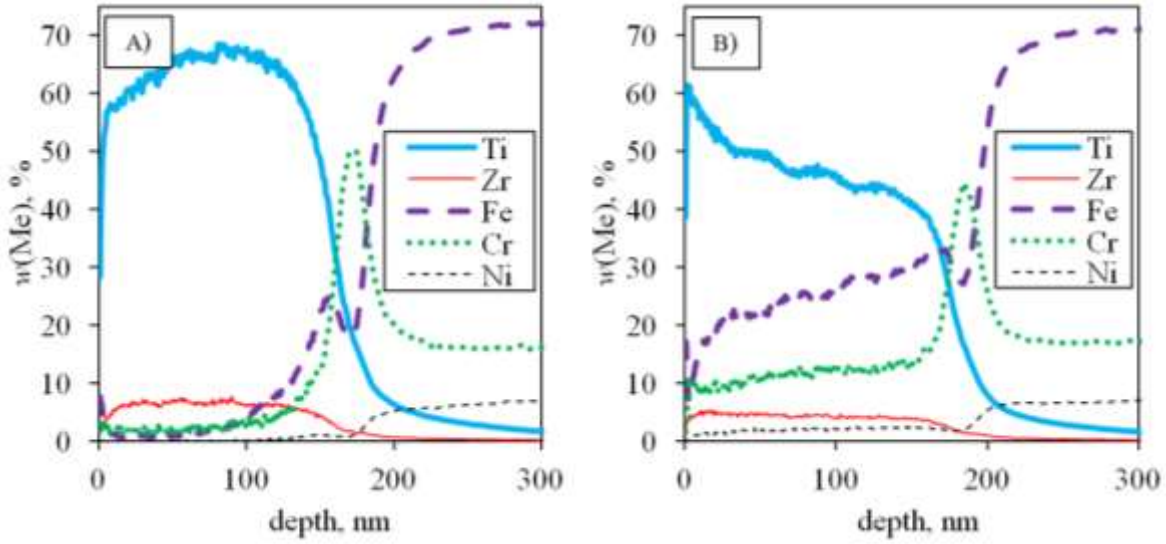

Figure 3. Quantitative depth profiling of samples (Me= Ti, Zr, Ni, Cr, Fe): sample 1 (A); sample 2 (B)
Slika 3. Kvantitativna dubinska profilna analiza (Me= Ti, Zr, Ni, Cr, Fe): uzorak 1 (A); uzorak 2 (B)

Distribution of the most important elements from surface to substrate for samples 1 and 2 is shown in Figure 3. This diagram shows the element mass fraction *w* (Me) in coating and in substrate. Titanium (Ti) and zirconium (Zr) are present in the coating (note: used device is not equipped with oxygen photomultiplier), while Ni, Cr and Fe are present in the substrate. It can be seen from the Figure 3 that the coating thickness was slightly higher than 150 nm for both samples. As the sample 2 was cracked, the notable diffusion of Fe and Cr from the substrate into the coating was noticed. It has also been noticed that Cr and Fe defunded into the coating. This diffusion was larger for those samples where calcination was conducted only once, after three dipping processes (Sample 2).

4. Testing of solid particle erosion

Particle erosion is a wear loss from surface of solid body caused by a relative motion of fluid with solid particles. When impact angle is low (between 0° and 30°), this kind of erosion is called the abrasive erosion. On the other side, if the impact angle is between 60° and 90°, it is considered the impact erosion [7].

The test of solid particle erosion with steel balls was performed in Laboratory for Tribology on Faculty of Mechanical Engineering and Naval Architecture in Zagreb. The particle erosion tester is shown in Figure 4.

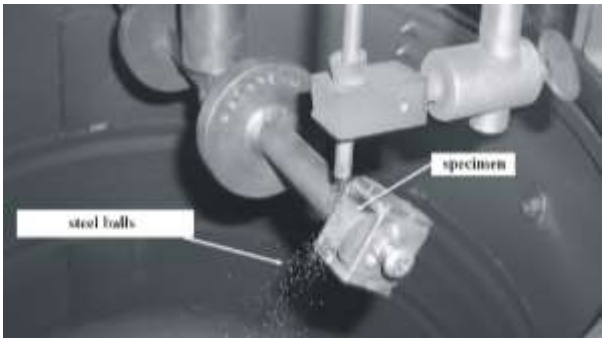

Figure 4. Testing of solid particle erosion
Slika 4. Ispitivanje otpornosti na eroziju česticama

Testing parameters:

- abrasive: steel balls (diameter: 700 μm),
- revolution: 1440 rpm,
- sample velocity: 24.3 m/s
- time of testing: 42 sec (~ 1000 impacts)
- impact angles: 30° and 90°
- sample dimension: 17×17×17 mm

The eroded samples were also subjected to the Quantitative depth profiling. The results are presented in Figure 5 and Figure 6.

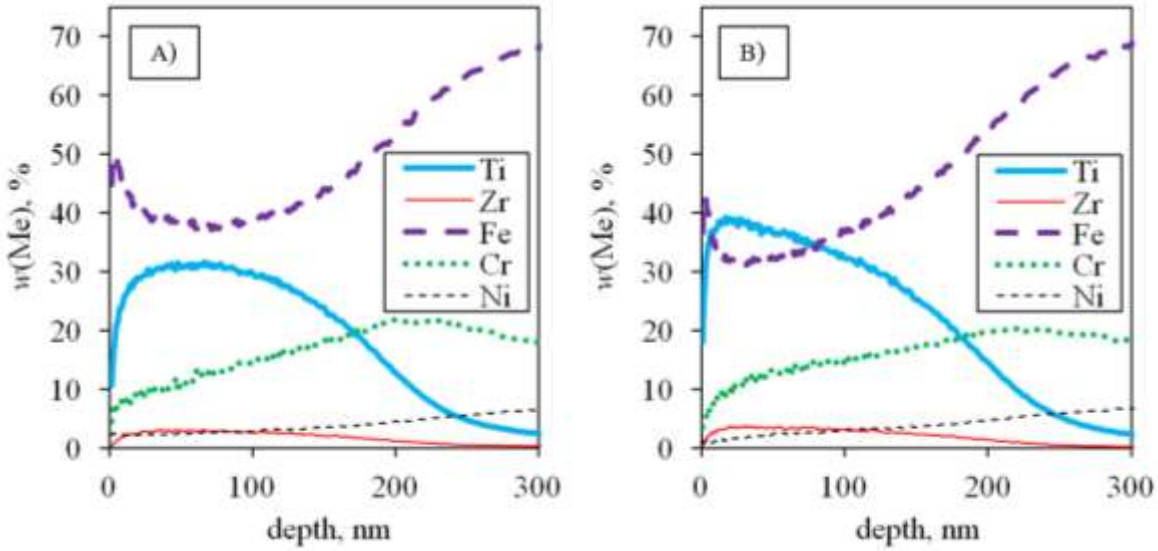

Figure 5. Quantitative depth profiling after erosion (angle 30°, 1000 impact): sample 1 (A); sample 2 (B)
Slika 5. Kvantitativna dubinska profilna analiza nakon erozije (kut 30°, 1000 udaraca): uzorak 1 (A); uzorak 2 (B)

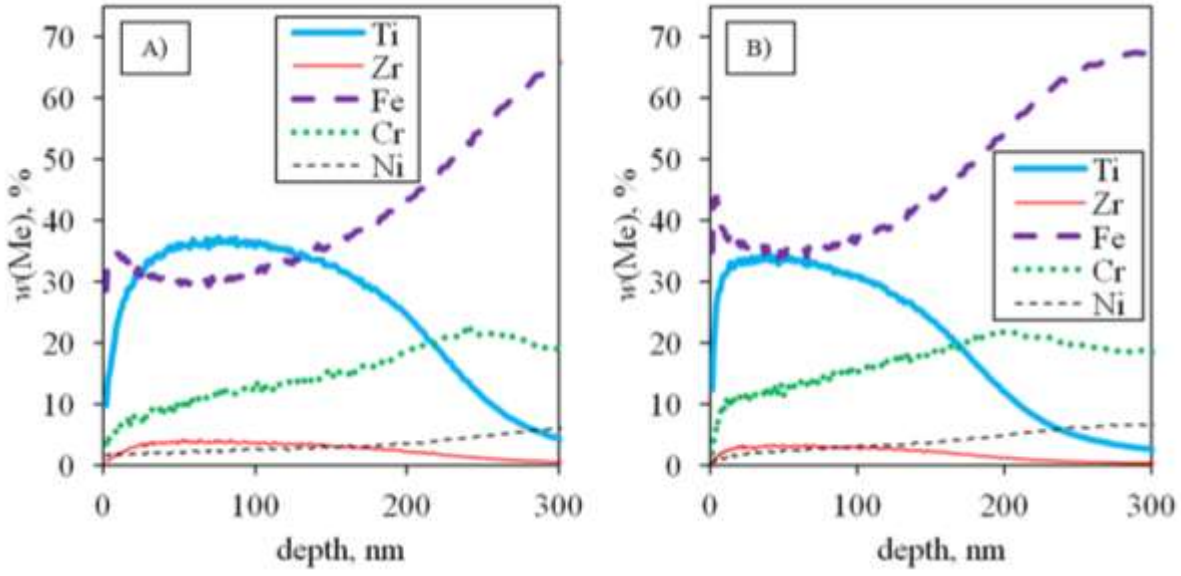

Figure 6. Quantitative depth profiling after erosion (angle 90°, 1000 impact): sample 1 (A); sample 2 (B)
Slika 6. Kvantitativna dubinska profilna analiza nakon erozije (kut 90°, 1000 udaraca): uzorak 1 (A); uzorak 2 (B)

The high amount of iron (Fe) is presented on sample surface after erosion, as it can be seen on Figures 5 and 6, because the coating was in places completely worn off, which is consistent with a great number of wear scars.

It is also visible from Figures 5 and 6 that the impact angle affects the distribution of the chemical elements on the surface. It is not visible that the occurred cracking caused higher wear. After erosion, there is lower mass portion of Ti on the surface, but Ti is present deeper inside of the substrate, suggesting that the coating is partially pressed into the substrate. This is

possible due to the significantly harder coating than the substrate.

Figure 7 and 8 show eroded surfaces analyzed by scanning electron microscope. Due to the surface cracking of the sample 2, the presence of the coating after erosion is evident. The coating still exists on the sample 1 as well, which it is not clear from the SEM image, but from the SEM-EDS image (energy dispersive spectrometry), presented with Figure 9. Titanium was found even in the large crater originated from the punch of steel balls at the impact angle of 90°. This also indicates that the hard coating was pressed into the soft substrate.

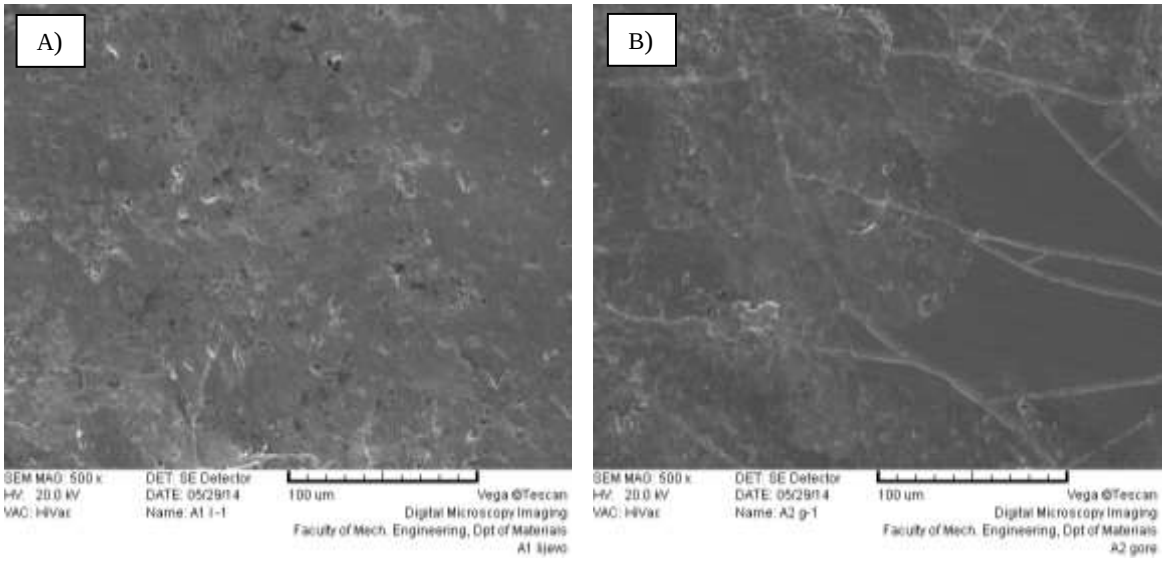

Figure 7. Specimen surfaces eroded at the impact angle of 30°: sample 1 (A); sample 2 (B)
Slika 7. Površine uzoraka erodiranih pod kutem od 30°: uzorak 1 (A); uzorak 2 (B)

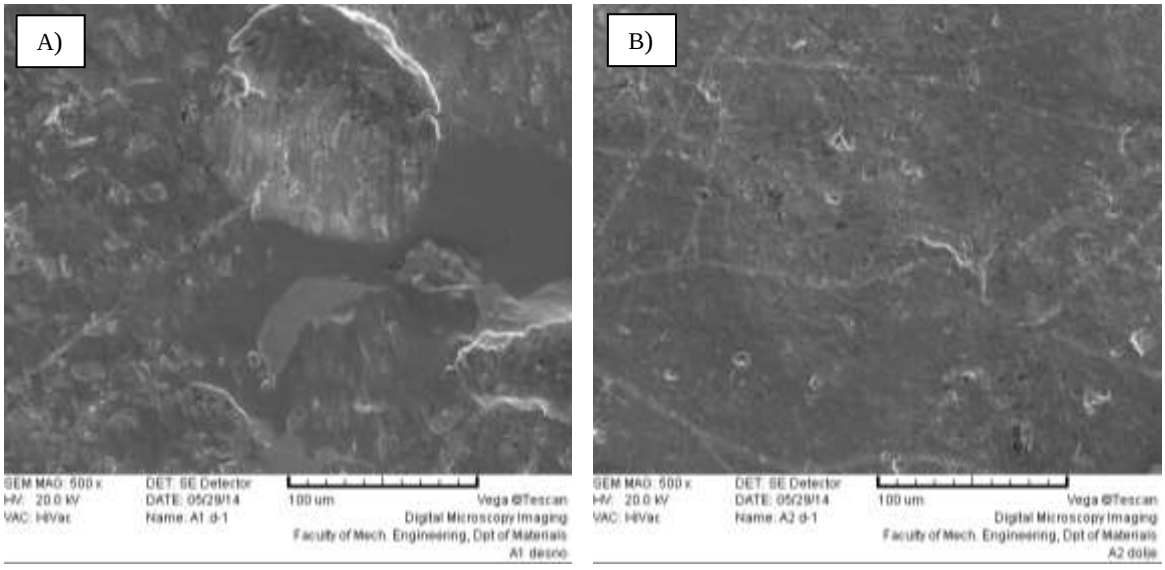

Figure 8. Specimen surfaces eroded at the impact angle of 90°: sample 1 (A); sample 2 (B)
Slika 8. Površine uzoraka erodiranih pod kutem od 90°: uzorak 1 (A); uzorak 2 (B)

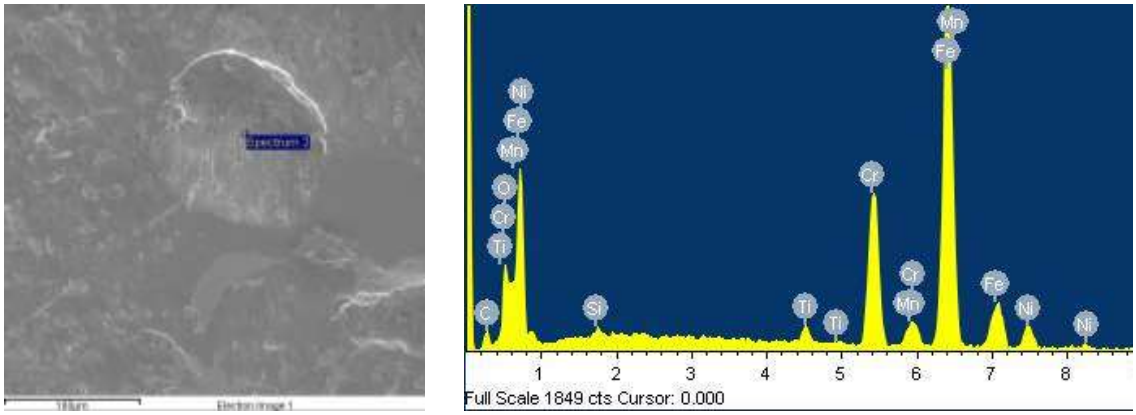

Figure 9. SEM-EDS analysis of the sample 1
Slika 9. SEM-EDS analiza uzorka 1

5. Conclusion

Sol-gel method and the dip coating technique are convenient for deposition of composite TiO_2–ZrO_2 coating on the stainless steel substrate. If the process parameters are well chosen, deposited coating can achieve high quality without visible cracks. During the calcination, the diffusion of elements, from substrate to coating and vice versa, has been noticed.

During the surface erosion, the coating is partially broken through. The erodent impact angle does not significantly influence the distribution of the chemical elements on the surface. After erosion, there is less Ti on the surface, but Ti is distributed deeper inside the substrate, indicating that the coating is partially pressed into the substrate. This is possible due to the higher hardness of the coating than the substrate.

REFERENCES

[1] Dai W. X., Chen X., Li E., Wang X. X., Liu P., Fu, X. Z.: *Influence of pH value of TiO_2 sol on surface gloss of corresponding TiO_2 film coated on ceramic tiles*, Surf. Eng. 25, 2009, 106-109

[2] Fu T., Wen C. S., Lu J., Zhou Y. M., Ma S. G., Dong B. H., Liu B. G.: *Sol-gel derived TiO_2 coating on plasma nitrided 316L stainless steel*, Vacuum, 86, 2012, 1402-1407

[3] Ćurković L., Otmačić Ćurković H., Salopek S., Majić Renjo M., Šegota S., *Enhancement of corrosion protection of AISI 304 stainless steel by nanostructured sol-gel TiO_2 films*, Corrosion Science, 77, 2013, 176-184

[4] Kitiyanan A., Sakulkhaemaruethai S., Suzuki Y., Yoshikawa S., *Structural and photovoltaic properties of binary TiO_2–ZrO_2 oxides system prepared by sol–gel method*, Composites Science and Technology, 66, 2006, 1259-1265

[5] Bensouyad H., Sedrati H., Dehdouh H., Brahimi M., Abbas F., Akkari H., Bensaha R., *Structural, thermal and optical characterization of TiO_2:ZrO_2 thin films prepared by sol–gel method*, Thin Solid Films, 519, 2010, 96-100

[6] Liang L., Sheng Y., Xu Y., Wu D., Sun Y., *Optical properties of sol–gel derived ZrO_2–TiO_2 composite films*, Thin Solid Films, 515, 2007, 7765-7771

[7] *Glossary of terms and definitions in the field of friction, wear and lubrication – tribology*, OECD Publications, Paris 1969

CARDBOARD BRIQUETTES FOR HEAT ENERGY PRODUCTION

Branimir LELA[1)]**,**
and Marin BARIŠIĆ[1)]

1) Fakultet elektrotehnike, strojarstva i brodogradnje, Sveučilišta u Splitu (Faculty of Electrical Engineering, Mechanical Engineering and Naval Architecture, University of Split) Ruđera Boškovića 32, 21000 Split, **Republic of Croatia**

blela@fesb.hr

Keywords

Cardboard/sawdust briquettes
Heating capacity of briquettes
Briquette pressing and drying

Ključne riječi

Briketi od kartona/piljevine
Ogrjevna moć briketa
Prešanje briketa i sušenje

Primljeno (Received): 20xx-xx-xx
Prihvaćeno (Accepted): 20xx-xx-xx

Original scientific paper

This study deals with the briquettes production out of the cardboard waste and sawdust. In order to determine the effect of pressure, cardboard/ sawdust ratio and draying temperature on calorific value of the produced briquettes experiments were carried out. Pressure was varied from 147,15 to 588,6 kN, sawdust/cardboard ratio was changed from 0 to 46,66% and drying temperature was within interval of 22 and 100°C. The results of experiments show that regarding the heating ability the briquettes made out of cardboard and cardboard/sawdust combination are able to successfully compete with the other heating elements (pellets and briquettes) made of various other biomasses.

Kartonski briketi za proizvodnju toplinske energije

Izvornoznanstveni članak

Ovo istraživanje se bavi proizvodnjom briketa od kartonskog otpada i piljevine. Kako bi se odredio utjecaj pritiska, omjera kartona i piljevine i temperature sušenja na ogrjevnu moć proizvedenih briketa provedeni su eksperimenti. Pritisak je varirao od 147,15 do 588,6 kN, omjer mase piljevine i kartona se mijenjao od 0 do 46,66%, a temperatura sušenja briketa se mijenjala od 22 do 100°C. Rezultati eksperimenata pokazuju da, uzimajući u obzir ogrjevnu vrijednost, se briketi izrađeni od kartona i kombinacije kartona i piljevine mogu uspješno natjecati sa drugim elementima za proizvodnju toplinske energije (peleti i briketi) izrađeni od drugih različitih biomasa.

1. Introduction

Global energy consumption has grown at an average annual rate of about 2% per year over the last two hundred years. Conventional energy sources (coal, oil, natural gas, nuclear and hydropower) account for 85-90% of global primary energy consumption. In the two last decades trends in global energy market are to utilize renewable energy resources and reduce dependency on fossil fuels. One of the renewable energy resources is the biomass out of which briquettes are made [1,2,3,4,5]. Right behind coal and oil, biomass is the third largest energy resource in the world [1]. Fuel briquettes can be made from various waste materials. In urban areas it is sawdust and shredded paper. In villages and rural areas, leaves, grass, rice husks and other agricultural waste in many combinations can serve the purpose. One of the interesting ideas is to utilize paper briquettes/pellets as a fuel [2,4,6]. Municipal solid waste typically consists of 40 to 45 % of paper products which are a potential valuable source of energy [6]. Paper waste is easy to segregate from the solid waste. It is free of metals and other noncombustible materials and has a high calorific value. It has excellent storage characteristics when it is densified and it has low sulfur content and low nitrogen oxides emissions [2,4,6]. With a comparable price to coal, paper briquettes can be used as a fuel. Major limitations for utilizing biomass for bioenergy products is its low bulk density, which ranges from 80–100 kg/m^3 for agricultural straws and grasses and 150–200 kg/m^3 for woody resources [1,7,8]. The low density makes the material difficult to store, transport and interface with biorefinery systems. One way to overcome this limitation is to increase biomass density. Common biomass densification systems have been adapted from other processing industries and include pellet mill, cuber, briquette press, screw extruder, tabletizer, and agglomerator [1]. The pellet mill, briquette press, and screw extruder are the most common used for bioenergy production. The quality of densified biomass depends on strength and durability of the particle bonds, which are influenced by a number of process variables: die diameter, die temperature, pressure, binders and pre-heating of the biomass mix [1]. Controlling the pelleting/briquetting system variables, including both process and feedstock variables, allows achieving the desired density, durability, and quality. That is a reason why this study deals with the influence of sawdust/cardboard mixture, densification force and drying temperature on the calorific value of paper briquettes produced as an alternative fuel.

Symbols/Oznake

HHV	- Higher heating value, *MJ/kg* - Gornja ogrjevna vrijednost, *MJ/kg*	DOE	- Design of experiment - Plan eksperimenata
BBD	- Box-Behnken design - Box-Behnken plan pokusa	RA	- Regression analysis - Regresijska analiza

2. Experimental procedure

The goal of this study is to obtain mathematical models that relate compression force, cardboard/sawdust ratio and drying temperature during the briquettes production with their heating value. Design of experiment (DOE), analysis of variance (ANOVA) and regression analysis (RA) have been used in order to get the mathematical model. The DOE was achieved using the Box-Behnken response surface design (BBD). In the experimental research and modelling BBD of experiment is very often used because it offers optimization possibility and reduction the number of experiments. Three factorial BBD of experiment demands 12 experiments (each factor on 3 levels), and 5 central experiments, what makes total of 17 experiments ($N = k^2 + k + c_p$, where k is the number of factors and c_p is the number of central point replications). The minimal and maximal values of chosen parameters as well as the coded input factors are presented in Table 1. To collect data for ANOVA and RA, software package Design-Expert was used to generate 17 experimental points. Overall experimental plan can be seen in Table 2.

Table 1. Physical and coded values of input factors
Tablica 1. Fizikalne i kodirane vrijednosti ulaznih faktora

Input factors	Coded values of input parameters		
	$x_{\text{-i,min}}$	$x_{\text{-i0}}$	$x_{\text{i,max}}$
	-1	0	+1
x_1 = Compression force, kN	147,15	367,88	588,6
x_2 = Sawdust weight, %	0	23,33	46,66
x_3 = Draying temperature, °C	22	50	100

The briquettes were made of three-layer corrugated cardboard (out of which packaging boxes are made) and sawdust in a specific weight ratios. Before compression cardboard was shredded into pieces of approximate dimensions 10 x 15 mm and chopped by a blender. The sawdust was made of fir. The mixture of cardboard and sawdust for each sample had the same mass of 15 grams. The mass of samples were determined by a digital scale shown on Fig1.b. An experimental rig for briquettes production was made consisting of a mould, punch and pressing plate. The rig is shown on Fig.1a. The bore in the mould was 38.6 mm in diameter and with the height of 110 mm. Cardboard/sawdust mixture was loaded in the mould and compressed up to a force specified by the plan of experiments. Depending on the compression force final height of the briquettes varied from 6 to 9 mm. Produced briquettes are shown on Fig.1c. The draying of briquettes was carried out in an electric furnace in duration of 30 min. In accordance with the plan of experiments one specimen at the time was placed in the furnace after the desired temperature had been reached. After achieving the desired draying time at a specific temperature the samples were taken out of the furnace and left to cool in still air. After completion experiments all seventeen samples in the form of briquettes were sent for calorific value analysis. The analysis of higher heating value (HHV) for all samples was carried out in the Central laboratory for chemical technology (CLFCT) which is a part of the HEP Inc. Group. HHV was obtained according to EU norm EN 14918.

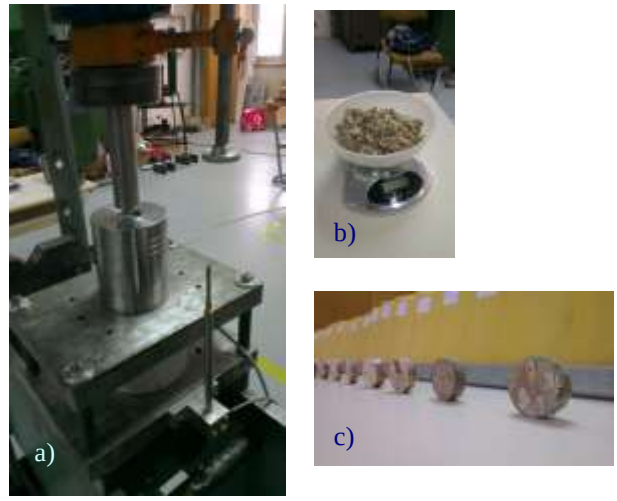

Figure 1. Experimental rig (a), preparation of cardboard/sawdust mixture (b) and briquettes after compression (c)

Slika 1. Oprema za eksperimentiranje (a), priprema mješavine kartona i piljevine (b) i briketi nakon prešanja (c)

The results of HHV measurements for all samples in accordance to the plan of experiments are shown in Table 2.

Table 2. Input factors according to BBD of experiment and results of measurements of higher heating values for produced briquettes
Tablica 2. Ulazni faktori prema Box-Behnken planu eksperimenata i rezultati mjerenja gornje ogrjevne vrijednosti proizvedenih briketa

Experiment number	*Compression force (kN)*	*Sawdust mass (%)*	*Draying temperature (°C)*	*Higher heating value (MJ/kg)*
1.	367.88	0.00	22.00	14.95
2.	588.60	46.66	50.00	15.62
3.	588.60	23.33	22.00	15.99
4.	367.88	0.00	100.00	15.18
5.	147.15	0.00	50.00	15.04
6.	367.88	46.66	100.00	15.89
7.	147.15	46.66	50.00	16.06
8.	367.88	23.33	50.00	15.05
9.	147.15	23.33	100.00	15.54
10.	588.60	0.00	50.00	14.88
11.	367.88	23.33	50.00	14.93
12.	367.88	23.33	50.00	15.2
13.	588.60	23.33	100.00	15.74
14.	367.88	46.66	22.00	16.1
15.	367.88	23.33	50.00	15.04
16.	147.15	23.33	22.00	16.94
17.	367.88	23.33	50.00	15.3

3. ANOVA and regression analysis

The measured values of HHV on each specimen (Table 2) are input data for the second-order regression models and ANOVA. The ANOVA and regression analysis have been carried out using program package "Design Expert 8". The ANOVA shows which factors and interactions have an important influence on the heating value of briquettes. Applying the regression analysis the coefficients of regression, multi-regression factors, standard false evaluation and the value of *t*-test were determined and mathematical models were obtained.
Mathematical model for the prediction of higher heating value (HHV) as a function of compression force, sawdust mass percentage and drying temperature was obtained as follows:

$$HHV = 17.22152 - 8.157 \cdot 10^{-3} \cdot A + 0.019396 \cdot B - 0.0349 \cdot C + 8.27778 \cdot 10^{-6} \cdot A^2 + 2.13316 \cdot 10^{-4} \cdot C^2 + 2.60505 \cdot 10^{-5} \cdot A \cdot C \quad (1)$$

where are:
A – Compression force (kN)

B – Mass of sawdust (%)

C – Draying temperature (°C)

The coefficients R-Squared, Adjusted R-Squared and Predicted R-Squared were obtained as 0.89, 0.82, and 0.43 respectively. ANOVA indicates that compression force does not have significant influence on HHV. However this parameter cannot be disregarded in the mathematical model because it supports mathematical hierarchy.
Graphical representation of the equation (1), when one factor is held fixed, is shown in Fig.2, Fig.3 and Fig.4.

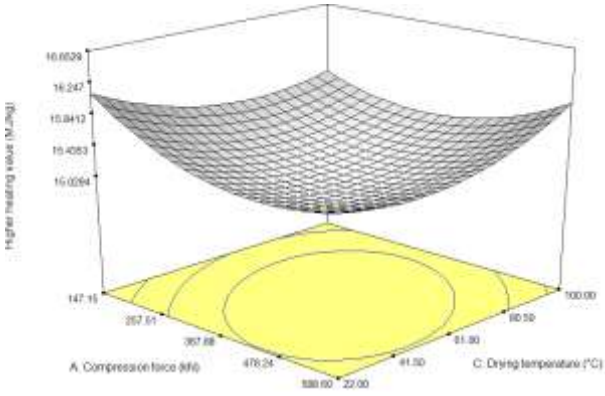

Figure 2. Graphical representation of the influence of compression force and drying temperature on HHV of briquettes when mass of sawdust is 25%

Slika 2. Grafički prikaz utjecaja sile sabijanja i temperature sušenja na gornju ogrjevnu vrijednost briketa kada je masa piljevine 25%

Surface on the Fig. 2 shows the effect of compression force and drying temperature on HHV when mass of sawdust is 25%. It can be seen that both factors has similar effect on HHV. At low drying temperatures, for example 22°C, HHV decreases with the increment of compression force, but for higher drying temperatures situation is reversed. Maximum value for HHV is obtained for compression force of 147,15 kN and without drying on higher temperatures.

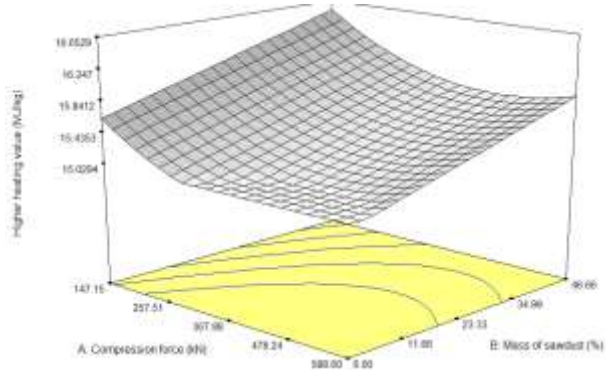

Figure 3. Graphical representation of the influence of compression force and mass of sawdust on HHV of briquettes when draying temperature is 22°C

Slika 3. Grafički prikaz utjecaja sile sabijanja i mase piljevine na gornju ogrjevnu vrijednost briketa kada je temperatura sušenja 22°C

Fig. 3 shows the effect of compression force and mass of sawdust on HHV when drying is undertaken at the room temperature of 22°C. Mass of sawdust shows significant influence on the HHV no matter what compression force is applied. The HHV decreases with decreasing mass of sawdust. Maximal HHV is achieved when the samples are composed of 46,66% of sawdust and when the compression force is 147,15 kN. Conclusion can be drawn that sawdust increases HHV of briquettes.

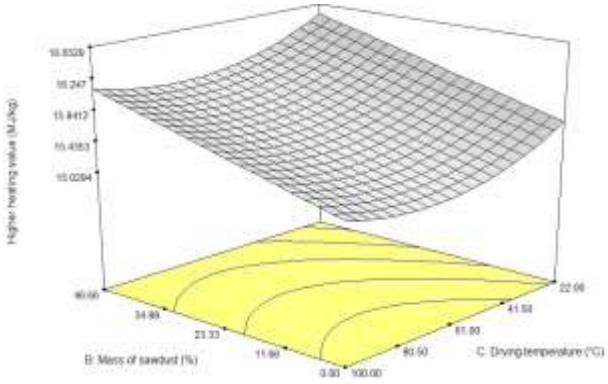

Figure 4. Graphical representation of the influence of drying temperature and mass of sawdust on HHV of briquettes when compression force is 147,15 kN

Slika 4. Grafički prikaz utjecaja temperature sušenja i mase piljevine na gornju ogrjevnu vrijednost briketa kada je sila sabijanja 147,15 kN

Fig. 4 shows the effect of mass of sawdust and drying temperature on HHV when compression force is 147,15 kN. Sawdust shows greater influence on HHV when compared to drying temperature influence. HHV again increases with mass of sawdust increment while drying temperature increment appears to decrease HHV. Maximal HHV is obtained when the samples are composed of 46,66% of sawdust and when drying at higher temperatures is not undertaken.

4. Conclusion

In this work the effect of compression force, drying temperature and cardboard/sawdust ratio on the higher heating value of briquettes were studied. Experiments were carried out in accordance with the Box-Behnken design of experiments. Utilizing ANOVA and regression analysis quadratic mathematical models for HHV prediction were obtained. In order to obtain high level of briquettes densification compression force is always needed, although according to ANOVA it has no significant influence on HHV. However compression force cannot be omitted from the mathematical model because it supports model hierarchy. According to ANOVA and RA major influence on HHV exhibits drying temperature and sawdust mass percentage in the briquettes. No matter what compression force is applied during the densification of briquettes the increment of sawdust in the briquettes increases their HHV. On the other hand for low compression forces HHV slightly decreases when drying temperature increases while for high compression forces HHV slightly increases for drying temperatures increment. The primary goal in briquette production is HHV as high as possible. Mathematical model obtained in this study shows that the highest HHV of 16,95 MJ/kg would be obtained if sawdust in the briquette is as high as possible, compression force as low as possible and without special drying at higher temperatures.

REFERENCES

[1] TUMULURU, J. S., WRIGHT, C. T., HESS, J. R., KENNEY, K. L.: A review of biomass densification systems to develop uniform feedstock commodities for bioenergy application, *Biofuels, Bioprod. Bioref.* 5, 2011, pp. 683–707; DOI: 10.1002/bbb.

[2] GADO, I. H., OUIMINGA, S. K., DAHO, T., YONLI, A. H., SOUGOTI, M., KOULIDIATI, J.: Characterization of Briquettes Coming From Compaction of Paper and Cardboard Waste at Low and Medium Pressures, Waste and Biomass Valorization 12, 2013; DOI:10.1007/s12649-013-9282-3

[3] TARASOV, D., SHAHI, C., LEITCH, M.: Effect of Additives on Wood Pellet Physical and Thermal Characteristics: A Review, ISRN Forestry, Vol. 2013, 2013, Article ID 876939, 6 pages.

[4] DEMIRBAS, A., SAHIN, A.: Evaluation of biomass residue 1. Briquetting waste paper and wheat straw mixtures, Fuel Processing Technology 55, 1998, pp. 175–183.

[5] KALIYAN, N., MOREY, R. V., Factors affecting strength and durability of densified biomass products, Biomass and Bioenergy, Vol.33(3), 2009, pp. 337–359; DOI: 10.1016/j.biombioe.2008.08.005

[6] LI, Y., LIU, H., High-pressure binderless compaction of waste paper to form useful fuel, Fuel Processing Technology 67, 2000, pp. 11–21.

[7] PLÍŠTIL, D., BROŽEK, M., MALAŤÁK, J., ROY, A., HUTLA, P.: Mechanical characteristics of standard fuel briquettes on biomass basis, Research in Agricultural Engineering., Vol.51(2), 2005, pp. 66–72.

[8] LI, Y., LIU, H., ZHANG, O.: High-pressure compaction of municipal solid waste to form densified fuel, Fuel Processing Technology 74, 2001, pp. 81–91.

Measuring of sand core casting with 3D digitalisator
Mjerenje pješčane jezgre odljevka 3D digitalizatorom

***Filip VALE*[1)], *Duško PAVLETIĆ*[2)], *Graciela ŠTERPIN*[2)] *i Mladen PERINIĆ*[2)]**

1)Trgometal d.o.o., Gorica 11b Sutivanac, 52341 Žminj, Hrvatska/Croatia

2)Sveučilište u Rijeci, Tehnički fakultet/ University of Rijeka, Faculty of Engineering, Vukovarska 58, 51000 Rijeka, Hrvatska/Croatia

duskop@riteh.hr

Keywords

Digizalization
Sand core
Polygonization
Uncoded measuring points
CAD model

Ključne riječi

Digitalizacija
Pješčana jezgra
Poligonizacija
Nekodirane mjerne točke
CAD model

'

Professional paper

Abstract: Nowadays, rhytm of industrial production is faster and faster so there is greater demand for fast and precise measuring of geometrical characteristics of products. When talking about products that have high degree of complexity we have a problem with imposibility of using conventional measuring devices or very slow and hard usage of them. Optical measuring instruments are more and more used instead of traditional coordinate 3D measuring devices, especially in case when measuring by conventional methods don´t give satisfying results. Data optained by measuring are proccessed in special programme package and in very short time they are disposable as true computer model of a measured object. Computer model of the taken object ensures precise measuring and analysis of product´s functional coordinates. Result of object digitalization is taken as model than can be compared with the original CAD model. Such analysis answers the question about needed process accuracy and precision in production of particular objects. It is also a starting point for possible tool and work correction. Measuring the shape of a sand core, that is used for production of turbo blower casting is shown in this paper. For sand core digitalization ATOS system first generation has been used. Data obtained by digitalization have been processed in GOM Inspect programme package.

Stručni članak

Sažetak: U današnje vrijeme ritam industrijske proizvodnje je sve brži pa samim time postoji sve veća potreba za brzim i preciznim mjerenjem geometrijskih karakteristika samih proizvoda. Govori li se o proizvodima koji imaju visok stupanj složenosti nailazi se na problem nemogućnosti korištenja konvencionalnih mjernih strojeva ili veoma sporo i mukotrpno korištenje istih. Optički mjerni instrumenti sve češće zamjenjuju tradicionalne koordinatne 3D mjerne strojeve, pogotovo u slučajevima kada mjerenja konvencionalnim metodama ne daju zadovoljavajuće rezultate. Podaci dobiveni mjerenjem se obrađuju u posebnom programskom paketu i u vrlo kratkom roku su raspoloživi kao vjeran računalni model mjerenog objekta. Računalni model snimanog objekta osigurava točno mjerenje i analizu funkcionalnih koordinata proizvoda. Rezultat digitalizacije objekta je snimljen kao model kojeg je moguće usporediti sa izvornim CAD modelom. Takve analize daju odgovor na pitanje o traženoj točnosti i preciznosti obrade u proizvodnji pojedinih objekata, te su polazište za eventualne korekcije alata i objekta. U radu je prikazano mjerenje oblika pješčane jezgre koja se koristi za izradu odljevka kućišta turbo-puhala. Za digitalizaciju pješčane jezgre korišten je ATOS sustav prve generacije. Podaci dobiveni digitalizacijom obrađeni su u programskom paketu GOM Inspect.

1. Uvod

Objekt koji je obrađen u ovome radu je pješčana jezgra koja se koristi za izradu hladnjaka zraka. Razlog za dimenzijsku kontrolu ovog objekta je pojava netočnih odljevaka hladnjaka zraka. Digitalizacija jezgre je u ovom slučaju potrebna kako bi se dobili rezultati mjerenja bez razaranja objekta. Mjerenja u skučenim i kompleksnim područjima vrlo su nezgodna a nekada i nemoguća, dok je mjerenje unutarnje šupljine odljevka vrlo teško bez metode razaranja. Nekada nema druge mogućnosti nego koristiti metodu razaranja kako bi se došlo do dijelova koji se žele izmjeriti. Kod odljevaka postoji mogućnost mjerenja pješčane jezgre koja zapravo predstavlja negativ šupljine koja se nalazi u objektu. Njezinim mjerenjem moguće je eliminirati potrebu za razaranjem objekta. Za brzo dobivanje preglednih rezultata koristi se postupak digitalizacije pješčane jezgre koji omogućuje usporedbu rezultata s računarskim modelom. Za mjerenje je korišten GOM–ov 3D digitalizator te uz softversku podršku istog napraviti će se provjera cjelokupnog oblika jezgre.

2. Digitalizacija pješčane jezgre

Potrebno je digitalizirati pješčanu jezgru te usporediti dobivene rezultate sa postojećim CAD modelom jezgre, slika 1. Jezgra se izrađuje Croning postupkom koji omogućava visoku razinu kvalitete površine i dimenzijsku točnost odljevka. Funkcija ove jezgre je izrada šupljine u odljevku kućišta hladnjaka zraka (eng. Intercooler). Proces digitalizacije biti će izvršen pomoću digitalizatora ATOS I. Pomoću njega se određuje detaljni trodimenzionalni oblik objekta kao i njegovih pojedinačnih dijelova.

Primjenom digitalizatora rezultati skeniranog objekta mogu se usporediti s CAD modelom, područja koja su od posebne važnosti mogu se pouzdano vidjeti. Sustav za digitalizaciju je mobilan tako da se može premještati i skenirati u raznim položajima i ne zahtjeva skupe uređaje za pričvršćivanje.

Figure 1. Digitalization process scheme

Slika 1. Shema procesa digitalizacije

2.1. Opis postupka digitalizacije

Za prikupljanje podataka koriste se dvije kamere koje su s centralno postavljenim projektorom integrirane u kompaktnu glavu ATOS–ovog senzora. Kamere koje se koriste za snimanje podataka su identične i temeljene na CCD čipu, elementu koji digitalizatoru omogućava pretvaranje svjetlosti (reflektirane od objekta) koji se digitalizira u niz digitalnih impulsa.

Sustav je zasnovan na kombinaciji triangulacije i projiciranja svjetlosnog uzorka linija, slika 2, koji se dobiva pomoću nekoherentnog izvora svjetla. U pojednostavljenom smislu, metoda funkcionira na način da centralno postavljen projektor slijedno projicira unaprijed određenu svjetlosnu strukturu na površinu mjernog objekta. To omogućava jednoznačnu prostornu rekonstrukciju površine temeljenu na analizi snimaka snimljenih s lijevom i desnom kamerom.

Određivanje koordinata provodi se postupkom triangulacije, pri čemu jedan vrh zamišljenog trokuta čini odabrana objektna mjerna točka, a ostala dva vrha su položaji slikovnih osjeta objektne mjerne točke u svakoj od kamera. Manje od 1 sekunde točnije 0,8 sekundi je ovakvom sustavu potrebno da pomoću dvije kamere prikupi informacije snimanog objekta i pretvori ih u piksele.

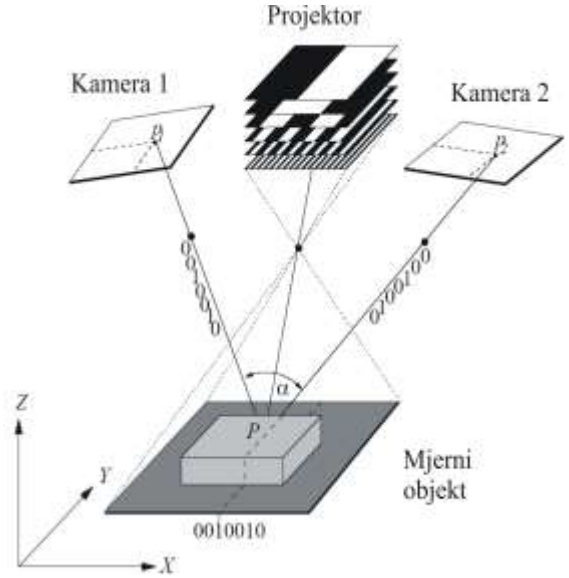

Figure 2. The principle of project system "Atos"

Slika 2. Princip projekcijskog sustava "Atos"

2.2. Umjeravanje uređaja

Pod pojmom umjeravanja sustava u fotogrametriji se podrazumijeva postupak koji omogućuje određivanje unutrašnjih i vanjskih parametara orijentacije kamera te eventualno, projektora. Umjeravanje je potrebno izvoditi prije početka prvog mjerenja. Za umjeravanje ATOS mjernog sustava može se upotrijebiti odgovarajuća ploča, slika 3a) ili križ, slika 3b), koji su dostupni u više dimenzija. Ovisno o tipu mjernog sustava njihov se izgled može neznatno razlikovati. Na tim pomagalima za umjeravanje nalaze se različite oznake koje se nazivaju referentne točke.

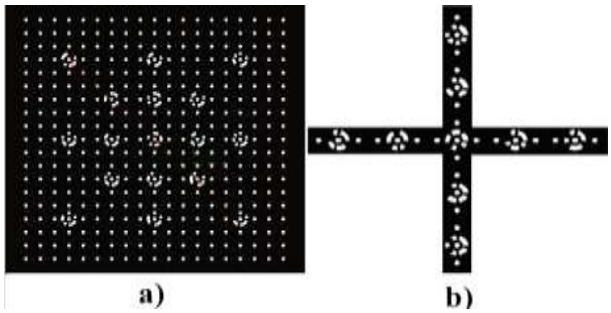

Figure 3. Calibration aid: a) board, b) cross

Slika 3. Pomagala za umjeravanje: a) ploča, b) križ

Da bi se umjeravanje izvelo pravilno potrebno je zagrijati sijalicu projektora te zagrijavanje traje okvirno pet minuta. Pri umjeravanju kao i pri snimanju projekata potrebno je mjerni laboratorij osigurati od utjecaja vanjskog svijetla. Umjeravanje je izvršeno pomoću aluminijske ploče dimenzija 250x200 mm što je prikazano na slici 4.

Figure 4. Calibration of device, upper position

Slika 4. Umjeravanje uređaja, gornji položaj

Ploča za umjeravanje postavlja se u vidno polje dviju kamera koje se nalaze u konvergentnoj postavi s fiksiranim unutrašnjim i vanjskim parametrima orijentacije. Nakon što je umjeravanje uređaja izvršeno i u granicama normalnih odstupanja vrši se njezina pohrana. Pohranjivanje umjeravanja je potrebno kako bi se moglo provjeriti stanje mjernog uređaja ukoliko se pojave greške u rezultatima mjerenja.

2.3. Mjerne strategije

Da bi se smanjile greške koje nastaju u procesu mjerenja potrebno je koristiti odgovarajuću mjernu strategiju koja je od posebnog značaja za rezultate mjerenja. Kako bi se smanjile tolerancije objekta, važno je da su mjerenja što pouzdanija sa što manje grešaka.
Nekodirane mjerne točke su neophodne za mjerenje te pomoću njih se dobiju poligonizirane slike mjernog objekta. Nekodiranih mjernih točaka postoji više vrsta i veličina te odabir veličine mjernih točaka ovisi o dimenzijama mjernog objekta. U našem slučaju odabrane su nekodirane mjerne točke unutarnjeg promjera 3 milimetra čija je okolina kvadratnog oblika, slika 5. Nekodirane mjerne točke prije procesa digitalizacije potrebno je nalijepiti na pješčanu jezgru. Njihov raspored, poziciju i broj određuje se na temelju iskustva, ali jedan od utjecajnijih faktora prilikom lijepljenja točaka je geometrijska kompleksnost same pješčane jezgre. U našem slučaju bilo je potrebno nalijepiti oko stotinjak nekodiranih mjernih točaka, slika 6. Nakon što su se na jezgru nalijepile nekodirane mjerne točke, potrebno ju je postaviti na okretni stol, samim time jezgra je spremna za sam proces digitalizacije.

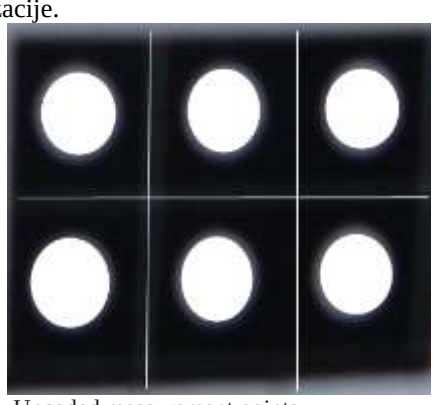

Figure 5. Uncoded measurement points

Slika 5. Nekodirane mjerne točke

Figure 6. Bonding of uncoded measurement points

Slika 6. Lijepljenje nekodiranih mjernih točaka

Osim pripreme same jezgre potrebno je prilagoditi uvjete u laboratoriju za početak mjerenja. U laboratoriju za mjerenje treba osigurati što manje okolne svjetlosti jer ona otežava sam proces digitalizacije i rezultira pojavom grešaka.

2.4. Procedura digitalizacije pješčane jezgre

Prije početka digitalizacije pješčane jezgre potrebno je učitati CAD model zbog kasnije usporedbe dobivenih rezultata. CAD model predstavlja idealni oblik pješčane jezgre te se prema njemu izrađuje jezgra. Rezultati digitalizacije uspoređuju se s idealnim CAD modelom koji se pomoću potprograma procesira u poligon podataka. Kada je učitavanje podataka završeno program GOM Inspect pruža mogućnosti definiranja osnovnih parametara modela. Potprogram je CAD model pretvorio u mrežu koja se sastoji od trokuta koji nastoje opisati konture površine modela. Moguće je regulirati veličinu mreže s obzirom da se zgušnjavanjem mreže dobiva bolji prikaz modela koji zauzima više memorije računala. Pošto je digitalizacija jezgre podijeljena na dva projekta najprije će se snimiti prvi projekt koji predstavlja gornji dio pješčane jezgre.

Na slici 7 prikazan je proces digitalizacije u postupku dok je na slici 8 prikazan gotov proces digitalizacije prvog projekta pješčane jezgre. Kako bi se digitalizirala jezgra u ovome projektu bilo je potrebno napraviti 140 slika pomoću digitalizatora.

Figure 7. Digitalization process of the first project in process

Slika 7. Proces digitalizacije prvog projekta u postupku

Figure 8. Final digitalization process of the first project

Slika 8. Završeni proces digitalizacije prvog projekta

Odstupanje ukazuje koliko u prosjeku referentne točke fotografije tj. skupa odstupaju od aritmetičke sredine. Usporedbom slika 7 i 8 vidi se kako se na slici 8 nalazi značajno manje nedostataka podataka na projektu što predstavlja prikaz projekta nakon digitalizacije prvog projekta. Da bi se dobila potpuna slika digitalizirane jezgre potrebno je snimiti drugi projekt, koji predstavlja doljnji dio jezgre Jezgru je potrebno okrenuti te fiksirati

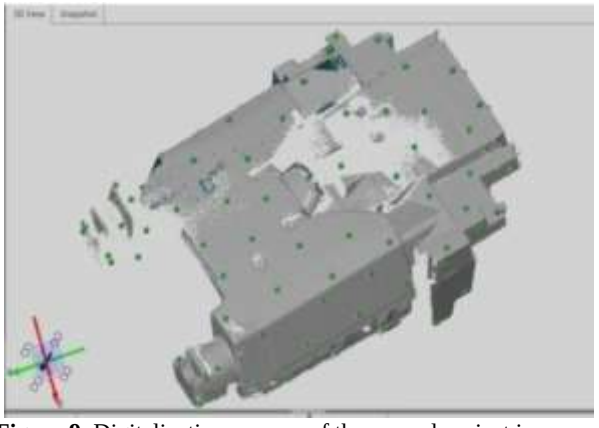

Figure 9. Digitalization process of the second project in process

Slika 9. Proces digitalizacije drugog projekta u postupku

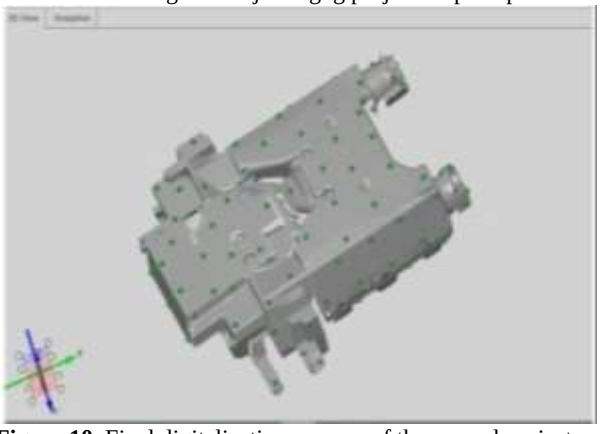

Figure 10. Final digitalization process of the second project

Slika 10. Završeni proces digitalizacije drugog projekta

Na slici 11 prikazana je lista napravljenih slika s brojem referentnih točaka za prvi projekt te se na njoj može vidjeti odstupanje referentnih točaka. Ako je odstupanje veće od 0,0783 mm, takve podatke je potrebno izbaciti iz liste što je vidljivo na slici 11.

jer je zbog njezine geometrije nestabilna. Na slici 9 prikazana je digitalizacija drugog projekta pješčane jezgre koji je u postupku, dok slika 10 prikazuje završeni postupak digitalizacije pješčane jezgre. Na projektima se nalaze zelene točke. To su zapravo nalijepljene referentne točke koje se koriste prilikom spajanja ova dva projekta.

Da bi se mogli spojiti projekti moraju se odabrati one referentne točke koje su vidljive u prvom i u drugom projektu.

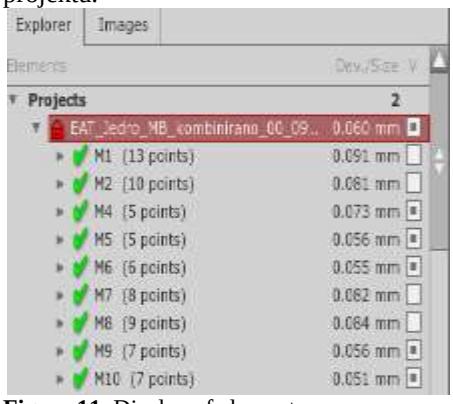

Figure 11. Display of elements

Slika 11. Slika elemenata

Nakon što se odaberu određene točke, one promijene svoj izgled u narančastu boju. Točke koje će biti upotrijebljene za spajanje ova dva projekta nalaze se na bočnim dijelovima prvog projekta iz tog razloga jer su iste vidljive i u drugom projektu. Na slici 12 i 13 mogu se vidjeti odabrane točke na bočnim dijelovima prvog i drugog projekta.

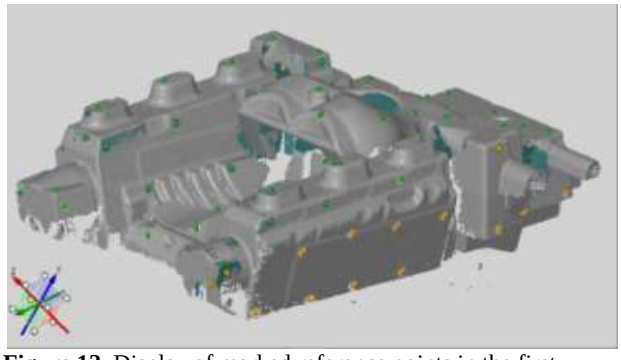

Figure 12. Display of marked reference points in the first project

Slika 12. Prikaz označenih referentnih točaka na prvom projektu

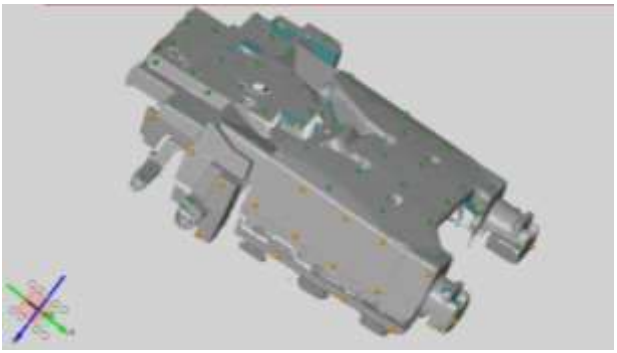

Figure 13. Display of marked reference points in the second project

Slika 13. Prikaz označenih referentnih točaka na drugom projektu

Pomoću odabranih točaka mogu se spojiti ova dva projekta u jedan. Spajanje kratko traje, nakon čega se pojavljuju preklopljene referentne točke i njihova odstupanja. Najbolje je da su ta odstupanja u nekom srednjem rasponu, jer odstupanja koja su blizu granične vrijednosti nisu poželjna, kao ni ona s vrlo malom vrijednošću. U pravilu ukupno odstupanje ne bi smijelo prelaziti vrijednost od 0,10 mm pa vrijednosti koje narušavaju ovu vrijednost je potrebno isključiti. Uspjelo se preklopiti 35 točaka koje su zajedničke prvom i drugom projektu. Ako bi se uzelo u obzir svih 35 točaka ukupno odstupanje bi iznosilo 8,956 mm pa je zbog toga potrebno isključiti kritične točke. Nakon selekcije točaka dobila se vrijednost ukupnog odstupanja od 0,026 mm što je prihvatljivo. Upravo to je uzrokovalo smanjenje broja točaka na 12 što je dovoljno jer su minimalan broj za spajanje dva projekta 4 točke. Slika 14 predstavlja rezultat spajanja oba projekta.

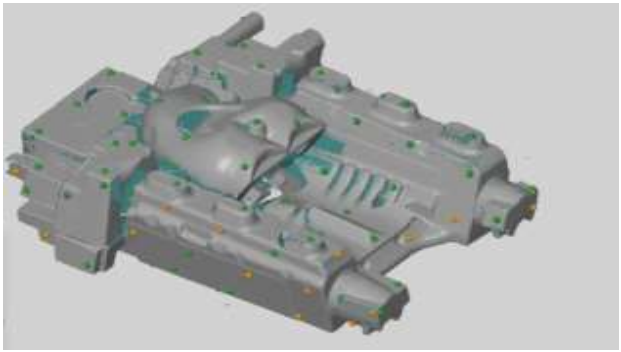

Figure 14. Results of project merging

Slika 14. Rezultat spajanja projekata

Da bi ovakav mjerni objekt, koji je sastavljen od dvaju projekata, dobio potpuno definiranu geometriju koja je digitalizirana u formi gustog oblaka točaka te vrlo precizno opisuje kompletnu površinu potrebno je napraviti poligonizaciju mreže. Nakon izvršene poligonizacije projekta, slika 15, isti je spreman za nastavak obrade, u ovom slučaju, u programu GOM Inspect V7.5 SR1.

Figure 15. Poligonization project

Slika 15. Poligonizirani projekt

3. Obrada podataka dobivenih digitalizacijom

Na početku je potrebno učitati dobivene podatke u program kako bi se mogli obraditi te nakon toga započinje obrada snimljenih podataka. Postoje dvije vrste podataka koje je potrebno učitati u program, a to su prikupljeni podaci koji nastaju kao rezultat snimanja i CAD model. CAD model predstavlja referentne podatke prema kojima se vrši daljnja analiza. Referentni model predstavlja idealni model snimanog objekta koji se učitava nakon obrade mjernih podataka. Dodatno se obrađuju samo rezultati snimanja kako bi se ispravile nastale greške u procesu digitalizacije.

3.1. Popunjavanje ne digitaliziranih dijelova u poligoniziranoj mreži

Prilikom snimanja mjernog objekta pojavljuju se nedostaci podataka na određenim dijelovima snimljenog projekta. Nedostaci podataka se pojavljuju zbog toga jer sustav stvara sliku objekta na principu triangulacije.
Ako prilikom snimanja objekta obije kamere ne vide istu točku na tome dijelu nastaje nedostatak podataka. Na slici 16 prikazan je snimljeni projekt koji još nije dodatno obrađen pa se prema tome mogu vidjeti ne digitalizirani dijelovi koji su nastali zbog nedostatka podataka. Prije početka obrade podataka može se saznati točan broj ne digitaliziranih dijelova na projektu koji u ovom slučaju iznosi 142.

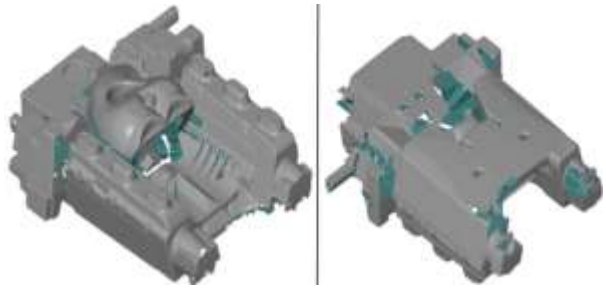

Figure 16. Display of measurement results

Slika 16. Prikaz rezultata mjerenja

Kako bismo mogli zatvoriti ne digitalizirane dijelove, koji su nastali zbog ograničenog vidnog polja kamera, možemo koristiti dvije osnovne funkcije. Koristeći funkciju interaktivnog zatvaranja moguće je zatvaranje svakog ne digitaliziranog dijela posebno.
Ne digitalizirani dijelovi koji se nalaze na kompliciranom dijelu objekta ili koji se nalaze na rubu objekta moguće je parcijalno zatvoriti. Pojavi li se ne digitalizirani dio prevelikih dimenzija pomoću ove funkcije možemo ih podijeliti na manje dijelove te postepeno popunjavati. Treća opcija je automatsko zatvaranje. Ova opcija je vrlo korisna pri zatvaranju grupe ne digitaliziranih dijelova koje se nalaze u bližem krugu na mjernom objektu. Za dobivanje najboljeg rezultata odabiru se točke oko površine koja se želi selektirati. U ovom slučaju odabrati će se pet točaka koje se mogu vidjeti na slici 17.
Na kraju je potrebno izvršiti popravak mreže kako bi se ispravio diskontinuitet mjernih podataka (udubljenja, ogrebotine, strugotine, pojava izbočenja izazvana nalijepljenim nekodiranim mjernim točkama ...) koje se nalaze na mreži.

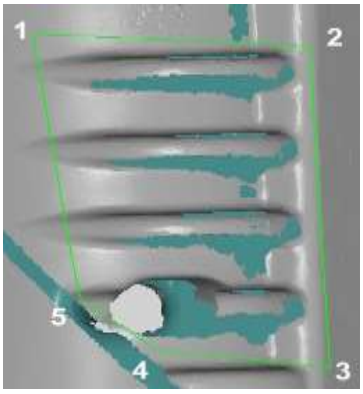

Figure 17. Selection of surfaces

Slika 17. Selektiranje površina

3.2. Preklapanje projekata

Kada je izvršena obrada dobivenih mjernih podataka potrebno ih je usporediti sa referentnim CAD modelom prema kojem će se uspoređivati dobiveni rezultati. Nakon što je učitan CAD model potrebno je izvršiti preklapanje mjernog objekta s referentnim modelom. Najbolje što se može desiti, nakon što su projekti učitani u program, je preklapanje koje je vidljivo na slici 18. Postojeće vidljivo stanje se dešava iz razloga neusklađenosti koordinatnih sustava, tj. koordinatni sustav mjernog projekta nije identičan koordinatnom sustavu CAD modela. Dakle do ovog rezultata se nije došlo korištenjem funkcija već samim učitavanjem.

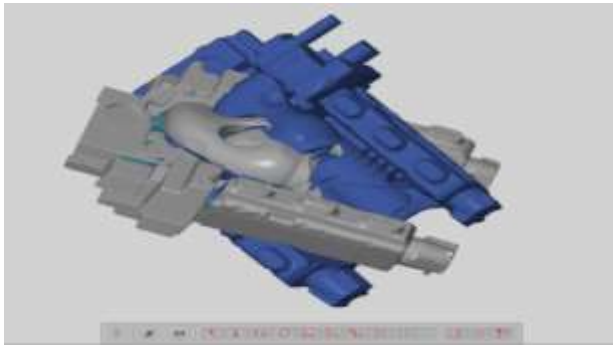

Figure 18. Display of objects after importing

Slika 17. Prikaz objekta nakon importiranja istih

Zatim je potrebno poravnati dobivene rezultate (mreža, mjerni rezultati, ...) automatski na nominalnu vrijednost neovisno o početnoj poziciji. Rezultat prikazuje transformaciju rezultata u [mm] koju program izračunava kao prosječnu vrijednost svih odstupanja

4. Usporedba površina s CAD modelom

Opcija usporedbe površina s CAD modelom koristi se kako bi se mogli dobiti rezultati odstupanja mjernog projekta pješčane jezgre u odnosu na referentni CAD model. Raspon odstupanja je prikazan na skali koja je označena plavom, zelenom i crvenom bojom. Plava boja predstavlja površinu mjernog projekta koja se nalazi ispod površine CAD modela. Ako su mjerni rezultati prikazani crvenom bojom, tada se površina mjernog projekta nalazi iznad površine referentog CAD modela. Površine koje su označene sa zelenom bojom označavaju područje koje je bez odstupanja, svi ostali slučajevi prikazani su kombinacijom navedenih boja. Kroz projekt se može napraviti presjek s proizvoljno definiranom ravninom. Nakon što se odredi položaj ravnine koja presjeca CAD model, program izračunava odstupanja koja se mogu vidjeti u ravnini presjeka a nalaze se između referentnog i mjernog projekta.

Potrebno je definirati ravninu kojom se želi presjeći model i njezinu udaljenost od ishodišta koordinatnog sustava. Kada se odredi presjek modela automatski se dobiva njegov prikaz, dok je ravnina presjeka označena zelenom bojom. U našem slučaju ravnina se postavila na udaljenost 20,000 mm od ishodišta koordinatnog sustava. Također je dobro napomenuti da je moguće postavljanje granica tolerancije koje su postavljene na ±0,800 mm. Da bi se dobio bolji prikaz presjeka potrebno je sakriti ostale elemente koji se nalaze u projektu. Na slici 20 može se vidjeti prikaz presjeka bez ostalih elemenata projekta.

CAD modela. Vrijednost prosječnog odstupanja u ovom slučaju iznosi 0,8983 mm. Na slici 19 vidi se rezultat preklapanja.

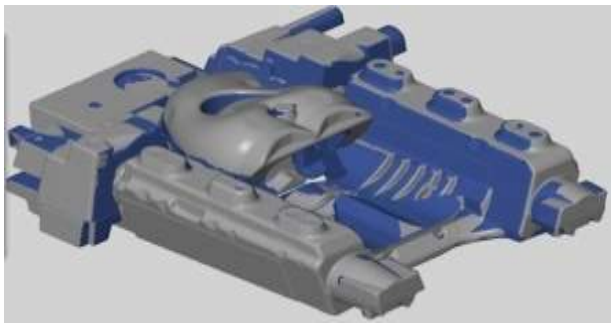

Figure 19. Results of project alignment

Slika 18. Rezultat preklapanja projekta

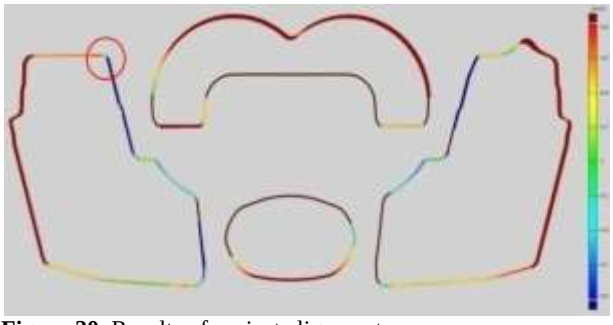

Figure 20. Results of project alignment

Slika 20. Rezultat preklapanja projekta

Pošto je slika relativno velika izvučen je detalj. Detalj je označen na slici 20 strelicom te je prikazan na slici 21. Udaljenost između točaka postavljena je na 20,000 mm te su preciznije prikazana odstupanja.

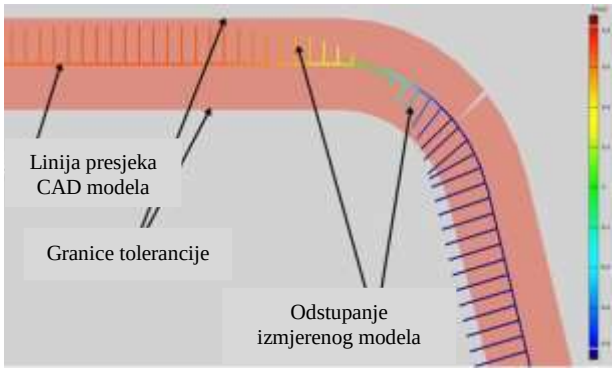

Figure 21. Detailed display

Slika 19. Prikaz detalja

Na slici 22 prikazan je presjek jezgre s oznakama odstupanja. Oznake na projektu su usklađene s bojom legende. Također mogu se vidjeti i oznake koje imaju

oblik [???]. One se nalaze na dijelovima presjeka koje nije moguće usporediti sa snimljenim projektom iz razloga što on na tom dijelu ne postoji, tj. nije snimljen.

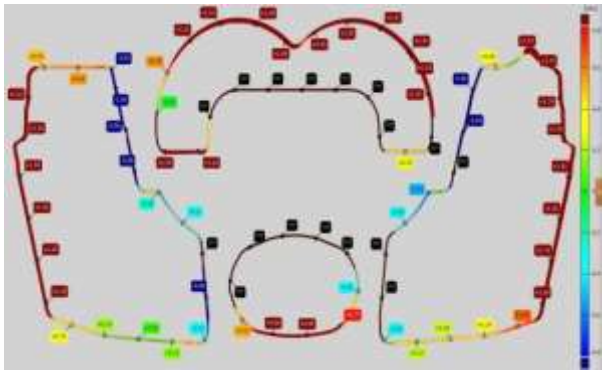

Figure 22. Display of deviation marks

Slika 20. Prikaz oznaka odstupanja

4.1. Rezultati preklapanja projekta

Rezultati koji su dobiveni usporedbom površina izmjerenog projekta i CAD modela su prikazani na slici 23. Rezultati su dobiveni na način da su postavljene granice odstupanja od ±0,8 mm te je prema njima formirana legenda. Prema bojama na legendi tj. projektu može se doći do zaključka da je kontrolirana jezgra nepravilno izrađena. Tamno crvena boja prikazuje zadebljanje, dok tamno plava boja predstavlja manjak materijala ili udubljenje. Zelenom bojom označene su površine koje su najbliže CAD modelu.

Na projektu je prikazano najveće i najmanje odstupanje. Najveće pozitivno odstupanje iznosi +2,61 mm, dok je najveće negativno -6,88 mm. Također prosječno odstupanje cijelog projekta iznosi 0,8983 mm što izlazi izvan granica tolerancije. Optimalno odstupanje površine iznosi +0,10 mm. Prilikom konstruiranja CAD modela došlo je do greške koja je utjecala na daljnju izradu jezgre. Konkretno u ovome slučaju je konstruktor pogriješio prilikom njenog dimenzioniranja. Rješenje za ovakav problem je izrada novog CAD modela pješčane jezgre te kalupa za izradu jezgri.

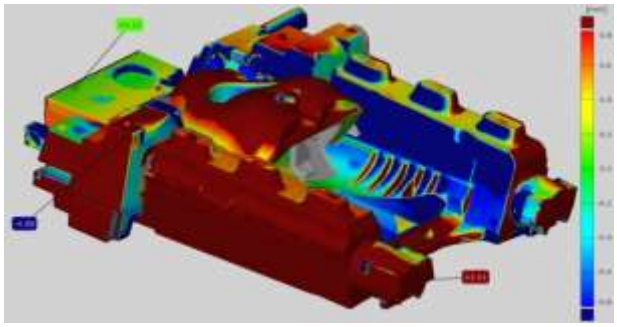

Figure 23. Surfaces comparison results

Slika 21. Rezultati usporedbe površina

5. ZAKLJUČAK

Jezgra odabrana u ovome radu služi za izradu kućišta hladnjaka zraka za teretna vozila. Kako bi se digitalizirala pješčana jezgra koristio se digitalizacijski sustav ATOS prve generacije. Za prikupljanje podataka koriste se dvije kamere koje su sa centralno postavljenim projektorom integrirane u kompaktnu glavu ATOS–ovog senzora. Sustav je zasnovan na kombinaciji triangulacije i projiciranja svjetlosnog uzorka linija. Umjeravanje uređaja je izvedeno pomoću aluminijske ploče. Na jezgru su nalijepljene nekodirane mjerne točke pomoću kojih su se dobile poligonizirane slike mjernog objekta. Digitalizacija jezgre podijeljena je na dva projekta te je potrebno dva projekta spojiti u jedan. Preklapanjem se dobilo 35 točaka koje su zajedničke prvom i drugom projektu. Nakon što je digitalizacija pješčane jezgre izvedena slijedi obrada rezultata. Potrebno je bilo usporediti snimljene i obrađene podatke s referentnim CAD modelom pješčane jezgre. Usporedbom projekata dobili su se rezultati koji su grafički prikazani bojama.

6. LITERATURA

[1] Vale, F., Mjerenje pješčane jezgre odljevka 3D digitalizatorom, diplomski rad, rujan 2013.

ISSN 1847-7917

SEM-EDS analysis of slip cast composite Al_2O_3-ZrO_2 ceramics

Marijana Majić RENJO, Lidija ĆURKOVIĆ, Krešimir GRILEC, Matija SAKOMAN and Suzana JAKOVLJEVIĆ

1) University of Zagreb, Faculty of Mechanical Engineering and Naval Architecture, Ivana Lučića 1, Zagreb, **Croatia**
Sveučilište u Zagrebu, Fakultet strojarstva i brodogradnje, Ivana Lučića 1, Zagreb, **Hrvatska**

lidija.curkovic@fsb.hr

Keywords

Slip casting
Al_2O_3–t-ZrO_2 ceramics
SEM-EDS

Ključne riječi

Lijevanje suspenzije
Al_2O_3–t-ZrO_2 keramika
SEM-EDS

Original scientific paper

Abstract: In this paper, composite Al_2O_3–t-ZrO_2 ceramics (composition: 95 wt. % Al_2O_3 – 5 wt. % t-ZrO_2 and 90 wt. % Al_2O_3 – 10 wt. % t-ZrO_2) was formed by slip casting in plaster mould.
After drying, green bodies were sintered in laboratory electric kiln under air environment at a temperature of 1650 °C.
Density of prepared samples was determined by the Archimedes' method. Surface morphology of sintered composite ceramics samples was determined by scanning electron microscope (SEM) equipped with energy dispersive spectrometer (EDS) analysis.
Distribution of the elements aluminium (Al), zirconium (Zr) and oxygen (O) on fracture surfaces of sintered samples was determined by EDS mapping.
SEM-EDS analysis of prepared composite ceramics samples confirmed the homogeneous distribution of ZrO_2 in Al_2O_3 matrix.

Izvorni znanstveni rad

Sažetak: U ovom radu, kompozitna Al_2O_3–t-ZrO_2 keramika (sastava: 95 % Al_2O_3 – 5 % t-ZrO_2 i 90 % Al_2O_3 – 10 % t-ZrO_2) oblikovana je lijevanjem u gipsani kalup.
Nakon sušenja sirovci su sinterirani u laboratorijskoj električnoj peći u atmosferi zraka pri temperaturi od 1650 °C.
Gustoća uzoraka određena je Arhimedovom metodom.
Sinteriranim uzorcima analizirana je morfologija površine pretražnim elektronskim mikroskopom (SEM) uz energetsko disperzivni spektrometar (EDS).
Mapiranjem uz EDS određena je raspodjela elemenata aluminija (Al), cirkonija (Zr) i kisika (O) na prijelomnim površinama sinteriranih uzoraka.
SEM-EDS analizom uzoraka kompozitne keramike potvrđena je homogena raspodjela ZrO_2 u Al_2O_3 matrici.

1. Introduction

Monolithic alumina (Al_2O_3) is widely used oxide ceramics, due to its satisfying properties, such as high strength and hardness, temperature stability, high wear resistance and corrosion resistance. However, low fracture toughness is its greatest disadvantage. The addition of yttria-stabilized tetragonal zirconia (t-ZrO_2) to alumina results in a composite ceramic material, which has higher fracture toughness and strength than alumina [1], [2].
Monolithic and composite ceramics can be produced by various technologies, one of which is slip casting. A slip is a suspension of fine powder in a liquid with small amounts of additives – dispersants, binders, plasticizers or sintering agents. Slip casting method provides superior surface quality, density and uniformity in casting of high-purity ceramic materials. Slip casting processing of ceramics is a relatively easy and economical technology. In order to produce high-quality green products and, subsequently, sintered material, it is essential to prepare stable suspension with adequate rheological properties. If the solid and liquid phase separate, due to the agglomeration of particles, the suspension is considered unstable. In order to prevent this, small amounts of dispersants are added to the suspensions. Suspension stability can be determined by sedimentation tests, zeta potential and particle size measurements, as well as determination of rheological parameters [3], [4] [5], [6], [7].
After choosing optimal slip casting parameters, suspensions are cast into the plaster mould and thus the green bodies are formed.
In this investigation, alumina and zirconia powders were dispersed in water, with DOLAPIX CE64 as a dispersant. One of the goals of this investigation was to find optimal dispersant amount, in order to improve slip casting process of composite Al_2O_3–t-ZrO_2 ceramics.

Symbols/Oznake

w	- mass portion, % - maseni udio, %	η	- dynamic viscosity, mPas - dinamička viskoznost
	Greek letters/Grčka slova	ρ	- Archimedes' density, g/cm^3 - Arhimedova gustoća, g/cm^3
γ	- shear rate, s^{-1} smična brzina, s^{-1}		

It was assumed that sintered material would have homogenous microstructure, containing dispersed particles of zirconia in alumina matrix, which was confirmed by SEM-EDS analysis.

2. Experimental procedure

2.1. Preparation of composite Al_2O_3–t-ZrO_2 ceramics

In this investigation, two groups of composite Al_2O_3–t-ZrO_2 ceramic suspensions were prepared (composition: 95 wt. % Al_2O_3 – 5 wt. % t-ZrO_2 and 90 wt. % Al_2O_3 – 10 wt. % t-ZrO_2). Solid content in all suspensions was 70 wt. %. In preliminary experiments, different amounts of the chosen dispersant, DOLAPIX CE 64, were added to each suspension, which were then subjected to the rheological measurements. Each suspension was homogenized for 120 minutes at a rate of 300 rpm in the planetary ball mill (PM 100, Retsch, Germany). The grinding jar and ten balls used for homogenization were made of alumina. In order to remove air bubbles and to achieve better homogeneity of prepared suspensions, each of them was treated in the ultrasonic bath. Figure 1 shows the planetary ball mill for suspension preparation (A), and removal of alumina balls used for homogenization (B).

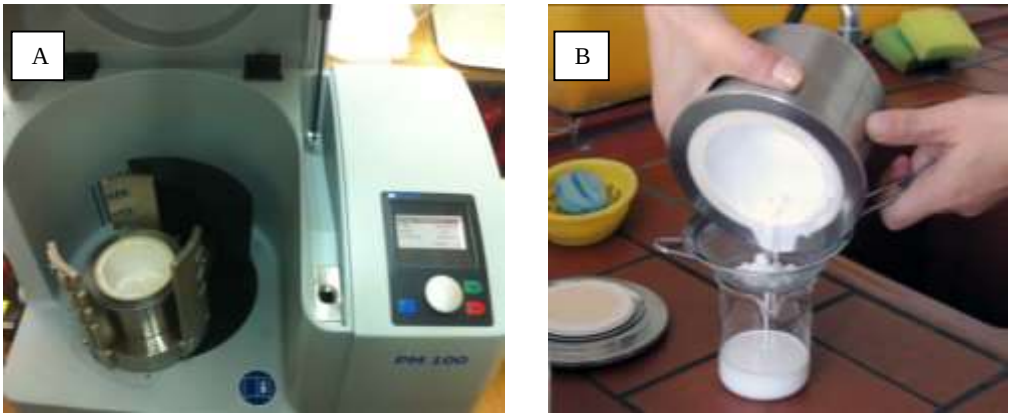

Figure 1. (A) Ball mill PM 100 Retch; (B) Separation of ceramic balls from the suspension
Slika 1. (A) Planetarni kuglični mlin PM 100 Retch; (B) Odvajanje keramičkih kuglica iz suspenzije

Rheological measurements were conducted on the Brookfield DV-III Ultra rheometer (USA). The optimal dispersant amount was determined by measuring the dynamic viscosity at the shear rate of 50 s^{-1}, which is the exact shear rate of the gravity slip casting. The optimal dispersant amount is characterized as the one that obtains the lowest viscosity at defined shear rate. Thus determined optimal content of the DOLAPIX CE 64 was chosen for further slip preparation. The overview of prepared suspensions is presented in Table 1.

Green bodies of alumina toughened zirconia ceramics were produced by slip casting process and formed in plaster mould. The plaster mould draws water from the poured slip and gives a form to the green body. This forms a dense cast form by removing deleterious air gaps and minimizing shrinkage in the final sintering process.

After moulding, green bodies were dried at a temperature of 100 °C in a drier, and sintered at 1650 °C in Nabertherm P 310 furnace.

2.2. Characterization of composite Al_2O_3–t-ZrO_2 ceramics

Sintered composite Al_2O_3–t-ZrO_2 ceramics (composition: 95 wt. % Al_2O_3 – 5 wt. % t-ZrO_2 and 90 wt. % Al_2O_3 – 10 wt. % t-ZrO_2) formed by slip casting in plaster mould was used for:

- determination of sintered density by the Archimedes' method,
- surface morphology by means of SEM-EDS method.

Table 1. Overview of prepared Al_2O_3–t-ZrO_2 suspensions

Tablica 1. Pregled pripravljenih Al_2O_3–t-ZrO_2 suspenzija

wt. (Al_2O_3+ ZrO_2), %/ *w* (Al_2O_3+ ZrO_2), %	*wt.* (H_2O), %/ *w* (H_2O), %	*wt.* (Al_2O_3, in powder mixture), %/ *w* (Al_2O_3, u mješavini praha), %	*wt.* (ZrO_2, in powder mixture), %/ *w* (ZrO_2, u mješavini praha), %	*wt.* * (DOLAPIX CE64), %/ *w** (DOLAPIX CE64), %	η, mPas/ η, mPas
70	30	95	5	0.4	8.54
70	30	90	10	0.5	10.62

**wt.*, weight percent based on the applied ceramic dry powder /
**w*, maseni udio preračunat na masu suhog praha

Density of sintered composite ceramics was determined by the Archimedes' method with density kit on the Mettler Toledo analytical balance. Samples were first weighed in air and then in liquid (water). Built-in software calculated their density by Archimedes' principle.

Surface morphology of sintered composite ceramics samples was determined by scanning electron microscope (SEM), Tescan Vega TS5136LS, equipped with energy dispersive spectrometer (EDS). Distribution of the elements aluminium (Al), zirconium (Zr) and oxygen (O) on fracture surface of sintered samples was determined by EDS mapping.

3. Results and discussion

Two groups of 70 wt. % aqueous ceramic suspensions were prepared: 95 wt. % of Al_2O_3 and 5 wt. % of t-ZrO_2; 90 wt. % of Al_2O_3 and 10 wt. % of t-ZrO_2. The minimal viscosity determined at the shear rate of 50 s^{-1} is given in Table 1. Obtained results indicate that the increase in zirconia content increases the optimal dispersant amount, as well as resulting dynamic viscosity.

Table 2. Archimedes' density of composite ceramics sintered samples

Tablica 2. Arhimedova gustoća sinteriranih uzoraka kompozitne keramike

Sample/ Uzorak	Mean value of Archimedes' density/ Srednja vrijednost Arhimedove gustoće	Standard deviation/ Standardno odstupanje
Al_2O_3–t-ZrO_2 (5% ZrO_2)	3.932	±0.0017
Al_2O_3–t-ZrO_2 (10% ZrO_2)	3.952	±0.0030

Determined Archimedes' density of sintered samples is given in Table 2. These results indicate that the increase in the zirconia content increases sintered density of composite Al_2O_3–t-ZrO_2 ceramics.

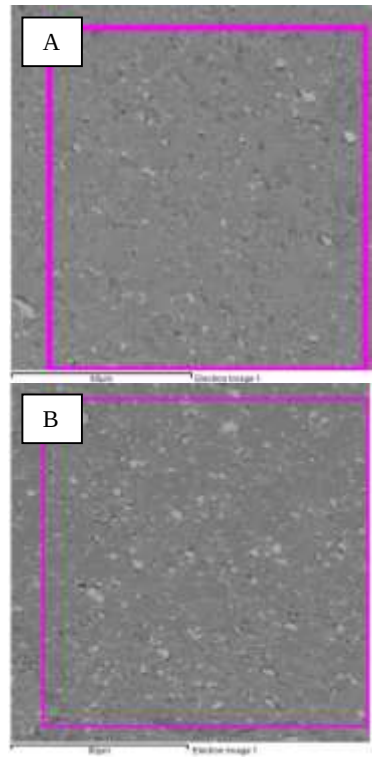

Figure 2. SEM images of composite Al_2O_3–t-ZrO_2 ceramics: (A) with 5 wt. % ZrO_2; (B) with 10 wt. % of ZrO_2

Slika 2. SEM snimke uzorka kompozitne Al_2O_3–t-ZrO_2 keramike: (A) uz 5 % ZrO_2; (B) uz 10 % ZrO_2

SEM analysis of the fractured surface of sintered Al_2O_3–t-ZrO_2 samples showed the zirconia distribution in alumina matrix. Figure 3 shows SEM images of the composite Al_2O_3–t-ZrO_2 ceramics: 95 wt. % of Al_2O_3 and 5 wt. % of t-ZrO_2 (A) and 90 wt. % of Al_2O_3 and 10 wt. % of t-ZrO_2 (B). White phase represents zirconia and dark phase represents alumina.

Scanning electron microscope equipped with energy dispersive spectrometer (SEM-EDS) was used for mapping of the following elements: aluminium (Al), oxygen (O) and zirconium (Zr) on fracture surface of sintered samples. Distribution of alumina, oxygen and zirconium is homogeneous in both composite ceramics.

The Zr mapping (Figure 3) shows an almost uniform distribution of ZrO_2 in the alumina matrix.

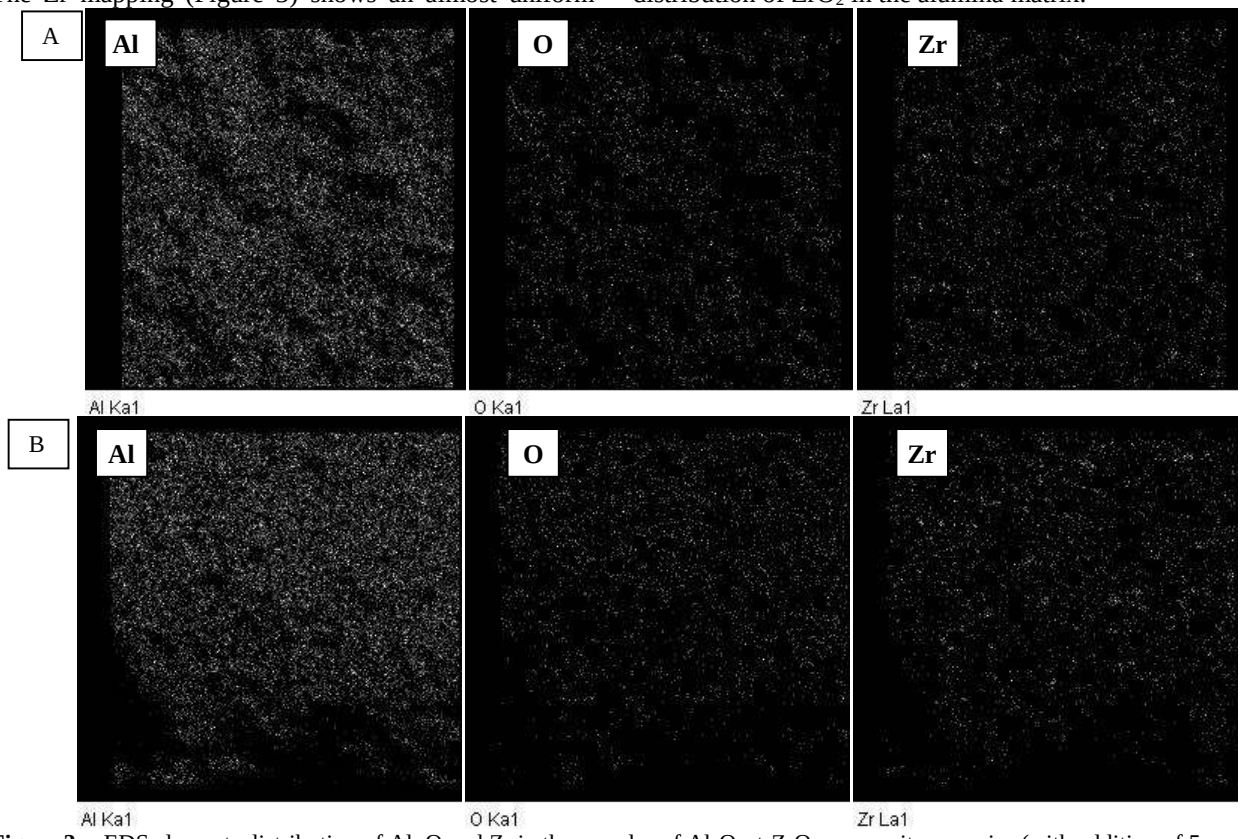

Figure 3. EDS elements distribution of Al, O and Zr in the samples of Al_2O_3–t-ZrO_2 composite ceramics (with addition of 5 (A) and 10 (B) wt. % of ZrO_2) from Figure 2A and 2B

Slika 3. EDS distribucija elemenata Al, O i Zr uzoraka Al_2O_3–t-ZrO_2 kompozitne keramike (s dodatkom 5 (A) i 10 (B) % ZrO_2) sa slike 2A i 2B

4. Conclusion

Green bodies of composite Al_2O_3–t-ZrO_2 ceramics (composition: 95 wt. % Al_2O_3 – 5 wt. % t-ZrO_2 and 90 wt. % Al_2O_3 – 10 wt. % t-ZrO_2) were formed by slip casting process in plaster mould. Preliminary results show that the obtained dynamic viscosity increases with the increasing amount of zirconia. Optimal amount of dispersant DOLAPIX CE 64 also increases with the increase in the zirconia content.

After drying, green bodies were sintered at a temperature of 1650 °C.

SEM-EDS analysis of prepared composite ceramics showed that ZrO_2 particles are homogenously dispersed in Al_2O_3 matrix, for both samples (containing 5 wt. % and 10 wt. % of ZrO_2).

REFERENCES

[1] Chinn R. E., (2002), *Ceramography: Preparation and Analysis of Ceramic Microstructures*, ASM International, USA

[2] Reed J. S., (1995), *Principles of Ceramics Processing*, John Wiley & Sons Inc., USA

[3] Tsetsekou A., Agrafiotis C., Milias A., (2001), *Optimization of the rheological properties of alumina slurries for ceramic processing applications; Part I: Slip casting*, Journal of the European Ceramic Society 2001, 21, 363

[4] Shojai F., Pettersson A. B. A., Mäntylä T., Rosenholm J. B., (2000), *Electrostatic and electrosteric stabilization of aqueous slips of 3Y-ZrO_2 powder*, Journal of the European Ceramic Society 2000, 20, 277

[5] Lewis J. A., (2004), *Colloidal Processing of Ceramics*, Journal of the American Ceramic Society 2004, 83, 2341

[6] Manjula S., Mahesh Kumar S., Raichur A. M., Madhu G. M., Suresh R., Lourdu Anthony Raj M. A., (2005), *A sedimentation study to optimize the dispersion of alumina nanoparticles in water*, Cerâmica, 2005, 51, 318, 121

[7] Binner J. G. P., McDermott A. M., (2006), *Rheological characterisation of ammonium polyacrylate dispersed, concentrated alumina suspensions*, Ceramics International 2006, 32, 803

Creating 3D models with scanner DAVID SLS-1
Izrada 3D modela primjenom skenera DAVID SLS-1

***Graciela ŠTERPIN*[1)]*, Branimir TADIĆ*[1)]*, Goran CUKOR*[1)] *i Zoran JURKOVIĆ*[1)]**

1) Sveučilište u Rijeci, Tehnički fakultet/ University of Rijeka, Faculty of Engineering, Vukovarska 58, 51000 Rijeka, Hrvatska/Croatia

gsterpin@riteh.hr

Keywords

Reference points
3D scanner DAVID SLS-1
Structured light
Cylindrical 3D model
Reflecting 3D model

Ključne riječi

Referentne točke
3D skener DAVID SLS-1
Strukturirano svijetlo
Cilindrični 3D model
Reflektirajući 3D model

Professional paper

Abstract: 3D scanners are getting more and more precise and also more accessible in the market. Every generation of optical scanners becomes more flexible and smaller. 3D scanner is a device which analyses a real object or environment with the purpose of collecting data about shape and sometimes look (e.g. colour) of the same. Collected data could be later use for creating digital 3D models whose applying is large. The purpose of 3D scanners is mostly to create point cloud of geometrical pattern on the object surface. These points can be used for shape reconstruction of scanned object. In most cases one scan is not enough to create a complete object model. More scans, even hundreds, are necessary to get information about all sides of an object. All scans must be brought into common reference system. This process is called alignment or registration. Then all the scans can be connected into a complete model. In this paper 3D scanning of three different models is shown, including cylindrical and reflecting model. The necessary scanning methods, which are needed to apply on the models, are explained herein. 3D scanner DAVID SLS-1 was used for scanning. It uses structured light technology. Model 1 shape measuring was done in programme package GOM Inspect.

Stručni članak

Sažetak: Trodimenzionalni optički mjerni uređaji (3D skeneri) postaju sve precizniji, ali i pristupačniji tržištu. Svaka generacija optičkih skenera je sve fleksibilnija i manja. 3D skener je uređaj koji analizira neki stvarni objekt ili okoliš u svrhu sakupljanja podataka o obliku i u nekim slučajevima izgledu (npr. boja) istog. Sakupljeni podaci mogu se kasnije koristiti za stvaranje digitalnih 3D modela čija je primjena velika. Namjena 3D skenera je najčešće stvoriti oblak točaka geometrijskog uzorka na površini objekta. Te točke mogu se koristiti za rekonstrukciju oblika skeniranog objekta. U većini slučajeva jedno skeniranje neće biti dovoljno za stvaranje kompletnog modela objekta. Potrebno je nekoliko skeniranja, nekad i stotine da bi se dobile informacije o svim stranama objekta. Sva skeniranja na kraju se moraju dovesti u zajednički referentni sustav. Ovaj proces zove se poravnavanje ili registracija. Sva skeniranja se onda mogu spojiti kako bi tvorila cjeloviti model. U radu je prikazano 3D skeniranje tri različita modela, uključujući cilindrični i reflektirajući model. Objašnjene su metode koje je potrebno primjeniti prilikom skeniranja istih. Za skeniranje je korišten 3D skener DAVID SLS-1 koji koristi tehnologiju strukturiranog svjetla. Mjerenje oblika modela 1 obrađeno je u programskom paketu GOM Inspect.

1. Uvod

Skeniranje objekata u tri dimenzije postaje sve zanimljivije područje za istraživanje, te je usko povezano s razvojem tehnologija 3D printanja. 3D skeniranje je proces koji omogućava mjerenje i snimanje oblika i boja postojećeg objekta, odnosno prikupljanje prostornih podataka o geometriji promatranog objekta, kako bi se dobio računarski kompatibilan digitalni oblik putem uređaja koji se u širem smislu nazivaju 3D skeneri. 3D skener je uređaj koji analizira stvarne objekte kako bi prikupio podatke o njegovom obliku (udubljenjima, izbočenjima, visini, ...) i izgledu (boji). Rezultat dobiven procesom 3D skeniranja predstavlja vezu između realnog objekta i CAD modela, tj. sakupljeni podaci se nakon toga mogu koristiti za konstrukciju digitalnih, trodimenzionalnih modela, slika 1.

Svrha 3D skeniranja je kreiranje skupa točaka u 3D Kartezijevom koordinatnom sustavu od geometrijskih uzoraka na površini objekta, tzv. oblak točaka (engl. *point cloud*). Ove točke mogu se dalje koristiti kako bi se dobio oblik objekta što se zove rekonstrukcija. Ako je informacija o boji prikupljena na svakoj točki, onda se boje na površini objekta također mogu odrediti. Proces 3D skeniranja ima sve veće područje primjene, od zabavne industrije (filmovi i video igrice), medicine (stomatologija – izrada ortoza, proteza ili dentalnih implantata), građevinske industrije (modeliranje mjesta, gradilišta, redizajniranje autocesta, …) do obrnutog

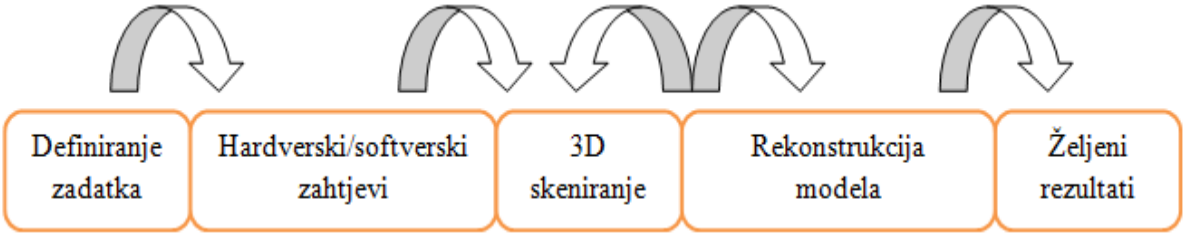

Figure 1. Process digitalization

Slika 1. Digitalizacija procesa

inženjeringa [1]. Postoje različite tehnologije 3D skeniranja odnosno izrade same 3D skenerske naprave. Svaka od tih tehnologija dolazi sa svojim ograničenjima, prednostima i cijenom. Danas je sve veća potražnja za jeftinim alternativnim rješenjima 3D skeniranja. Postoji mnogo različitih tehnika za konstrukciju 3D objekata, ali oni često zahtijevaju kompleksnu i skupu opremu. Na temelju poznavanja oblika objekta mogu se odabrati hardverski zahtjevi i metoda skeniranja s obzirom na željene rezultate. Važno je napomenuti da rezultat skeniranja ovisi o hardverskom zahtjevu kao i o softverskom zahtjevu za naknadnu obradu rezultata, slika 1.

Skenirani 3D model može koristiti procesu dizajniranja tako što povećava efektivnost rada s kompleksnim dijelovima i oblicima, pomaže u dizajniranju objekta za prilagođavanje nekom drugom dijelu, zatim ako su CAD modeli stariji, 3D skeniranje će omogućiti noviju verziju te za zamjenu starijih dijelova ili dijelova koji nedostaju.

Jedno od jeftinijih alternativnih rješenja 3D skeniranja je primjena skenera DAVID SLS-1. Na Tehničkom fakultetu Sveučilišta u Rijeci, na Zavodu za industrijsko inženjerstvo i management, primijenjena je inovativna tehnologija strukturiranog svijetla DAVID SLS-1 skenera u izradi 3D modela. U ovom radu opisan je proces 3D skeniranja pomoću spomenutog skenera, poravnanje i spajanje dobivenih skenova u cjeloviti model te metode rješavanja problema skeniranja reflektirajućih i cilindričnih objekata.

2. Optička mjerna metoda

Tehnologija optičkog 3D mjerenja jedna je od najefektivnijih metoda za dobivanje trodimenzionalnih informacija nekog objekta. Pripada bezkontaktnim mjernim metodama čije su prednosti upravo mjerenje bez fizičkog dodira te moguća velika brzina mjerenja. Princip rada optičke metode sa strukturiranim svijetlom zasniva se na projiciranju nekoherentnog kodiranog svjetla na mjerni objekt. Metoda strukturiranog svjetla radi na principu da se na objekt pomoću projektora projiciraju svjetlosne trake (linije), jedna po jedna ili više njih istovremeno, te se trake očitavaju iz drugog smjera CCD (engl. *Charge-Coupled Device*) kamerom. Veličina rešetke linija obrnuto je proporcionalna rezoluciji slike. Oblik skeniranog objekta utječe na oblik projicirane linije te se ona lomi ovisno o obliku objekta ukoliko se ne gleda iz smjera projektora. CCD kamerom očitavaju se "izlomljene" linije, te se ovisno o obliku linije određuje geometrija mjerenog objekta. Razmak između pregiba linija i visine objekta može se kroz umjeravanje dovesti u odnos sa standardnim veličinama.

2.1. Metoda kodirane svjetlosne zrake

Metoda strukturiranog svjetla koju koristi DAVID SLS-1 je metoda kodirane svjetlosne zrake. Kod ove metode informacije o visini dobivaju se iz višestrukog snimanja mreže linija različitih rastera. Snimke se uzimaju sekvencijalno. Prilikom snimanja mjereni se objekt ne smije pomicati. Na slici 2 prikazana triangulacija s binarno kodiranim svjetlosnim rasterom predstavlja metodu kodirane svjetlosne linije. Takav svjetlosni raster nastaje uz pomoć LCD (engl. *Liquid Crystal Display*) projektora. Pikseli na LCD matrici mogu se, liniju po liniju, prebacivati između "svijetlih" i "tamnih". Sa šire raspoređenim rasterima mogu se snimati veći predmeti, ali sa smanjenom rezolucijom.

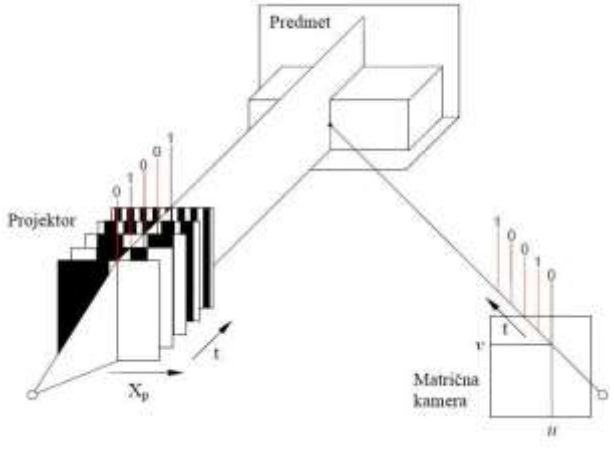

Figure 2. Coded light beam method [2]

Slika 2. Metoda kodirane svjetlosne zrake [2]

3. Proces skeniranja 3D modela

DAVID SLS-1 skener koristi inovativnu tehnologiju strukturiranog svjetla, što omogućuje precizno 3D skeniranje u samo nekoliko sekundi. Skener je mobilan i na jednostavan način se može postaviti ispred skeniranog objekta. Na taj način se može skenirati objekt sa svih strana i na kraju spojiti u 360° zatvoreni model. U ovom slučaju skener je statičan dok se objekt rotira kako bi se dobila skeniranja iz različitih kutova, tj. kako bi se dobile informacije o svim stranama objekta. Sva skeniranja na kraju moraju biti dovedena u zajednički referentni sustav, proces koji se obično naziva poravnanje ili registracija te nakon toga spojena kako bi se dobio cjeloviti model. Točnost ovog skenera je do 2% veličine objekta tj. oko 0,1 mm. Što se tiče hardverskih zahtjeva potrebno je računalo, projektor s posebnim objektivom za veliki raspon fokusa, industrijska kamera s mogućnošću fokusiranja objektiva i ugao za umjeravanje kamere. U tablici 1 su navedene tehničke karakteristike DAVID SLS-1 skenera [3].

Table 1. Technical characteristics of 3D scanner

Tablica 1. Tehničke karakteristike 3D skenera

Size of the object/ Veličina objekta	10-500 mm
Scanning time/ Vrijeme skeniranja	2-4 s per scanning/ 2-4 s po skeniranju
Data output/ Izvoz podataka	OBJ, STL, PLY
Mobility/ Mobilnost	Easy transport of scanner/ Lako prenošenje skenera
Object surface data/ Podaci o površini objekta	Surface texturing/ Teksturiranje površine

3.1. Umjeravanje uređaja

Precizno umjeravanje specifične konfiguracije mjernog sustava ključno je za preciznu 3D rekonstrukciju. Umjeravanje je proces temeljen na matematičkom modelu sustava koji se vrši kako bi se procijenili nepoznati parametri sustava putem poznatih referenci za umjeravanje. Kako bi se osigurala preciznost umjeravanja, razni činitelji moraju biti uzeti u obzir. Ambijentalno svjetlo mora biti regulirano tako da je ugao za umjeravanje osvijetljen homogeno u svim pozicijama, te da se uz to postigne i visoki kontrast. Refleksije (npr. od projektora) trebaju se izbjegavati. Ugao za umjeravanje se mora sastojati od dva jednaka zida/ploče koje se spajaju u ugao od točno 90°, slika 3.

Figure 3. Calibration corner

Slika 3. Ugao za umjeravanje

3.2. Procedura skeniranja 3D modela

Model (dalje u tekstu model 1) koji je skeniran pomoću 3D skenera DAVID SLS-1 prikazan je na slici 4. Potrebno je devet skeniranja iz različitih kutova, uključujući skeniranje gornje i donje strane modela, kako bi se prikupile informacije o svim stranama modela 1, slika 5.

Figure 4. Model 1

Slika 4. Model 1

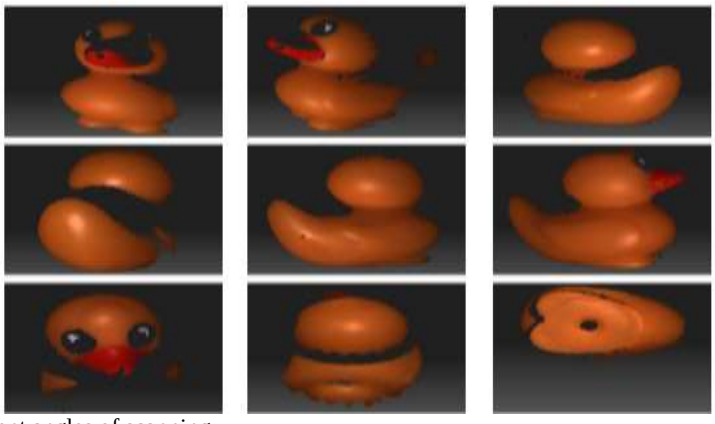

Figure 5. Scans from different angles of scanning

Slika 5. Skenovi iz različitih kutova skeniranja

Softver nudi međusobno poravnavanje skenova i njihovo spajanje u jedan 360° zatvoreni model. Pomoću naredbe *"Align Scans"* vrši se poravnavanje. U 3D prostoru najprije je potrebno odabrati sken koji se želi poravnati tzv. *"Scan A"*, te zatim odaberemo sken koji želimo poravnati s prethodnim skenom, tzv. *"Scan B"*. Softver omogućuje dva načina poravnanja, poravnanje pomoću teksture na površini skenova tzv. *"Use Texture"* i *"Contact Pair Selection"*. Koristeći naredbu *"Contact Pair Selection"* potrebno je odabrati specifičnu točku na objektu koja je zajednička između dva skena koja se žele poravnati. Nakon što se poravnaju svi skenovi potrebno je odabrati *"Fuse"* kako bi se započelo spajanje poravnatih skenova te uključivanjem opcije *"Close Holes"* zatvaraju se dijelovi koji su ostali ne digitalizirani [4]. Na slici 6 je prikazan 360° zatvoreni model 1.

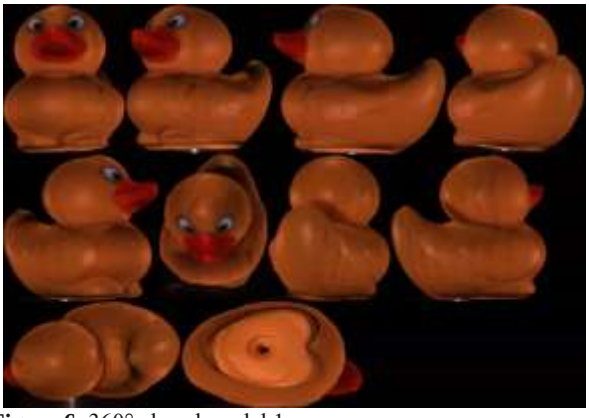

Figure 6. 360° closed model 1

Slika 6. 360° zatvoreni model 1

3.2.1. Usporedba rezultata modela 1 s referentnim CAD modelom

Nakon što je 3D skeniranjem dobiven model 1, izvršena je usporedba rezultata s CAD modelom kako bi se dobila odstupanja istog. Usporedba rezultata je provedena u programskom paketu GOM Inspect. Kako bi se skenirani model 1 mogao učitati u GOM Inspect potrebno ga je spremiti kao .stl format. Osim modela 1 potrebno je učitati i referentni CAD model kako bi usporedba rezultata bila izvršena, slika 7.

Zatim je potrebno izvršiti preklapanje modela 1 s referentnim modelom, slika 8. Ovakva metoda gdje se mjerni objekt automatski pokušava preklopiti s CAD modelom naziva se "best fit" metoda. Program traži istu geometriju na CAD modelu i na mjerenom obliku. Vrijednost prosječnog odstupanja koju izračunava program kao prosječnu vrijednost svih odstupanja CAD modela iznosi 0,2092 mm.

Raspon odstupanja je prikazan na skali koja je označena plavom, zelenom i crvenom bojom. Plava boja predstavlja površinu modela koja se nalazi ispod površine CAD modela. Ako su mjerni rezultati prikazani crvenom bojom, tada se površina modela nalazi iznad površine CAD modela. Rezultati mjerenja i preklapanja s CAD modelom mogu se prikazati kao grafički model s odstupanjima, slika 9. Zelenom bojom označene su površine koje su najbliže CAD modelu.

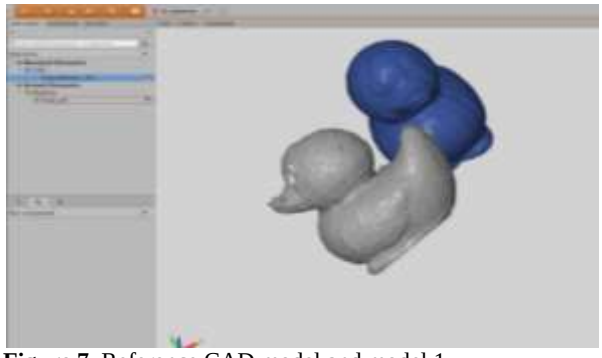

Figure 7. Reference CAD model and model 1

Slika 7. Referentni CAD model i model 1

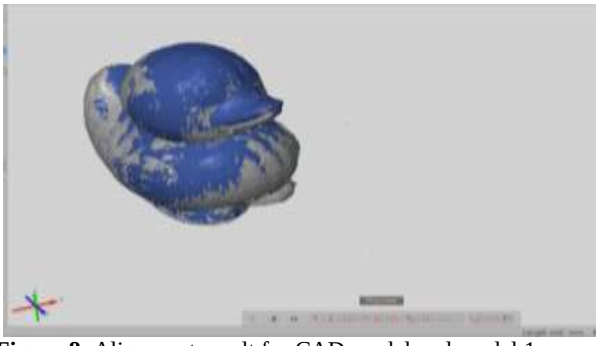

Figure 8. Alignment result for CAD model and model 1

Slika 8. Rezultat preklapanja CAD modela i modela 1

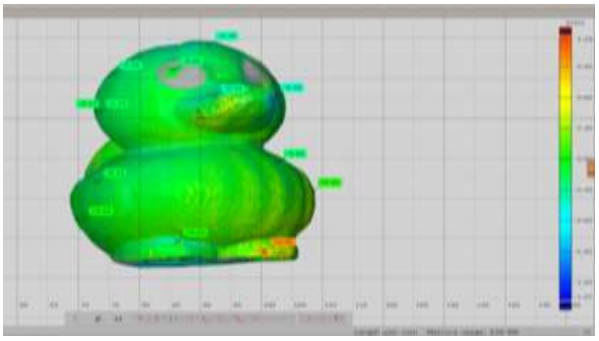

Figure 9. Surface comparison result

Slika 9. Rezultat usporedbe površine

3.3. Procedura skeniranja cilindričnih 3D modela

Iz poglavlja 3.2 može se zaključiti da su prikupljene sve potrebne informacije modela 1 kako bi se dobio 360° zatvoreni model. Prikupljeni su podaci o obliku (udubljenjima, izbočenjima, visini, ...) i izgledu (boji) te je na taj način u potpunosti definiran 3D model.

Primjenom procedure skeniranja prethodnog modela, skenovi cilindričnog modela (dalje u tekstu model 2) se nisu uspjeli dovesti u zajednički referentni sustav, jer softver ne prepoznaje različite kutove skeniranja istog. Drugim riječima softver prilikom pokušaja poravnanja skenova preklapa skenove jedan preko drugog.

U ovom slučaju potrebno je koristiti referentne točke kako bi skener prepoznao različite kutove skeniranja. Prije početka procesa skeniranja potrebno je nalijepiti referentne točke na model. Nalijepljeno je 6 referentnih točaka. Strategija koja je primijenjena u ovom slučaju je da u svakom različitom kutu skeniranja je drukčiji raspored referentnih točaka. Upravo takvom strategijom došlo se do skenova koji se prilikom poravnanja ne preklapaju u potpunosti jedan preko drugog.

Figure 10. Model 2, reference points

Slika 10. Model 2, referentne točke

Kako bi se u potpunosti dobio 360° zatvoreni model 2, slika 11, potreban je bio proces skeniranja iz pet različitih kutova skeniranja, slika 12.

Figure 11. 360°closed model 2

Slika 11. 360° zatvoreni model 2

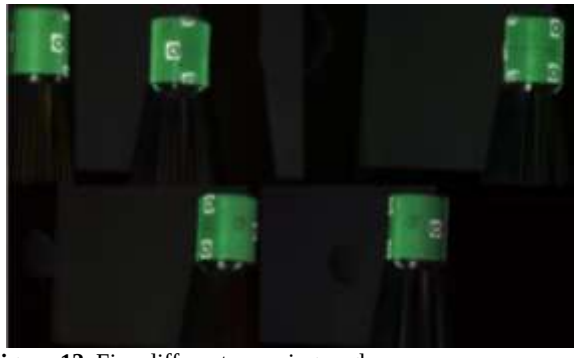

Figure 12. Five different scanning angles

Slika 12. Pet različitih kutova skeniranja

3.4. Procedura skeniranja reflektirajućih 3D modela

Metoda strukturirane svjetlosti ne može se primijeniti na visoko reflektirajućim plohama (ogledalo), te na plohama koje imaju slabu refleksiju (mat crne plohe).

Prilikom skeniranja reflektirajućih 3D modela naišlo se na problem odbijanja strukturirane svijetlosti od

reflektirajuće površine modela (dalje u tekstu model 3) te je iz tog razloga kao rezultat dobivena rasipana površina modela 3, slika 13.

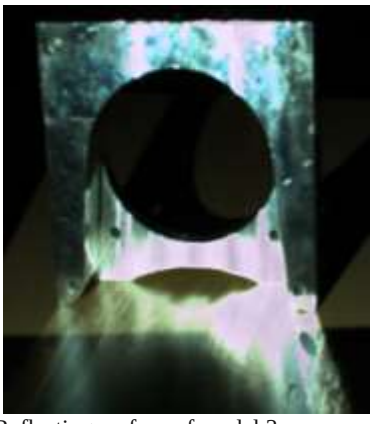

Figure 13. Reflecting surface of model 3

Slika 13. Reflektirajuća površina modela 3

U ovom slučaju potrebno je koristiti bijeli puder u prahu i bijeli sprej koji se nanese na reflektirajuću površinu modela 3 te se na taj način postiže mat bijela ploha objekta, slika 14.
Izrađena je i crna kutija kako bi se svijetla pozadina zamijenila tamnom. Na taj način kontrolira se utjecaj vanjske svijetlosti na model. Također, i u ovom su se slučaju koristile referentne točke kako bi se u procesu skeniranja prepoznali različiti kutovi skeniranja. Rezultati procesa skeniranja dobiveni primjenom navedene metode prikazani su na slici 15.

Figure 14. Unreflecting surface of model 3

Slika 14. Mat bijela površina modela 3

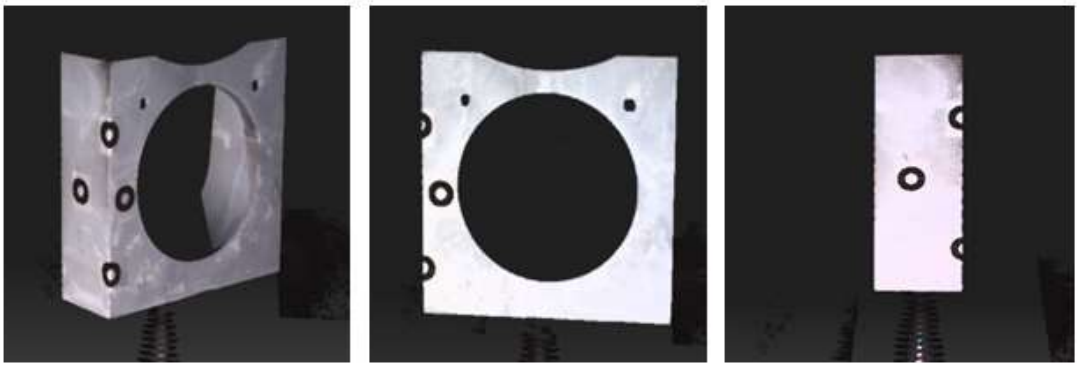

Figure 15. Result of scanning process for model 3

Slika 15. Rezultat procesa skeniranja modela 3

4. Zaključak

Uređaji za 3D skeniranje moćan su alat na području strojarstva, a najviše se koriste u kontroli kvalitete, reverzibilnom inženjerstvu i brzoj izradi prototipova. Osim u strojarstvu, 3D skeneri našli su primjenu u zabavnoj industriji, medicini te u zaštiti kulturne baštine. Pri radu s 3D skenerom najbitnije je definirati dimenzije najmanjeg/najvećeg predmeta koji će se skenirati, potrebnu preciznost, područje primjene (kontrola kvalitete, reverzibilni inžinjering, zabavna industrija ili ostalo), frekventnost korištenja, potrebnu brzinu korištenja i materijal predmeta koji se skenira. DAVID SLS-1 predstavlja 3D skener koji spada u kategoriju optičkih uređaja koji rade s kodiranom svjetlošću. Uređaji koji rade s kodiranim svjetlosnim zrakama su brzi kada se skeniraju predmeti jednostavnije geometrije, imaju zadovoljavajuću preciznost i laki su za korištenje. Nedostatke uređaja predstavlja vrijeme skeniranja složenijih geometrija, a također ovi uređaji zbog fizikalnih svojstava svjetlosti imaju problema s refleksijom i ambijentalnom svjetlošću. Korištenjem sredstva poput bijelog pudera u prahu i bijelog spreja koji je nanešen na reflektirajuću površinu modela 3, dobila se mat bijela površina koja predstavlja idealnu površinu za skeniranje koristeći

kodiranu svjetlost. Alati za kontrolu poput programskog paketa GOM Inspect omogućuju preciznu usporedbu rezultata 3D skeniranja s ulaznim CAD modelom te na temelju rezultata može se donijeti odluka o daljnjoj rekonstrukciji objekta. S obzirom da je sve veća potražnja za jeftinim alternativnim rješenjima 3D skeniranja, uređaj DAVID SLS-1 predstavlja kvalitetnu platformu koja ne zahtjeva kompleksnu i skupu opremu, a kvaliteta skeniranih objekata zadovoljava praktičnu primjenu na području strojarstva.

Zahvala

Rad je financiran potporom Sveučilišta u Rijeci broj: OJ 212, MT 137.

Literatura

[1] Mehmedbašić, E.; DAVID 3D skener; http:// www.am.unze.ba/pzi/2010/MehmedbasicEnisa/index.html, 18.09.2013.

[2] Groš, J., Medić, S., Brozović, M.; Metode trodimenzionalnog optičkog mjerenja i kontrole geometrije oblika; Zbornik Veleučilišta u Karlovcu, UDK/UDC 004.352

[3] DAVID Laserscanner; http://shop.david-vision-systems.de/product_info.php/info/p124_DAVID-Structured-Light-Scanner.html, 18.09.2013.

[4] DAVID Vision Systems GmbH; DAVID SLS-1 Getting Started Guide, Version 3.6.; Koblenz, Germany, 2013.

ISSN 1847-7917

Preparation of stable suspensions for slip casting of monolithic and composite ceramics

Marijana MAJIĆ RENJO, Lidija ĆURKOVIĆ, Krešimir GRILEC and Matija SAKOMAN

University of Zagreb, Faculty of Mechanical Engineering and Naval Architecture, **Croatia**
Sveučilište u Zagrebu, Fakultet strojarstva i brodogradnje,
Ivana Lučića 5, 10000 Zagreb, **Hrvatska**

marijana.majic@fsb.hr

Keywords

Al_2O_3–t-ZrO_2
Slip casting
Viscosity
Flow curves

Ključne riječi

Al_2O_3–t-ZrO_2
Lijevanje suspenzija
Viskoznost
Krivulje tečenja

Original scientific paper

Abstract: Stability of highly concentrated (70 wt. %) aqueous suspensions of monolithic and composite ceramics suitable for slip casting was monitored by rheological properties measurements (flow curves and rheological parameters). Three groups of suspensions were prepared: monolithic Al_2O_3 and composite Al_2O_3–t-ZrO_2 ceramics (composition: 95 wt. % Al_2O_3 – 5 wt. % t-ZrO_2 and 90 wt. % Al_2O_3 – 10 wt. % t-ZrO_2) with different amount of dispersant DOLAPIX CE 64. Recorded flow curves were fitted to the power law, Herschel-Bulkley and Bingham models. Minimal viscosity was determined for each prepared suspension, in order to determine optimal slip casting parameters. Obtained results showed that the amount of dispersant for required minimal viscosity increases with the increase of the t-ZrO_2 amount.

Izvorni zanstveni rad

Sažetak: Stabilnost visokokoncentriranih (70 %-tnih) vodenih suspenzija monolitne i kompozitne keramike prikladnih za lijevanje praćena je određivanjem reoloških svojstava (krivulje tečenja i reološki parametri). Pripravljene su tri skupine suspenzija: monolitna Al_2O_3 i kompozitna Al_2O_3–t-ZrO_2 keramika (sastava : 95 % Al_2O_3 – 5 % t-ZrO_2 i 90 % Al_2O_3 – 10 % t-ZrO_2) s različitim udjelima disperzanta DOLAPIX CE 64. Snimljene krivulje tečenja opisane su potencijskim modelom, Herschel-Bulkley i Binghamovim modelom. Kako bi se odredili optimalni uvjeti lijevanja, minimalna viskoznost određena je za svaku pripravljenu suspenziju. Dobiveni rezultati pokazali su da minimalna viskoznost raste s porastom sadržaja t-ZrO_2.

1. Introduction

Slip casting is the most adequate technology for production of complex ceramic components. It is a simple, reliable, flexible, cost effective and pollution-free procedure, but it requires adequate understanding of colloid suspensions and their behaviour [1-11]. The slip casting process can be used for manufacturing both monolithic and composite ceramic products of different sizes and shapes. In order to use all the benefits of slip casting technology, the procedure must be prepared and carried out appropriately. It means that suspension viscosity, stability, density and composition must be optimal, as well as the casting parameters ([1-5], [7-9], [14], [15]). High suspension viscosity causes difficulties in moulding. In order to lower the viscosity, but keep the required suspension density, various additives are used. Their purpose is to electrostatically and/or sterically stabilize the ceramic particles in the suspension ([3], [4], [12], [13], [14]). The influence mechanism of polyelectrolytes on the rheological properties of ceramic suspensions (alumina, titania, zirconia) is already known and had been researched ([1], [14]).

Rheological flow curves are used for estimation of suspension stability. They show the dependence of shear stress and viscosity on shear rate and can be used for predicting the nature of interactions among suspension particles [1]. A number of models, such as Power law, Herschel-Bulkley or Bingham plastic model, have been developed in order to describe non-Newtonian systems. These models are effectively used to explain, characterize and predict the flow and pseudoplastic behaviour of various suspensions ([1], [12], [15]).

The aim of this study was to investigate the influence of a dispersant concentration (DOLAPIX CE 64) on viscosity of the monolithic Al_2O_3 and composite Al_2O_3–t-ZrO_2 ceramic suspension. The suspension flow curves were recorded and fitted to the Power law, Herschel-Bulkley and Bingham plastic model. Obtained results can be used to determine if the investigated suspensions show pseudoplastic behaviour and to determine which of the applied rheological models is the most appropriate to describe each suspension.

Symbols/Oznake

k	- consistency coefficient (flow index) - indeks konzistencije (tečenja)	**Greek letters/Grčka slova**	
n	- shear rate exponent - konstanta smične brzine	γ	- shear rate, s^{-1} - smična brzina, s^{-1}
R^2	- correlation coefficient, % - koeficijent korelacije, %	η	- dynamic viscosity, mPas - dinamička viskoznost
w	- mass portion, % - maseni udio, %	ρ	- plastic viscosity, Pa - plastična viskoznost, Pa
		τ	- shear stress, Pa - smično naprezanje, Pa
		τ_0	- yield stress, Pa - granica tečenja, Pa

2. Experimental

2.1. Suspension preparation

For preparation of highly concentrated aqueous suspension following components were used:

- high purity Al_2O_3 powder; average particle size 900 nm (according to manufacturer specification),
- high purity t-ZrO_2 powder stabilized with 8 mol % of Y_2O_3; average particle size is 300 nm (according to manufacturer specification)
- DOLAPIX CE 64 (Zschimmer & Schwarz GmbH &Co KG, Chemische Fabriken) – 70 wt. % aqueous solution of the ammonium salt of polymethacrylic acid (PMAA-NH4) as a dispersant
- deionised water

Three groups of suspensions were prepared: monolithic Al_2O_3 and composite Al_2O_3–t-ZrO_2 ceramics (composition: 95 wt. % Al_2O_3 – 5 wt. % t-ZrO_2 and 90 wt. % Al_2O_3 – 10 wt. % t-ZrO_2). Dry powder content was 70 wt. % in all prepared suspensions. The amount of DOLAPIX CE 64 was varied within each group, in order to determine its optimal content, which is reflected in obtained minimal viscosity. The dispersant content was: 0.2, 0.25, 0.3, 0.4, 0.6, 0.8 and 1.0 wt. %, calculated on the applied dry ceramic powder.

All suspensions were prepared by adding deionised water, containing dissolved DOLAPIX CE 64, into the grinding jar of planetary ball mill, after which ceramic powder was added. The grinding jar and ten balls used for homogenization were made of alumina ceramics. Each of the prepared suspensions was homogenized for 120 minutes at a rate of 300 rpm in the planetary ball mill (PM 100, Retsch, Germany). In order to remove air bubbles and to achieve better homogeneity of prepared suspensions, each of them was treated in the ultrasonic bath, so the results of rheological measurements would be as reliable as possible.

2.2. Determination of rheological properties

Rheological characterization includes recording of flow curves and describing obtained results by appropriate model. Flow curves show dependence of shear stress and viscosity on shear rate.

After the homogenization, all suspensions were subjected to rheological measurements, one at the time. Eight millilitres of each prepared suspension was used to measure rheological properties on the rotational viscometer Brookfield DV-III Ultra, USA, with accompanying software Rheocalc. The testing temperature was held constant at 23 ± 1°C. In order to avoid influence of all previous occurrences ("sample history") on the results, each suspension was subjected to pre-shearing at the shear rate of 100 s^{-1} for 2 minutes. Subsequently, flow curves were recorded. The shear rate, γ, was increased from 0 s^{-1} to 180 s^{-1} with 50 equal intervals, which lasted fo r 5 seconds. Measurements were made just before each rate change.

This study was focused on the influence of the DOLAPIX CE 64 on alumina and alumina-zirconia suspensions prepared for slip casting. Three rheological models were used: Power law, Herschel-Bulkley model and Bingham plastic model. Obtained rheological curves show the dependence of shear stress and viscosity on the shear rate.

The shear rate, γ, of 50 s^{-1} is the exact shear rate achieved during the gravity slip casting. One of the goals of this investigation was also to determine which amount of the DOLAPIX CE 64 will enable minimal viscosity at this shear rate.

All experiments were carried out under ambient laboratory conditions.

3. Results and discussion

3.1. Rheological properties

The aim of this research was to investigate how the concentration of the dispersant DOLAPIX CE 64 influences the viscosity of prepared ceramic suspensions and how does the added zirconia reflect on the

rheological properties of ceramic suspensions. Three groups of suspensions were prepared: monolithic Al_2O_3 and composite Al_2O_3–t-ZrO_2 ceramics (composition: 95 wt. % Al_2O_3 – 5 wt. % t-ZrO_2 and 90 wt. % Al_2O_3 – 10 wt. % t-ZrO_2). Prepared suspensions contained 70 wt. % of ceramic powder and variable amount of dispersant DOLAPIX CE 64 (0.2, 0.25, 0.3, 0.4, 0.6, 0.8 and 1.0 wt. %, calculated on the applied dry ceramic powder).

Rheological measurements were used to determine optimal dispersant amount, which is in correlation with lowest achieved viscosity at the shear rate of 50 s^{-1}. It is the exact shear rate of the gravity slip casting. Dependence of the obtained viscosity on the dispersant amount is given in Figure 1.

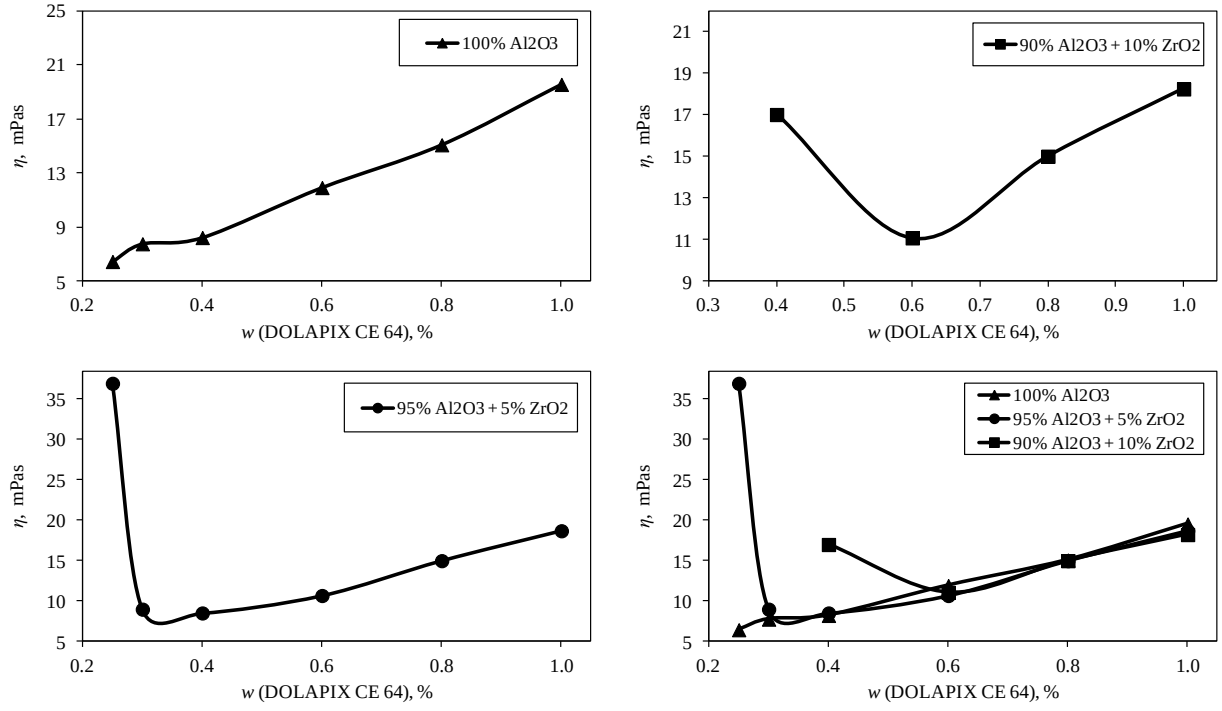

Figure 1. The dependence of viscosity on the concentration of DOLAPIX CE 64 for all investigated suspensions
Slika 1. Ovisnost viskoznosti o povećanju udjela DOLAPIX-a CE 64 za sve ispitivane suspenzije

Suspensions which endured the lowest viscosity were chosen for further analysis and were slip cast into plaster mould. Their composition and viscosity is given in Table 1.

Rheological measurements of investigated suspensions showed the relationship between viscosity and shear rate, shown in Figure 2.

Figure 2 represents the dynamic viscosity, η, as a function of shear rate, γ, for monolithic Al_2O_3 and composite Al_2O_3–t-ZrO_2 suspensions (composition: 95 wt. % Al_2O_3 – 5 wt. % t-ZrO_2 and 90 wt. % Al_2O_3 – 10 wt. % t-ZrO_2). Obtained results showed that the suspension viscosity decreases with the increasing shear rate. It is also noticeable that dynamic viscosity generally increases with the increasing of the zirconia content.

Table 1. Dinamic viscosity of prepared suspensions at the shear rate of 50 s^{-1}

Tablica 1. Dinamička viskoznost pripravljenih suspenzija pri smičnoj brzini od 50 s^{-1}

Sample (70 wt. % suspensions)/ Uzorak (70%-tne vodene suspenzije)	Optimal amount of DOLAPIX CE 64, wt. %/ Optimalni udio DOLAPIX-a CE 64, %	Dinamic viscosity, mPas / Dinamička viskoznost, mPas
Al_2O_3	0.25	6.47
95% Al_2O_3 + 5% ZrO_2	0.4	8.54
90% Al_2O_3 + 10% ZrO_2	0.6	11.09

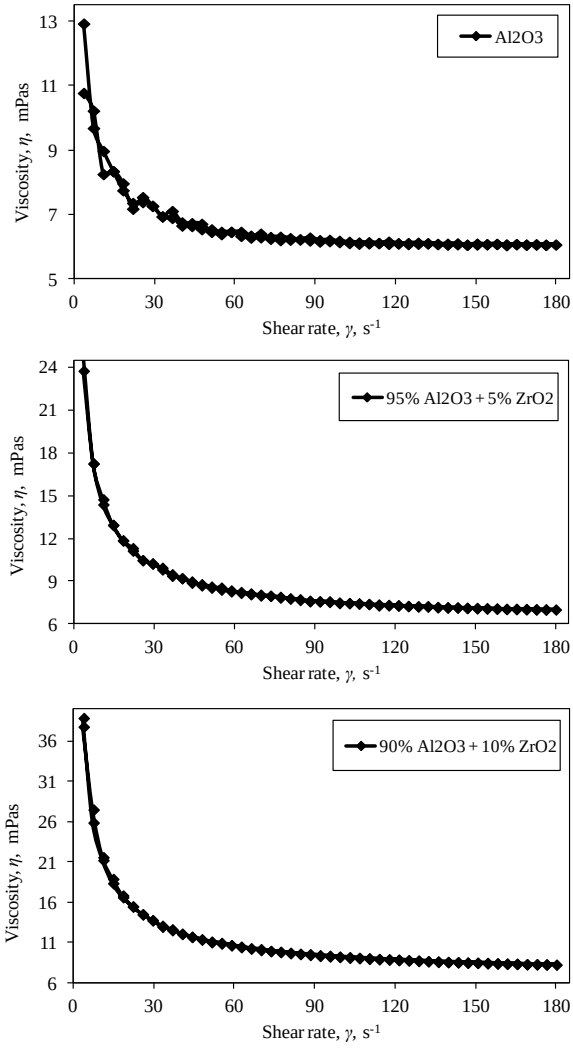

Figure 2. Flow curves of prepared suspensions – the dependence of the viscosity on the shear rate

Slika 2. Krivulje tečenja pripravljenih suspenzija – ovisnost viskoznosti o smičnoj brzini

3.2. Rheological flow models

It is clear from the Figure 2 that investigated monolithic and composite ceramic suspensions show typical shear thinning or pseudoplastic behaviour, which is characterized by decreasing in viscosity when shear rate increases.

To evaluate this experimental data, three different flow models were used:

- Power law, presented with:

$$\tau = k\gamma^n, \quad (1)$$

- Herschel-Bulkley model:

$$\tau = \tau_0 + k\gamma^n, \quad (2)$$

- Bingham plastic model:

$$\tau = \tau_0 + \rho\gamma, \quad (3)$$

Obtained values of all parameters are represented in Table 2.

According to obtained correlation coefficients R^2 (Table 2), all models are adequate to describe investigated Al_2O_3 and Al_2O_3–t-ZrO_2 suspensions, but the best results gives the Herschel-Bulkley model, with its correlation coefficient of 100%.

The shear rate exponent, *n*, decreases with the increasing zirconia content in observed suspensions. The value of shear rate exponent *n* stays below 1 for monolithic Al_2O_3 and composite Al_2O_3–t-ZrO_2 ceramics (composition: 95 wt. % Al_2O_3 – 5 wt. % t-ZrO_2 and 90 wt. % Al_2O_3 – 10 wt. % t-ZrO_2), indicating that these suspensions behave pseudoplastic, according to the Power law and Herschel-Bulkley model. The Herschel-Bulkley and Bingham plastic model also show that yield stress, τ_0, increases with the increasing zirconia concentrations. Plastic viscosity obtained from Bingham plastic model also increases with the increasing zirconia content.

4. Conclusion

The rheological measurements were conducted on highly concentrated ceramic suspensions, containing 70 wt. % of solid content. Three groups of suspensions were prepared: monolithic Al_2O_3 and composite Al_2O_3–t-ZrO_2 ceramics (composition: 95 wt. % Al_2O_3 – 5 wt. % t-ZrO_2 and 90 wt. % Al_2O_3 – 10 wt. % t-ZrO_2). All suspensions contained DOLAPIX CE 64 as a dispersant. The amount of DOLAPIX CE 64 was varied for each group of suspensions, in order to determine its optimal content. The optimal dispersant content is the one that gives the lowest viscosity values at the shear rate of 50 s^{-1}, because it is the exact shear rate of the gravity slip casting. The minimal viscosity for 70 wt. % suspensions was as follows:

- monolithic Al_2O_3 ceramics endured the lowest viscosity of 6.47 mPas for 0.25 wt. % of DOLAPIX CE 64,
- composite Al_2O_3–t-ZrO_2 ceramics (composition: 95 wt. % Al_2O_3 – 5 wt. % t-ZrO_2) ceramics endured the lowest viscosity of 8.54 mPas for 0.4 wt. % of DOLAPIX CE 64,
- composite Al_2O_3–t-ZrO_2 ceramics (composition: 90 wt. % Al_2O_3 – 10 wt. % t-ZrO_2) ceramics endured the lowest viscosity of 11.09 mPas for 0.6 wt. % of DOLAPIX CE 64.

It is clear that the increase in the zirconia content resulted in higher viscosity and in required higher amount of dispersant.

When the optimal dispersant amount was determined, it was used for further preparation of suspensions. These suspensions were used for rheological measurements.

After the rheological measurements were carried out, it can be concluded that all suspensions were well dispersed, stable and suitable for slip casting.

Table 2. Rheological parameters of prepared suspensions, according to used mathematical models

Tablica 2. Reološki parametri pripravljenih suspenzija prema upotrijebljenim matematičkim modelima

Sample / Uzorak	Power law model / Potencijski model			Herschel-Bulkley model / Herschel-Bulkley model				Bingham plastic model / Binghamov plastični model		
	k	n	R^2	τ_0	k	n	R^2	τ_0	ρ	R^2
Al_2O_3	12.2	0.86	96.5	0.03	5.73	0.99	100	0.03	5.86	98.5
95% Al_2O_3 + 5% ZrO_2	27.5	0.72	95.5	0.08	8.96	0.94	100	0.10	6.45	97.7
90% Al_2O_3 + 10% ZrO_2	48.8	0.64	95.3	0.12	13.50	0.89	100	0.18	7.29	97.2

To evaluate obtained results, three rheological flow models were used: Power law, Herschel-Bulkley model and Bingham plastic model. All models are considered applicable to all investigated suspensions, but the Herschel-Bulkley model showed the best correlation between experimental data and theoretical model.

The flow curves of observed alumina and alumina-zirconia suspensions show typical shear thinning (pseudoplastic) behaviour, which is confirmed with the shear rate exponent, n, which is less than 1 for all suspensions. It has been noticed that the shear rate exponent decreases with the increasing zirconia content.

The Herschel-Bulkley and Bingham models also show that yield stress, τ_0, increases with the increasing zirconia content. Plastic viscosity obtained from Bingham plastic model also increases with the increasing zirconia content.

Further investigations should focus on the mechanical and tribological properties of sintered ceramics obtained by slip casting.

REFERENCES

[1] Sarraf H., Havrda J., (2007), *Rheological behavior of concentrated alumina suspension – effect of electrosteric stabilization*, Ceramics-Silikáty 2007, 51, 147

[2] Navizi T., Salahi E., Ghafari M., Mobasherpour I., (2010), *Influence of Tiron concentration on dispersability and sintering behaviors of hydroxyapatite in an aqueous system*, Ceramics International 2010, 36, 1945

[3] Tsetsekou A., Agrafiotis C., Milias A., (2001), *Optimization of the rheological properties of alumina slurries for ceramic processing applications; Part I: Slip casting*, Journal of the European Ceramic Society 2001, 21, 363

[4] Shojai F., Pettersson A. B. A., Mäntylä T., Rosenholm J. B., (2000), *Electrostatic and electrosteric stabilization of aqueous slips of 3Y-ZrO_2 powder*, Journal of the European Ceramic Society 2000, 20, 277

[5] Ramesh S., Siah L.F., Nor Azmah A. K., (2000), *Sintering behaviour of slip-cast Al2O3 – Y-TZP composites*, Journal of Materials Science 2000, 35, 5509

[6] Santacruz I., Nieto M. I., Moreno R., (2005), *Alumina bodies with near-to-theoretical density by aqueous gelcasting using concentrated agarose solutions*, Ceramics International 2005, 31, 439.

[7] Xu X., Oliveira M. I. L. L., Fu R., Ferreira J. M. F., (2003), *Effect of dispersant on the rheological properties and slip casting of concentrated sialon precursor suspensions*, Journal of the European Ceramic Society 2003, 23, 1525

[8] Li Y., Lin J., Gao J., Qiao G., (2008), *Fabrication of reaction-bonded SiC ceramics by slip casting of SiCC suspension*, Materials Science and Engineering: A, 2008, 483-484, 676

[9] Karimian H., Babaluo A. A., (2006), *Effect of Polymeric Binder and Dispersant on the Stability of Colloidal Alumina Suspensions*, Iranian Polymer Journal 2006, 15, 879

[10] Boufi S., Baklouti S., Pagnoux C., Baumard J. F., (2002), *Interaction of cationic and anionic polyelectrolyte with SiO_2 and Al_2O_3 powders*, Journal of the European Ceramic Society 2002, 22, 1493

[11] Boschini F., Guillaume B., Rulmont A., Cloots R., Moreno R., (2006), *Slip casting of barium zirconate aqueous concentrated suspensions*, Journal of the European Ceramic Society 2006, 26, 1591

[12] Zhang Y., Binner J., (2008), *Effect of dispersants on the rheology of aqueous silicon carbide suspensions*, Ceramics International 2008, 34, 1381

[13] Olhero S. M., Ferreira J. M. F., (2002), Ceramics International 2002, 28, 377

[14] Pradhan M., Bhargava P., (2005), *Influence of Sucrose Addition on Rheology of Alumina Slurries Dispersed with a Polyacrylate Dispersant*, Journal of the American Ceramic Society 2005, 88, 833

[15] Shin Y. J., Su C. C., Shen Y. H., (2006), *Dispersion of aqueous nano-sized alumina suspensions using cationic polyelectrolyte*, Materials Research Bulletin 2006, 41, 1964

[16] Hang J., Shi L., Feng X., Xiao L., (2009), *Electrostatic and electrosteric stabilization of aqueous suspensions of barite nanoparticles*, Powder Technology 2009, 192, 166

[17] Binner J. G. P., McDermott A. M., (2006), *Rheological characterisation of ammonium polyacrylate dispersed, concentrated alumina suspensions*, Ceramics International 2006, 32, 803

ISSN 1847-7917

Wear mechanisms of mold for high pressure die casting in "LTH Metal Cast" manufacturing plant

Zvonimir DADIĆ[1)]***, Dražen ŽIVKOVIĆ***[1)]***, Nikša ČATIPOVIĆ***[1)]
1) Fakultet elektrotehnike, strojarstva i brodogradnje, Sveučilišta u Splitu
(Faculty of Electrical Engineering, Mechanical Engineering and Naval Architecture, University of Split)
Ruđera Boškovića 32, 21000 Split, Republic of Croatia

zdadic@fesb.hr
drazen.zivkovic@fesb.hr
ncatipov@fesb.hr

Keywords
High pressure die casting mold
Wear mechanisms
Casting parameters

Ključne riječi
Kalup za visokotlačno lijevanje
Mehanizmi trošenja
Parametri lijevanja

Review paper
Abstract: "LTH Metal Cast" manufactures aluminum alloy automotive parts using high pressure die casting process. During this process, under certain loads, mold wear appears. The tool has to be repaired or replaced which implies significant expenses.
This article has been made within the project "Computer optimization of parameters of metal thermal treatment processes". Goal of the article is to analyze and define the mold wear in relation with: mold material, casting alloy and casting parameters in "LTH Metal Cast" manufacturing plant. Using this information, it is possible to simulate the process of high pressure die casting and obtain enough data to reduce the wear of the mold.

Pregledni članak
Sažetak: „LTH Metalni Lijev" proizvodi automobilske dijelove od legura aluminija procesom visokotlačnog lijevanja. Prilikom ovog procesa, pod određenim opterećenjima, dolazi do trošenja kalupa. Kalup je potrebno popraviti ili zamijeniti što podrazumijeva znatne troškove.
Ovaj članak izrađen je unutar projekta „Računalno optimiranje parametara termalnih procesa obrade metala". Cilj članka je definiranje trošenja kalupa u odnosu na: materijala kalupa, ljevačke legure te parametara lijevanja u pogonu „LTH Metalni Lijev". Koristeći ove informacije, moguće je simulirati proces visokotlačnog lijevanja te pribaviti dovoljno podataka kako bi se smanjilo trošenje kalupa za lijevanje.

1. Introduction

High pressure die casting is mostly used for non-iron casting alloys such as alloys: with zinc, copper, aluminum, magnesium, led and tin. It is appropriate for mass produced casts with large dimensions and narrow cross sections. Casts produced using this process require very little subsequent machining [1].
Crucial part of high pressure die casting equipment is the mold. It is very expensive, considering the cast prices with other casting technologies, as shown in table 1. The prices of molds used in "LTH Metal Cast" are in the range of 30.000 to 100.000 €. Every mold has a certain life span, usually around 100.000 to 120.000 casting cycles. After that cycle period it is not possible to achieve the required dimensions of the cast. The tool has to be repaired or changed with a new one. Premature excessive wear significantly increases the cost of production [2].

Table 1. Comparison of casting methods [1]

	Sand casting	**Low pressure die casting**	**High pressure die casting**
Cast weight, kg	0.1 … 500	1 … 70	0.01 ... 30
Mold price	Low	Moderate	High
Minimal wall thickness, mm	4 ... 6	3 ... 4	0.8 ... 1.5
Dimension accuracy	Good	Very Good	Excellent
Surface roughness Ra, μm	>6.3-12.3	≥3.2	≥1.6(0.8)
Casting alloys	AlSi10Mg AlSi7Mg AlSi9Cu2 AlSi7Cu2	AlSi12 AlSi10Mg AlSi7Mg	AlSi9Cu3Fe AlSi12 AlSi10Mg AlSi11Cu2 (Fe)

2. Die casting process

Because of the high melting point of aluminum (about 660 °C) in the "LTH Metal Cast" manufacturing plant cold chamber die casting is used. For materials with lower melting point (Pb, Sn, Zn) hot chamber die casting is used. Cold chamber die casting implies introducing the molten metal for casting to the shot chamber from an external source. This is the reason way the die casting machinery is able to stay cool [3].

Casting alloy chemical composition is verified by spectral analysis. The alloy is mixed with the recycled scrap material at a certain ratio. Molten metal is obtained at a separate furnace from aluminum alloy ingots Al 226, Al 231 and Al 239 [2].

The temperature of molten metal is 690±20˚C. Molds are preheated to 170±10˚C. Hydraulic powered piston forces the molten metal into the mold under pressure of 300 to 1000 *bar* depending on the material and the required casting quality. Speed of molten aluminum at the entrance of mold is in the range of 30 to 50 m/s, depending on the pressure and density of the casting alloy. It takes 0.01 to 0.2 seconds to fill the mold, depending on the molten metal mass, mold entrance size, pressure and metal density. [3]

When the molten metal solidifies, the mold is opened and the cast is pushed out. The mold surface is lubricated after every casting cycle with a solution of molybdenum disulfide (MoS_2) at room temperature. Force needed to keep the mold closed during the injection and solidification of the molten metal is in the range from 3.400 to 12.000 kN. [2]

3. Mold material

Mold material has to have stability of properties at elevated temperatures, which significantly narrows the range of possible material selection. High strength and toughness is needed at temperatures of about 690 ˚C. The mold surfaces that shape the product and are in direct contact with the molten metal are made from steel EN X38CrMoV51, which has: a high resistance to annealing, wear, dynamic loads, thermal fatigue and corrosion [4]. Maximum percentage of phosphorus and sulfur is 0.03%. Chemical composition of steel X38CrMoV51 is shown in table 2.

Table 2. Steel X38CrMoV51 chemical composition [5]

C, %	Si, %	Mn, %	Cr, %	Mo, %	V, %
0.36-0.42	0.9-1.2	0.3-0.5	4.9-5.8	1.1-1.4	0.24-0.5

Mold production from this material includes the following steps[3]:

- incoming material inspection;
- rough machining;
- heat treatment for removal of residual stresses (high temperature annealing at 600 ˚C);
- hardening to achieve hardness of 50 to 55 HR_c;
- annealing to 43 HR_c;
- machining to final dimensions;
- inspecting the dimensions;
- carbonitration - Tenifer procedure (for surface hardness and resistance to wear and corrosion).

Trade mark of this steel is "Böhler W300". It was specifically made for severe operating conditions of tools and molds. It is suitable for quenching by air. It is also mostly used for casting light metal alloys [4]. Physical properties of steel X38CrMoV51 are shown in table 3.

Table 3. The physical properties of steel X38CrMoV51 at certain temperatures [4]

Temperature	**20 °C**	**500 °C**	**600 °C**
Density, [kg/dm3]	7.80	7.64	7.60
Specific heat, [J/kgK]	460	550	590
Modulus of elasticity, [MPa]	215×10^3	176×10^3	165×10^3

4. Mechanisms of wear

Mold is heated by the molten metal and cooled by heat conduction into the bulk of the mold and also by irradiation and convection when the mold is open. Before every cycle, the surface is sprayed with molybdenum disulfide which causes additional heat loss. Sudden temperature changes cause **thermal fatigue** of the mold material surface layer. Thermal fatigue is the dominant mold failure mechanism in die casting [6].

Expansion and contraction of the material in the mold surface layer represents a dynamic load cycle. A certain amount of cycles results in fatigue of the material. Cracks caused by thermal fatigue are usually smaller and are cross linked at the surface. Propagation of cracks causes particle separation. Oxidation can contribute significantly to propagation of cracks caused by thermal fatigue [6]. Figure 1 shows a mold with significant wear due to thermal fatigue on the left side and a cast made with the same mold on the right side.

Figure 1. Mold damaged by thermal fatigue and cast made with the same mold [7]

Erosion is induced by molten metal high kinetic energy at the entrance and also enhanced by the presence of solid particles in the molten metal (Al_2O_3). Damage can be seen on the spot where the molten metal comes in contact with the mold for the first time. [6]

Figure 2. Mold erosion wear [8]

Damage is also caused by **corrosion** originating from the dissolution of the mold material in the molten metal and emerging intermetallic compounds [6].

Local adherence between the mold surface and molten metal during filling and the solidification process causes remains of molten metal on the mold surface. The intensity of wear can be decreased by achieving lower friction between mold surface and molten metal, by increasing mold hardness and by achieving a lower chemical reactivity between the mold and the molten metal [6, 9].

Mentioned mechanisms of wear can increase the production costs significantly by additional expenses of maintenance, faulty products and expensive mold repairs.

5. Casting alloy

Material used for casting is an alloy of aluminum and silicon – AlSi12Cu1 (Fe). This is a eutectic alloy with excellent casting properties and resistance to thermal fatigue. Silicon allows low viscosity in the molten state. This alloy was made for production of casts with complex shapes and narrow cross sections. It is suitable for machining [10].

Disadvantage of these alloys is poor weld ability. It is not recommended for anodizing for decorative purposes. Mechanical properties of the casting alloy are improved by adding manganese and nickel [9]. Chemical composition and properties of the casting alloy are shown in tables 4, 5, 6 and 7.

Table 4. Casting alloy chemical composition [10]

Si, %	Fe, %	Cu, %	Mn, %	Mg, %	Cr, %	Ni, %	Zn, %	Pb, %	Ti, %
10.5-13.5	0.6-1.1	0.7-1.2	0.5	0.4	0.1	0.3	0.5	0.2	0.1

Table 5. **C**asting properties [10]

Solidification range, °C	Casting temperature, °C	Shrinkage, %
580-530	650-700	0.5-0.8

Table 6. Mechanical properties [10]

Tensile strenght, R_m, Mpa	Proof stress, $R_{p0,2}$, Mpa	Elongation A_{50}, % (min.)	Brinell Hardness, HB (min.)
240	140	1	70

Table 7. Other mechanical and physical properties [10]

Density, kg/dm3	Linear thermal expansion, (293-373 K), K-1	Thermal conductivity, W/mK
2.65	20x10-6	120-150

6. Controlling parameters

The thermally induced stresses cause accumulation of compressive plastic strains in the surface layer during the heating phase of the first cycle. The plastic yield of the mold material during the heating phase is, in turn, the perquisite for development of tensile stresses in the mold surface layer during the cooling phase. The presence of stress raising defects may cause that tensile stresses exceed the mold steel yield stress. The gradual softening of the mold steel, which occurs during the thermal cycling, degrades the initial yield strength values of the steel. Thus, the surface material locally will be exposed to cyclic stresses that cause accumulation of plastic strains after a certain number of thermal cycles [6]. If the mold preheating temperature is higher, the difference between mold preheating temperature and the molten metal temperature is lower and the amplitude of the load cycle is lower. Therefore, wear can be mitigated by optimal adjustment of the mold preheating temperature. According to this, one of the most important parameters is the **mold preheating temperature**.

As it was mentioned before, erosion wear occurs during the mold filling process with molten metal due to high relative **speed of molten metal.** It is to be expected that

the wear would decrease with the decrease of molten metal speed. Wear can be reduced by lowering the pressure of the hydraulic cylinder or by a different mold design.

Mold material is also an important parameter. Casting process takes place at high temperatures and most of wear occurs due to material fatigue. Thermal crack evaluations revealed that the crack length and crack density decreases with higher initial tool steel hardness [6]. Also, with high strength and hardness, high toughness is necessary to withstand as many cycles of load as possible and to extend the mold lifetime.

7. Conclusion

Taking into consideration the high cost of mold, investigating the cause of wear is justified. According to the data in this paper, the most influential parameters are mold preheating temperature, speed of molten metal and mold material. Research data show that parameters in "LTH Metal Cast" plant are not optimal which suggests wear can be moderated. According to various sources wear can be decreased by increasing the mold preheating temperature from the minimum of 180 to 350 ˚C ([3],[11],[12]). "LTH Metal Cast" uses preheating temperatures of around 170 ˚C.

To most effectively reduce wear it is necessary to try out different combinations of parameters and analyze the long term effects. It is inconvenient to do this in the manufacturing plant because it would imply loss of time and money. To avoid this, a device that simulates real conditions of high pressure die casting has to be designed. The device has to be able vary the mold preheating temperature, relative speed of molten metal and different mold materials.

REFERENCES

[1] Alteams Tech Center: „High pressure die casting", http://www.alteams.com/alteams-tech-centre/casting-methods/high-pressure-die-casting.html , april 2014.

[2] „LTH Metal Cast d.o.o.", Benkovac

[3] Danko Fuštin: „Alati za izvorno oblikovanje", http://www.ss-industrijska-strojarska-zg.skole.hr/upload/ss-industrijska-strojarska-zg/multistatic/52/9.%20Alati%20za%20izvorno%20oblikovanje-kalupi.pdf , april 2014.

[4] Böhler: „W300", http://www.bohler-edelstahl.com/english/files/W300DE.pdf , april 2014.

[5] Steel Grades: „X38CrMoV51", http://www.steel-grades.com/Steel-grades/Tool-steel-Hard-alloy/x38crmov5-1.html , august 2014.

[6] Anders Persson: „On Tool Failure in Die Casting", ACTA Universitatis Upsaliensis, Uppsala 2003. ISBN 91-554-5659-6

[7] Petar Ljumović;"Analiza triboloških mehanizama trošenja na kalupima za visoko – tlačno lijevanje", specijalistički projekt, Sveučilište u Splitu; Sveučilišni odjel za stručne studije, Split 2013.

[8] N.N.: „Mold erosion", http://www.giessereilexikon.com/en/foundry-lexicon/?tx_contagged%5Bsource%5D=default&tx_contagged%5Buid%5D=4594&tx_contagged%5BbackPid%5D=3&cHash=5127b12a9da411d323d4f20959e0dfab , april 2014.

[9] B. Kosec: „Failures of dies for die-casting of aluminium alloys", University of Ljubljana, Ljubljana 2007. ISSN 0543-5846

[10] N.N.: „Aluminium alloy EN AB-47100", http://www.stenametall.com/NR/rdonlyres/3B738B52-121E-41AD-8DA4-AB040E6F48BE/0/engENAB47100.pdf , june 2014.

[11] Uddeholm: „DIE STEELS AND IMPROVED PRODUCTIVITY IN DIE CASTING", http://www.empiredie.com/empire-die-casting/resource-center/downloads/pdf/UddeholmDiecastingoverview.pdf , june 2014.

[12] R. Molina, P. Amalberto: „Mechanical characterization of aluminium alloys for high temperature applications Part1: Al-Si-Cu alloys", Metallurgical Science and Technology, Vol. 29-1 – Ed. 2011.

ISSN 1847-7917

Cold and hot forging die wear

Nikša ČATIPOVIĆ[1)]
Dražen ŽIVKOVIĆ[1)]
Zvonimir DADIĆ[1)]
1) Fakultet Elektrotehnike, Strojarstva i Brodogradnje, Sveučičišta u Splitu (Faculty of Electrical Engineering, Mechanical Engineering and Naval Architecture, University of Split) Ruđera Boškovića 32, 21000 Split, **Republic of Croatia**

ncatipov@fesb.hr
drazen.zivkovic@fesb.hr
zdadic@fesb.hr

Keywords

wear mechanisms
wear types
dies for cold and hot forging
die wear
precise hot forging

Ključne riječi

mehanizmi trošenja
tipovi trošenja
kalupi za hladno i toplo kovanje
trošenje kalupa
precizno toplo kovanje

Review article

Abstract: This article analyses the basic mechanisms of tribological wear due to tribological processes that occur during cold and hot forging. Forging dies surface wear has a large influence on the product surface quality so it is necassary to reduce the waer intensity as much as possible. Also very important is to maintain needed tolerances of the final product, especially in hot precision forging. Understanding the tribological wear processes, that occur on the forging die surfaces, is necessary for analyses of die wear intensity. Tribological meethods that are used to decrease the intesity of wear are listed in this paper.

Trošenje kalupa za hladno i toplo kovanje

Pregledni članak

Sažetak: U ovom radu analizirani su osnovni tribološki mehanizmi trošenja u odnosu na tribološke procese koji se javljaju prilikom hladnog i toplog kovanja.
S obzirom na veliki utjecaj površinskog trošenja kovačkih kalupa na kvalitetu konačnog proizvoda potrebno je što više smanjiti intezitet trošenja kalupa. Također je važno zadržati zadane tolerancije gotovog proizvoda, posebno kod toplog preciznog kovanja. Da bi se smanjio intezitet trošenja kalupa potrebno je poznavati procese trošenja koji nastaju unutar tribosustava kalupa za kovanje i obratka.
U ovom radu navedene su tribološke mjere kojima se postiže manji intezitet trošenja tj. veća postojanost kalupa za hladno i toplo kovanje.

1. Introduction

Tribology is a scientific discipline which comprehensively addresses the problems of friction and wear. Friction is caused by the normal force between the surfaces of two bodies in contact. When the surfaces that are in contact, move relatively in opposite directions, the friction between the two objects converts kinetic energy into heat. A third of the world's energy is consumed in various forms of friction, which generally represents a loss of energy. Dynamic contact of two solid body surfaces leads to a gradual loss of material on the surface. That is material wear. Friction causes enormous losses of energy. Wear causes large lose of material. The main tribological goal is to obtain a satisfactory friction and wear. It may be said that control of friction and wear is the main task of tribology [1]. Approximately 70% of failures of mechanical components are the result of tribological phenomena, [2]. There are different ways that knowledge about mechanisms of wear and tear makes it easy to predict the degree of danger. Unfavourable wear on mechanical components often results in a decline in accuracy and efficiency of equipment, increased clearance between the moving components, vibration, increased mechanical wear and sometimes fatigue. In 1976 American experts in the field of tribology and representatives of various industries had attempted to measure the costs caused by wear. The results of this study are shown in Table 1 and are expressed in US dollars from 1976. Due to inflation the equivalent in today's US dollars is 5.4 times higher than in 1976.

Table 1. Expenses due to wear [3].

Category	Expense (in US dollars 1976.)	Expense (in US dollars 2014.)
War airplanes	$243.87 per flight hour	$1316.89 per flight hour
War ships	$38.92 per hour	$210.17 per hour
Tool wear due to machining	$9,000,000,000 per year	$48,600,000,000 per year
Car maintenance and repair costs	$40,000,000,000 per year	$216,000,000,000 per year

2. Wear processes and mechanisms

Wear is the gradual loss of material from the surface of a rigid body due to dynamic contact with other rigid body, fluid and/or particles [1]. For example: wear of tires, wear of a variety of cutting tools, wear wooden floors etc. Wear is often complex and can not be described by a single mechanism. It usually consists of two or more of the wear mechanism, acting at the same time or in a time sequence. Each wear process can be broken down into four basic wear mechanisms:

- **abrasion**

Abrasion is wear that occurs as a result of micro-cutting by hard particles with irregular geometry of the blade and is not extruding material. It results in a more material removal at the interface of a softer material, which is manifested by surface roughnesses, Figure 1a.

- **adhesion**

Adhesive wear occurs when irregularities – bumps, that are due to sliding contact, sliding one on eachother, which may result in the separation of parts from one and further "sticking" parts of one surface to another surface as shown in Figure 1b.

- **fatigue**

Fatigue is the gradual phenomena of material damage due to of long periodic fluctuating loads, Figure 1c. Mainly occurs in dynamicly stressed structures. Most of all fractures of the material are due to material fatigue.

- **tribo-corrosion**

Tribo-corrosional or tribo chemical wear is one of the wear mechanism in which dominates the chemical or electrochemical reactions of materials with the environment. Under the influence of the gas or liquid a reaction product in the form of thin films on the surface of the material is possible, as shown in Figure 1d.

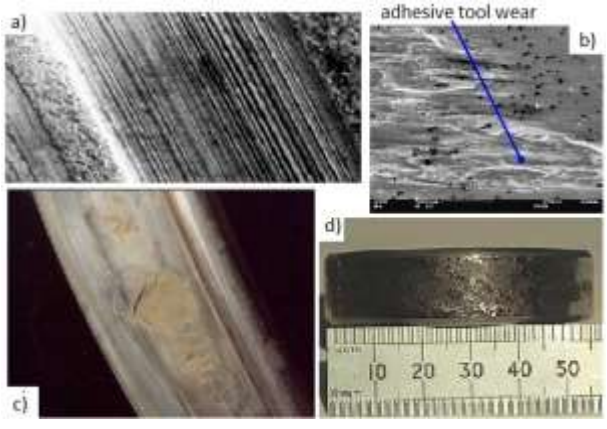

Figure 1. Basic wear mechanisms; a) abrasive wear [4], b) adhesive wear [5], c) surface fatigue [6], d) tribo-corrosion [7].

3. Cold and hot forging die wear

In forging die failure can be a significant portion of the overall production cost. The dies that fail must be either repaired or replaced. The replace cost includes the basic cost of the die that encompasses: material costs, machining, coating, and surface treatment as well as the cost of labor, [8].

Complex precision-forged parts are almost exclusively produced in closed dies. Therefore, the dies have to withstand high contact pressures well above the flow stress of the billet material at the forging temperature. Also, the amount of surface generation and the sliding velocities at which the billet material moves along the die surface are very large.

The high pressures and sliding velocities as well as the sudden changes in temperature may induce die failure due to several mechanisms. When a failure occurs, the production must stop to replace or repair the die. Consequently, the production cost will be significantly reduced if the die life can be increased.

3.1. Wear and fracture mechanisms

In hot forging, die wear is responsible for nearly 70% of die failures. In cold forging, die failure is primarily caused by fatigue.

In order to maximize die life, it is important to understand the primary mechanisms of fatigue, summarized as follows:

- **mechanically induced fatigue**

It occurs when a crack is induced and propagates through a die due to mechanical loading. Crack initiation occurs if the tool load exceeds the yield strength of the tool material in the area of a stress concentration, and a localized plastic zone forms.

- **thermaly induced fatigue**

It occurs when a crack is induced and propagates through a die due to thermal loading. Thermal-induced fatigue is not as common as mechanically induced fatigue, because the bulk die temperature does not fluctuate drastically during typical metal forming operations.

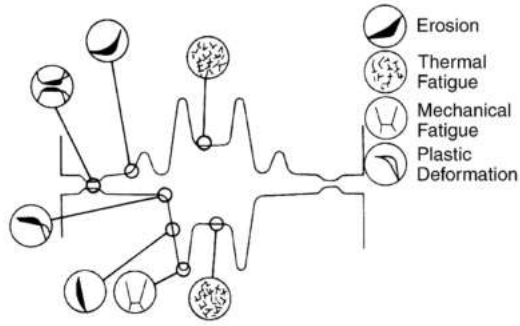

Figure 2. Typical failure modes and locations in

precision-forging die [8].

In order to maximize die life, it is also important to understand the primary mechanisms of wear. In metal forming four primary wear mechanisms may occur. These mechanisms, summarized below, work simultaneously and may be difficult to distinguish in an actual die:

- **adhesive wear;**

Adhesive wear occurs when two surfaces slide relative to one another. Material from one surface is sheared and remains adhered to the other surface. When there is metal-to-metal contact between the surface asperities of the workpiece and the die, some small portion of the workpiece surface may be sheared and remain attached to the die surface.

- **abrasive wear;**

Abrasive wear occurs when material is removed from a softer surface due to interaction with a hard asperity on another surface (two-body abrasion) or due to interaction with hard, loose particles trapped between two surfaces (three-body abrasion). A major concern is the abrasive wear of the die by hard oxides such as scale or intermetallics on the surface of the workpiece.

- **fatigue wear;**

Fatigue wear occurs when small cracks form on the surface or subsurface of the die and subsequently break off in the form of small fragments, thus leaving small voids in the die surface. This phenomenon is a result of the repeated mechanical loading and unloading that dies are subjected to. In hot forging, the repeated thermal loading and unloading also contributes to fatigue wear and die failures that can be seen in Figure 3, [9].

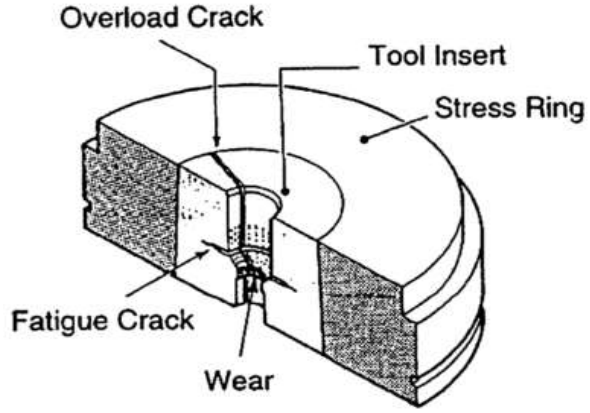

Figure 3. Fatigue fracture in forward extrusion die [9].

- **corrosive/chemical wear.**

Corrosive/chemical wear occurs when surface films (i.e., oxidation) are removed as a result of the relative sliding between the die and the workpiece in a corrosive environment. In general, corrosive wear is accelerated by the use of lubricants. However, this level of wear is generally accepted in order to prevent the more severe forms of adhesive wear that would result if lubricants were not used.

3.2. Analytical wear models

Some of the earliest analytical wear models were developed by Holm (1940s), Archard (1950s), and Rabinowicz (1960s). In general, these models characterized adhesive and abrasive wear as follows:

$$V = \frac{K \cdot p \cdot S}{H} \qquad (1)$$

V is the wear volume, K is the experimental wear coefficient, P is the normal pressure, S is the sliding length and H is the hardness of the softer material. Thus, it was recognized very early that adhesive and abrasive die wear could be decreased by minimizing: the wear coefficient, the normal pressure, and the sliding length and although by maximizing the die hardness.

Approximate values of the experimental wear coefficient (K) have been determined for many die/workpiece material combinations. For adhesive wear K_{adh} varies upon the material pair and the lubricant used. Table 2 summarizes these values, [8]. For abrasive wear, K_{abr} depends on the size, shape, and orientation of the asperity/particle interacting with the die surface. It usually varies from 0.02 to 0.2 for two-body abrasive wear and 0.001 to 0.01 for three-body abrasive wear.

Table 2. Summary of wear coefficient K_{adh} for adhesive wear [8].

Surface condition	Like metallic pairs	Unlike metallic pairs
Clean	5×10^{-3}	2×10^{-4}
Poor lubrication	2×10^{-4}	2×10^{-4}
Average lubrication	2×10^{-5}	2×10^{-5}
Excellent lubrication	2×10^{-6} do 10^{-7}	2×10^{-6} do 10^{-7}

4. Tribological measures to reduce cold and hot forging die wear

There are numerous parameters that influence die failure in cold and hot forging processes. The interaction of these parameters is complex. They may increase or decrease the die failure. In order to maximize die life tribological trends are important to be understand.

- **incoming bar;**

The workpiece material flow stress of influences the normal pressure at the die/workpiece interface. Considering that wear is proportional to interface pressure, a material with a lower flow stress will produce less pressure at the die/workpiece interface and thus less die wear, [8].

In addition, adhesive wear is inversely proportional to the workpiece material hardness. Therefore, a material with a high hardness (but less than die hardness) will produce less adhesive die wear.

The scale that is present on the workpiece surface influences the interface conditions. It acts as an insulator and thus protects the die against increased heating and thermal fatigue, but if it is hard and brittle, it causes abrasive wear.

The geometry of the billet influences the amount of sliding that will take place during the forging process. Because abrasive and adhesive wear are proportional to sliding length, the use of preforms where die wear is a concern will increase die life.

Die wear increases with increasing billet weight. This is likely the effect of increased interface pressure and contact time.

- **billet separation;**

The separation method influences obtainable weight tolerances. In general, cropping and sawing are the primary methods by which billets are separated.

Sorting of billets either by weight or size can help to extend the useful life of the dies. Billets can be sorted into two or more groups based on weight or size. The smaller billets should be forged first. As the dies begin to wear and the cavities become larger, larger billets may be introduced. The largest billets are forged at the end of the die life when the cavity is the largest. This technique helps to reduce the risk of excessive interface pressures generated as a result of premature die fill.

- **billet heating;**

The billet heating process must be closely controlled in order to keep the billets in the optimum forging temperature range and to reduce scale formation.

- **forging equipment;**

The press or hammer type influences the length of the contact time. Increased contact times result in increased wear. The reason for this is that the longer the die is in contact with the hot billet, the more the temperature of the dies increases and the temperature of the billet decreases. The increased die temperatures cause decreased die hardness due to thermal softening. Therefore, abrasive wear increases.

In general, hydraulic presses transfer energy from the ram to the workpiece and die slower than other press types. Thus, the contact time is longer. Hammers typically transfer energy very quickly. The contact time is shorter. However the fatigue fracture is a major concern for dies with low toughness, [8].

The press (ram) speed influences the relative sliding velocity between the billet and the dies.

- **forging dies;**

Peremeters as: strength (i.e., flow stress), toughness, resistance to thermal softening and hardness at higher temperature of the hot forging die material influence die wear resistance. It is known that abrasive and adhesive wear are inversely proportional to the strength/hot hardness of the die material. In addition, good toughness is also important for resistance to fatigue wear/fatigue fracture. Because toughness is a function of strength and ductility, it usually increases with increasing temperature.

A typical temperature-hardness curve for material H-10 (Cr-Mo alloy) is shown in Figure 4 [8].

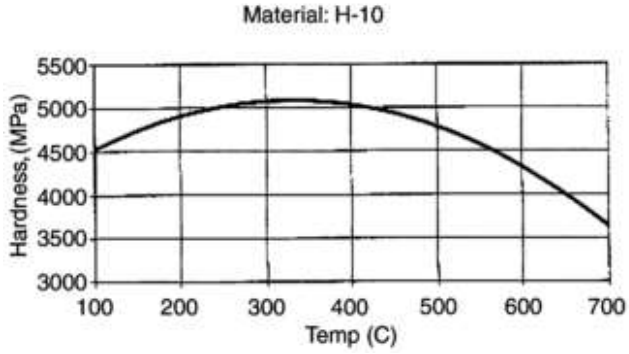

Figure 4. Temperature-hardness curve for material H-10 [8].

Alloying elements such as chromium, tungsten, vanadium and molybdenum are typically employed in hot forging dies in order to improve the wear resistance of the die. In particular, molybdenum is responsible for resistance to thermal softening at hot forging temperatures. Vanadium improves the resistance to abrasion and thermal fatigue. Tungsten increases toughness (resistance to mechanical fatigue) and resistance to thermal softening

Because dies simultaneously require high hardness to prevent wear and high toughness to prevent fatigue fracture, many dies incorporate a surface treatment, such as nitriding or boriding in hot forging or a coating such as TiN or TiAlN in cold forging. That improves the hardness of the surface while leaving the bulk of the die relatively soft.

- **lubrication;**

The lubricant type influences the interface pressure and the heat transfer between the die and the billet. Generally decreasing lubricity results in increased interface pressure. Increased pressure increases the die wear and thus decreases fatigue life. Also, the lubricant

acts as an insulator in order to protect the die against extreme temperature changes and thermal fatigue wear.
In hot forging, the lubricant application parameters, i.e., spray time, spray angle, spray distance, and flow rate, influence how the lubricant covers the die. Inadequate lubrication results in the case of increased interface pressure reduce insulation against extreme die-temperature changes.

- **process conditions**

The die hardness is under the die temperature influence. In general, the die hardness is inversely proportional to the die temperature. Thus, because abrasive and adhesive die wear are inversely proportional to die hardness, die wear is proportional to die temperature, which is significantly affected by contact periods.
The billet temperature influences the flow stress of the material. As discussed previously, increased flow stress results in increased interface pressure and thus increase wear and decrease fatigue life.
Increased sliding velocity between the die and the workpiece increases die wear. In general, the relative sliding between the die and work piece creates heat. The higher sliding velocity, the more heat is produced.
While the exact number of forging operations is not important, what is important is that there are enough operations so that the severity of the deformation at one station is not excessive. Excessive deformation in one die cavity causes large sliding between the billet and the die, which results in increased die wear.
The transfer time, i.e., amount of time required to transfer the billet from the furnace to the press, influences the temperature of the billet.
If the heated billet is allowed to rest on the die for a long period of time before deformation occurs, the billet will cool and the die will heat. Thus, wear will be increased, because the flow stress of the billet will be increased and the hardness of the dies will be decreased.

Wear prediction using FEM

Several studies have been conducted in an attempt to estimate die life in hot forging. The ability to predict die wear allows for the optimization of process variables such that die life is improved. Many researchers have applied FEM to estimate die wear in hot forging. In general, all of the results have been similar.
The die wear prediction (fatigue fracture as well) with FEM has the following specific advantages:

- Die changes can be scheduled, based on estimated die lives, in order to reduce unexpected machine downtime.
- Forging parameters such as: press speed, die materials, workpiece and die temperatures can be optimized to increase die life in an economical manner. That is opposed to expensive experimental studies.
- The effects of die geometry changes on die wear can be rapidly investigated, again avoiding the high cost of experimental studies.

Measurement of die wear for the hot precision forging process was carried out at the IFUM at the University of Hannover in Germany, under the conditions given in Table 3.

Table 3. Forging conditions used in die wear tests [10], [11].

PRESS
Type: mechanical Capacity: 3.09 MN (347 tonf) Stroke: 180 mm (7.1 in.) Stroke rate: 2/s Cycle time: 13 s
BILLET
Material: čelik 1045 Temperature: 1100 °C (595 °F) Diameter: 30 mm (1.2 in.) Height: 40 mm (1.6 in.)
DIES
Material: H-10, H-12, H-13 Hardness: 1200/1500/1700 Pa (0.17/0.22/0.25 psi) Temperature: 140/220/300 °C (285/430/570 °F) Lubrication: various
The cycle time includes placing the billet on the lower die, the billet resting on the lower die, the forging stroke, the forged billet resting on the lower die, removal of the forged billet, and lubrication (when applied).

Figure 5 shows the precision forging die used in the experiments. Typical wear profiles after forging are shown in Fig. 6. The experimental wear depths for three different lubricants are summarized in Fig. 7. [8].

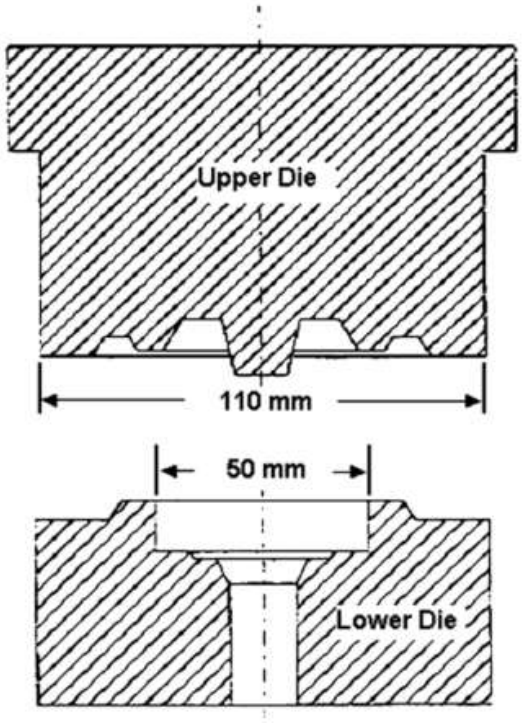

Figure 5. Hot precision forging die [10].

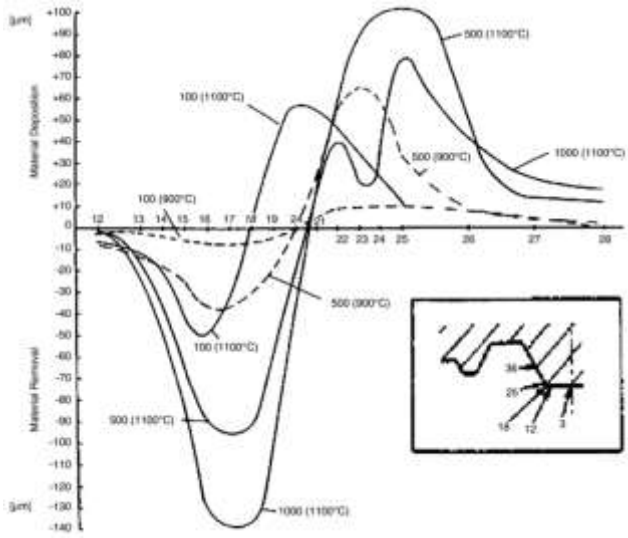

Figure 6. Measured die wear profile vs. die temperature vs. number of forging cycles [10].

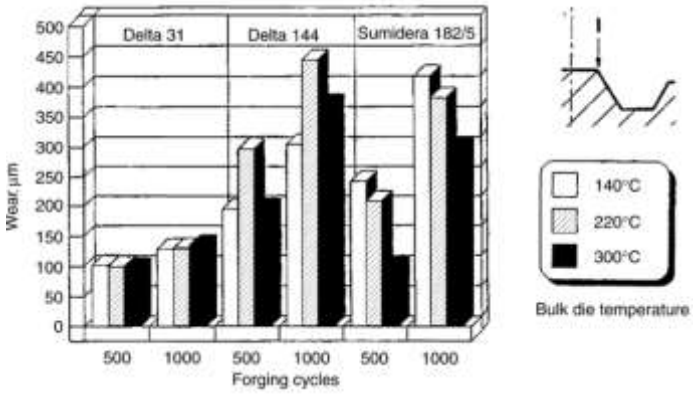

Figure 7. Measured die wear at location 1 vs. die temperature vs. lubricant vs. number of forging cycles [10].

It was assumed that abrasive wear was the dominant wear mechanism in hot precision forging. Therefore, the wear model in Eq 2 was used [8].

$$Z_i = \sum_{J=1}^{M} K_{abr}\left[\frac{p_{ij}U_{ij}\Delta t}{H_{ij}^{m}}\right]...i = 0, N \qquad (2)$$

where Z_i is the accumulated wear depth at the ith node, Δt is the time interval of the calculation step, M is the total number of calculation steps (2 for steels), N is the total number of nodes on the die surface, i represents the ith node, and j represents the jth time step, H is the die hardness, K_{abr} is the dimensionless abrasive wear coefficient, p is the interface pressure and U is the sliding velocity.

Figure 8 shows the FEM model of the hot precision forging process. On completion of each step, the parameters needed for the die wear model were extracted from the FEM simulation, and the wear depth was predicted, as discussed previously. Based on typical experimental values for two-body abrasion, the wear coefficient was assumed to be $K_{abr} = 0.02$ [8].

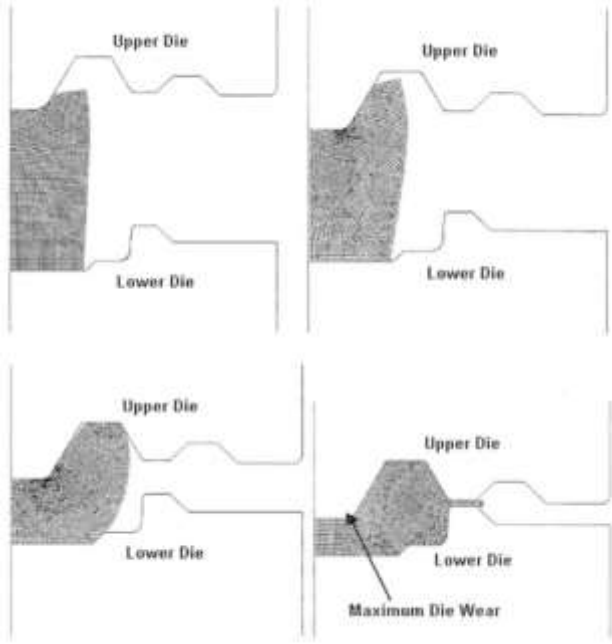

Figure 8. FEM model of hot precision forging process [8].

The maximum predicted die wear and the maximum measured die wear both occurred at the corner of the upper die (Fig. 6, measurement location 18). In general, the model predicted that die wear increases with decreasing corner radius, decreases with increasing friction factor, and increases with decreasing die hardness (i.e., different materials have different temperature-hardness curves). This illustrates the advantage of being able to predict die wear. It is not intuitive that die wear would decrease with increasing friction factor.

5. Conclusions

During any form of material treatment tends to have as much tool life as possible. That is the greater useful processing time after which further work tool is no longer economically feasible.

The same applies for dies for hot and cold forging. Prolonged use of the die: reduces the precision of machining, increases surface roughness, increases cutting forces and cutting temperatures and also vibrations occur. All these are consequences of different types of wear that occur in the die-workpiece system and may occur alone or in combination with one another. Some of the factors that affect the stability of the die are: the die and workpiece temperature, the geometry of the die and the workpiece, the mechanical properties of the die material and the lubricant type.

Wear of the forging tools has significant proportion in the total cost of the production process. Dies that are too worn out and failed, must be either repaired or replaced. Price includes replacement of the die, which includes cost of materials, the cost of processing, surface protection as well as the labor price. In any case, the most important factor in failure of the die is associated with slowdown of the manufacturing process, which ultimately reduces the overall productivity.

The mechanical properties of the die depend on the die material. High material hardness provides greater wear resistance, while higher toughness enables dynamic impact resistance. Since these properties are inversely proportional there is no universal material that would be ideal for any treatment. So forging material is selected according to the purpose. In addition to the hardness and toughness properties, stability of materials at high temperature and chemical resistance are also very important (ie. wear resistance of the materials surface layers).

High pressures, high sliding speeds and sudden changes in temperature can lead to a variety of wear mechanisms which result in the die failures. When an error occurs in the die, the production process must be stopped to repair or replace the die. It is therefore understandable that the production costs will considerably reduce if the lifetime of the die is extended.

It is extremely important to detect early and even predict the wear mechanisms that will occur in die-workpiece system. Thus directly affect the reduction in die repair costs but also the costs that will take place in the case of unforeseen extended downtime of the production process.

REFERENCES

[1] Vinko Ivušić: „Tribologija", Zagreb, 1998.

[2] H. G. Phakatkar, R. R. Ghorpade: „Tribology", http://books.google.hr/books?id=db7dEFk9qw0C&printsec=frontcover&dq=tribology&hl=hr&sa=X&ei=BDDkUOW2NPCP4gSkkIG4DA&ved=0CEYQ6AEwAg , 22. Prosinac. 2012.

[3] William A. Glaeser, Richard C. Erickson, Keith F. Dufrane, Jerrold W. Kannel: „Tribology: The science of combatting wear", http://www.stle.org/UserFiles/File/certification/Combatting%20Wear%20pt2.pdf , 23. Prosinac. 2012.

[4] N. N.: „DUCOM Tribology Instruments", http://www.ducom.com/Products/ , 23. Prosinac. 2012.

[5] Dmitri Kopeliovich: „Mechanisms of wear", http://www.substech.com/dokuwiki/doku.php?id=mechanisms_of_wear , 2. siječanj. 2013.

[6] N.N.: „Wear management", s Interneta, http://www.wear-

management.ch/?path=root+coatings&lang=en, 7. veljače. 2013.

[7] N.N.: „Bearing Corrosion and its Causes“, http://www.vibanalysis.co.uk/technical/corrosion/corrosion.html, 8. veljače. 2013.

[8] T. Altan; G. Ngaile, G. Shen: „Cold and Hot Forging – Fundamentals and Applications“, Materials Park, Ohio, veljača 2005.

[9] K. Lange, L. Cser, M. Geiger, J.A.G. Kals, M. Hansle; „Tool Life and Tool Quality in Bulk Metal Forming“ *Annals of the CIRP*, 1992, p 667-675.

[10] T. Bobke; „Phenomenon of Edge Layer at Sealing Process of Drop Forge Tools“ No. 237, IFUM, University of Hannover, 1991.

[11] H. Liug; „Influence of Wear Protective Coating and Scaling of Raw Parts on Forging Wear“No. 315, IFUM, University of Hannover, 1993.

.

ISSN 1847-7917

Influence of drawing with shear technology on the structure and properties of low-carbon wire

Elena PASHINSKA[1)],

Anna MAKSAKOVA[1)],

Anatoliy ZAVDOVEEV[1)],

Victor TKACHENKO[1)]

1) Donetsk Institute for Physics and Engineering named after O.O. Galkin, R.Luxemburg Str., 72, Donetsk, 83114, **Ukraine**

annymax@gmail.com

Keywords

drawing
shear
wire
low carbon steel
ferrite grain
EBSD-analysis

Ključne riječi

Professional article

Abstract: The technology of drawing with shear for low-carbon wire without heat treatment is developed. The effect of this technology on the structure and physical properties of low-carbon wire is studied.

It is shown that developed technology leads to a significant increase in number of small grains (less than 4 microns) and reduction of amount of big grains. It is set that the formation of small grains is explained with development of competing processes of fragmentation of large grains and dynamic recrystallization.

It is determined that the hallmark of this technology is the reduction of the structural anisotropy. This effect is related with the use of dies with a shear, that causes the change of direction of metal flow.

.

1. Introduction

Various methods of severe plastic deformation (SPD) with a shear are used for obtaining materials with ultrafine-grained (UFG) structure while hot or cold material state. Application of such treatments can significantly improve the strength of materials while maintaining a certain reserve of plasticity.

Modern production is very interested in getting a new technological and operational characteristics of long wire products [1,2]. One of the limitations in wire manufacture with UFG structure is that the volumes of materials, which obtained by SPD methods, is produced in kilograms and tons. In comparison, the required capacity of drawing production is hundreds of thousands of tons. For long wire products this problem can be solved with using of drawing with shear.

Papers [1-9] describe the various methods of intensive plastic deformation of metal for long products of different configurations. Of greatest interest are the works [5,6,9].

Thus, the authors [5] consider the application of alternating bending on cold-drawn fitting without additional heating. The main advantages of this method are its continuity and the ability of manufacturing of long products with enhanced mechanical properties.

Paper [6] describes a method for long-dimensional material structuring and a device for its implementation. Work of the device is based on alternating deformation in intersecting channels. The hearth of deformation zone is formed by shifting the axes of channel symmetry with uniaxial tension. This method is discontinuous, it allows to make long product with a finite length of several meters. Its advantage is the formation of fine-grained structure. However the deforming unit more complex than in case [5]. Moreover, both methods [5,6] does not allow to make small wire diameters.

Another way to obtain the UFG structure for long items, based on drawing, described in [9]. Its main advantage - the continuity of the process and the possibility of its usage in mass drawing production. The

disadvantage of this method is the laboriousness of the drawing process as a complex technical unit is used. The main disadvantage is the need for a new assembly and dismantling of this node while changing of dies.

The purpose of this article is to show the influence of the drawing with a shear technology on changes in structure of wire compared with the classical drawing technology with standard dies.

Symbols/Oznake

c	- Aspect ratio	D_2	- grain length perpendicular to the drawing direction, mm
D_1	grain length towards to the drawing direction, mm		**Subscripts/Indeksi**
	-	*	- die with shear

Table 1. The chemical composition of steel wire 08G2S, %

C	Mn	Si	S	P	Cr	Ni	Cu	N
0.071	1.98	0.84	0.015	0.018	0.015	0.009	0.016	0.0055
Ti	As	B	Al	V	Mo	W	Co	
< 0.005	< 0.005	< 0.0005	0.005	0.006	< 0.01	0.024	0.01	

Table 2. Routes of drawing wire, which obtained from the experimental and classical technologies

Technology	Diameter of dies, mm						
Experimental	6.15	5.45*	5.0	4.7*	4.20	3.85	3.30
Classical		5.45		4.40			
Experimental	2.95	2.75	2.42	2.13	1.88	1.70	1.55
Classical						-	-

Note: * – die with shear

2. Experimental methods

The experiment was performed on the rod from 08G2S steel (Table 1). Drawing was performed on the drawing machine AZTM 7000/1 using the developed (experimental) technology (dies with shear) and classic (with standard round dies). Drawing routes for both types of technology are shown in Table. 2 The microstructure of the annealed and deformed samples were studied at magnifications of 100-2000 on the microscope «Neophot-32» after repeated polishing and etching on the grain boundaries (etchant composition: 4% nitric acid, 97% alcohol). Photographing was performed on an optical microscope Axiovert 40 MAT. On the samples in the transverse and longitudinal directions the size of the grains and their fragments were quantified. For each photo was hold about 100 measurements. Aspect ratio was calculated according to the formula.

$$c = D_1/D_2, \qquad (1)$$

where D_1, D_2 – grain length, mm in longitudinal direction of sample section towards and perpendicular to the drawing direction.

The closer the value of the coefficient c is to 1, the higher the isotropy of the structure under investigation.

The microstructure of the samples was also examined using a scanning electron microscope JSM-6490LV of backscattered electron diffraction (EBSD-analysis). Sample preparation was performed by standard procedure.

3. The experimental results

3.1. Optical microscopy

One of the features of an experimental technology is the reduction the structural anisotropy. In the longitudinal section in the "classic" samples anisotropy is expressed more than in "experimental" samples, ferrite grain is smaller, pearlite colonies are extended in strips. In the "experimental" samples pearlite colonies less elongated, more rounded. The same effect is observed in the cross-section. The confirmation of this effect can be observed in the Table 3, where the aspect ratio is given.

In the standard technology of drawing it can be observed a decrease of the aspect ratio while drawing samples to smaller diameter. It is associated with the fact that drawing refers to an uniaxial strain. During

such strain grains orientate and extend along the strain axis and at the same time they decrease in width. That is why Aspect ratio when using classical drawing decreased gradually from 0.65 to 0.12.

Table 3. Aspect ratio *c* for steel wire 08G2S

Technology	*c*			
	ø 6.5	ø 5.0	ø 3.9	ø 1.55/ ø 1.88
Experimental	1	0,47	0,72	0,28
Classical		0,65	0,44	0,12

It is also observed a decrease of aspect ratio while experimental technology, but it is not linear. For diameter ø 3.9 we observe an increase of the coefficient to 0.72 compared to 0.47 for the diameter ø 5.0. This effect is associated with the use of the dies with shear, which changes a direction of metal flow.

Analysis of structures using optical microscope allowed to see the following main structural features.

1. When drawing on classical technology with increasing degree of deformation the grain size decreases according to the principle of Taylor-Polanyi (Table 4). It has been established that the axial drawing with classical technology leads to an increase in grain size and to its reduction the cross-section. Changes of the grain size in the experimental drawing are not monotonous like in classical drawing. Grain refinement processes are periodically replaced by increasing of grains size. Experimental technology in longitudinal section does not lead to increasing of grain size; it leads to its reduction (compare 9.02 and 4.53 mkm). This phenomenon can be explained with a process of metal flow in dies with shear. It can also be associated with the development of competing processes: fragmentation and dynamic polygonization / recrystallization.

To solve this dilemma it was held as analysis of the structure involving a scanning electron microscope. To understand the picture of structure formation the EBSD data analysis will be given below.

2. Fig. 1 shows curves of the grain size distribution along the axis of the drawing. It is clearly seen that the experimental technique of drawing leads to a substantial increase in the amount of small grains (less than 4 mm) and a decrease in the amount of large grains. For example, for a classical drawing technology it can be observed the presence of grains more than 44 microns while for experimental technology grains more than 32 microns are absent.

3. During experimental drawing it can be observed the healing of pores and microcracks [10].

3.2. Scanning electron microscopy

Studies have shown that at low deformation degree the state of the grain boundaries for both technologies are similar: there are relatively large grains decorated with high angle boundaries (Fig. 2, a and b). A thin structure is formed inside the grains, which represents dislocation clusters, cells and low-angle boundaries (subboundaries). However, the overall density of the low-angle boundaries after experimental drawing is higher than after drawing on the classical scheme.

At the same time, while increasing the deformation degree a picture of formed boundaries changes. In the classical drawing it can be seen the general grain refinement and a forming of subboundaries from dislocations. Due to these effects, relatively clean of defects areas appear inside the grains. In experimental drawing an amount of high angle boundaries increase significantly. It happens due to the relatively large grains, which increase the angle of disorientation during the deformation and due to a very small fragmented grains less than 4 microns.

In addition, the backscattered electron diffraction enabled an analysis of different types of grains: deformed, substructure, recrystallized. Fig. 3 shows the grain types EBSD-maps after different kinds of drawing. These maps support the idea that formed small grains (less than 4 microns) are recrystallized. Probable mechanism of the formation of such grains is the fragmentation of large grains. Thus they split up into small grains less than 4 microns in size. These grains had to show structural imperfections due to the large number of defects and therefore noticeable curvature of the crystal lattice. However, the maps of crystallographic orientations show that the crystallographic orientation inside the grains do not vary smoothly due to bending of the crystallographic planes, but they change abruptly. In other words, grains are structurally "perfect", in "small" grains lattice is not curved. It is typical for the case of formation of deformed structure due to grain boundary sliding (GBS), or joint occurrence of dynamic recrystallization and GBS. The consequences of these processes are the change of grain boundaries from smooth to notched and high angle boundaries formation.

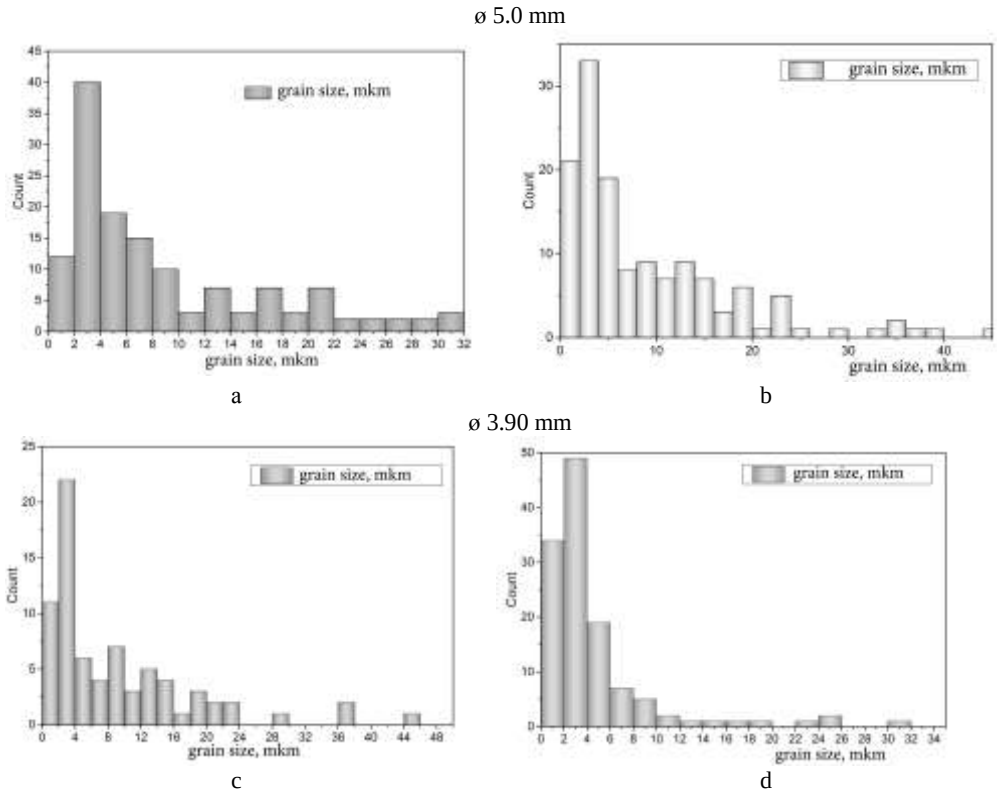

Figure. 1. The grain size in wire from 08G2S steel obtained by the classical (a, c) and experimental (b, d) technologies. Section along the axis of the drawing

Table 4. Grain sizes of wire 08G2S after drawing

Diametres, mm	Grain size, mkm			
	Drawing technology			
	Classical		Experimental	
	Along the drawing axis	Across the drawing axis	Along the drawing axis	Across the drawing axis
5.0	8.70	5.72	8.78	4.14
3.9	9.02	4.02	4.53	3.28

In favor of the latter considerations attests the data shown in Fig. 3, c and d. After drawing with experimental technology the number of recrystallized grains increases the from 2.5% to 4.8% compared with the classical technology of drawing. Besides the number of deformed grains increase from 12.5% to 22%. Recrystallized grains indicates the occurrence of a mechanically activated dynamic recrystallization.

Thus, at high degrees of deformation structure formed by drawing on classical and experimental technology differs fundamentally. Experimental technology leads to more intensive grain refinement than classical technology. Experimental technology of drawing leads to a significant increase in number of small grains (less than 4 microns) and reducing the number of large grains. At the boundary there is a large number of small grains with high angle boundaries.

4. Conclusions

The structure formed by drawing with classical and experimental technology at high degrees of deformation differs fundamentally: the experimental technology leads to more significant grain refinement than the classical drawing technology. Experimental technology of drawing leads to a significant increase in number of small grains (less than 4 microns) and reducing the number of large grains. At the boundary there is a large number of small grains with high angle boundaries.

Formation of such grains can be explained with the development of competing fragmentation processes of the large grains and dynamic recrystallization. This leads to the fact that the grain boundaries are changed from smooth to notched and form incomplete high angle

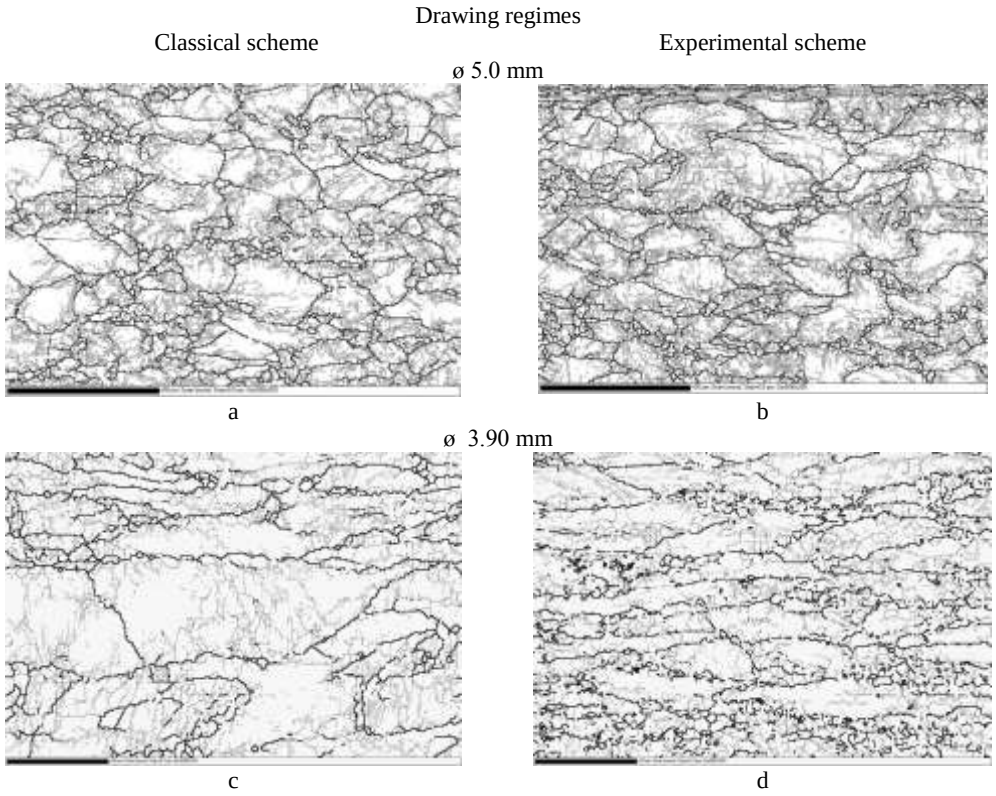

Figure. 2. Grain boundary EBSD-maps of low-carbon steel: a,c – classical scheme; b,d – experimental scheme. a,b – scale bar 50 μm; c,d – scale bar 20 μm. Black line – HAB, gray line – LAB. Longitudinal section.

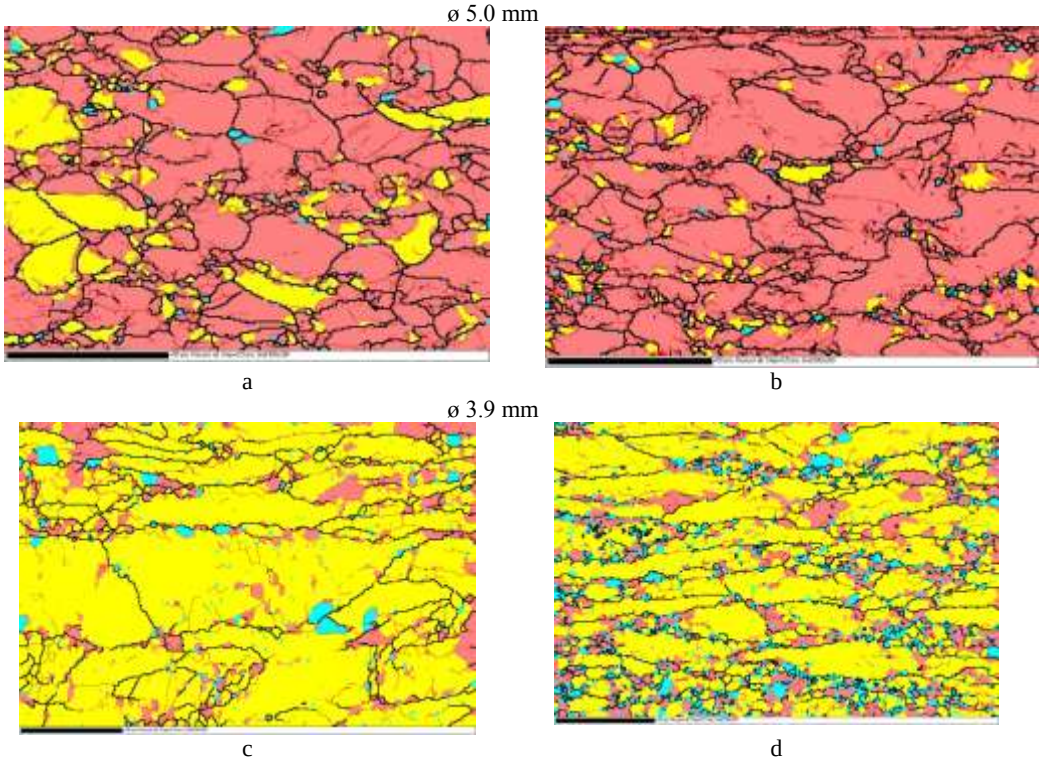

Figure. 3. Grain types EBSD-maps of low-carbon steel: a,c – classical scheme; b,d – experimental scheme. a,b – scale bar 50 μm; c,d – scale bar 20 μm. Pink – deformed grains, yellow – substructured grains, blue – recrystalline grains. Longitudinal section.

boundaries. Also it is shown that some of the small grains provides grain boundary sliding.

One of the features of an experimental technology is the reduction of the structural anisotropy. This effect is related with the use of dies with a shear, that causes the change of direction of metal flow.

REFERENCES

[1] Astafurova E.G., Zaharova G.G., Najdenkin E.V., Raab G.I., Odesskij P.D., Dobatkin S.V., (2011) *Features of the microstructure and the mechanical behavior of steel 06MBF after equal channel angular pressing*, Letters about materials 1, issue. 4, 198

[2] Astafurova E.G., Zaharova G.G., Najdenkin E.V., Dobatkin S.V., Raab G.I., (2010) *Effect of equal channel angular pressing on the structure and mechanical properties of low carbon steel*, FMM 110, 275.

[3] Kolbasnikov N. G., Zotov O. G., Duranichev V. V., (2009), *Influence of large deformations in hot state on the structure and properties of low carbon steel*, Metalloobrabotka №4, 25.

[4] Jakovleva S.P., Maharova S.N., (2010) *Mechanical properties of 09G2S at low temperature annealing after cold equal channel angular pressing*, Proceedings of the Samara Scientific Center, Russian Academy of Sciences, V. 12, №1(2), 589.

[5] Kireev E.M., Shhuljak M.N., Stoljarov A.V., (2009), *Effect of finishing strain with alternating curve at the formation of the mechanical properties of cold fittings*, Steel, №3, 56.

[6] *Patent of RF* № 2440865, The method of plastic material structuring of long workpieces and device for its implementation, A.S. Matveev, R.A. Kazakov, Ju.S. Shumkina, V.V Kurganskij, Application № 2010121631/02, 27.05.2010.

[7] Astafurova E.G., G Zaharova.G., Najdenkin E.V., Raab G.I., Dobatkin S.V., (2010) *Structure and mechanical properties of low-carbon ferrite-pearlite steel 10G2FT after severe plastic deformation and subsequent high-temperature annealings*, FMM.,V. 13, № 4, 91.

[8] Zakirova A. A., Zaripova R. G., Semenov V. I., (2012) *Structure and mechanical properties of carbon steel subjected to severe plastic deformation by torsion*, Mechanical engineering and materials science and thermal processing of metals V. 11, №2 (29), 123

[9] *Patent of RF* № 2347633, A method for producing ultrafine semifinished products by drawing shift, G.I. Raab, A.G. Raab, Application № 2007141899/02, 12.11.2007.

[10] Pashinska E.G. Varykhin V.N. Maksakov A.I. Maksakova A.A. Tolpa A.A. Makarova A.V., (2014) *The impact of technology of drawing with a shear on a structure and properties of low-carbon wire*, FTHP, №1, V 24,120-126

Konstrukcijske karakteristike aktivnog modularnog motora s unutrašnjim izgaranjem

univ.bacc.ing.mech.Antonio Mijić[1)]

prof.dr.sc.Gojmir Radica[1)]

univ.bacc.ing.mech. Dino Dodig[1)]

mag.ing.mech.Nikola Matulić[1)]

1) Fakultet Elektrotehnike, Strojarstva i Brodogradnje, Sveučilišta u Splitu (Faculty of Electrical Engineering, Mechanical Engineering and Naval Architecture, University of Split) Ruđera Boškovića 32, 21000 Split, **Republic of Croatia**

amijic@fesb.hr
goradica@fesb.hr
ddodig@fesb.hr
nimatuli@fesb.hr

Keywords

AMICES
Hybrids
New construction concepts
Ceramic piston coatings
Carbon pistons

Ključne riječi

AMICES
Hibridi
Novi konstrukcijski koncepti
Keramikom presvučeni klipovi
Karbonski klipovi

Review article

Abstract: This article analyzes construction characteristics of AMICES concept, which include ways of cylinder design and the use of materials that are able to withstand the given conditions inside of the engine. AMICES stands for active modular internal combustion engine system, and it is conceptually designed as a two stroke, three cylinder engine with external compression. It would be in accordance with all of the default rules and standards of air pollution, with extremely high engine efficiency and performance, and with very low fuel consumption in comparison with other similar engines. We are presenting a description and specifications of the concept, and analyzed problems related to the construction of engine and materials needed for its production.

Pregledni članak

Sažetak: Ovaj rad se bavi konstrukcijskim karakteristikama koncepta AMICES, u koje spadaju načini izvedbe cilindra, te korištenje materijala koji su u stanju izdržati zadane uvjete unutar motora. AMICES je kratica koja prevedena s engleskog znači aktivni modularni motor s unutrašnjim izgaranjem, a zamišljen je kao dvotaktni, trocilindrični motor s vanjskom kompresijom. Bio bi u skladu sa svim zadanim propisima i normama o onečišćenju zraka, te bi mu stupanj iskorištenja energije bio iznimno visok u usporedbi sa ostalim sličnim motorima, uz vrlo malu potrošnju goriva. U ovom radu je iznesen opis i specifikacije koncepta, te su analizirani problemi vezani uz konstrukciju motora i materijali potrebni za njegovu izradu.

Symbols/Oznake

W	- specific work , kW - rad
p	- pressure, bar - tlak
Q	- heat, J - toplina
σ_V	- tensile strength, MPa - vlačna čvrstoća

Greek letters/Grčka slova

α	- coefficient of thermal expansion, 1/K - koeficijent linearnog toplinskog širenja
E	- modulus of elasticity, GPa - modul elastičnosti
λ	- conduction coefficient, $Wm^{-1}K^{-1}$ - koeficijent kondukcije
ρ	- density, gcm^{-3} - gustoća

Subscripts/Indeksi

MUI	- internal combustion engine - motor s unutrašnjim izgaranjem
AMICES	- active modular internal combustion engine system - aktivni modularni motor s unutrašnjim izgaranjem
GMT	- top dead center - gornja mrtva točka
DMT	- down dead center - donja mrtva točka
DOPPELWELLE	- two crankshafts system - sistem s dva koljenasta vratila

1. Uvod

Posljednjih nekoliko godina sve se više priča o štetnom učinku automobilskih štetnih plinova, koji uzrokuju onečišćenje atmosfere, te zagađenje okoliša. Svake godine sve stroži i stroži propisi tjeraju inženjere na nova i bolja rješenja koja će riješiti problem emisije štetnih plinova. Osnovnu učinkovitost pretvorbe energije svakog motora s unutarnjim izgaranjem predstavlja toplinska učinkovitost. Ona je kod automobila vrlo mala(otprilike 25-30 %) što znači da se vrlo mali dio energije pohranjene u gorivu pretvara u koristan mehanički rad. To predstavlja neracionalno raspolaganje Zemljinim energentima te se veliki dio energije bespovratno baca. Vodeći proizvođači automobila su se uvelike angažirali oko razvijanja koncepta automobila kojeg će pogoniti obnovljivi izvor energije kako bi spremni dočekali vrijeme kada će zbog nestašice nafte ili zbog posljedica globalnog zatopljenja i onečišćenja okoliša korištenje motora s unutrašnjim izgaranjem biti strogo ograničeno ili u potpunosti zabranjeno. Rješenje tih problema se već nazire, u obliku hibridnih automobila kako električnih tako i pneumatskih koji nude kompromis između željenih performansi pogona i potrošnje goriva. Ovaj rad se bavi konstrukcijskim karakteristikama koncepta AMICES, hibridnog motora koji bi svojom visokom učinkovitošću te čistim ispuhom reducirao
gubitke energije i sveo emisiju štetnih plinova na minimum.

2. Analiza problema

2.1. Hibridi

Hibridni automobili su oni koji za pokretanje koriste dva ili više izvora energije, umjesto jednog kao kod tradicionalnih automobila. Najčešća je kombinacija benzinskog ili dizelskog motora s elektromotorom. Hibridni motori imaju znatno manju emisiju štetnih plinova koji onečišćuju zrak i uzrokuju kisele kiše. Cilj hibrida je, kombinirajući elektromotor i standardni motor s unutrašnjim izgaranjem, dobiti vozilo sa čistim ispuhom.

2.2. AMICES koncept

Idejni začetnik i vlasnik patenta za koncept AMICES je gosp. Hrvoje Šalinović, diplomirani inženjer strojarstva koji je kombinirajući dugogodišnje iskustvo rada u automobilskoj tvrtki BMW sa novim pratećim trendovima u autoindustriji postavio teorijske izračune motora koji bi uvelike trebao nadmašiti performanse svih poznatih hibrida. AMICES koncept motora je zamišljen kao dvotaktni, trocilindrični motor od 500 cm^3. Kao što je vidljivo na slici, srce pogona je trocilindrični dvotaktni motor, napajan zrakom od krilnog kompresora koji je pogonjen direktno preko razdjelnika snage ili elektromotora. Rekuperacijski modul se sastoji od turbine pogonjene ispušnim plinovima koja predaje snagu generatoru za punjenje baterija ili preko planetarnog prijenosnika na razdjelnik snage. Turbina i kompresor nisu u direktnoj vezi kao kod turbopuhala, već su pogonjeni svaki zasebno. To

omogućuje korištenje efikasnijih turbina, kao i specijalnih kompresora u svrhu postizanja što većih efikasnosti sustava, kao i iskorištavanje energije ispušnih plinova koja se kod turbopuhala iz sigurnosnih razloga izbacuje preko obilaznih ili ispušnih ventila.

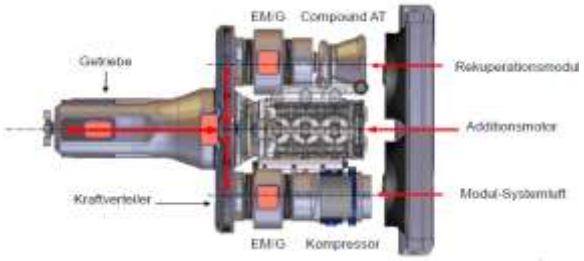

Slika 2. 1. *Pogonski sklop [5]*

Figure 2. 1. *Powertrain of AMICES [5]*

Oznake sa slike 2.1. su:
Rekuperationsmodul- rekuperacijski modul,
Additionsmotor- adicijski motor- trocilindrični dvotaktni motor,
Modul-Systemluft- modul za pripremu zraka,
Compound AT- turbina,
EM/G- elektromotor/generator,
Kraftverteiler- razdjelnik snage,
Getriebe- mjenjačka kutija.

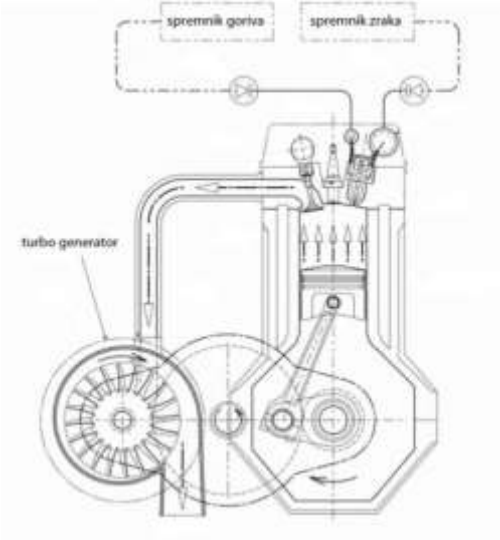

Slika 2.2. *Konstrukcija motora [5]*

Figure 2.2. *Engine construction [5]*

Zahvaljujući nesinkroniziranoj vanjskoj kompresiji, istodobnom ubrizgavanju i regulaciji snage temeljenoj na ubrizgavanju mješavine zraka i goriva pri konstantnom tlaku, krivulja okretnog momenta je gotovo linearna.

Pogon se temelji na start-stop sistemu te ne treba nikakav period uhodavanja iz stanja mirovanja.

Procesi u cilindru se odvijaju sljedećim redom:

Početak je ubrizgavanje zraka i goriva pod tlakom od 50 bar-a. Ubrizgavanje počinje u GMT a traje do nekih 20° koljenastog vratila (KV). Postoji mogućnost ranije pripreme smjese i ubrizgavanje iste pod tlakom od 50 bara ili ubrizgavanje čistog zraka pod tlakom od 50 bara, a gorivo se ubrizgava direktno u cilindar. Zatim slijedi paljenje smjese na 20° KV vratila nakon GMT. Paljenje se može vršiti klasičnom svjećicom ili kako je projektno zamišljeno laserom. Laserska tehnologija paljenja još nije ušla u primjenu, ali je u visokom stupnju razvoja i očekuje se uskoro. Nakon paljenja događa se ekspanzija. Zadnji ciklus je ciklus ispuha. U ispušnom taktu osim ispiranja cilindra dobiva se i rad na turbini. Očekuju se visoke vrijednosti rada na turbini zbog produljene ekspanzije uzrokovane kasnim paljenjem tj. realno je očekivati znatno viši tlak na ulazu u turbinu u odnosu na konvencionalne motore.

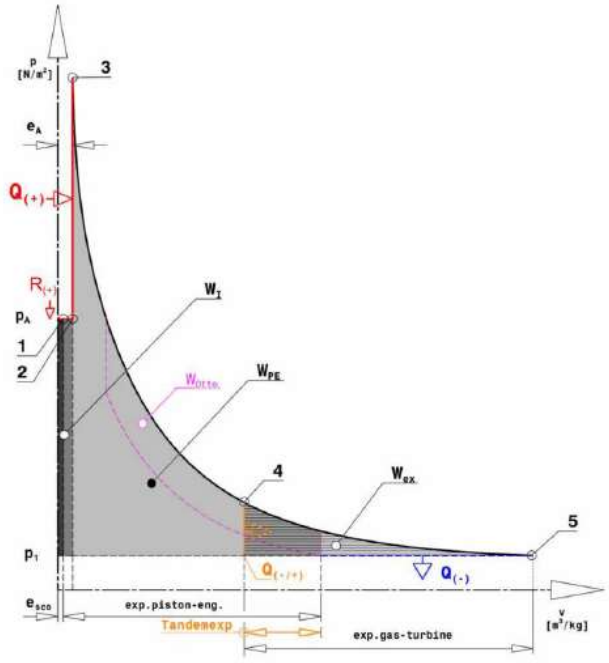

Slika 2.3. *AMICES ciklus [5]*

Figure 2.3. *AMICES cycle [5]*

Proces počinje od točke 0 i tada ja klip u GMT, te pri konstantnom tlaku od 50 bara počinje ubrizgavanje smjese zraka i goriva unutar cilindra, sve do točke 1.Od točke 1-2 slijedi ugrijavanje smjese energijom iz prošlog ciklusa koja se prenosi konvekcijom i to traje vrlo kratko. Nakon toga slijedi lasersko zapaljenje smjese te klip ide sve do DMT(točka 3). Slijedi ekspanzija od 3-4, tijekom koje se otvara ispušni ventil a zatim i ekspanzija ispušnih plinova u turbinu od točke 4-5. Na dijagramu se jasno vidi da se ta dva područja u dijelu svoga rada preklapaju (Tandemexp). Svaka površina ispod krivulje predstavlja rad. Svi ovi radovi se međusobno zbrajaju

i čine ukupan rad procesa. Za usporedbu imamo i rad izvršen Otto ciklusom . Ukupni rad AMICES-a je:
– rad kompresije plus rad koji je predala toplina R(+) konvekcijom;
- rad primarne ekspanzije koji nastaje ekspanzijom plinova u cilindru;
– rad sekundarne ekspanzije koji nastaje kada ispušni plinovi predaju rad turbini,
– toplina koja se razvija laserskim paljenjem smjese.

U proračunu kod AMICES ciklusa proces punjenja ili ubrizgavanja zraka se promatra kao izobara, izgaranje kao izohora, a ekspanzija kao adijabata

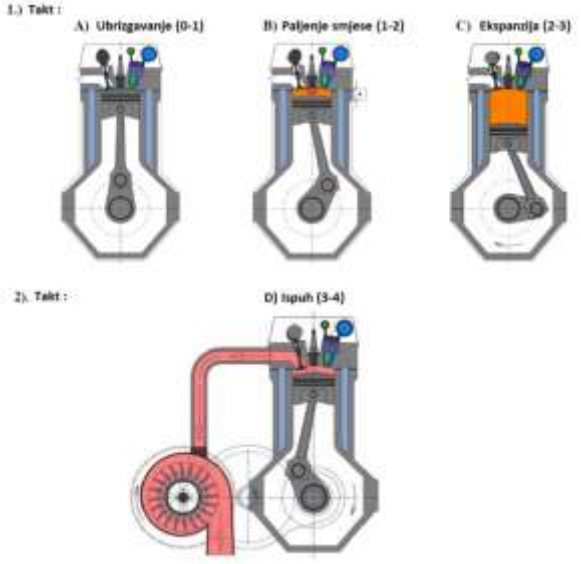

Slika 2.4. *Taktovi u cilindru*

Figure 2.4. *Strokes inside of cylinder*

2.3. Razlika AMICES-a i ostalih hibrida

AMICES koncept unutar automobila zauzima mnogo manje mjesta nego standardni motori istih izvedbi i snaga, kompaktniji je, a manja nam je i sama težina motora te troškovi izrade. Na slici 2.5 se jasno vidi razlika u dimenzijama između standardnih hibrida i AMICES-a. Uz to, prema teorijskim proračunima, AMICES bi trebao razvijati i do 4 puta veće snage (pri tlaku kompresije 50 bara) nego standardni hibridi (Toyota Prius) . Standardni hibridi troše 4.5-6.5 l/100 km (Toyota Prius, Honda Insight), dok bi predviđena potrošnja AMICES-a trebala biti unutar 1-3 l/100 km uz ekstremno malu emisiju CO_2 manje od 50 mg. Veliki minus standardnih hibrida je i znatno veća težina o odnosu na normalne automobile i to do 500 kg više, upravo zbog baterija i sustava hlađenja koji služi za odvod topline (Tesla Roadster).

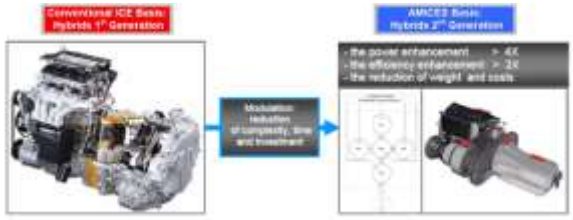

Slika 2.5. *Razlika običnih hibrida i AMICES-a [5]*

Figure 2.5. *Difference between standard hybrids and AMICES [5]*

Oznake sa slike 2.5. su:
Conventional ICE Basis: Hybrids 1st Generation – Standardni MUI: hibridi prve generacije
AMICES Basis : Hybrids 2nd Generation – AMICES : Hibridi druge generacije
Power enhancment – Povećanje snage
Efficiency enhancment – Povećanje iskoristivosti
Reduction of weight and costs – Redukcija mase i troškova

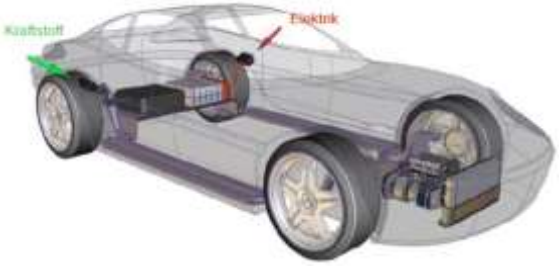

Slika 2.6. *Shema koncepta AMICES [5]*

Figure 2.6. *AMICES car appearance [5]*

Oznake sa slike 2.6. su:
Kraftstoff - Gorivo
Elektrik – Struja

Koncept s ciklusom kompresije van motora je u osnovi hibrid koji nudi integraciju električnog sustava na motor, a kompresiju vrši vanjskim kompresorom koji je pokretan elektromotorom. Temperatura smjese prilikom ubrizgavanja nije povezana s kompresijskim omjerom motora, dakle ne postoji klasičan problem toplinske barijere. Nema potrebe za dodatnim izvorom električne energije iz razloga što bateriju pune generatori pokretani kočenjem, energijom ispušnih plinova, a po potrebi preko sustava spojki i samim motorom. Baterija može biti manjeg kapaciteta (1-10 kW) s mogućnošću punjenja u kućanstvu. Ovako koncipiran motor mogao bi svesti potrošnju goriva i emisiju ispušnih plinova na vrlo niske vrijednosti, uz vrlo visoku specifičnu snagu. Sa veličinom tanka od oko 30 l moguće je voziti i do 1000 km bez punjenja ili ulijevanja goriva.

Hibridi 1.generacije temelje se na Otto/Diesel pogonu kombiniranim sa električnim pogonom. Njihova glavna odlika je da prikupljaju energiju kočenja te je skladište u baterije, te na taj način štede energiju. Korisni su samo gradske vožnje, jer im je domet na električni pogon vrlo malen, dok bi na otvorenoj cesti trošili znatno više zato pri vožnji na veće udaljenosti koriste isključivo pogon MUI-a, što znači da nam sustav baterija i elektromotora predstavlja nepotrebnu težinu jer ga uopće ne koristimo.

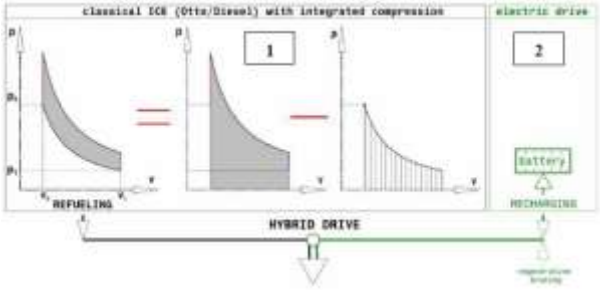

Slika 2.7. *Hibridi prve generacije*

Figure 2.7. *1st generation hybrids*

Oznake sa slike 2.7. su:
Integrated compression - Unutarnja kompresija
Electric drive – Električni pogon
Refueling – Punjenje gorivom
Recharging – Električno punjenje
Regenerative breaking – Pohrana energije kočenja

Kao što vidimo iz slike 2.7, rad dobiven na izlazu odgovara sivo obojanoj površini, a rad utrošen na kompresiju predstavlja okomitim linijama šrafirana površina ispod. Rad dobiven na izlazu jest rad dobiven ekspanzijom umanjen za rad utrošen na kompresiju. Dosadašnja iskustva s ubrizgavanjem, turbopunjačima, sistemima paljenja smjese i ostalim tehničkim inovacijama, omogućavaju tehnički iskorak i pokušaj prebacivanja takta kompresije iz ciklusa motora na vanjski izvor energije.

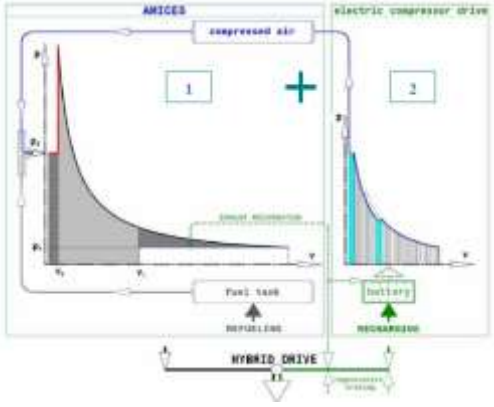

Slika 2.8. *AMICES hibrid*

Figure 2.8. *AMICES hybrid*

Oznake sa slike 2.6. su:
Fuel tank - Tank goriva
Compressed air – Komprimirani zrak

Toyota Prius Hybrid je već u kolovozu 2013.-e premašio brojku od 3 milijuna prodanih automobila diljem svijeta, dok je sama Toyota, općenito, dosad prodala preko 7.5 milijuna modela svojih hibrida. Ukupno gledajući, kada bi zbrojili broj prodanih automobila od 10 tipova najprodavanijih hibrida na svijetu, oni bi još uvijek bili iza Toyote Prius Hybrid.

Uspoređujući podatke Toyote Prius [1] sa AMICES-om lako je zaključiti da AMICES koristi trocilindrični 0.5L motor koji razvija 200 kW na 10000 okretaja, dok Prius sa četverocilindričnim 1.798L ima maksimalno 98 kW na 5200 ok/min. AMICES-ov električni motor je puno slabiji i razvija samo 5-10 kW, dok je kod Toyote 59 kW.
AMICES-ov električni motor i sustav baterija je mnogo manji zbog činjenice da pri svakom ciklusu skladištimo energiju kočenja i energiju ispušnih plinova na turbini u baterije. No, to nam je sasvim dovoljno s obzirom na karakteristike MUI-a, a samim time nam je težina automobila manja kako imamo manje baterija.
Naravno, moramo kazati da je Toyota Pirus već gotov i izrađen auto dok je koncept AMICES tek u razradi, te su sve dobivene brojke samo teorijske što ne znači da će se i u praksi pokazati takvima.

2.4. Problemi u realizaciji AMICES-a

AMICES koncept je još uvijek u teorijskoj razradi, a da bi ga pokušali pretočiti u praksu moraju se riješiti sve nedoumice i mnogobrojna pitanja koja se pojavljuju. Neki od problema, kao i sama usporedba sa Otto motorom već su analizirani u prijašnjim radovima [3], te ukazuju na to da, iako AMICES u teoriji pokazuje svoje prednosti, postoje i mnogi nedostatci pri njegovoj izvedbi koji su najčešće vezani uz vanjsku kompresiju. Najveći problemi su vezani uz hlađenje motora s obzirom na to da su nam temperature i tlakovi povišeni, te to da još uvijek nije proizveden odgovarajući kompresor koji bi nam ubrizgavao zrak u cilindar pri pritisku od 50 bara. Zrak pod tim tlakom mora proći kroz dovoljno veliki otvor da bi u kratkom vremenu u cilindar ubacili potrebnu masu zraka. Javlja se i problem hlađenja komprimiranog zraka jer temperatura na kraju jednostupanjske kompresije iznosi 896 K. AMICES definira temperaturu ubrizgavanja od 293K, stoga komprimirani zrak treba ohladiti. AMICES koristi 2-stupanjsku kompresiju koja daje manju temperaturu na izlazu iz kompresora, ali i zahtjeva hlađenje u među-stupnju kao i na izlazu iz kompresora da bi postigli ciljanu temperaturu. Veliki problem je i stabilnost čitavog sustava s obzirom na to da nam je ekspanzijski takt vrlo snažan te nam klip vrlo brzo

dođe u GMT. Tu će nam veliku ulogu igrati balansiranje motora i pokušaj što veće kontrole ekspanzijskog takta. Također, moguće je i smanjenje tlaka kompresora sve do 20-ak bara kako bi nam krivulja okretnog momenta i snage bila što linearnija, jer nam je pri većem tlaku teže kontrolirati pulsacije, te dolazi do rušenja snage i okretnog momenta.
No, ti svi problemi se javljaju kod klasičnog načina konstruiranja cilindra i gibanja klipa unutar cilindra. Promjenom toga, moguće je da većinu problema riješimo.

3. Konstrukcijska rješenja

3.1. Mogućnosti izvedbe cilindra kod AMICES-a

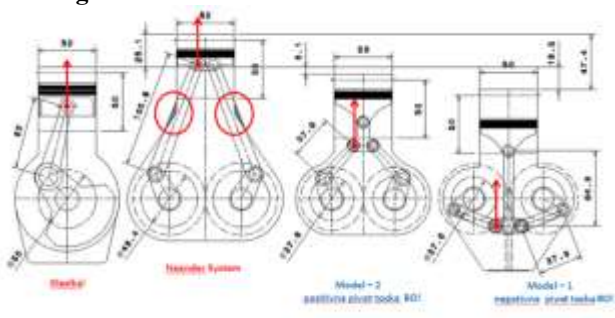

Slika 3.1. *Konstrukcijske izvedbe cilindra*

Figure 3.1. *Different construction concepts*

Na slici 3.1 vidimo razne konstrukcijske izvedbe cilindra koje bi bile u primjeni za AMICES koncept. Svaka od njih ima svoje prednosti i svoje mane, te s obzirom da zadane karakteristike trebamo odabrati onu najpoželjniju kako bi mogli upravljati procesom bez većih poteškoća [6].

3.2. Neander system

To je sistem sa dvije klipnjače vezane na dva koljenasta vratila. Izrazito je velik što nam predstavlja problem. Silazak klipa cca. 187°, te povratak cca. 173°.Mana mu je što su klipnjače direktno vezane na klip, a hod klipa matematički uvjetuje dužinu para klipnjača koje ulaze duboko u cilindar te postaju izuzetno duge što uvjetuje, značajni porast oscilacijskih masa klipnjača te povećanu visinu i težište motora u odnosu na klasične sisteme. Budući da par klipnjača ulazi duboko u cilindar motora, kod zakreta vratila od otprilike 300-330° dolazi do kolizije između klipnjača i donjeg ruba cilindra koji je moguće riješiti samo na dva načina: nezgrapno visoki položaj radnog dijela cilindra iznad osi vratila ili, kao što su to i napravili kroz vrlo nepovoljan odnos (S/D = cca. 0,6!) što značajno povećava toplinske i radne gubitke motora, te u pogledu iskoristivosti poništava potpuno pozitivan efekt tek neznatno produženog ekspanzijskog takta.

3.3. Doppelwelle system

Razlikujemo dva tipa ovog sistema: onoga sa pozitivnom pivot točkom i onog sa negativnom. Kada imamo sistem sa pozitivnom pivot točkom ležaj se kreće iznad vratila, dok je kod negativne pivot točke kretanja ležaja ispod vratila. Sistem rješava prije svega probleme trenja i bočnih oscilacija motora kroz izbjegavanje snažne normalne sile između klipa i stjenke cilindra. Sistem krije u svojoj kinematici jednu daleko značajniju prednost. Naime, kod klasičnih sistema s jednom klipnjačom vremensko trajanje silaska i povratka klipa je potpuno izjednačeno (silazak=180°, povratak=180°). Kod Doppelwelle sistema put klipa od GMT-a u DMT traje dulje nego njegov povratak u gornju mrtvu točku (GMT). Kod AMICESA ovo predstavlja izuzetnu prednost vezano za ubrizgavanje i paljenje nakon gornje mrtve točke što znači da nam ekspanzijski takt traje duže od ispušnog takta. Proračuni s brzinama klipa pokazuju izuzetne prednosti ovih sistema kako u odnosu na značajno smanjenje motora kod istog radnog volumena (downsizing), tako i u smanjenju mase pokretnih dijelova u mehanizmu koljenastih vratila. Najveću prednost predstavlja radni takt koji traje 240° dok sam ispuh traje svega 120°. Tako se kod potencijalnog trocilindričnog motora, dva cilindra trajno preklapaju u radnom taktu (Dvostruko radno područje).

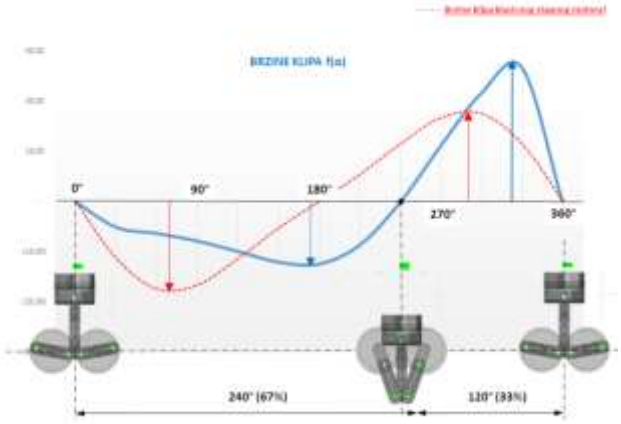

Slika 3.2. *Doppelwelle sistem*

Figure 3.2. *Doppelwelle system*

3.4. Usporedba klasičnog i Doppelwelle sistema

Teorijski gledano, Doppelwelle sistem nam se čini kao izvrsno konstrukcijsko rješenje za AMICES. No, prije bilo kakvih zaključaka potrebno je izvršiti ispitivanja u računalnim programima te na osnovu rješenja dobivenih u tim simulacijama izvršiti usporedbu te odabrati najbolje rješenje. Za potrebe našeg ispitivanja, koristili smo program Ricardo Wave. Rezultati su vidljivi na slikama 3.3 i 3.4.

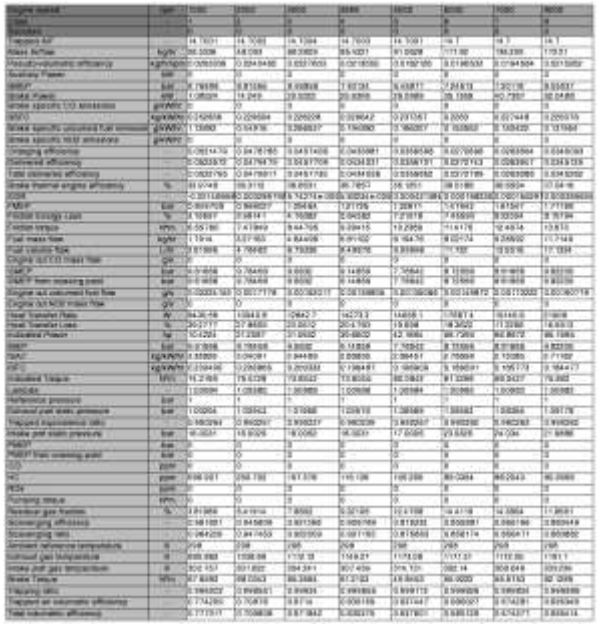

Slika 3.3. *Specifikacije Doppelwelle sistema*

Figure 3.3. *Doppelwelle Specifications*

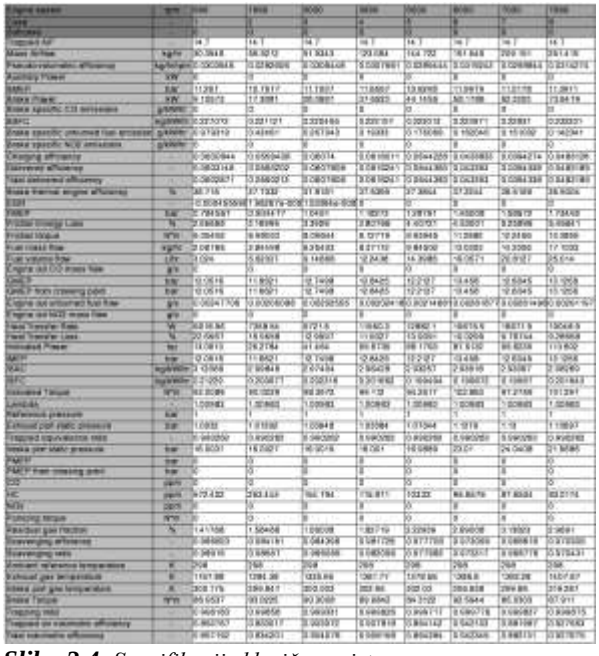

Slika 3.4. *Specifikacije klasičnog sistema*

Figure 3.4. *Specifications for classical engine construction*

Svi bitni rezultati mogu se očitati i usporediti iz tablica, ali nama je najvažnija usporedba snage i okretnog momenta. Dobivene vrijednosti ne moraju nužno biti u potpunosti točne, ali pretpostavka je da bi stvarne vrijednosti trebale biti u nekom približnom intervalu kao i ove.

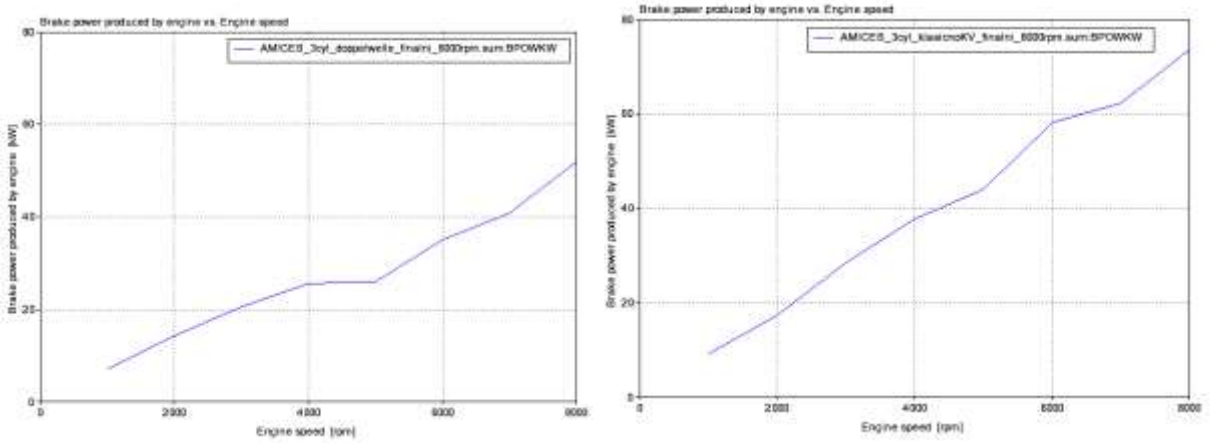

Dijagram 1. *Ovisnost snage o broju okretaja za Doppelwelle sistem (lijeva slika) i klasičan sistem (desna slika)*

Diagram 1. *Power - RPM diagram for Doppelwelle system (left picture) and classical engine construction (right picture)*

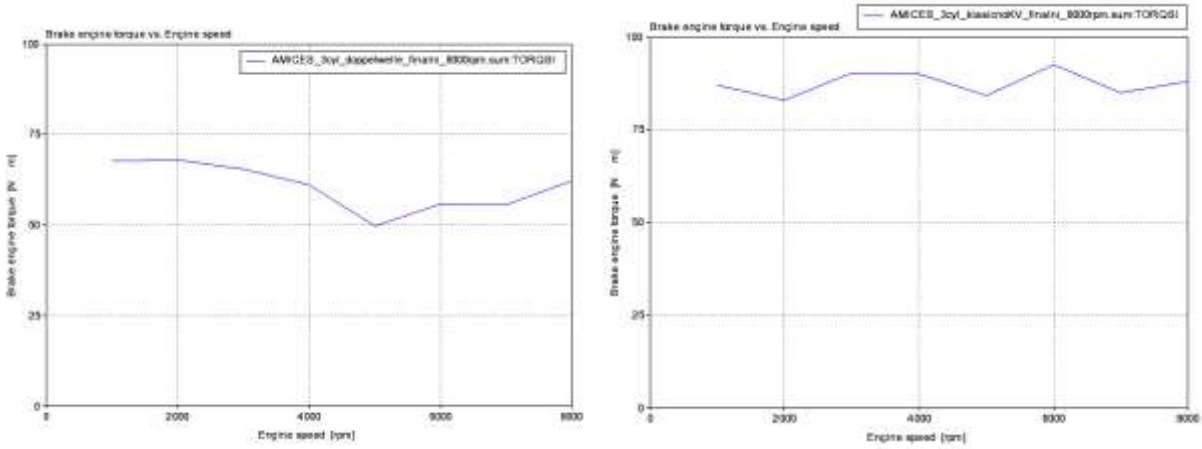

Dijagram 1. *Ovisnost zakretnog momenta o broju okretaja za Doppelwelle sistem (lijeva slika) i klasičan sistem (desna slika)*

Diagram 1. *Torque - RPM diagram for Doppelwelle system (left picture) and classical engine construction (right picture)*

Iz prikazanih vrijednosti se može zaključiti da nam je klasični sistem puno bolji nego Doppelwelle. Iznosi snage klasičnog sistem su mnogo veći za isti broj okretaja nego od Doppelwelle-a kao npr. na 8000 min^{-1} klasični sistem razvija 73 kW, dok Doppelwelle razvija 52 kW što je velika razlika od čak 21 kW. Isto se može primijetiti i za okretni moment. Klasični sistem je puno stabilniji i to sa vrijednostima između

82 Nm i 90 Nm, dok nam Doppelwelle pokazuje veći pad vrijednosti na 5000 min^{-1} , a same vrijednosti mu se kreću od 68 – 50 Nm. Važna napomena je da smo pri dobivanju što realnije slike Doppelwellea izvršili određene aproksimacije u programu Ricardo kako bi dobili podatke, jer program nema opciju biranja pravog Doppelwelle sistema sa kojim bi onda provodili eksperiment.

4. Materijali za izradu klipa

S obzirom na dobivene krivulje snage i momenta za pojedinu konstrukcijsku izvedbu, odlučit ćemo se za onu nama tehnološki i energetski najpovoljniju. Zbog velikih tlakova i izrazito visoke temperature u komori izgaranja, materijali za izradu dijelova motora će biti drugačiji nego inače. Općenito govoreći, najopterećeniji dio motora je klip i to njegova glava. On se radi od materijala koji može izdržati najveća termička opterećenja kojima će biti podvrgnut. Oblik vrha glave nam zajedno s oblikom glave motora definira prostor izgaranja. Iako se smatra da klip ima oblik valjka, to u stvarnosti nije tako, jer je gornji dio glave nešto manjeg promjera zbog nejednakih termičkih naprezanja i nejednakog širenja materijala. Standardni materijali za izradu su aluminij (za promjere 200 – 250 mm) i čelik (za sve veće promjere). Alternativni materijali za korištenje za AMICES su nam ili standardni klip presvučen keramikom ili klip izrađen od grafita.

4.1. Klipovi presvučeni keramikom

Keramika je kao materijal znatno tvrđa i bolje podnosi veće temperature nego čelik ili aluminij. Keramički klipovi sa većim temperaturama mogu i bolje sagorjeti smjesu, a to automatski znači bolja iskoristivost unesenog goriva čime nam snaga raste, a postotak štetnih plinova opada.

Slika 4.1. *Klipovi presvučeni keramikom*

Figure 4.1. *Ceramic piston coatings*

Testovi su pokazali da potpuno jednaki motori sa jednakim parametrima, ali samo razlikom u materijalu klipa (jedan je s običnim, a drugi s keramičkim) pokazuju razliku u kompresijskom omjeru i to na stranu motora s keramičkim klipom.

4.2. Grafitni klip

Veliki novitet u svijetu MUI-a je klip u potpunosti izrađen od grafita. Grafit kao materijal ima značajne prednosti pred ostalim materijalima koji se trenutno upotrebljavaju u autoindustriji: lakši je, ima manji koeficijent termalnog širenja, te veći koeficijent toplinskog otpora.

Karakteristike	Ozn.	Mjerna jedinica	**Al legure**	**Grafit**
Gustoća	ρ	gcm^{-3}	2.7	1.83
Koef.lin.topl. širenja	α	1/K	$21 \cdot 10^{-6}$	$6 \cdot 10^{-6}$
Modul el.	E	GPa	80	11
Koeficijent kondukcije	λ	$Wm^{-1}K^{-1}$	150	80
Vlačna čvrstoća	σ_V	MPa	225	70

Tablica 1. *Usporedba aluminija i grafita*

Table 1. *Difference between Al and graphite*

Vlačna čvrstoća mu je na nižim temperaturama manja, ali za razliku od aluminija, ona raste s povećanjem temperature.

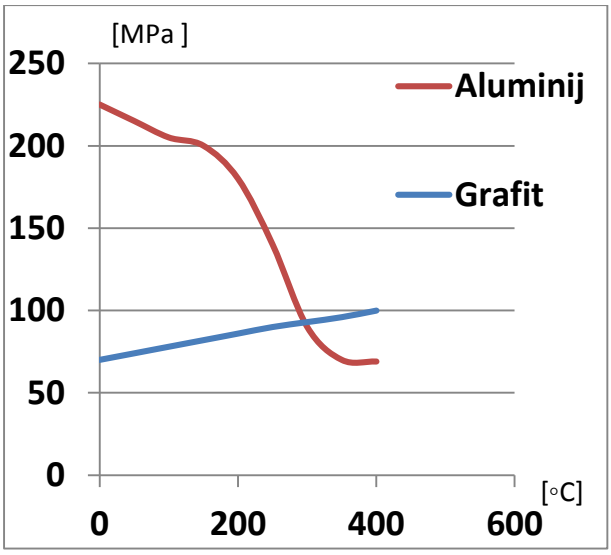

Dijagram 5. *Ovisnost vlačne čvrstoće o temperaturi*

Diagram 5. *Tensile strength – temperature diagram*

Prednosti karbonskih klipova su [7]:
• Manja masa klipova i do 30 % ;
• Bolje performanse motora (manje vibracija, potrošnja goriva manja i do 5 %) ;
• Toplinska i mehanička postojanost pri velikim temperaturama ;
• Stabilnost ;
• Vrlo malo toplinsko širenje klipa ;
• Manje emisije štetnih plinova i to 20 % HC, 30 % CO, 3 % NOx ;
• S obzirom na izvrsne karakteristike grafita što se tiče trenja najveći uspjeh je smanjenje potrošnje ulja za podmazivanje i to za 44 %. Rad motora je čak moguć i u uvjetima kada nestane ulja ;
• Konstantna tvrdoća pri svim temperaturama ;
• Otpornost na oksidaciju, sve do 600 °C ;
• Izvrsna tribološka svojstva ;
• Jednaka raspodjela topline unutar cilindra.

Slika 4.2. *Karbonski klip, klipnjača i koljenasto vratilo [2]*

Figure 4.2. *Carbon piston, connecting rod and crankshafts [2]*

Proizvođač, Schunk Kohlenstofftechnik GmbH, navodi da su već sada uspjeli proizvesti kompletne dijelove (klip, klipnjača i koljenasto vratilo) za sljedeća vozila :
• Ford Focus RS Mk1, Mk2 and Mk3
• Honda Civic Type-R
• Mazda Bongo Friendee
• Mitsubishi Lancer Evolution
• Nissan Silvia S15
• Nissan Skyline and GT-R
• Subaru Impreza WRX/STi
• Suzuki Swift Sport
• Toyota MR2

Slika 4.3. *Izgled karbonskih (B), čeličnih (A) i aluminijskih klipova (C)*

Figure 4.3. *Appearance of carbon(B), steel (A) and aluminum pistons (C)*

S obzirom na navedene karakteristike klipovi od karbonskih vlakana se čine kao najbolja opcija, jer nam donose velike uštede kod potrošnje ulja,ukupne mase motora i njegovih dijelova te smanjuju emisije štetnih plinova. Rad motora je puno lakši, uz manje vibracije i veću stabilnost.

4.3. Raspodjela temperature po klipu za odabrane materijale

Za svaki od opisanih materijala klipa, u SOLIDWORKS-u smo za jednake dimenzije klipa odabrali svaki od materijala sa zadanim svojstvima,te proučavali razlike u raspodjeli topline kroz klip. Rezultati se mogu vidjeti na slikama 4.4 , 4.5 , 4.6.

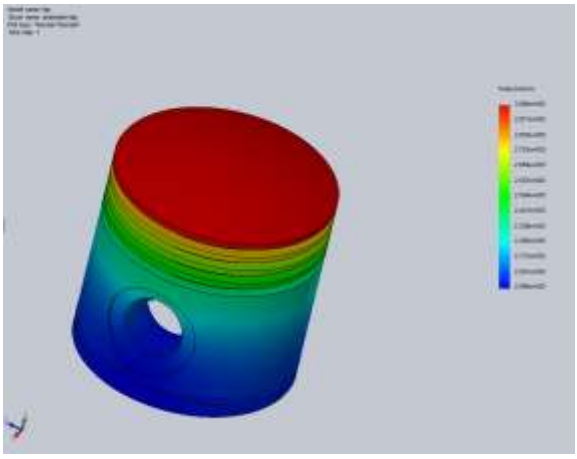

Slika 4.4. *Standardni aluminijski klip*

Figure 4.4. *Aluminum piston*

Za standardni aluminijski klip uzeli smo aluminijsku leguru sa sljedećim svojstvima :
- Modul elastičnosti *E=70 GPa*
- Gustoća $\rho = 2700\ kg/m^3$
- Koeficijent kondukcije $\lambda = 150\ W/mK$
- Vlačna čvrstoća $\sigma_V = 225\ MPa$
- Koeficijent linearnog toplinskog širenja
$\alpha = 2.1 \cdot 10^{-5}\ 1/K$

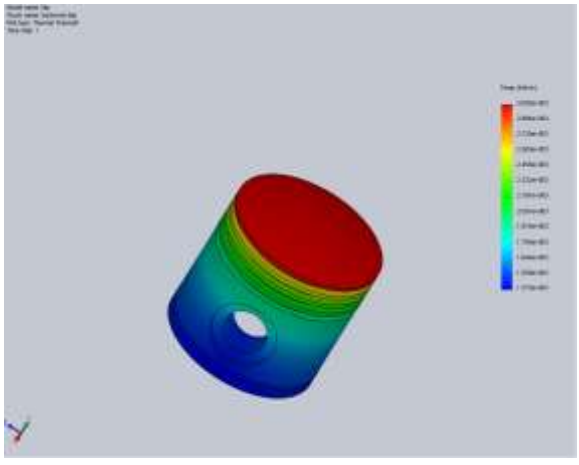

Slika 4.5. *Karbonski klip*

Figure 4.5. *Carbon pistons*

Za karbonski klip uzeli smo grafit sa sljedećim svojstvima :
- Modul elastičnosti *E=11 GPa*
- Gustoća $\rho = 1830\ kg/m^3$
- Koeficijent kondukcije $\lambda = 80\ W/mK$
- Vlačna čvrstoća $\sigma_V = 172\ MPa$
- Koeficijent linearnog toplinskog širenja
$\alpha = 6 \cdot 10^{-6}\ 1/K$

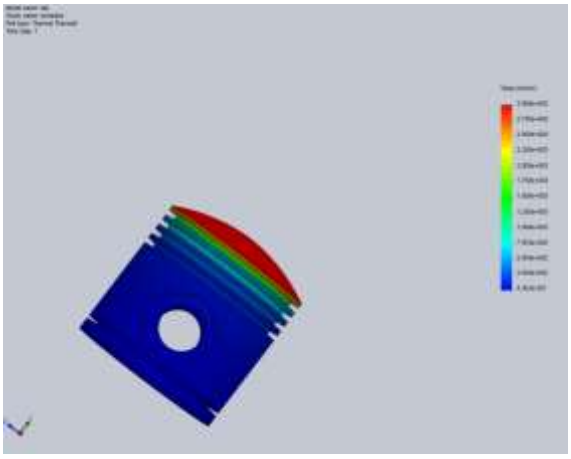

Slika 4.6. *Keramikom presvučeni klip*

Figure 4.6. *Piston with ceramic piston coatings*

Za keramički klip uzeli smo keramiku sa sljedećim svojstvima :
- Modul elastičnosti *E=220 GPa*
- Gustoća $\rho = 2300\ kg/m^3$
- Koeficijent kondukcije $\lambda = 1.5\ W/mK$
- Vlačna čvrstoća $\sigma_V = 70\ MPa$
- KoeficIjent linearnog toplinskog širenja
$\alpha = 2.4 \cdot 10^{-5}\ 1/K$

Očekivano, najmanji prijenos topline imaju nam keramički klipovi, s obzirom na to da im je koeficijent kondukcije od 50 do 100 puta manji u odnosu na karbon odnosno aluminij. Ali, velika mana karbonskih klipova je u tome što im je vlačna čvrstoća i do 2-3 puta manja u odnosu na karbon i aluminij, što nam može stvoriti velike probleme. Uz to, i koeficijent toplinskog širenja joj je manji nego kod karbona, a gustoća joj je veća čime povećavamo ukupnu težinu što nam nije poželjno.
Karbon nam se čini kao trenutno najpoželjniji materijal, spajajući međusobno najbolje karakteristike aluminija i keramike. Ima dovoljno veliku čvrstoću, relativno mali koeficijent kondukcije, te izvrsno podnosi velike temperature i tlakove. Također, gustoća mu je znatno manja nego kod druga dva materijala što nam motor čini lakšim, a samim time auto bržim. Važno je napomenuti da raspodjela temperatura dobivena u SOLIDWORKSU, ne mora nužno biti u potpunosti točna tj. dobivene temperature (izuzev početne) mogu biti u stvarnosti različite s obzirom na utjecaj mnogobrojnih faktora (konvekcija, sustav hlađenja i brojni drugi) koji su unošenjem u simulaciju bili pretpostavljeni, ali i jednaki za sva 3 klipa, čime smo samo željeli ukazati na razliku i prednosti između zadanih materijala pri raspodjeli temperature.

Zaključak

Koncept AMICES, u svojoj teoriji, predstavlja izraziti napredak u odnosu na hibride koji se trenutno koriste u svijetu. No, kako bi u potpunosti zaživio potrebno je riješiti probleme korištenja vanjske kompresije, koja sa sobom vuče i pulsacije unutar cilindra,. Uz taj glavni problem nam se javlja i problem balansiranja motora, jer nam je ekspanzijski takt prejak, te moramo pronaći način kako da usporimo gibanje klipa prema GMT. Pri ugradnji zamašne mase bi nam se stvorio problem, jer bi nam ona trebala biti vrlo velika da bi uravnotežila motor. Time, nepotrebno povećavamo masu motora i gubimo na brzini automobila. Problemi, poput laserskog paljenja smjese, te povećanih temperatura i tlakova unutar cilindra bi trebali biti vrlo lako riješeni, s obzirom da nam je laserska tehnologija sve dostupnija, a napredak kod istraživanja materijala nas je doveo do toga da su se unutar motora već počeli ugrađivati karbonski klipovi, klipnjače i koljenasta vratila koji uvelike smanjuju masu motora te vibracije, a izvrsno funkcioniraju pri visokim temperaturama i tlakovima. Također smanjuju i emisije štetnih plinova, te potrošnju ulja za podmazivanje.

S daljnjim istraživanjem i rješavanjem opisanih problema, te praćenjem inovacija unutar autoindustrije, ali i ostalih grana strojarstva nadamo se kako će za nekoliko godina svi hibridi biti pogonjeni AMICES konceptom. Samim time onečišćenje zraka bi bilo znatno manje, a iskoristivost energije na zavidnom nivou.

Literatura

[1] Toyota:" Toyota Prius Specifications" , s Interneta, http://www.toyota.hr/cars/new_cars/prius/index.tmex, Nagoya , 2011

[2] Schunk Kohlenstofftechnik GmbH : " Carbon pistons for ICE engines " , s Interneta , http://www.schunk-group.com/uploads/tx_rmsschunktest/08-06_Carbon-Pistons-for-Internal-Combustion-Engines_02.pdf , Heuchelheim , 2006

[3] Matulić , N. : "Analiza i optimizacija radnih parametara hibridnog sustava", Diplomski rad , FESB Split , 2013

[4] Dodig, D: " Analiza radnih parametara aktivnog modularnog motora s unutarnjim izgaranjem" , Završni rad, FESB Split , 2014.

[5] Šalinović, H: „Von AMICES I-2008 zu AMICES II-2011", München, 2011.

[6] Basshuysen, R., Schaefer, F. : Handbuch Verbrennungsmotor, MTZ, GWV Fachverlag GmbH, Wiesbaden, 2010.

[7] J. Heuer : „Development and testing of carbon pistons" , Research, Structural Materials Daimler-Benz Aktiengesellschaft, Sttutgart

Murko je prije stalno trčao za macama po susjedstvu...
...a sada, uz EVN, više voli biti doma.

Kad je vani hladno, puno je ugodnije biti u kući, pogotovo ako se grijete uz EVN. Uz zemni plin, hlađenje i grijanje vašeg doma ili ureda postaje jednostavno, ugodno i dostupno, a temperatura uvijek idealna neovisno o godišnjem dobu. Odaberite zemni plin i učinit ćete ogromnu uslugu sebi, svom kućnom budžetu i okolišu. Kontaktirajte nas i rado ćemo vam dati detaljne informacije o instaliranju zemnog plina u vaš dom.

Saznajte više o plinofikaciji Dalmacije na:
www.evn.hr, info@evn.hr
ili na besplatnom info telefonu 0800 820 820.

Za ugodniji život.

EVN

ISSN 1847-7917